

**A Thesis Submitted for the Degree of PhD at the University of Warwick**

**Permanent WRAP URL:**

<http://wrap.warwick.ac.uk/117577>

**Copyright and reuse:**

This thesis is made available online and is protected by original copyright.

Please scroll down to view the document itself.

Please refer to the repository record for this item for information to help you to cite it.

Our policy information is available from the repository home page.

For more information, please contact the WRAP Team at: [wrap@warwick.ac.uk](mailto:wrap@warwick.ac.uk)

**Evaluating the suitability of Nanoparticles and Microspheres  
for diagnostics and biopharmaceutical delivery in Medicine**

**By**

**Ajit Singh Thakur**

A thesis submitted in partial fulfillment of the requirements for the degree of  
Doctor of Philosophy by published work

Division of Health Sciences

Warwick Medical School

University of Warwick

September 2018

## TABLE OF CONTENTS

ACKNOWLEDGEMENTS	1
SUBMISSION DECLARATION	1
WORD COUNT	1
INDEX OF PUBLICATIONS SUBMITTED AND STATEMENT OF CONTRIBUTION	2
LIST OF ILLUSTRATIONS AND TABLES	4
LIST OF ABBREVIATIONS	5
<b>ABSTRACT</b>	<b>6</b>
<b>BACKGROUND</b>	<b>7</b>
NANOPARTICLES FOR DIAGNOSTICS AND BIOPHARMACEUTICAL DELIVERY IN MEDICINE	7
MICROSPHERES FOR BIOPHARMACEUTICAL DELIVERY IN MEDICINE AND TRANSPLANTATION	
IMMUNOLOGY	14
GENE THERAPY WITH VIRAL NANOCARRIERS	17
<b>AIMS AND OBJECTIVES</b>	<b>19</b>
<b>METHODS</b>	<b>19</b>
<b>SUMMARY OF PUBLISHED WORK</b>	<b>20</b>
<b>PAPER 1:</b> "CHARACTERIZATION OF QUANTUM DOT BEHAVIOUR IN LIVE MAMMALIAN CELLS" (2005) <i>CANADIAN UNDERGRADUATE PHYSICS JOURNAL</i> . 3(3), pp.7-12.	20
<b>PAPER 2:</b> "STRATEGIES FOR OCULAR siRNA DELIVERY: POTENTIAL AND LIMITATIONS OF NON- VIRAL NANOCARRIERS" (2012) <i>JOURNAL OF BIOLOGICAL ENGINEERING</i> . 6(1) pp. 7.	25
<b>PAPER 3:</b> "TEMPERATURE-SENSITIVE POLYMERS FOR DRUG DELIVERY" (2012) <i>EXPERT REVIEW     OF MEDICAL DEVICES</i> . 9(4) pp. 339-351.	28
<b>PAPER 4:</b> "CHARACTERIZATION OF VIABILITY AND PROLIFERATION OF ALGINATE-POLY-L-LYSINE- ALGINATE ENCAPSULATED MYOBLASTS USING FLOW CYTOMETRY" (2010) <i>JOURNAL OF     BIOMEDICAL MATERIALS RESEARCH: PART B</i> . 94B(2) pp. 296-304.	30
<b>PAPER 5:</b> "SINGLE-COLOUR FLOW CYTOMETRIC ASSAY TO DETERMINE NK CELL-MEDIATED CYTOTOXICITY AND VIABILITY AGAINST NON-ADHERENT HUMAN TUMOR CELLS" (2012) <i>BIOTECHNOLOGY LETTERS</i> . 34(3) pp. 447-53.	36
<b>PAPER 6:</b> "RETROVIRAL EXPRESSION OF MIR2 DECREASES BOTH SURFACE MHC CLASS I AND THE ALLOIMMUNE CTL RESPONSE" (2011) <i>JOURNAL OF TISSUE ENGINEERING AND     REGENERATIVE MEDICINE</i> . 5(7) pp. 520-528.	38
<b>PAPER 7:</b> "SUPPRESSION OF THE MHC CLASS I-MEDIATED ALLOIMMUNE RESPONSE IN HUMAN CELLS USING A SINGLE-STEP RETROVIRAL TRANSDUCTION PROTOCOL TO EXPRESS KSHV'S STEALTH PROTEIN MIR2" (2011) <i>UNIVERSITY OF TORONTO MEDICAL JOURNAL</i> . 89(1) pp. 27-32.	43

<b>PAPER 8: "RECURRENT HOSPITALIZATIONS IN A RARE CASE OF HEMICORPECTOMY: A CHALLENGING CASE FOR MEDICAL MANAGEMENT" (2018) <i>BRITISH MEDICAL JOURNAL CASE REPORTS</i>. DOI 10.1136 PP. 1-5.</b>	<b>46</b>
<b>DISCUSSION</b>	<b>48</b>
<b>FUTURE WORK</b>	<b>52</b>
<b>CONCLUSION</b>	<b>55</b>
<b>BIBLIOGRAPHY</b>	<b>56</b>
APPENDIX A: PUBLICATIONS INCLUDED IN THE THESIS	67
APPENDIX B: STATEMENT OF CONTRIBUTION SIGNED BY PRINCIPAL INVESTIGATORS	68
APPENDIX C: LIST OF ADDITIONAL PAPERS SUBMITTED AS SUPPLEMENTARY MATERIAL	69

## ACKNOWLEDGEMENTS

I sincerely thank my PhD thesis supervisor Dr. Daniel Mitchell for his support and guidance throughout the thesis writeup. I am most grateful to my research supervisors including Dr. Cecile Fradin, Dr. Gonzalo Hortelano, Dr. Kim Jones, Dr. Bhagwati Gupta, and Dr. Heather Sheardown for their advice, technical help and providing me with all the means and materials for this research. In addition, I would like to thank all members of these lab groups, especially Dr. Kaplan Kugathasan, Dr. Scott Fitzpatrick, Dr. Vasudha Gupta, Dr. Abeyat Zaman and Brian Moody for their support and friendship over the years. Furthermore, I would like to thank my research sponsors including the National Science and Engineering Research Counsel (NSERC), McMaster University and the University of Toronto.

Finally, I thank my family for their continued support and encouragement throughout my research projects. I am eternally grateful to my parents for all their sacrifices made on my behalf. I dedicate this work to them.

## SUBMISSION DECLARATION

I declare that this thesis is my own work based on collaborative research as outlined in the statement of contribution. I declare that the submitted material is not substantially the same as published or unpublished material that I have previously submitted, or currently submitting, for a degree, diploma, or similar qualification at any university or similar institution.

This thesis submitted to the University of Warwick in support of my application for the degree of Doctor of Philosophy. It has been composed by myself and has not been submitted in any previous application for any degree.

## WORD COUNT

~10000

## INDEX OF PUBLICATIONS SUBMITTED AND STATEMENT OF CONTRIBUTION

The following eight papers make up the body of work for my thesis:

- 1) **A. Thakur** and C. Fradin. (2005). "Characterization of quantum dot behaviour in live mammalian cells." *Canadian Undergraduate Physics Journal*. 3(3), pp.7-12. **This article was featured on the cover-art of the journal.** [12 citations; 4325 words]

Ajit Thakur conceived the idea for the study and took the lead role in experimental work and data analysis. He was the lead author as well as the corresponding author who submitted the manuscript and corresponded with reviewers for paper revisions prior to publication.

- 2) **A. Thakur**, S. Fitzpatrick, A. Zaman, K. Kugathasan, B. Muirhead, G. Hortelano, H. Sheardown. (2012). "Strategies for ocular siRNA delivery: potential and limitations of non-viral nanocarriers." *Journal of Biological Engineering*. 6(1) pp. 7. [17 citations; 10941 words]

Ajit Thakur conceived the idea for this paper and was the lead author involved in the literature review, write-up and critical review. He designed the smart universal nanoparticle for intracellular oligonucleotide delivery. He was also the corresponding author who submitted the manuscript and corresponded with reviewers for paper revisions prior to publication.

- 3) S. Fitzpatrick, L. Fitzpatrick, **A. Thakur**, M. Mazumder and H. Sheardown. (2012). "Temperature-sensitive polymers for drug delivery." *Expert Review of Medical Devices*. 9(4) pp. 339-351. [25 citations; 5807 words]

Ajit Thakur co-authored this manuscript with S. Fitzpatrick and was involved in the literature search, write-up, critical review and multiple revision of the paper.

- 4) **A. Thakur**, R. Sengupta, H. Matsui, D. Lillicrap, K. Jones and G. Hortelano. (2010). "Characterization of viability and proliferation of alginate-poly-L-lysine-alginate encapsulated myoblasts using flow cytometry." *Journal of Biomedical Materials Research: Part B*. 94B(2) pp. 296-304. [15 citations; 6488 words]

Ajit Thakur conceived the idea for the study and took the lead role in writing the paper, critical data analysis and multiple paper revisions prior to publication. He was assisted by coauthor R Sengupta for experimental work.

- 5) **A. Thakur**, A. Zaman, J. Hummel, K. Jones, G. Hortelano. (2012). "Single-colour flow cytometric assay to determine NK cell-mediated cytotoxicity and viability against non-adherent human tumor cells." *Biotechnology Letters*. 34(3) pp. 447-53. [2 citations; 3889 words words]

Ajit Thakur conceived the idea for the study, and took the lead role in experimental work and data analysis. He was the lead author as well as the corresponding author who submitted the manuscript and corresponded with reviewers for paper revisions prior to publication.

- 6) **A. Thakur**, J. Hummel, R. Sengupta, V. Gupta, K. Mossman and K. Jones. (2011). "Retroviral expression of MIR2 decreases both surface MHC Class I and the alloimmune CTL response." *Journal of Tissue Engineering and Regenerative Medicine*. 5(7) pp. 520-528. [3 citations; 6491 words]

Ajit Thakur conceived the idea for the study and took the lead role in experimental work and data analysis. He was the lead author of the paper who submitted the manuscript and corresponded with reviewers for paper revisions prior to publication.

- 7) **A. Thakur**, A. Zaman, S. Fitzpatrick, J. Hummel and K. Jones. (2011). "Suppression of the MHC Class I-mediated alloimmune response in human cells using a single-step retroviral transduction protocol to express KSHV's stealth protein MIR2." *University of Toronto Medical Journal*. 89(1) pp. 27-32. [4707 words]

Ajit Thakur conceived the idea for the study and took the lead role in experimental work and data analysis. He was the lead author of the paper who submitted the manuscript and corresponded with reviewers for paper revisions prior to publication.

- 8) **A. Thakur**, R. Naik, B. Elliott, S. Mcquaid, N. Khan, C. Arsene. (2018). "Recurrent hospitalizations in a rare case of hemicorporectomy: A challenging case for medical management." *British Medical Journal Case Reports*. doi 10.1136 pp. 1-5. [2500 words]

Ajit Thakur conceived the idea for this paper and was the lead author involved in patient care, design, data analysis, critical review and write-up of the paper. He was also the corresponding author for the paper who submitted the manuscript and corresponded with reviewers for paper revisions prior to publication.

## LIST OF ILLUSTRATIONS AND TABLES

FIGURE A: PATHWAYS OF ALLOGRAFT RECOGNITION	16
FIGURE 1: SCHEMATIC OF A QUANTUM DOT	22
FIGURE 2: IMMOBILISED SINGLE QD AND QD AGGREGATES	22
FIGURE 3: BLINKING OF SINGLE QD COMPARED TO AGGREGATES	23
FIGURE 4: CONFOCAL MICROSCOPY OF CdSe-ZNS QD IN RAT FIBROBLASTS	23
FIGURE 5. DIRECTED QD TRAFFICKING ALONG MICROTUBULES IN LIVE RAT FIBROBLASTS	24
FIGURE 6: NANOCARRIER UPTAKE AND INTRACELLULAR siRNA DELIVERY	26
FIGURE 7: SCHEMATIC OF FOUR-COMPONENT 'UNIVERSAL' NANOCARRIER FOR siRNA DELIVERY	27
FIGURE 8. MURINE MYOBLASTS ENCAPSULATED WITHIN APA MICROCAPSULES	32
FIGURE 9. RELATIONSHIP BETWEEN FVIII SECRETION RATE OF NON-IMPLANTED ENCAPSULATED FVIII SECRETING MYOBLAST CELLS AND VIABILITY	32
FIGURE 10. REPRESENTATIVE FS/SS PLOTS OF NON-IMPLANTED ENCAPSULATED FVIII SECRETING MYOBLAST CELLS CULTURED IN VITRO	33
FIGURE 11. REPRESENTATIVE FS/SS PLOTS OF ENCAPSULATED FVIII SECRETING MYOBLAST CELLS RETRIEVED 6 WEEKS POST-IMPLANTATION IN MICE	33
FIGURE 12. RELATIONSHIP BETWEEN FVIII SECRETION RATE AND VIABILITY OF ENCAPSULATED MYOBLAST CELLS CULTURED IN VITRO AFTER BEING RETRIEVED FROM MICE	34
FIGURE 13. PROLIFERATION OF NON-IMPLANTED ENCAPSULATED (BLACK) AND FREE (WHITE) FVIII SECRETING MYOBLAST CELLS CULTURED IN VITRO	34
FIGURE 14. PROLIFERATION OF IMPLANTED-ENCAPSULATED (BLACK) AND NON-IMPLANTED ENCAPSULATED (WHITE) FVIII SECRETING MYOBLAST CELLS	35
FIGURE 15: COMPARISON OF NK CYTOTOXICITY	37
FIGURE 16: COMPARISON OF VIABILITY	37
FIGURE 17: EFFECT OF MIR2-GFP TRANSDUCTION ON HLA-ABC EXPRESSION OVER 100 DAYS	39
FIGURE 18: TREND SHOWING MIR2-GFP DOSE-RESPONSE EFFECT ON HLA-ABC EXPRESSION.	40
FIGURE 19: CELL SURFACE CHARACTERIZATION OF U937-LACZ AND U937-MIR2-GFP CELLS	41
FIGURE 20: CTL ASSAY	42
FIGURE 21: NK ASSAY	42
FIGURE 22: MIR2-GFP EXPRESSION IN U937 CELLS AFTER MMLV TRANSDUCTION.	44
FIGURE 23: CELL-SURFACE CHARACTERIZATION OF U937-LACZ AND U937-MIR2-GFP CELLS	44
FIGURE 24: CTL ASSAY	45
FIGURE 25: NK ASSAY	45
FIGURE 26: HEMICORPECTOMY PATIENT.	47
FIGURE 27: EVOLUTION OF PRESSURE ULCERS	47
FIGURE 28. IN VIVO QD IMAGING IN LIVE C. ELEGANS EMBRYOS	50
FIGURE 29: PROTOTYPE OF A SMART BIODEGRADABLE POLYMERIC NANOPARTICLE FOR INTRACELLULAR NUCLEOTIDE DELIVERY	54



## LIST OF ABBREVIATIONS

Alginate-poly-L-lysine-alginate (APA), Quantum Dots (QD), near infrared (NIR), immunohistochemistry (IHC), fluorescence *in situ* hybridisation (FISH), single particle tracking (SPT), reticuloendothelial system (RES), photodynamic therapy (PDT), sentinel lymph node (SLN), hematoxylin and eosin (H&E), small-interfering RNA (siRNA), reactive oxygen species (ROS), graphene quantum dots (GQD), mannuronic acid (M), glucuronic acid (G), insulin-dependent diabetes mellitus (IDDM), allogeneic antigen presenting cells (APC), CD8+ Cytotoxic T Lymphocytes (CTL), Major Histocompatibility Complex (MHC), Regulatory T cells (Tregs), adeno-associated viral (AAV), self-complementary AAV vectors (scAAV), carboxyfluorescein diacetate succinimidyl ester (CFSE), damage associated molecular patterns (DAMPs), flow cytometry- based cytotoxicity assay (FCC), forward scatter (FSC), side scatter (SSC), Effector:Target ratio (E:T), Major Histocompatibility Complex Class I (MHC class I), Kaposi's sarcoma-associated herpesvirus (KSHV), modulator of immune recognition (MIR2), mean fluorescence intensity (MFI), green fluorescent protein (GFP), pathogen-associated molecular patterns (PAMPs), transacting activator of transcription (TAT), aggregation-induced emission (AIE).

## ABSTRACT

Nanoparticle and microsphere technologies have enormous diagnostic and therapeutic potential in medicine. We characterised the behaviour of Quantum Dots (QD) in live mammalian cells and discovered that QD surface coating deficiencies can lead to the formation of aggregates, which are recognised as foreign objects by the innate immune defenses of cells and actively transported along microtubules within lysosomes. Applying the principles of viral nucleotide delivery systems, we designed a nature-inspired, smart 'universal' nanoparticle for intracellular oligonucleotide delivery using a combination of natural and synthetic stimuli-responsive polymers. We then developed and tested a nature-inspired polymer alginate-poly-L-lysine-alginate (APA) microcapsule to encapsulate allogeneic cells for Factor VIII delivery in a mouse model of haemophilia A. We also developed a novel flow cytometry-based assay to evaluate the behaviour of encapsulated cells and discovered that both implanted and non-implanted APA microcapsules reduced the viability of cells, induced changes in the cytoplasmic composition and morphology of the cells, and altered the proliferation rate, suggest that the local microenvironment can significantly alter the behaviour of encapsulated cells. We then developed and tested a novel single-colour flow cytometry-based *in vitro* cytotoxicity assay to measure both necrotic and apoptotic cell death. We then developed and tested a novel method to potentially delay or prevent organ rejection upon transplantation using viral nanoparticles to selectively modify allogeneic donor cells *ex vivo* using viral mechanisms of immune evasion. To our knowledge, this was the first study to employ viral immune evasion strategies to simultaneously reduce CD8+ T cell-mediated cytotoxicity without altering Natural Killer cell-mediated cytotoxicity against allogeneic human cells. Finally, we present a rare clinical case of hemicorporectomy due to chronic non-healing pressure ulcers to highlight the potential role for nanoparticles, microspheres and tissue-engineered constructs for wound healing applications via suppression of inflammation and promotion of tissue regeneration.

# BACKGROUND

## NANOPARTICLES FOR DIAGNOSTICS AND BIOPHARMACEUTICAL DELIVERY IN MEDICINE

Over the past two decades, the field of nanotechnology has evolved from a subject of mere academic inquiry to a burgeoning arena in the pharmaceutical industry, giving rise to cutting edge materials that can be implemented in clinical medicine, especially for diagnosis and drug delivery [1,2]. Nanoparticles can be broadly classified into two major types: non-viral and viral. Although non-viral nanoparticles vary significantly in their physical size and shape, chemical composition, electrical charge and optical properties, their applications in clinical medicine have been limited to date due to several challenges, including the innate and adaptive immune response to nanomaterials. Given the sheer diversity of non-viral nanoparticles, this review will focus on small semiconductor nanoparticles called Quantum Dots (QD) to illustrate the salient features and current applications *in vitro*, *in vivo* and in clinical settings. This discussion will serve to highlight some of the major challenges that limit the application of all nanoparticles in clinical medicine.

Quantum dots are small semiconductor nanocrystals (2-15 nm core) with highly customisable optical and chemical properties (Figure 1) [3]. Optically, QD have excellent photostability, high quantum yields, large two-photon cross sections, broad excitation spectra, large effective Stokes shifts and narrow size-dependent emission spectra. Quantum dots also have a long fluorescence lifetime (10-100x longer than organic fluorophores) and exhibit a tendency to blink [4–6]. Blinking is a photophysical effect where the QD alternate between a light state and a dark state at irregular intervals [6]. These qualities provide an unambiguous optical signature that allows single QD to be easily distinguished among other fluorophores using epifluorescence microscopy. Chemically, QD have a three-layered core-shell-hydrophilic structure (Figure 1). The inorganic (typically CdSe-ZnS) core-shell is then protected with a hydrophilic layer, which renders them water-soluble and allows them to be functionalised with biomolecules. This feature provides QD with a highly customisable surface chemistry that permits their use in various *in vitro* and *in vivo* applications. Furthermore, the inorganic composition of QD makes them highly resistant to photobleaching and biodegradation, which permits their use in long-term imaging applications [7]. With the development of functionalised QD, it is possible to circumvent the limitations of organic fluorophores to label biomolecules of interest, study subcellular processes and design experiments with greater flexibility [3,4,8,9].

More recently, QD have increasingly been exploited for their imaging and therapeutic potential *in vivo*. Fluorescent QD emitting in the visible range (400-700nm) have shown promising results for superficial imaging, while near infrared-emitting (NIR) QD (700-850nm) have been successfully applied for whole body imaging of small animals in preclinical studies [10–13]. In 2008, the first *in vivo* human clinical trials were performed for sentinel lymph node (SNL) imaging in oncology using NIR organic dyes, paving the way for other NIR fluorophores to be tested [13–16]. However, the efficacy and potential toxicity of using QD as biological probes has not been well-established. This review will explore the potential applications of QD as biological probes *in vitro* and *in vivo* and assess their suitability for clinical applications, especially for diagnosis and treatment.

### **Quantum dots as biological probes *in vitro*:**

#### ***Quantum dot applications in histological and live cell imaging:***

Histological imaging techniques such as immunohistochemistry (IHC) and fluorescence *in situ* hybridisation (FISH) have traditionally been performed using organic fluorophores to evaluate the phenotype of cells and detect protein biomarkers within cell and tissue specimens with high sensitivity, specificity and spatial resolution. In 1998, Bruchez *et al* and Chan *et al* were the first to demonstrate the potential application of QD for *in vitro* histological imaging of cell and tissue samples [13–18]. Bruchez *et al* successfully labeled F-actin filaments in fixed mouse 3T3 fibroblasts using biotinylated QD interacting with phalloidin-biotin and streptavidin [17]. Alternatively, QD have also been successfully employed in FISH analysis [19]. In 2007, Knoll demonstrated that QD conjugates can be used in human metaphase chromosome FISH to visualise single copy sequence DNA probes as short as 1500 nucleotides in length, which significantly enhances the sensitivity of conventional cytogenetic analysis to detect subtle chromosomal rearrangements and to provide diagnostic and prognostic information for chromosomal disorders [20]. Quantum dots have also been successfully applied for high-resolution immunofluorescence imaging of fixed cells and subcellular structures, such as membrane proteins [21,22], microtubules [21], actin filaments [17], cytoplasmic organelles and nuclear proteins [21,23].

Although QD imaging of fixed cells and tissues can provide useful information about biomolecule expression, distribution and cellular and subcellular structure, it provides little information about function and the dynamic interactions between subcellular biomolecules. Hence, many studies are employing QD in live cell and tissue imaging to label intracellular targets such as cytoskeletal components and nuclear antigens, and to investigate complex subcellular dynamic processes such as cell-surface receptor or lipid transport [24–26]. In 2003, pioneering studies by Dahan *et al* demonstrated the Single Particle Tracking (SPT) of

individual glycine receptors in neuronal membranes of live cells over periods ranging from milliseconds to at least 20 minutes [27]. This was in stark contrast to their SPT of glycine receptors with organic dye Cy3, when tracking was limited to only 5 seconds [27]. In following studies, Howarth *et al* successfully employed streptavidin-conjugated QD and *E. coli* biotin ligase to label and track the motion of cell-surface epidermal growth-factor receptors (tagged to an acceptor peptide sequence) in live HeLa cells with high sensitivity using a versatile approach that can be applied to virtually any cell-surface protein [28]. In 2016, Verela *et al* advanced this technique to label neocortical neuron dopamine receptors with QD in rats *in vivo* and subsequently used SPT in acute rat brain slices *ex vivo* [29]. In other live cell imaging studies, FRET technology has also been applied successfully to increase signal to noise ratio and to unambiguously track the subcellular motion of biomolecules [30–32]. Given the proliferation of modern cancer drugs that alter gene expression and target subcellular processes and structures, numerous studies are employing QD to study endocytosis, nuclear and cytoplasmic transport of biomolecules in order to improve subcellular drug delivery [17,21,33–38].

#### **Quantum dots as biological probes *in vivo*:**

The application of QD *in vivo* presents a special optical challenge. First, the elevated levels of autofluorescence from cells and tissues precludes the use of visible light (400-700nm) for *in vivo* imaging. Second, the absorption and scattering of visible light wavelengths severely restricts the imaging of tissues beyond a few millimeters in depth. However, near infrared (NIR) wavelengths (700-1100nm) are located within a region of the spectrum where the absorption coefficients of tissue ( $\lambda < 600\text{nm}$ ) and water ( $\lambda > 1150\text{nm}$ ) are minimal [39]. This minimises the tissue autofluorescence and increases the signal to noise ratio for imaging purposes. Moreover, these NIR wavelengths have a tissue penetration depth of several centimeters and minimise the photodamage to cytosolic and nuclear material induced by shorter wavelengths [40–42]. Taken together, this presents an opportunity to use NIR wavelengths to take advantage of this 'optical tissue window' for *in vivo* imaging [39]. As opposed to using NIR emitting QD, pioneering studies by Larson *et al* have successfully demonstrated that two-photon excitation of green-emitting QD can also be used to image dynamic processes in mice within capillaries several hundred micrometres deep [41]. Since then, other research groups have further developed multiphoton excitation of QD to image various dynamic processes such as the vascular circulation and subsequent extravasation of tumor-labelled QD into lung tissue *in vivo* [43].

Despite all the optical and chemical advantages of employing QD for human clinical applications, the vast majority of research *in vivo* has been done using animal models due to the concerns of potential QD accumulation and toxicity within cells and tissues [44,45].

However, it is important to highlight the advances being made in this *in vivo* frontier in animal models. Over the last decade, QD have been used for six major applications *in vivo*: 1) biodistribution studies such as pharmacokinetics, histological analysis, renal and reticuloendothelial system (RES) clearance [46], 2) vascular imaging studies such as blood and lymphatic vessel imaging [41], and sentinel lymph node mapping [45,47], 3) QD tracking studies of stem cells [48], metastatic cancer cells [43,49,50], and embryological and malignant cell division, 4) tumor imaging studies such as superficial and deep tissue imaging for image-guided surgery [51,52], 5) therapeutic studies for cancer such as Photodynamic therapy (PDT) [53], and 6) theranostics for cancer, where QD are employed for simultaneous diagnostic imaging (fluorescence combined with MRI, PET, CT contrast agents) and therapeutic interventions, including active targeting and drug delivery in tumors [54–56].

## **Potential clinical applications of Quantum Dots**

### **Tissue diagnostics**

*In vitro* and *ex vivo* tissue diagnostics of patient samples are perhaps the most important clinical applications of currently available QD technologies. It allows for the simultaneous collection of multi-dimensional information from both the tumor microenvironment and from cancer cells to foster a personalised medicine approach to patient care. For example, Chen *et al* quantitatively determined the cell-surface receptor distribution of invasive breast cancer cells recovered from 700 patients, using QD-based spectral analysis techniques [57,58]. When compared with conventional IHC, the QD-conjugate IHC approach was found to be much more sensitive, specific and cost-efficient [57,58]. In a follow up study by the same group of researchers, Li and colleagues enhanced the prognostic potential of QD IHC by adding a new macropathologic indicator, namely tumor size [59]. Through this approach, they were able to identify a new subgroup of HER2-expressing breast cancer patients with a drastically reduced 5-year disease-free survival, who were not identified by traditional HER2 gene amplification methods [59]. The results of such studies will likely be instrumental in early detection and formulating a more personalized targeted therapy for breast cancer.

The multiplexing capabilities of QD have enormous potential for clinical biomarker detection and imaging using IHC techniques [58,60–63]. In 2011, Liu *et al* conducted a QD-based double color imaging of HER2-overexpressing breast cancer invasion by simultaneously labelling cell surface HER2 and type IV collagen in the tumor matrix [64]. Furthermore, the authors demonstrate the inverse correlation between cell surface HER2 expression level and the amount of type IV collagen in the cancer matrix, suggesting a metastatic progression sequence. In another study by Yezhelyev *et al*, QD multiplexing was used for the simultaneous characterization of multiple biomarkers (HER2, ER, PR, EGFR and mTOR) in the MCF-7 breast cancer cell line, as well as formalin-fixed paraffin-embedded clinical specimens of

breast cancer [65]. Importantly, this study demonstrated the ability of QD-conjugates to detect low levels of HER2 cell surface expression that correlate closely with HER2 gene amplification, quantified using traditional techniques including FISH, Western blot analysis and IHC. This study clearly demonstrated the multiplexing potential of QD for the molecular profiling of single tissue specimens in anatomic pathology. Such advances suggest that QD will have significant implications in anatomic pathology and become a powerful diagnostic and prognostic tool in clinical medicine for the quantitative detection of multiple biomarkers simultaneously in small biopsy specimens.

### **Sentinel lymph node mapping**

Ever since the pioneering studies by Kim *et al* in 2003, where they successfully demonstrated the application of NIR type II QD for sentinel lymph node (SLN) mapping in mice and pigs *in vivo*, many other research groups have subsequently explored NIR QD for solid tumor studies [66]. Given the steady rise in the incidence of lymph node-negative breast cancer, there has been increasing interest in axillary lymphatic system mapping to determine cancer metastasis by identifying the SLN, plan for biopsy/surgery and evaluate patient prognosis [67]. The multiplexing potential of QD enables the simultaneous mapping of multiple lymphatic drainage territories in real time. For example, Huma *et al* employed the use of two types of NIR QD with different emission spectra to simultaneously visualize two separate lymphatic flows draining the breast and upper extremity in mice [68]. A subsequent study by the same group of researchers expanded the multiplexing potential of QD to simultaneously image five separate lymphatic basins using five colours of QD in mice [69]. Moreover, a similar SLN mapping study by Robe *et al* did not reported any detectable levels of QD accumulation in RES organs like the liver, spleen and kidney in mice [70]. Such studies suggest that QD can provide a non-invasive alternative for axillary lymphatic system mapping to determine the lymphatic drainage pattern for SLN biopsy and the path of cancer cell migration *in vivo* for periods over 24h [70].

### **Micrometastatic detection**

Efforts to elucidate the path of cancer cells as they emigrate outside the primary tumor site has become increasing important in determining effective therapy and improving patient prognosis [71,72]. This 'micrometastasis' of individual and small aggregates of cancer cells is believed to be the earliest form of metastasis and happens long before clinically recognized macroscopically visible metastasis [71]. However, conventional histological techniques using hematoxylin and eosin (H&E) staining are not sensitive enough to reliably detect micrometastasis during intraoperative frozen section analysis [73]. In 2013, Ojima *et al* implemented a QD-based double labeling technique with IHC and H&E staining to demonstrate that when compared to conventional H&E staining alone, their technique significantly reduced the false-negative rate of micrometastasis detection (single cells and

small aggregates of cancer cells) in intraoperative frozen section specimens collected from the lymph nodes of 100 breast cancer patients [73]. The *in vivo* imaging potential of QD for tracking micrometastasis was established by Gonda *et al*, where they employed anti-protease-activated receptor 1 antibody conjugated QD to identify four distinct stages of cancer cell micrometastasis: cancer cells within the tumor and away from blood vessels, near blood vessels, in the blood stream, and adherent to the inner luminal surface of blood vessels in normal tissues near the primary tumor [74]. Such advances in QD-based imaging *in vivo*, have led to the development of high-resolution 3D imaging [75] and multimodal imaging techniques [76] for diagnosis and image-guided surgery [52][67]. For example, Ma *et al* developed multilayered, targeted core-shell nanoparticles composed of ferric oxide (core), visible-fluorescent QD (inner shell), NIR QD (outer shell) and conjugated to anti-HER2 antibodies (surface) for multimodal imaging of human breast cancer-bearing mice *in vivo* [77]. This study successfully demonstrated the multimodal imaging potential of QD for fluorescence, MRI and NIR imaging in real-time at tissue depths of greater than 1cm. The inclusion of various MRI contrast agents (within nanoparticles) can significantly increase the diagnostic potential of these hybrid nanoparticles by permitting deep tissue imaging using MRI scanners widely available at modern clinical facilities [78]. Therefore, it is expected that this technology will make a significant contribution to noninvasive SLN mapping, biopsy techniques and surgical excision of tumors in clinical medicine.

### **Theranostic Quantum Dots for cancer treatment**

Recently, theranostic QD have also been employed in breast cancer treatment. In 2007, Tan *et al* conjugated QD with small-interfering RNA (siRNA) oligonucleotides targeted towards HER-2, and successfully downregulated the receptor expression in breast cancer cell lines [79]. In 2008, Park *et al* synthesized a multifunctional nanoparticle composed of NIR QD, iron oxide and the anti-cancer drug doxorubicin to perform QD-based fluorescence imaging, MRI and drug delivery in breast cancer-bearing mice *in vivo* [56]. These studies highlight the theranostic potential of QD for simultaneous dual-mode diagnosis and therapy for cells *in vitro* and organs *in vivo* or *ex vivo* by combining the advantages of optical imaging and MRI. Another dynamic area of research that exemplifies the theranostic potential of QD is PDT, where light of a specific wavelength is used to irradiate a photosensitizer drug, triggering the generation of reactive oxygen species (ROS) from intracellular oxygen [80]. The locally produced ROS induce cell death and necrosis in surrounding tissues, making PDT an attractive therapeutic option for non-invasively targeting cancer cells. Photosensitizer drugs are typically highly hydrophobic and have limited solubility, which has prompted a number of attempts to incorporate the photosensitizer into a carrier system, such as polymeric nanoparticles, gold nanoparticles, liposomes, carbon nanotubes and graphenes in order to enhance solubility [81–86]. Other research groups have conjugated nanocarriers with targeting ligands, such as peptides, proteins, monoclonal antibodies, steroids and folic acid in



order to enhance cellular targeting and cellular internalization and reduce damage to healthy tissues [87–91]. Alternatively, Ge *et al* recently developed a novel PDT agent using non-cadmium-based graphene quantum dots (GQD) [92]. The GQD possessed high singlet oxygen quantum yields, a broad absorption band spanning the entire visible region as well as the UV region, and a strong deep-red emission. Promising *in vivo* PDT efficacy of the GQD was demonstrated against subcutaneous breast cancer xenografts in female BALB/nu mice. Tumors treated in the PDT GQD group initially turned dark and festered, increasing in volume slightly, then began to decrease in volume around day 9 and were destroyed 17 days post treatment. Tumor regrowth was not observed in the PDT CQD group over the course of 50 days. Tumors in the control groups however, which included mice receiving GQD injections but no irradiation and mice receiving irradiation but no GQD treatment, continued to grow significantly throughout the study period and exhibited a strong fluorescent signal, indicating that neither GQD injection or light irradiation alone were sufficient to kill tumor cells. Thus, Ge *et al* have demonstrated the theranostic potential of QD PDT agents, which may be used for imaging and treating breast cancer.

#### **Active and passive targeting of solid tumors with nanoparticles**

One major advantage of using nanoparticles for drug delivery is their ability to employ active and passive targeting of solid tumors. As a case in point, approximately 25% of all breast tumors overexpress HER2 [93]. In treating this type of breast tumor, an FDA-approved humanised monoclonal antibody against HER2, called Herceptin (trastuzumab), is usually administered in conjunction with other chemotherapeutic drugs [94]. The availability of Herceptin immediately presents an opportunity to create targeted nanoparticle drug delivery systems, through which many anti-cancer therapeutics can be delivered to the cancer site. This type of antibody-targeted delivery system is referred to as active targeting.

In contrast, passive targeting in breast cancer constitutes the accumulation of macromolecules, between 5-200 nm in diameter, at the tumor site. It is believed that this accumulation occurs primarily for two reasons: first, the tumors are known to have abnormal vasculature, which may be disorganized, unresponsive to vasoactive stimuli and up to 10 times more permeable than normal capillaries. This allows for nanoparticles 5-200nm in diameter to extravasate and accumulate in solid tumors. However, nanoparticles less than ~5nm extravasate at the same rate as the inverse diffusion process, thus do not accumulate in solid tumors. Second, tumors are also known to have poor lymphatic drainage, decreasing the rate of macromolecular clearance from the solid tumor. Together, these factors result in the selective accumulation of nanoparticles (5-200 nm) at the tumor site. Originally documented in 1986 for solid tumors in mice, this enhanced permeability and retention (EPR) effect has been reported for many types of solid tumors in humans as well [95][96,97].

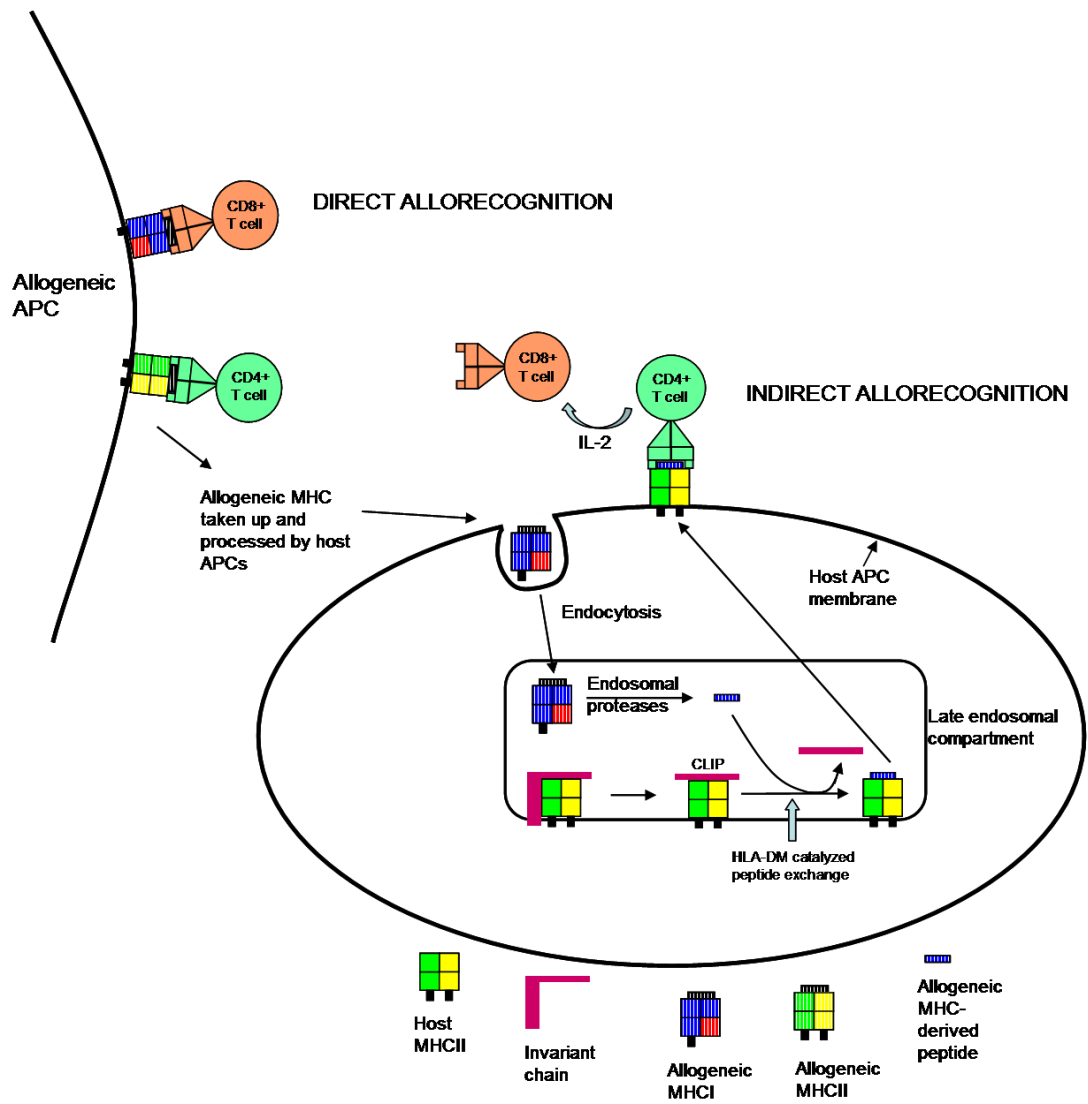
## MICROSPHERES FOR BIOPHARMACEUTICAL DELIVERY IN MEDICINE AND TRANSPLANTATION IMMUNOLOGY

Microspheres are small (usually 100-800um) spherical structures that can be used for drug and cell delivery. Given the diversity in the size, structure, composition and application of these microspheres, this review will focus on hollow alginate-based microspheres, known as microcapsules, for drug and cell delivery. Alginate is among the few biomaterials that has passed most stages of the scientific and regulatory approval for human applications. Alginate is a natural linear polymer derived from algae and is composed of mannuronic (M) and glucuronic (G) acid units in homopolymers of M-M, G-G and G-M [98]. Controlling the amount of each homopolymer in the mixture determines the alginate biomaterial properties including its permeability, which allows it to serve as a selectively-permeable membrane for biological applications such as immuno-isolation.

Immuno-isolation is a relatively simple idea to the tissue rejection problem. It proposes to encapsulate the transplanted cells in a selectively-permeable membrane that allows nutrient and gas exchange, while preventing the humoral and cellular immune system from contacting the foreign cells. The transplanted cells can then provide a means of long-term, continuous sensing, synthesising and delivering cell-derived biological molecules of interest *in vivo* in a localised manner [98]. Moreover, this microencapsulation technology can be configured into a medical device such that it can be scalable and retrievable [99]. In 1964, T.M.S Chang proposed the idea of using ultra-thin polymer membrane microcapsules for immunoprotection of transplanted cells [100]. Since then, there have been many allogeneic and xenogeneic transplantation trials of various kinds of cells, with varying results. For example, pancreatic islet beta-cells are perhaps the most commonly transplanted cell type since they provide a solution to insulin-dependent diabetes mellitus (IDDM) that affects a great proportion of the diabetes population. Such bioencapsulation has provided a range of therapeutic treatments for diabetes, renal failure, haemophilia and cancer. However, a lack of reproducibility and consistency of previous studies has been a major problem, which can generally be attributed to variability in microcapsule manufacturing protocols and the immune response. First, the lack of clinical-grade polymers has hindered the success of the bioencapsulation strategy. Although many natural and synthetic polymers are being explored, most of them have compatibility issues and illicit a deleterious immune response. Second, current methods of encapsulating cells are inconsistent and tend to be non-uniform. Third, the variability in the polymer membrane types necessitates their individual characterisation to determine compatibility with the immune system [100]. Fourth, encapsulated cells undergo a period of ischemia post-implantation, which alters their viability and growth characteristics. Hence, a method to reliably evaluate the viability, proliferation and secretory ability of encapsulated cells can greatly improve our understanding of the factors that influence their survival.

## **Transplantation immunology**

The mammalian immune system is divided into two parts: innate and adaptive. The innate immune system responds immediately to foreign antigen with limited strength. In contrast, the adaptive system has a delayed onset; however, it can be tuned to be much more effective against the foreign antigen. The adaptive immune system can be activated by two separate pathways: direct and indirect (Figure A). The direct pathway depends critically on the migration of allogeneic antigen presenting cells (APC) (e.g., dendritic cells) from within the grafted tissue to host lymphoid tissue, where they directly present peptide to CD4+ T cells and induce their activation [101]. An encapsulating membrane that prevents allogeneic APC migration would effectively prevent graft rejection through this mechanism. The direct pathway is considered the major mechanism of graft rejection. In contrast, the indirect pathway is a relatively minor mechanism of acute graft rejection. In this mechanism, protein fragments normally shed from allogeneic cells are internalised by host APCs and presented to CD4+ T cells to induce their activation [101]. Encapsulating cells in a membrane does not prevent the indirect pathway of activating the immune system since some soluble protein fragments are too small to be retained within currently employed microcapsule membranes. The indirect pathway is considered to play a greater role in chronic graft rejection, which can occur over weeks to months post-transplant. Once the immune system is activated, either through the direct or the indirect pathway, the effector cells of the immune system such as CD8+ Cytotoxic T Lymphocytes (CTL) bind the foreign major histocompatibility complex (MHC) molecules and kill the allogeneic cells. This cytotoxic effect can also be mediated through soluble factors such as reactive aldehydes, oxygen free radicals and granzymes, which are all too small to be excluded by most encapsulating membranes [101]. Overall, it seems inevitable that immuno-isolation alone is not sufficient to prevent graft rejection and can only be a temporary solution to the many challenges encountered in allogeneic transplantation. Thus, many mechanisms of peripheral tolerance induction are currently being investigated, including the inhibition of CD8+ T cell activation, antigen presentation without costimulation, inhibition of CD4+ T cell cytokine production and induction of Regulatory T cells (Tregs). It is important to note that tolerance induction requires time to take effect and immuno-isolation provides a simple solution to attenuate aggressive immune responses while the induction of tolerance is being processed. Hence, it follows that a combination of immuno-isolation and tolerance induction strategies would provide a long-term solution to the graft rejection problem.



**Figure A: Pathways of allograft recognition.** This figure illustrates the direct and indirect pathways of allograft recognition. Self-created figure based on theory presented by Game *et al* [102].

## GENE THERAPY WITH VIRAL NANOCARRIERS

The American Society of Gene and Cell Therapy defines gene therapy as the “introduction of genetic material and/or cells in the body to treat or prevent disease.” Over the years, gene therapy has been successfully applied to several conditions including known protein deficiencies such as haemophilia, in addition to cancer, neurodegenerative disorders, cardiovascular conditions and infectious diseases.

The bioengineered adeno-associated viral (AAV) vector has been exploited for the purposes of gene delivery mainly due to its high transduction efficiency, replication-deficient nature, reduced chance of integration into the host genome, and convenience to produce in the laboratory with high titres. The AAV genome is a 7kb single stranded DNA molecule and requires a helper virus such as adenovirus for replication. This makes AAVs ideal to bioengineer and use in humans as a ‘single-shot’ gene delivery system, since they do not have the ability to replicate themselves in human cells. Despite all these advantages, several initial clinical trials were unsuccessful in long-term gene expression at therapeutic levels in humans. However, there are several other bioengineered variants of AAV, such as self-complementary AAV vectors (scAAV) that are able to increase Factor IX expression by 20 times compared to regular AAV vectors, which are currently being developed to enhance long-term gene expression in clinical trials [103]. If successful, this AAV-based gene therapy strategy may be used to treat many multiple genetic disorders with known protein deficits [104].

Adenoviruses are (80-100nm) non-enveloped icosahedral double stranded DNA (dsDNA) viruses [105]. They can be used as highly effective gene delivery vectors with transduction efficiencies approaching 100%. Furthermore, they can be used to deliver gene fragments up to 30kb in length. However, the major drawback with adenoviral vectors is their transient gene expression, which can last from a few days to about a month. This is a result of their inability to integrate the introduced DNA segment into the chromosomes of the transduced cell.

In contrast, retroviruses are enveloped RNA viruses (80nm-120nm) that can be used to deliver genes up to 10kb in length [105]. Retroviruses have three salient features that make them ideal for gene delivery: First, the retrovirus can integrate into the host cell genome for long-term gene delivery. Although integration into the host genome raises the concern for oncogene activation, many new site-specific insertion techniques have been developed to minimise the chance of insertional mutagenesis. Second, the retroviral genome can be modified to tailor gene delivery for various tissue and cell types despite having a smaller gene delivery capacity.

Third, high gene product levels can be achieved using cell-specific promoters [105]. These three characteristics make retroviral nanoparticles ideal for gene delivery in cell-based tissue engineering constructs and for the allogeneic transplantation of cells, tissue and organs. It is evident that viral nanoparticles can be employed for efficient, targeted gene delivery for the long-term modification of human cells. Strategies to enhance gene transduction efficiency in human cells, understanding and modulating the immune response to viral nanoparticles *in vivo*, and the potential of using genome editing techniques for the treatment of diseases are all subjects of investigation [103].

## AIMS AND OBJECTIVES

The aim of this study is to evaluate the suitability of nanoparticles and microspheres for biopharmaceutical delivery in medicine, with an emphasis on biomaterial interactions with the innate and adaptive immune system. Specifically, we study the behaviour of QD nanoparticles in live mammalian cells, design a smart non-viral nanocarrier for intracellular oligonucleotide delivery, develop and test viral nanoparticles for gene delivery in tissue engineering and allogeneic transplantation, develop and test microspheres for cell encapsulation and biopharmaceutical delivery, and discuss the potential applications of these technologies in the clinical context of chronic non-healing pressure ulcers.

### **Objectives:**

1. Characterize QD behavior in aqueous solution and within live mammalian cells
2. Design a smart non-viral nanocarrier for intracellular oligonucleotide delivery
3. Develop and test microspheres for cell encapsulation and biopharmaceutical delivery
4. Develop a flow cytometry assay to study the behaviour of encapsulated cells and measure cell-mediated cytotoxicity
5. Develop viral nanoparticles for gene delivery and test the transduced human cells against allogeneic immune cells *in vitro*
6. Highlight the suitability of nanoparticle and microsphere technologies in a rare case of hemiporectomy due to chronic non-healing pressure ulcers

## METHODS

Please refer to the published papers in the appendix for details.

## SUMMARY OF PUBLISHED WORK

**PAPER 1:** “CHARACTERIZATION OF QUANTUM DOT BEHAVIOUR IN LIVE MAMMALIAN CELLS” (2005) *CANADIAN UNDERGRADUATE PHYSICS JOURNAL*. 3(3), PP.7-12.

Until recently, studies of live cells were limited to the use of organic fluorescent probes to label molecules of interest. However, organic probes have many undesirable optical, physical and chemical properties that limit their use in live cells. With the development of functionalised QD, it has become possible to circumvent the limitations of organic fluorophores and design experiments with greater flexibility [3,4,8]. However, the application of QD as fluorescent probes in live cells remains a challenge mainly due to manufacturing deficiencies in their outer hydrophilic layer and difficulty in their intracellular delivery.

In this paper, we first characterised the optical behaviour of three types of QD in aqueous solution using fluorescence correlation spectroscopy. We found that although all the QD were made of the CdSe-ZnS core-shell material (Figure 1), their optical and physical characteristics differed significantly in aqueous solution. We observed that the hydrodynamic radius of single QD varied up to 30% (radius 13.9- 19.8nm) and their molecular brightness varied up to 4x based on their hydrophilic coating. Interestingly, in some types of QD, we observed the presence of a larger second component diffusing in solution. We modified our mathematical model of diffusion to include a second diffusing component in solution and determined that these larger diffusing components were approximately 150nm in radius and were aggregates of QD. We then immobilized QD in polyacrylamide gel to further characterise the optical behaviour of single QD and aggregates (Figure 2). Aggregates are collections of QD, held together mainly through electrostatic interactions due to an imperfect hydrophilic layer [106]. We observed that single QD exhibit the unique phenomenon of ‘blinking,’ a on-and-off fluorescence behaviour that allows them to be distinguished from other fluorophores in the system, including aggregates of QD, which do not blink (Figure 3).

We then studied the behaviour of three types of QD in live mammalian cells cultured *in vitro*. Most significantly, we discovered that QD aggregates are recognized by innate immune defenses of cells as foreign bodies and packaged into lysosomes (Figure 4). We also observed the directed and saltatory motion of QD within cells (using colocalization and SPT studies) and measured their average velocity to be 0.18-0.26  $\mu\text{m/s}$ , suggesting that QD are trafficked via motor proteins along microtubules (Figure 5). In contrast to QD aggregates, we

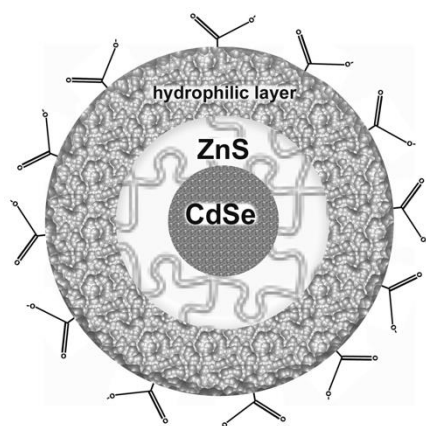


observed that single QD with an uncompromised surface coating are not recognized as foreign objects and therefore can be useful as biological probes.

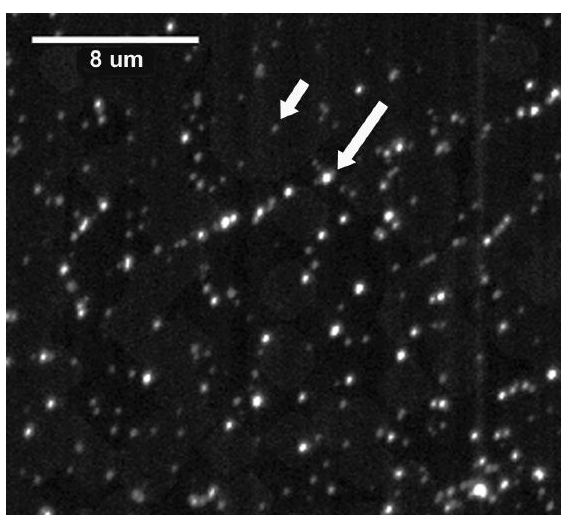
To our knowledge, this was the first study to show how the QD surface coating significantly influences their optical properties (molecular brightness and blinking) and behaviour in solution (deficient coatings promote aggregation in aqueous environments). In our live mammalian cell studies, we were also the first to suggest that QD were not innocuous and that subcellular innate immune defenses are recognizing these QD aggregates as foreign objects and packaging them into lysosomes and trafficking them along microtubules. Furthermore, we learned that a multicomponent diffusion model is required to analyze the diffusive behaviour model of QDs due to the presence of aggregates. In the complex intracellular environment of living cells, equations like the Stokes-Einstein relationship and equations modeling Brownian motion in solution are harder to apply given the multitude of possible interactions with intracellular proteins.

Our published results highlight the importance of preventing QD aggregation by using a proper hydrophilic surface coating. In addition, our research also serves to emphasise the limitations of currently available commercial QD nanoparticles and the potential consequences of their use in studying biological processes.

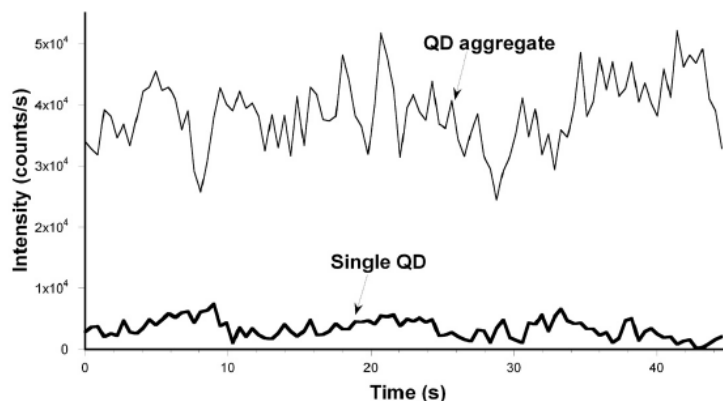
Perhaps the most complete study to date of QD behaviour at the subcellular and systemic level involved the QD targeting of HER2-overexpressing breast cancer conducted by Tada *et al* in 2007 [107]. The authors quantitatively tracked single NIR-emitting QD-anti-HER2 antibody conjugates injected into HER2-overexpressing tumor-bearing mice in real-time, using high-speed confocal microscopy. Importantly, the authors were able to identify six stages of QD delivery: 1) initial circulation within blood vessels, 2) extravasation from blood vessels, 3) diffusion in the extracellular region, 4) binding to cell surface HER2, 5) transport from the cell surface to the perinuclear region, and 6) accumulation in the perinuclear region. This seminal study provides a unique perspective of all the stages of delivery, as well as the challenges that an anti-cancer theranostic QD-conjugate injected *in vivo* will have to overcome for it to successfully reach its target site (cell cytoplasm) and have the intended effect. Interestingly, this study also revealed that movement of the QD-conjugate within cells was “stop-and-go,” a type of saltatory motion highly suggestive of retrograde active transport along microtubules using molecular motors. This study not only confirms our experimental observations that QD are actively transported within cells along microtubules (Figure 5), but also provides new insight into nanoparticle behavior in complex biological environments such as intravascular, extracellular and intracellular compartments.



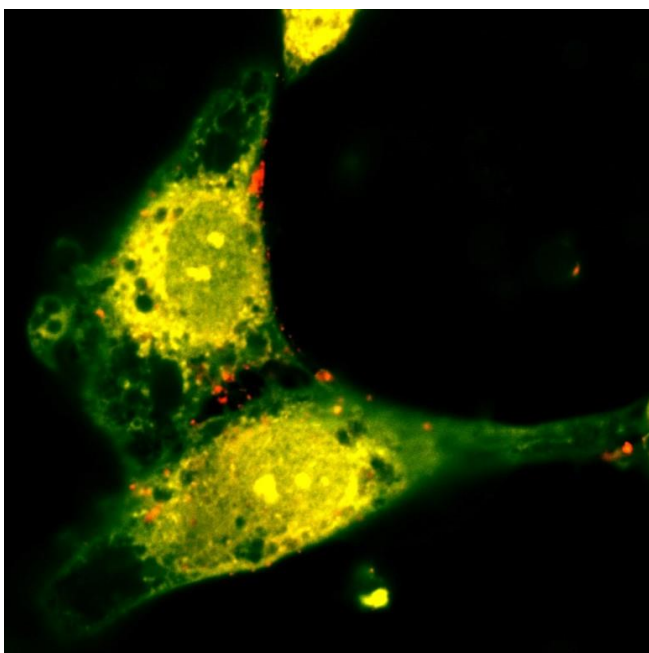
**Figure 1: Schematic of a quantum dot.** A typical CdSe-ZnS core-shell QD with a hydrophilic layer that terminates in carboxylic acid functional groups for covalent coupling to other molecules of interest. This figure was reproduced from the publication being presented in this section.



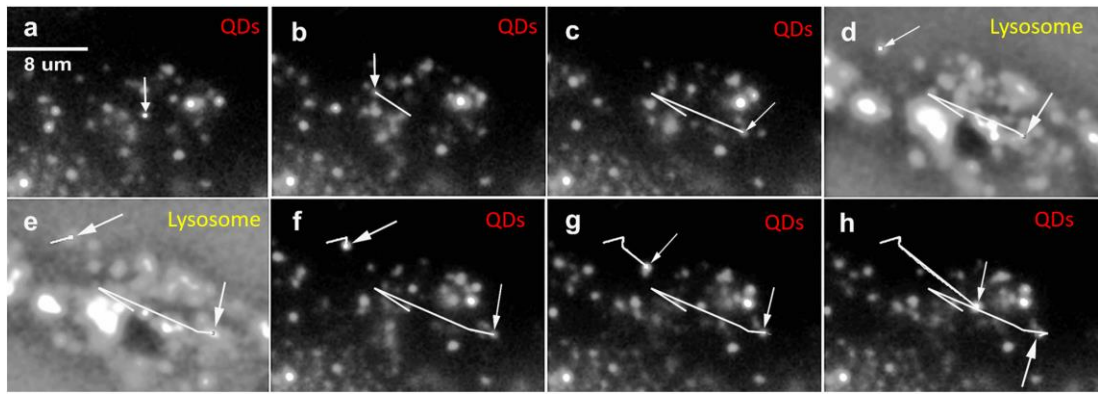
**Figure 2: Immobilised single QD and QD aggregates.** Fluorescence microscopy image of unfiltered QD embedded in a 5% polyacrylamide gel. The long arrow points to an aggregate and the short arrow points to a single QD. Self-acquired image reproduced from the publication being presented in this section.



**Figure 3: Blinking of single QD compared to aggregates.** Fluorescence intensity as a function of time for a particle identified as a single QD (thick black line) and a particle identified as an aggregate (thin grey line). These QD were embedded in 5 % polyacrylamide gel and imaged using time-lapse video microscopy with a time resolution of 100 milliseconds. A background intensity has been subtracted. This figure was reproduced from the publication being presented in this section.



**Figure 4: Confocal microscopy of CdSe-ZnS QD in Rat fibroblasts.** QD (orange) were introduced into the cytoplasm of live Rat fibroblasts (yellow) using pinocytotic loading and confocal imaging shows single QD and aggregates within the cytoplasm and on the cell surface. Rat fibroblasts appeared unperturbed by the presence of QD within the cytoplasm and the QD were extremely photostable over the imaging period of 8h. Self-acquired image captured using a Nikon Eclipse upright confocal microscope.

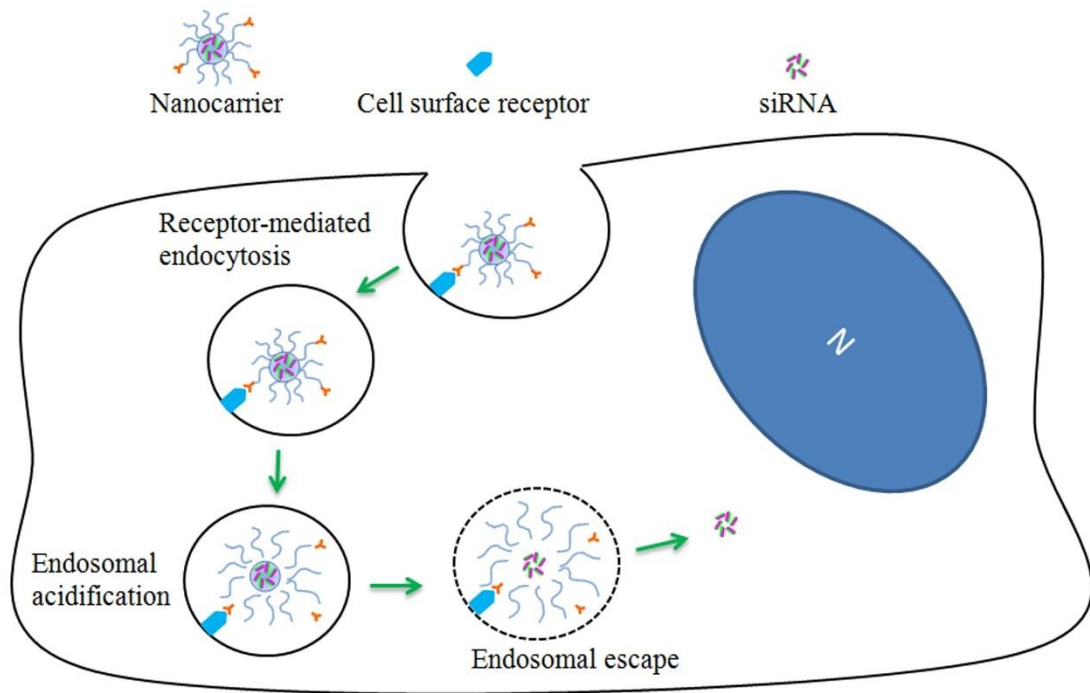


**Figure 5. Directed QD trafficking along microtubules in live Rat fibroblasts.** Chronological image sequence of a region of the cytoplasm in a live Rat fibroblast showing the saltatory directed trafficking of commercial CdSe-ZnS QD (images a, b, c, f, g, h) along microtubules within lysosomes (images d, e) stained with LysoTracker dye. Self-acquired image reproduced from the publication being presented in this section.

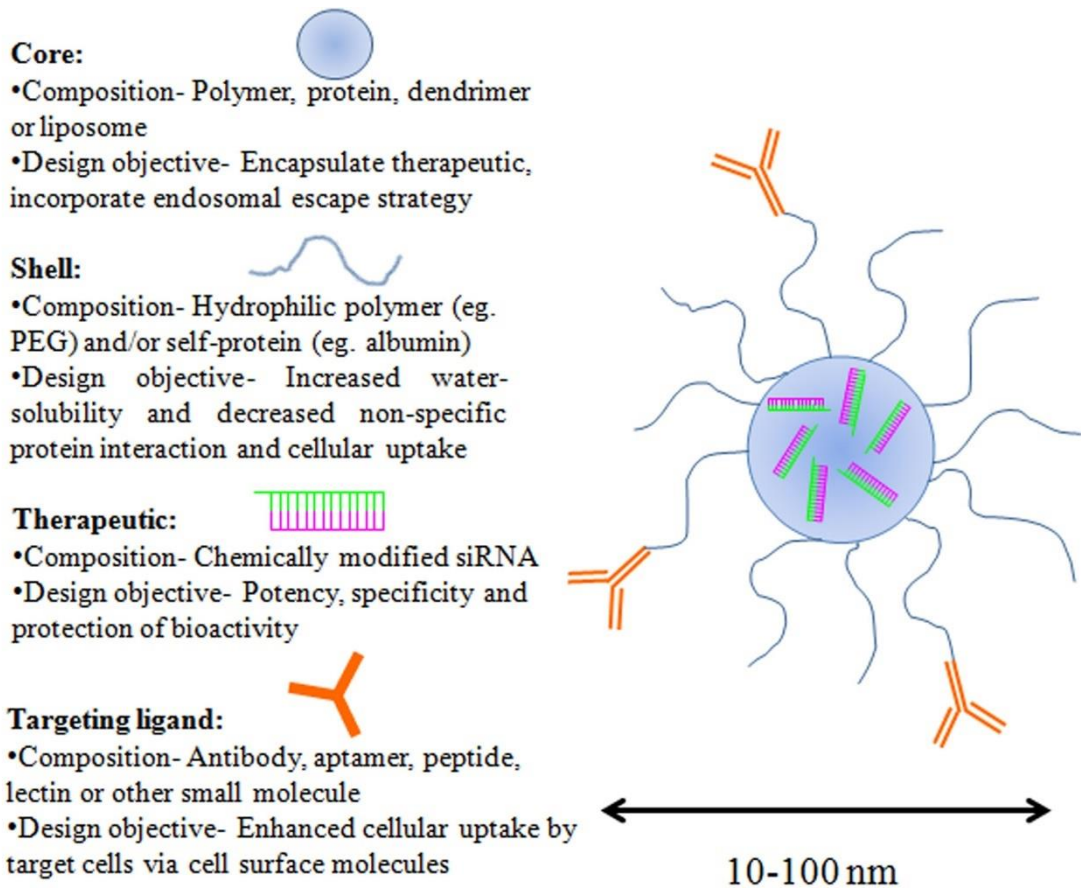
**PAPER 2: “STRATEGIES FOR OCULAR siRNA DELIVERY: POTENTIAL AND LIMITATIONS OF NON-VIRAL NANOCARRIERS” (2012) *JOURNAL OF BIOLOGICAL ENGINEERING*. 6(1) PP. 7.**

Ribonucleic acid interference (RNAi) can provide a novel therapeutic modality to treat many human diseases by interfering with disease-causing and disease-promoting genes in a sequence-specific manner. Theoretically, RNAi can be used to selectively alter the expression of any transcribed gene. This new paradigm in therapeutics allows one to address disease states previously considered ‘undruggable.’ However, most nanoparticle drug delivery systems have numerous limitations, including a short blood half-life, poor specificity and uptake in target tissues, and undesirable off-target effects, which significantly hamper the successful application of siRNA therapeutics in medicine. Intracellular siRNA delivery poses the additional challenge of siRNA recognition by the innate immune system and their inability to passively diffuse across cell membranes (Figure 6).

In this review paper, we evaluate other types of non-viral nanoparticles for oligonucleotide delivery, specifically siRNA delivery for ophthalmic applications. We study the eye as a special case since it is a relatively immune privileged and accessible site, which allows the direct application of drugs, thereby bypassing the systemic circulation and avoiding many innate and adaptive immune defenses. We review common non-viral siRNA delivery systems: polymer, liposome, protein and dendrimer. Although various types of oligonucleotide delivery systems are currently being developed for specific applications, a general strategy for intracellular oligonucleotide delivery has not been proposed to our knowledge. Our major contribution to the field in this article was to outline the general design features of a ‘universal’ smart nanoparticle for intracellular oligonucleotide delivery, based on our previous work with nanoparticles as well as ideas presented in reviewed literature. We note that many human viruses sequentially deploy strategies to overcome common barriers at the systemic, organ, tissue, cellular and subcellular level to deliver their genetic material within cells. We apply the principles of viral nucleotide delivery systems for the design of a nature-inspired, smart ‘universal’ nanoparticle for intracellular oligonucleotide delivery (Figure 6,7). Initial results from prototypes of this type of smart nanoparticle are shown in Figure 29 (Future Work section), where we successfully demonstrate that degradable polymer nanoparticles with a core-shell structure can be used in mammalian cells. Our proposed four component core-shell system incorporates stimuli-responsive biodegradable materials, stealth from the immune system, targeting ligands for tissue and cell-specific targeted therapeutic delivery, endosomal escape strategies for intracytoplasmic delivery, and controlled release and protection of the therapeutic agent from biodegradation. We believe that a nature-inspired design to sequentially deploy strategies to overcome each barrier for intracellular oligonucleotide delivery would significantly improve the biodistribution and bioavailability, reduce toxicity and enhance therapeutic outcome.



**Figure 6: Nanocarrier uptake and intracellular siRNA delivery.** This illustration shows that uptake of antibody targeted nanocarriers (10-100 nm) occurs via receptor-mediated endocytosis. The key step in cytoplasmic siRNA delivery involves low pH-triggered nanocarrier disassembly and endosomal escape. A smart nanocarrier can induce endosomal escape by lysing or fusing with endolysosomes upon acidification. The pH change can also be used to trigger the dissociation of the nanocarrier, therefore releasing the siRNA cargo into the cytosol. Self-created figure reproduced from the publication being presented in this section.



**Figure 7: Schematic of four-component ‘universal’ nanocarrier for siRNA delivery.** This illustration highlights the salient features of a four-component, targeted core-shell nanocarrier for siRNA delivery. Self-created figure reproduced from the publication being presented in this section.

**PAPER 3: “TEMPERATURE-SENSITIVE POLYMERS FOR DRUG DELIVERY” (2012) *EXPERT REVIEW OF MEDICAL DEVICES*. 9(4) PP. 339-351.**

In this paper, we present a targeted review on stimuli-responsive polymers, focusing on thermoresponsive polymers for drug and cell delivery. First, we review the main types of natural (elastin-like polypeptides, chitosan, cellulose derivatives, xyloglucan) and synthetic (polyphosphazenes, poly(N-isopropylacrylamide) and poly(ethylene oxide)-based copolymers) polymers. We report that natural biomaterials have the benefit of improved biocompatibility, non-toxic biodegradability and have defined cellular and biological interactions. However, given the limited number of natural polymers and challenges in their chemical modification, they have a restricted range of biomaterial properties. Moreover, natural materials have greater batch-to-batch variability, limited mechanical strength and the possibility of biological impurities that can have been known to trigger an immune response [98]. In addition, sterilisation of natural biomaterials for clinical applications is more challenging using conventional sterilisation techniques. In contrast, synthetic biomaterials have the benefit of greater compositional diversity and synthetic flexibility that offers more control over biomaterial properties such as molecular weight, mechanical strength, elasticity, scaffold shape and size, drug release profile, stimulus-response, biodegradation and immune activation. Moreover, synthetic biomaterials can be more easily sterilised with conventional techniques for clinical applications. These features make synthetic biomaterials more customisable, so that they can be engineered to suit the intended application.

Second, we review polymer architecture (hydrogels, micelles, polymerosomes, interpenetrating networks, films and bulk gels) and the common internal (pH, temperature changes, ionic charge, antigen-antibody interactions, enzymes) or external stimuli (light, electricity, magnetism, ultrasound) that can be used to illicit desired changes in biomaterial properties. A case in point, Poly(N-isopropylacrylamide) copolymers have been shown to form thermoresponsive hydrogels that can be used as scaffolds for drug and cell delivery as minimally invasive therapeutics [108]. Interestingly, this material is in a fluid state and therefore injectable below its lower critical solution temperature of 33°C, but undergoes a reversible phase transition upon heating above that temperature. Hence, this material provides a means to deliver biopharmaceuticals including live cells and drugs *in vivo*, where the fluid polymer would transition to a hydrogel and provide a scaffold for cell growth and controlled release of the encapsulated drug. This *in situ* phase transition is particularly useful in hard-to-access applications such as the spinal cord and posterior ocular compartment, which require minimally invasive techniques.



As a contribution to the field, this paper provided a comprehensive review of the state-of-the-art on thermoresponsive polymers and provided insight into the biomaterial characteristics for the design of novel stimuli-responsive and biocompatible drug delivery devices. Finally, we conclude that a combination approach, with natural and synthetic stimuli-responsive polymers engineered to respond to internal physiologic feedback from disease-specific stimuli and external signals will provide the optimal solution to designing novel drug and cell delivery scaffolds for clinical applications.

**PAPER 4: “CHARACTERIZATION OF VIABILITY AND PROLIFERATION OF ALGINATE-POLY-L-LYSINE-ALGINATE ENCAPSULATED MYOBLASTS USING FLOW CYTOMETRY” (2010) *JOURNAL OF BIOMEDICAL MATERIALS RESEARCH: PART B*. 94B(2) PP. 296-304.**

One solution to the organ rejection problem has been to create protective barriers (natural or synthetic) between the transplant recipient’s immune system and the allogeneic cells. These immunoprotective barriers are designed to be impermeable to cells and large molecules such as antibodies, but permit the exchange of small molecules such as oxygen and nutrients. Previous studies with such barriers, however, have had limited reproducibility with varied success rates [109]. One of the major challenges with immunoprotective membranes is their immunocompatibility, which can play a significant role in determining the success of the transplanted cells. Many previous studies suggest that the cell-biomaterial interaction after encapsulation likely influences their behaviour. However, no prior studies examine the behaviour of transplant cells once they have been encapsulated and implanted *in vivo*. Immuno-isolation of allogeneic and xenogeneic cells within a microcapsule likely triggers an immune response via the escape of membrane permeable antigens and damage associated molecular patterns (DAMPs) from encapsulated cells, via the composition of the microsphere including immunogenic impurities, and also via the surface characteristics of the microsphere [98,110].

In this paper, we develop and test nature-inspired hybrid polymer alginate-poly-L-lysine-alginate (APA) microspheres to encapsulate live allogeneic cells for the delivery of coagulation Factor VIII in a mouse model of haemophilia A (Figure 8). In order to assess the behaviour of APA encapsulated cells, we developed a novel flow cytometry assay to evaluate their viability, granularity and proliferation. Viability is a very important parameter to determine accurately and precisely in cell encapsulation studies, as it correlates with the secretion of the therapeutic product of interest. First, we validated our novel flow cytometry assay by comparing the viability of encapsulated cells *in vitro* against the traditional trypan blue exclusion method and found them to be comparable, both correlating to FVIII secretion levels (Figure 9).

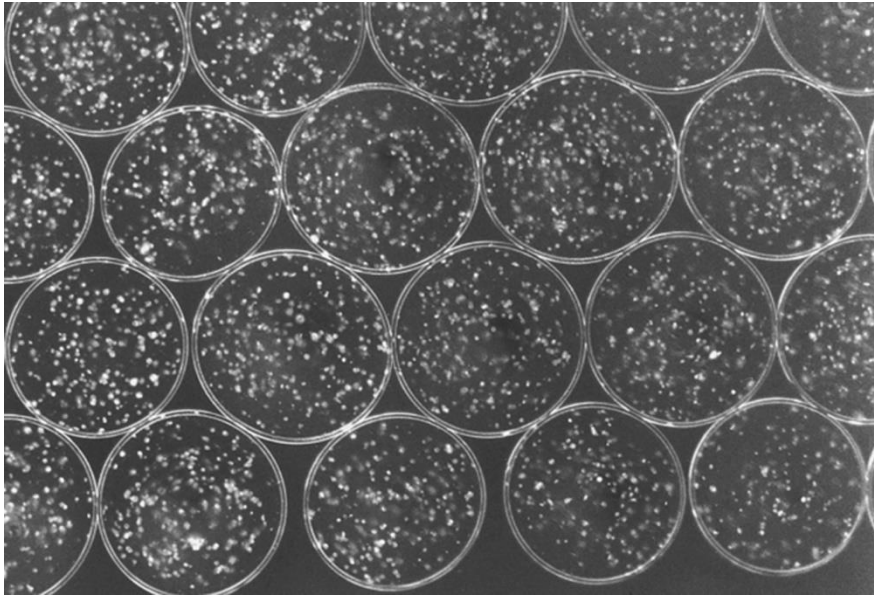
Our novel flow cytometry assay also allowed us to evaluate the behaviour of encapsulated cells in terms of their morphology and proliferation, which can both potentially alter secretion of therapeutic product. To our knowledge, neither of these parameters have been previously assessed in any type of encapsulated cell preparation. We found that encapsulated cells within APA microspheres were morphologically more granular both *in vitro* and *in vivo*, when compared to non-encapsulated cells (Figure 10-11). We also found that encapsulation itself decreases the viability and increases the granularity of cells over the seven-day period observed (Figure 10). Moreover, implanted (for 6 weeks) encapsulated cells were significantly

smaller in size, with a lower viability than non-implanted encapsulated cells (Figure 11). However, when implanted encapsulated cells (retrieved after 6 weeks) were cultured *in vitro* (encapsulated), their average cell size, viability and granularity increased, which correlated with FVIII secretion levels (Figure 11-12).

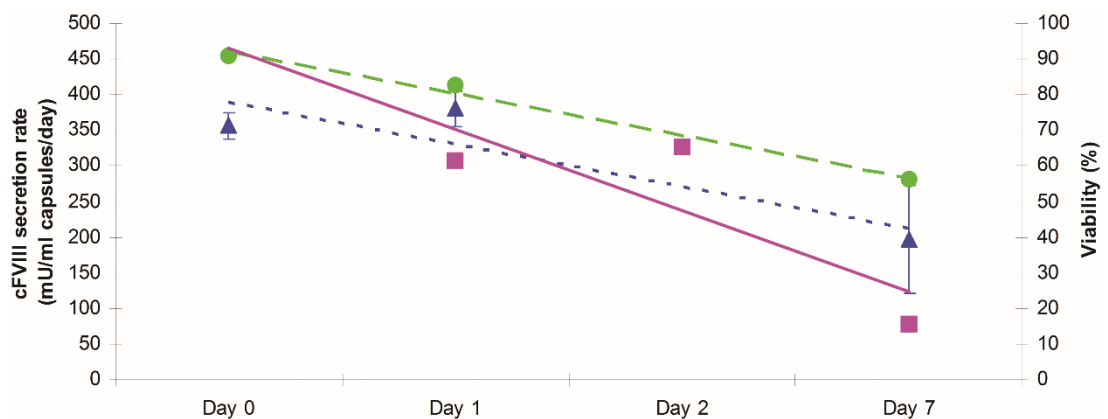
In our cell proliferation studies, we found that non-implanted encapsulated cells proliferate slower compared to free cells (Figure 13). In order to study *in vivo* proliferation rates, cells were labelled with a fluorescent dye, carboxyfluorescein diacetate succinimidyl ester (CFSE), encapsulated and implanted, and then retrieved after 7 days. Interestingly, implanted-encapsulated cells proliferated faster *in vivo* (over 7 days) and were more heterogenous than non-implanted encapsulated cells, suggesting that encapsulated cell proliferation is influenced by the local microenvironment (Figure 14).

Together, these data provide new insight into the behaviour of encapsulated cells, suggesting that encapsulating cells within the APA biomaterial itself reduced the viability of cells, induced changes in the cytoplasmic composition and morphology of the cells, and decreased the proliferation rate of encapsulated cells. Furthermore, the enhanced proliferation rate and heterogeneity of implanted encapsulated cells suggest that the local *in vivo* microenvironment can significantly alter the behaviour of encapsulated cells.

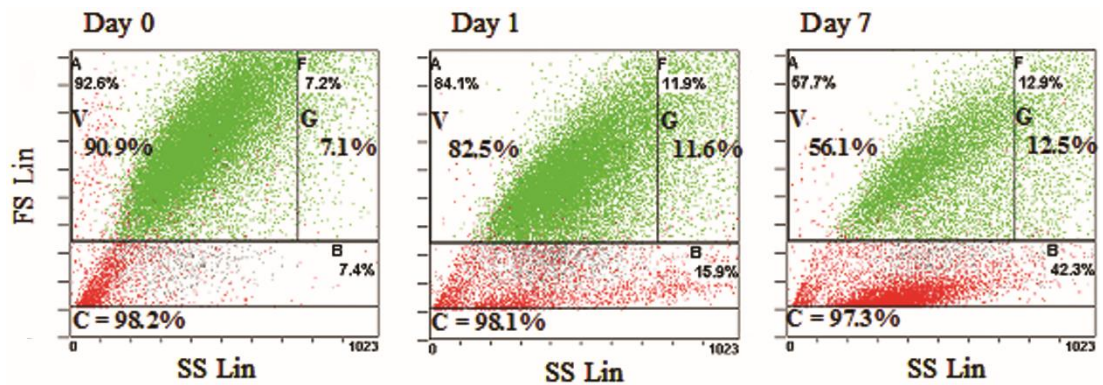
To our knowledge, this was the first published study to characterise and compare encapsulated cells *in vitro* and *in vivo* using flow cytometry. We also demonstrate the use of de-encapsulation protocols in conjunction with flow cytometry to more consistently and comprehensively study the behavior encapsulated cells that have been retrieved from the complex multicellular *in vivo* environment. Our flow cytometry assay has four significant advantages: 1) can analyse thousands of cells per minute to allow a fast assessment of a representative sample population, 2) multiple parameters of cell health can be analysed, 3) discriminate between host immune cells and the encapsulating cells in a mixed population, 4) and provide objective and quantifiable data. We expect this knowledge to help in the development of cell and gene therapy protocols.



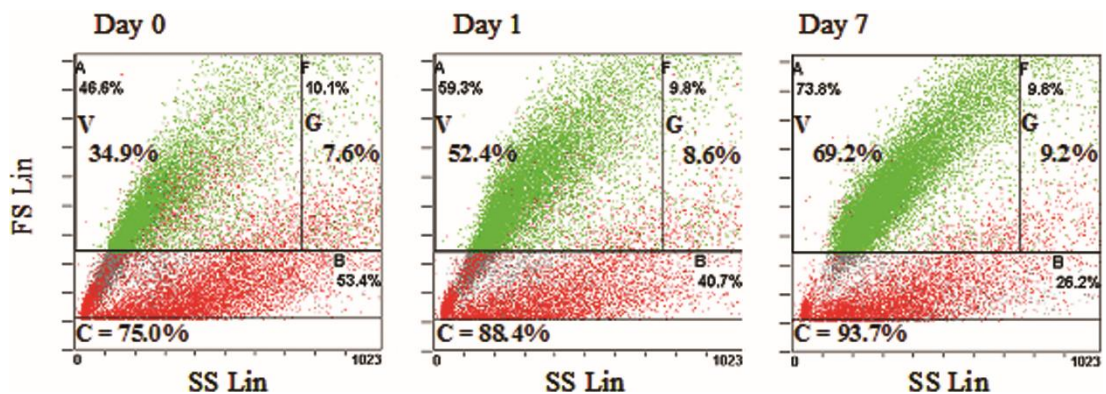
**Figure 8. Murine myoblasts encapsulated within APA microcapsules** (approximately 300-400  $\mu\text{m}$  in diameter). This image was reproduced from the publication being presented in this section.



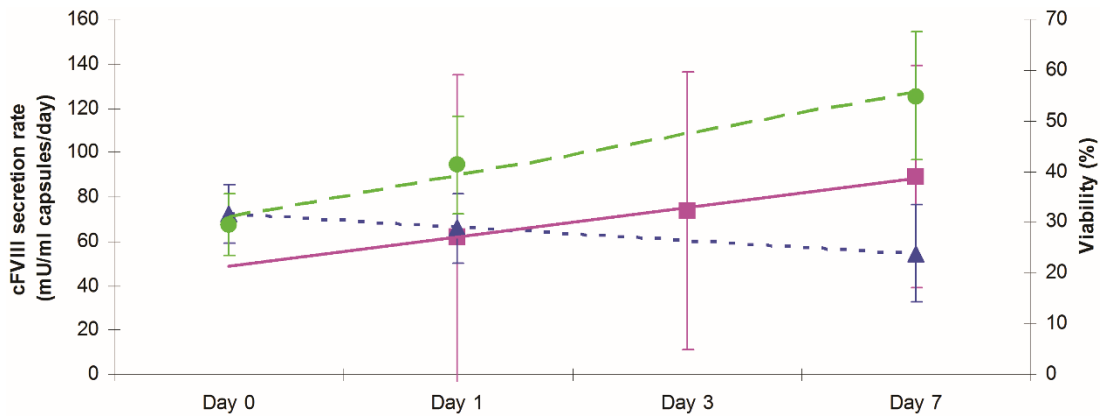
**Figure 9. Relationship between FVIII secretion rate of non-implanted encapsulated FVIII secreting myoblast cells and viability.** Secretion rate ( $\blacksquare$ ), trypan blue-based viability ( $\blacktriangle$ ) and flow-based viability ( $\bullet$ ) all significantly ( $p < 0.05$ ) decreased from day 0 to day 7. Trypan blue-based viability and flow cytometry-based viability were not significantly ( $p < 0.05$ ) different. Solid and dashed lines represent the linear regression fit of data presented. (Error bars indicate standard deviation;  $n=3$ ). This figure was reproduced from the publication being presented in this section.



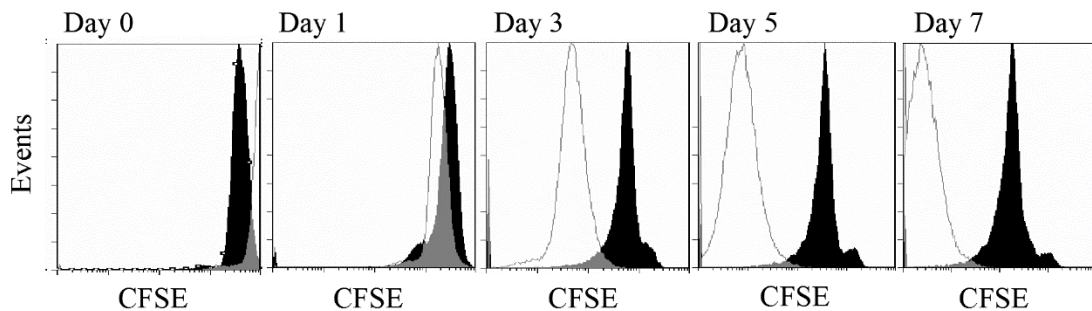
**Figure 10. Representative FS/SS plots of non-implanted encapsulated FVIII secreting myoblast cells cultured *in vitro*.** Samples of myoblast cells were de-encapsulated on day 0, 1 and 7, and their viability assessed by flow cytometry. Viability significantly ( $p < 0.05$ ) decreases over the week, as indicated by the increased movement of live cells (green) from box A into box B. Granularity also increases ( $p < 0.05$ ) over the week, as indicated by the movement of cells into box F. (Data presented from ~30,000 events collected). This figure was reproduced from the publication being presented in this section.



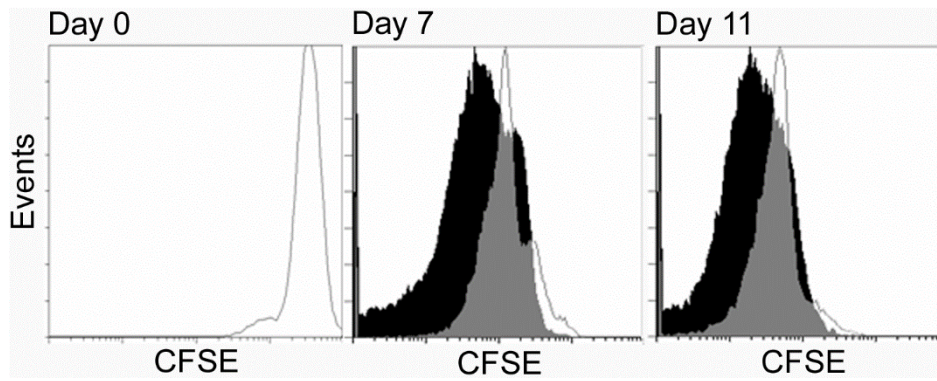
**Figure 11. Representative FS/SS plots of encapsulated FVIII secreting myoblast cells retrieved 6 weeks post-implantation in mice.** The recovered FVIII secreting myoblast cells were subsequently cultured *in vitro*, and samples de-encapsulated on day 0, 1 and 7 to assess their viability using flow cytometry. Viability significantly increases over the week, as indicated by the movement of cells into box B. Granularity slightly increases over the week, as indicated by the movement of cells into box F. (Data presented from >25,000 events collected). This figure was reproduced from the publication being presented in this section.



**Figure 12. Relationship between FVIII secretion rate and viability of encapsulated myoblast cells cultured *in vitro* after being retrieved from mice.** Secretion rate (■) did not significantly increase from day 0 to day 7. Flow-based viability (●) significantly ( $p < 0.05$ ) increased from day 0 to day 7. Trypan blue-based viability (▲) did not significantly decrease from day 0 to day 7. Trypan blue-based viability and flow-based viability were significantly ( $p < 0.05$ ) different. Solid and dashed lines represent the linear regression fit of data presented. (Error bars indicate standard deviation;  $n = 3$ ). This figure was reproduced from the publication being presented in this section.



**Figure 13. Proliferation of non-implanted encapsulated (black) and free (white) FVIII secreting myoblast cells cultured *in vitro*.** Encapsulated fluorescently-labelled FVIII secreting myoblast cells proliferated slower (on average) than free cells. This figure was reproduced from the publication being presented in this section.



**Figure 14. Proliferation of implanted-encapsulated (black) and non-implanted encapsulated (white) FVIII secreting myoblast cells.** Implanted capsules were retrieved after 7 days and cultured *in vitro* until day 11. Implanted-encapsulated fluorescently-labelled FVIII secreting myoblast cells proliferate slightly faster (on average) than non-implanted encapsulated cells. Representative data presented from one implantation. This figure was reproduced from the publication being presented in this section.

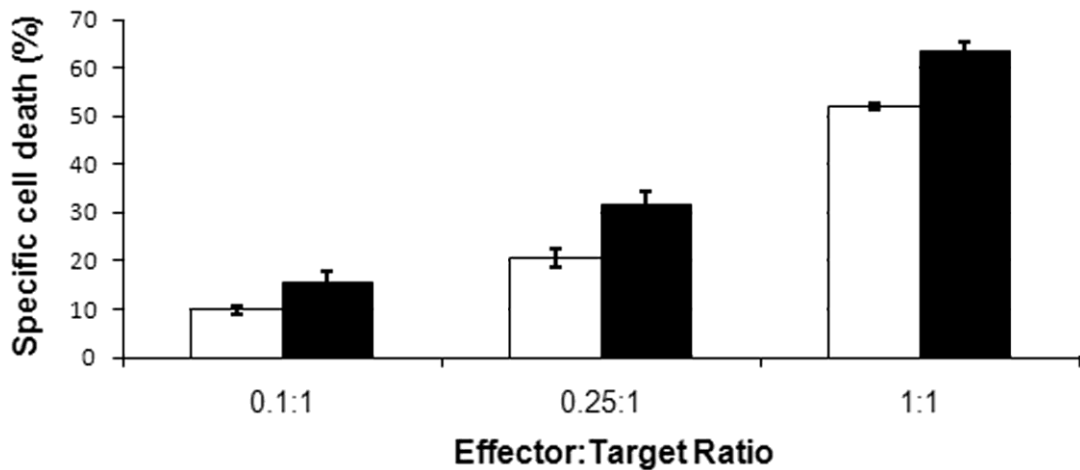


**PAPER 5: “SINGLE-COLOUR FLOW CYTOMETRIC ASSAY TO DETERMINE NK CELL-MEDIATED CYTOTOXICITY AND VIABILITY AGAINST NON-ADHERENT HUMAN TUMOR CELLS” (2012) *BIOTECHNOLOGY LETTERS*. 34(3) PP. 447-53.**

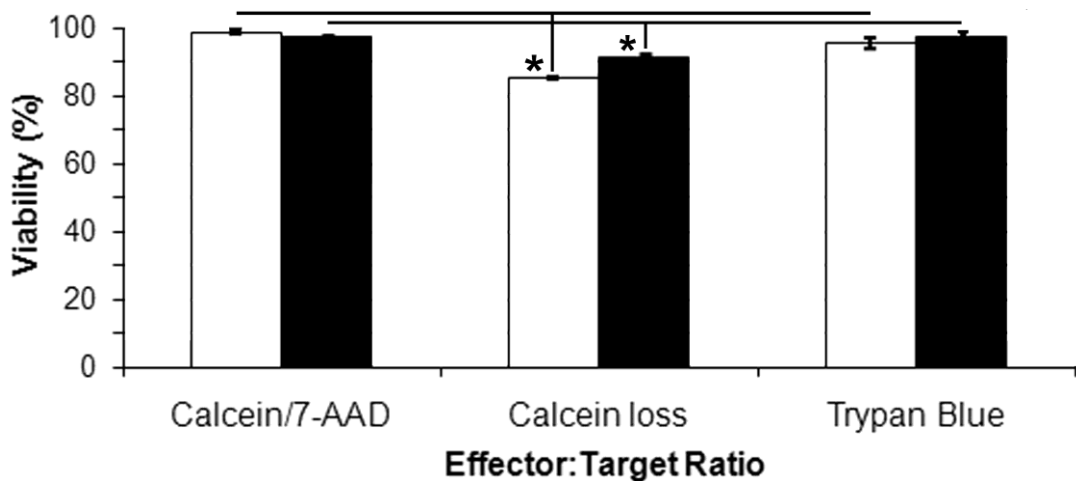
Cell-mediated cytotoxicity assays are essential tools in immunology to quantify effector cell-mediated cytotoxicity against target cells. The chromium release assay is considered the standard technique for measuring cell-mediated cytotoxicity. However, it requires the use of radio-isotopes and lacks speed and sensitivity. In this paper, we developed and tested a novel flow cytometric assay to measure percent specific target cell death in a cytotoxicity assay (FCC) using a single fluorophore, namely Calcein-AM. In our cytotoxicity assay, Calcein-labelled target cells that have been killed by the effector cells will either have a compromised cell membrane or be completely lysed. Target cells with a compromised cell membrane (presumably by apoptotic mechanisms) will leak membrane-impermeable Calcein, which diffuses out of the target cell reducing the overall target cell brightness. Flow cytometry can simultaneously analyse cell size (forward scatter, FSC), granularity (side scatter, SSC) and Calcein staining intensity, thereby providing a measure of the target cells compromised by effector cells in our cytotoxicity assay. In order to quantify the number of completely lysed target cells (by perforin and granzyme mediated necrosis), we employed fluorescent polymeric microspheres to measure the reduction in absolute target cell count. We then created an equation that uses flow cytometry data to compare viability in the control sample and the test sample (accounting for both types of target cell death- apoptosis and necrosis/lysis), to provide a measure of the specific cell death in our cytotoxicity assay. We validated this assay using two different human cell lines, K562 and U937 (Figure 15). We also used this method to measure the viability of cells, which was comparable to Trypan blue and Calcein/7-AAD double labelling methods, although it underestimated it by 5-10% due to the stringent live gate used in our analysis (Figure 16).

To our knowledge, this is the first single-colour flow cytometry assay to determine cell-mediated cytotoxicity that measures both necrotic and apoptotic cell death. This provides several advantages over more expensive dual-labelling techniques and the traditional chromium release assay. Moreover, flow cytometry provides a more comprehensive and precise analysis of viability and health of cells. This FCC assay can be extended to other fluorophores and any effector and target cell type to measure cytotoxicity and viability. We expect this technique to be employed in the field of transplantation immunology and tissue engineering.





**Figure 15: Comparison of NK cytotoxicity.** Determined using Calcein-loss technique in K562 (white bars) and U937 (black bars) cell lines at three different Effector:Target (E:T) ratios. Specific cell death values increased with the E:T ratios in both cell lines. Specific cell death values were also significantly ( $p < 0.05$ ) different between all E:T ratios in both cell lines. Error bars indicate standard deviation;  $n = 3$ . Flow cytometry data presented from ~30,000 events collected per sample. This figure was reproduced from the publication being presented in this section.



**Figure 16: Comparison of viability.** Determined using Calcein/7-AAD, Calcein-loss and Trypan blue techniques in K562 (white bars) and U937 (black bars) cell lines. Viability determined using Calcein-loss is significantly ( $p < 0.05$ ) different in U937 (\*) and K562 (\*) cell lines. Viabilities determined using Calcein/7-AAD and Trypan Blue are not significantly ( $p > 0.05$ ) different in both cell lines. Error bars indicate standard deviation;  $n = 3$ . Flow cytometry data presented from ~30,000 events collected per sample. This figure was reproduced from the publication being presented in this section.

**PAPER 6: “RETROVIRAL EXPRESSION OF MIR2 DECREASES BOTH SURFACE MHC CLASS I AND THE ALLOIMMUNE CTL RESPONSE”**  
(2011) *JOURNAL OF TISSUE ENGINEERING AND REGENERATIVE MEDICINE*. 5(7) PP. 520-528.

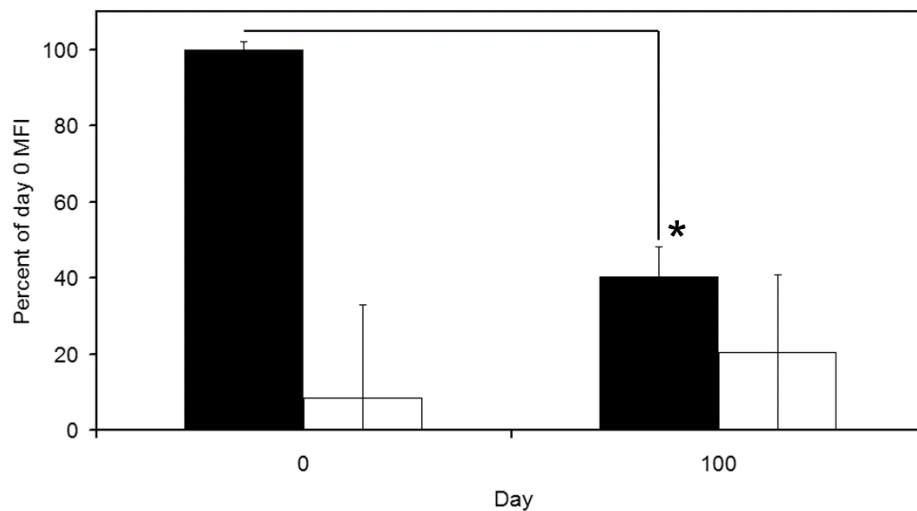
In clinical practice, organ transplantation is a solution of last resort to many incurable diseases including chronic renal failure, heart disease and end-stage liver disease. However, transplanting organs such as the kidney, heart and liver require the recipients of these organs to possess a permanently suppressed immune response against the foreign organs – often maintained with an aggressive regime of anti-rejection, immunosuppressant drugs. In addition, the limited intrinsic supply, and the extensive list of requirements for matching the tissue compatibility of the donor to the recipient further reduces the number of organs available for transplantation. Together, these factors present a substantial challenge for organ transplantation as a solution for many human diseases. Fortunately, the field of tissue engineering offers many potential solutions to these medical challenges. In tissue engineering, biomaterials provide the physical structure, and allogeneic stem cells and stem cell-derived cells are typically incorporated to provide the biological function. Since the cells will be sourced in advance, this provides the opportunity to use genetic engineering to evade or manipulate and suppress the immune response of the host using viral nanoparticles for gene delivery.

In this paper, we propose a novel method to potentially delay or even prevent organ rejection upon transplantation using viral nanoparticles as gene delivery vehicles. Viruses were the inspiration to our work. It is known that viruses have evolved complex mechanisms to evade and suppress detection by the immune responses of the host. Tissue engineering a human organ that also utilises these mechanisms might potentially elicit a similar response, where a fully functional donor organ would not be recognised by the host immune system as ‘foreign,’ thus preventing organ rejection. The immunogenicity of allogeneic cells is primarily due to the Major Histocompatibility Complex Class I (MHC class I) molecules expressed on these cells and is the key factor in acute cellular rejection mediated via alloreactive T cells of the adaptive immune system.

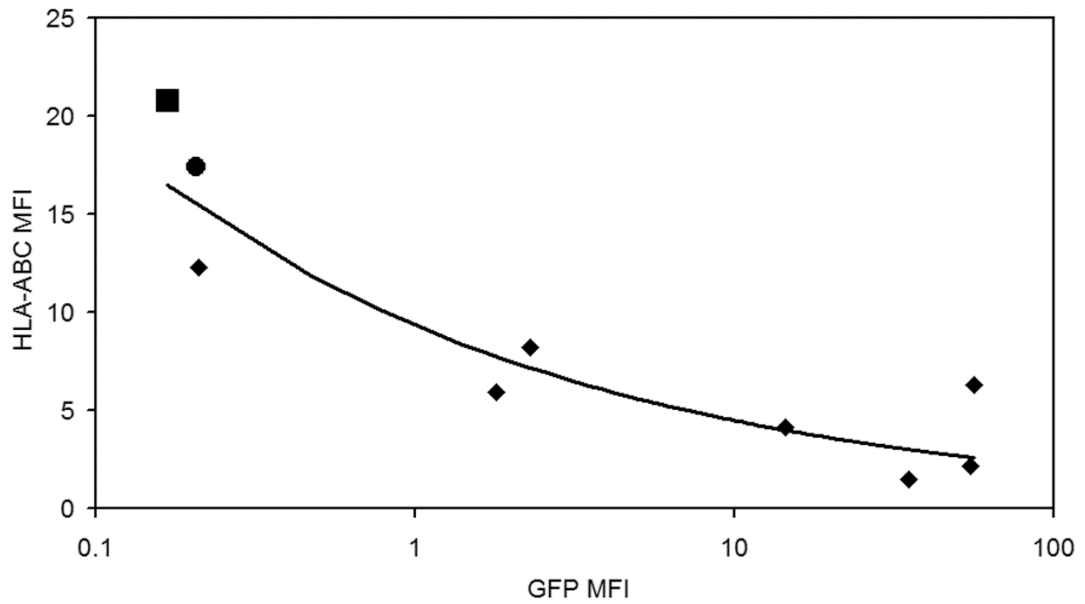
Here we construct a retroviral nanocarrier to stably express a viral immune modulator protein (KSHV MIR2) in model human cells with high transduction efficiency. Figure 17 shows that retroviral nanocarrier delivery resulted in stable and long-term MIR2-GFP expression with HLA-A/B/C downregulation over 100 days of observation. Figure 18 illustrates a dose-response effect, with an inverse relationship between MIR2-GFP copy-number and HLA-A/B/C expression. We then selected (high copy-number) and clonally expanded MIR2-GFP transduced cells and used flow cytometry to demonstrate that MIR2-GFP expression differentially downregulate multiple immunoactive cell surface molecules including MHC class

I, ICAM-1 and CD86 (B7-2) (Figure 19). In a functional test of immune evasion, we performed a flow cytometry-based CTL and Natural Killer (NK) assays. The allogeneic CD8+ T cells and NK cells were isolated from whole blood with healthy human donors to simulate the *in vivo* setting. The CTL assay showed a statistically significant 52% reduction in MIR2-expressing target cell death at a 2:1 Effector:Target (E:T) ratio (Figure 20). The NK assay showed no statistically significant difference in cell death between MIR2-transduced target cells and mock-transduced (LacZ-transduced) cells at multiple E:T ratios (Figure 21).

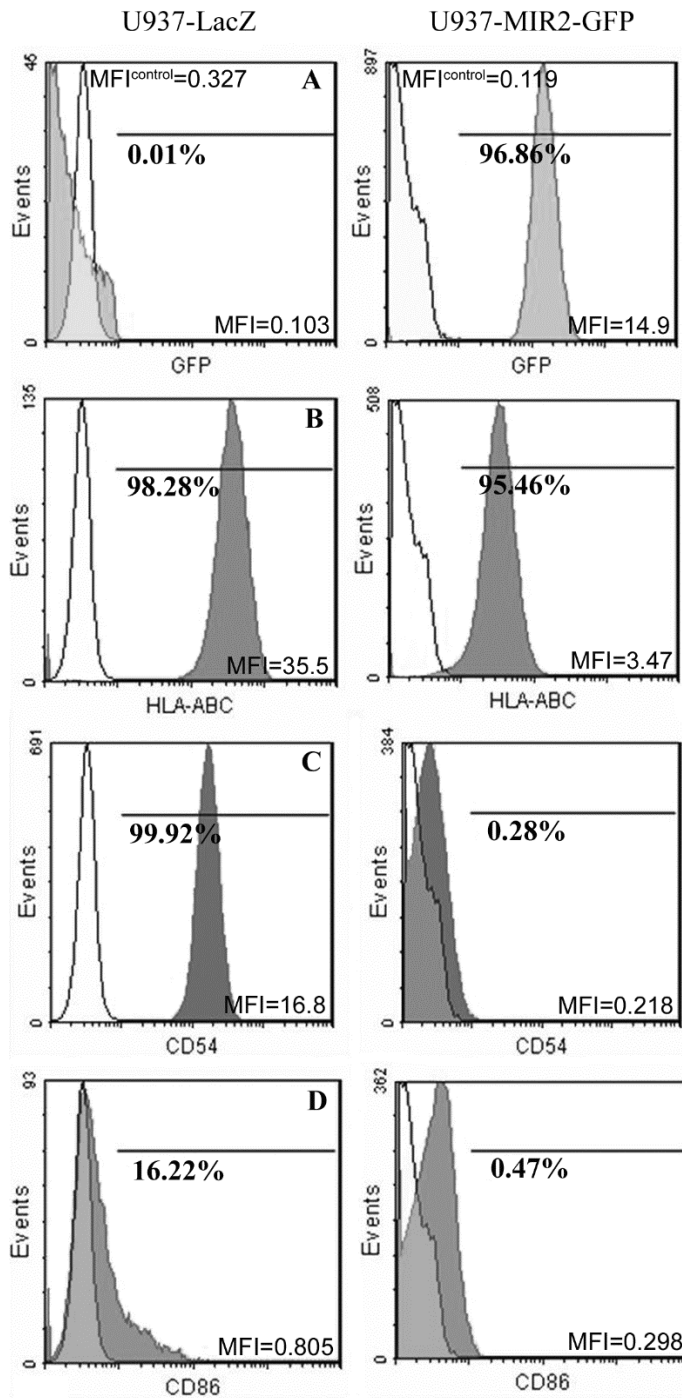
In this paper we employ viral nanoparticles to engineer immune acceptance by selectively modifying allogeneic donor cells using viral mechanisms of immune evasion without altering the host immune system. To our knowledge, this was the first study to use viral immune evasion strategies to simultaneously reduce CTL-mediated cytotoxicity without altering NK-mediated cytotoxicity against allogeneic human cells. Controlling the acute cellular immune response represents a significant advance since it can be integrated into a multipronged strategy to induce selective donor cell tolerance and therefore extend the life of allogeneic tissue-engineered constructs and organs. It could also facilitate the development of ‘universal’ cells for allogeneic transplantation.



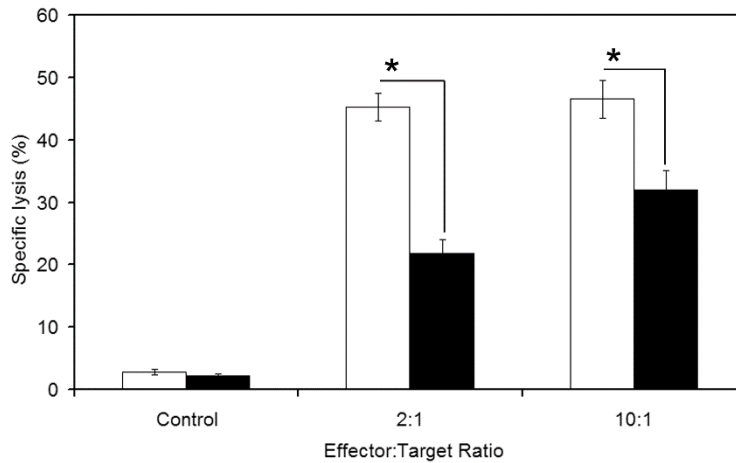
**Figure 17: Effect of MIR2-GFP transduction on HLA-ABC expression over 100 days.** The black bars show the percent of day 0 Mean Fluorescence Intensity (MFI) for MIR2-GFP expression in U937-MIR2-GFP cells. The white bars show the percent of HLA-ABC MFI measured in U937-MIR2-GFP cells relative to its value measured in U937-LacZ cells on day 0. These measurements were acquired from a clonal population of U937-MIR2-GFP cells in active culture for 100 days. Data presented from 100,000 cells analyzed per sample; n = 3 replicates. (Student’s paired *t*-test: \* indicates significant difference ( $p < 0.05$ ); Error bars indicate standard deviation). This figure was reproduced from the publication being presented in this section.



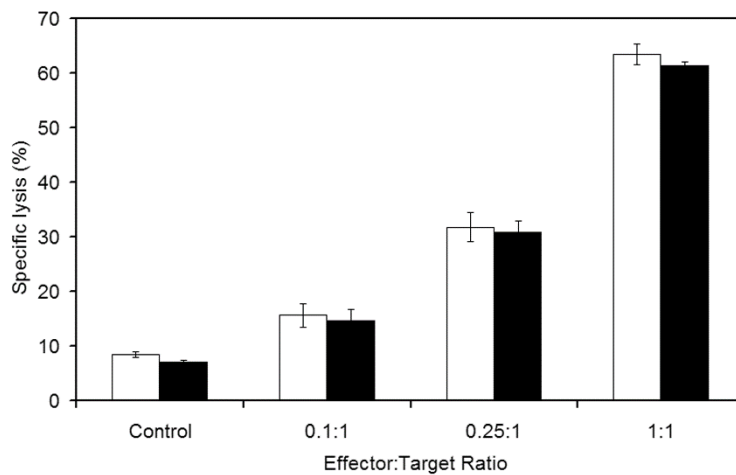
**Figure 18: Trend showing *MIR2-GFP* dose-response effect on *HLA-ABC* expression.** Figure depicts a decreasing trend in the cell surface *HLA-ABC* level with increasing levels of *MIR2-GFP* expression (MFI of GFP) as measured by flow cytometry in each of the seven U937-*MIR2-GFP* clones (◆). Untransduced U937 cells (■) and U937-*LacZ* cells (●) have high levels of *HLA-ABC* expression. Line of best fit data presented from 100,000 cells analyzed per sample. This figure was reproduced from the publication being presented in this section.



**Figure 19: Cell surface characterization of U937-LacZ and U937-MIR2-GFP cells.** HLA-ABC, CD54 and CD86 were all (shaded curves) downregulated in U937-MIR2-GFP cells. Expression of MIR2-GFP was quantified by GFP fluorescence, while antibodies were used to quantify all other markers. Mean fluorescence intensity (MFI) values for the shaded curves are indicated at the bottom right corner of each graph, while MFI values of unlabelled cells (white curves) are indicated as MFI<sup>control</sup>. Representative data presented from 100,000 cells analysed per sample. This figure was reproduced from the publication being presented in this section.



**Figure 20: CTL Assay.** Specific lysis of Calcein-labelled target cells (U937-LacZ [white bars] or U937-MIR2-GFP [black bars] cells) in control samples (without CTLs) and test samples (with CTLs) with varying Effector:Target ratios. (Student's paired *t*-test: \* indicates  $p < 0.05$  between cell lines for both Effector:Target ratios; Error bars indicate standard deviation;  $n = 3$  replicates). This figure was reproduced from the publication being presented in this section.

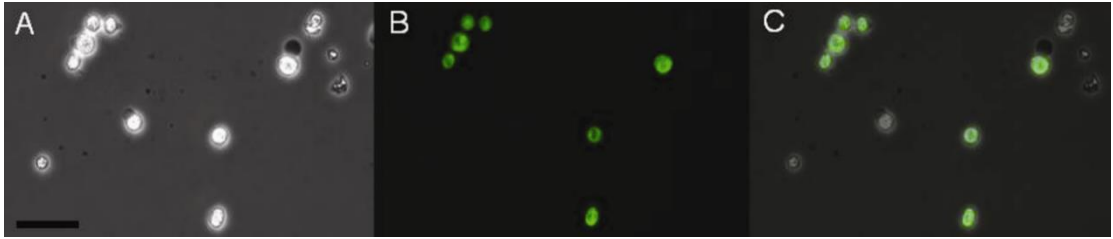


**Figure 21: NK Assay.** Specific lysis of Calcein-labelled target cells (U937-LacZ [white bars] or U937-MIR2-GFP [black bars] cells) in control samples (without NK cells) and test samples (with NK cells) with varying Effector:Target ratios. (Student's paired *t*-test: No significant difference between cell lines ( $p < 0.05$ ); Error bars indicate standard deviation;  $n = 3$  replicates). This figure was reproduced from the publication being presented in this section.

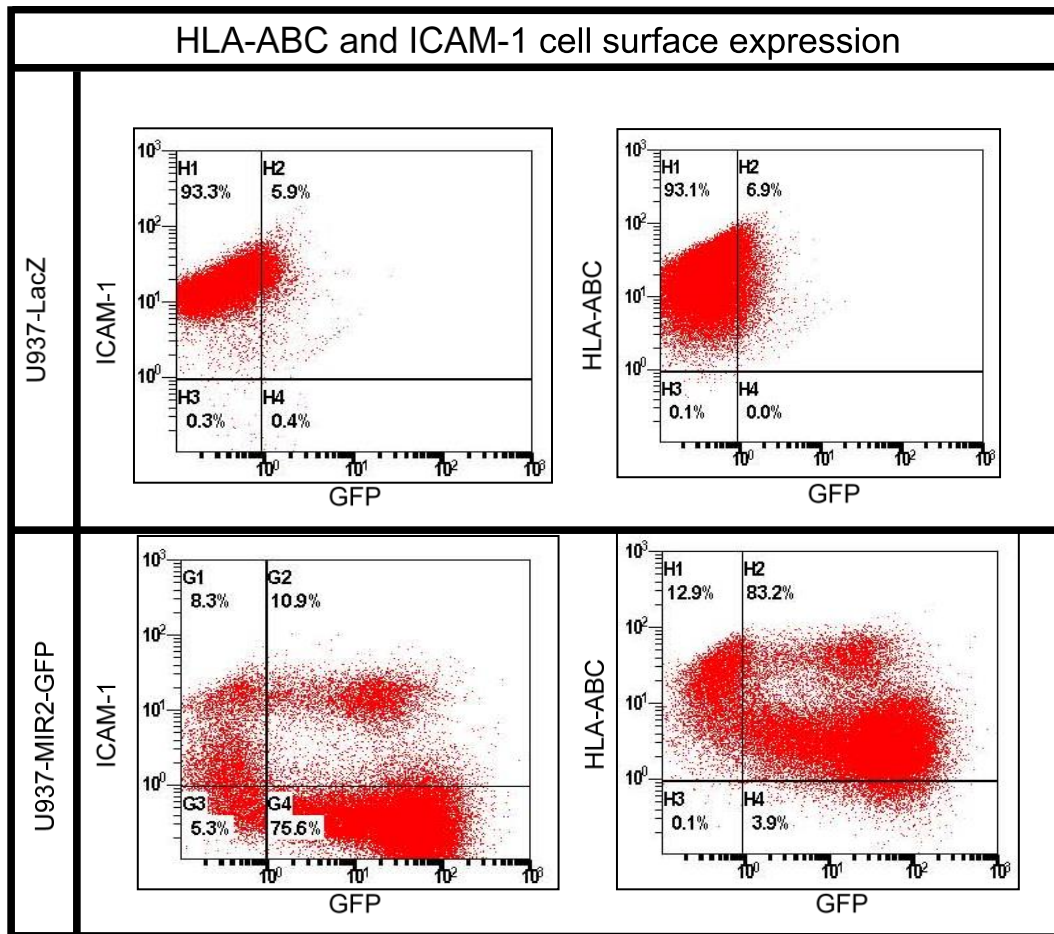
**PAPER 7: “SUPPRESSION OF THE MHC CLASS I-MEDIATED ALLOIMMUNE RESPONSE IN HUMAN CELLS USING A SINGLE-STEP RETROVIRAL TRANSDUCTION PROTOCOL TO EXPRESS KSHV’S STEALTH PROTEIN MIR2” (2011) UNIVERSITY OF TORONTO MEDICAL JOURNAL. 89(1) PP. 27-32.**

In our previous work, we employ viral nanoparticles to genetically modify allogeneic cells *ex vivo* for immune evasion in allogeneic transplantation. These transduced cells were selected *in vitro*, clonally expanded, characterised and then tested in functional CTL and NK assays. In the field of tissue engineering, cells are usually sourced in advance. This approach would be useful for developing ‘universal’ cells and allogeneic cell-based tissue-engineered constructs for off-the-shelf products. However, in clinical transplantation, many types of allogeneic cells, tissues and organs from human donors require transplantation within a limited time-frame, restricting the ability to select, clonally expand and characterise virally transduced cells. Hence, in this paper, we extended our viral gene delivery approach to simulate such a clinical scenario, where allogeneic donor cells are transduced with a viral nanoparticle in a single step without any clonal expansion or selection. Using fluorescence microscopy, we measured the transduction efficiency after a single step transduction protocol and found that it varied from 50%-80% (Figure 22). As a result, this single step transduction protocol creates in a heterogeneous population of allogeneic cells with varying copy-numbers (MIR2-GFP) as well as non-transduced cells (Figure 22). We characterised this heterogeneous population of MIR2-GFP transduced cells with flow cytometry and found that approximately 80% of live cells significantly downregulated (>90% decrease in MFI) both HLA-ABC and ICAM-1, while approximately 10% of cells expressed GFP without downregulating cell-surface HLA-ABC or ICAM-1, and the remaining 5-10% did not express GFP or downregulate cell-surface HLA-ABC and ICAM-1 (Figure 23). We then functionally tested this heterogeneous population of allogeneic cells in flow cytometry-based CTL and NK assays. The CTL assay showed a significant (30%) decrease in allogeneic target cell death at the 2:1 E:T ratio (Figure 24), without increasing the NK cell-mediated target cell death *in vitro* (Figure 25).

This study provides proof of concept that a single step *ex vivo* retroviral gene delivery strategy can potentially be implemented in clinical transplantation to extend the life of transplanted allogeneic organs, tissues and cell-based tissue engineering constructs. In addition, this method of employing viral nanocarriers to transduce cells for allogeneic transplantation would greatly increase the flexibility of producing tissue-engineered constructs. Furthermore, this form of tissue engineering would accelerate the development of biomaterials that better integrate into the recipient and provide new mechanisms for drug delivery.

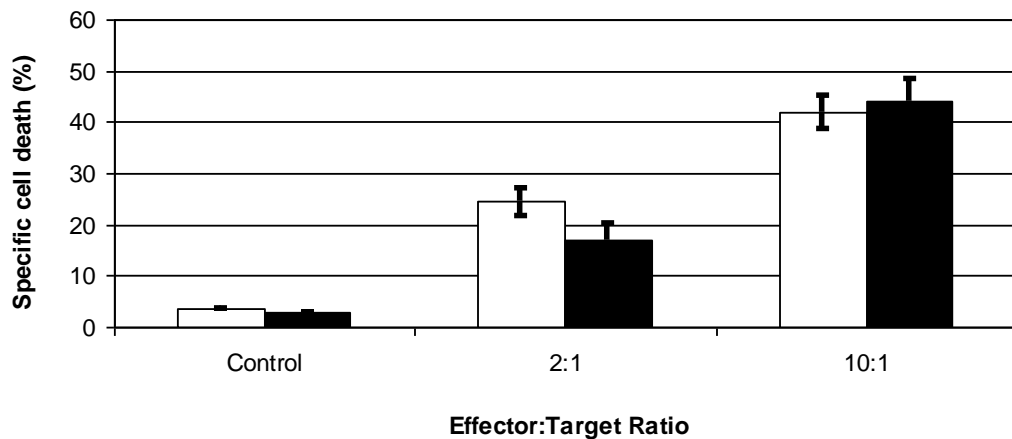


**Figure 22: MIR2-GFP expression in U937 cells after MMLV transduction.** U937 cells express MIR2-GFP (green) after transduction with retrovirus. Images collected in transmission (A) and fluorescence (B) channels. Image C overlays the two channels. Scale bar is 20  $\mu\text{m}$ . Self-acquired image reproduced from the publication being presented in this section.

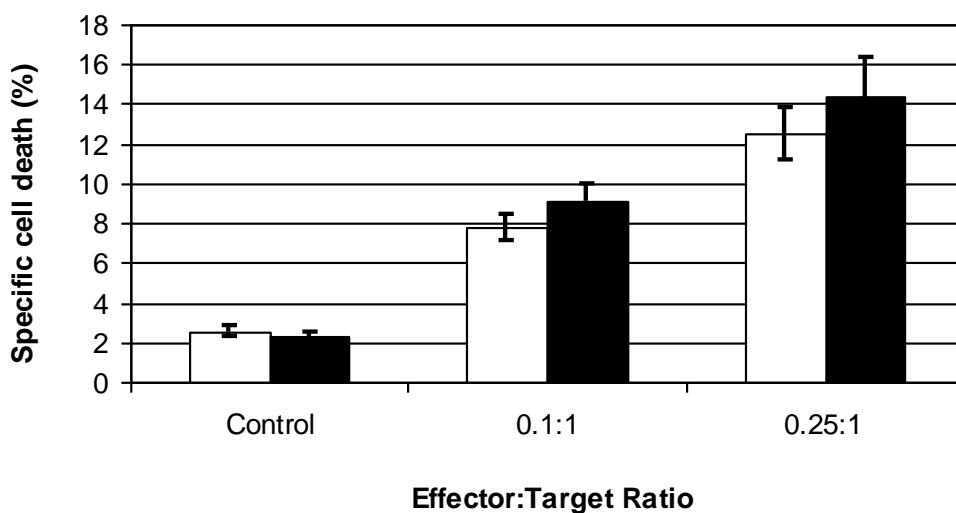


**Figure 23: Cell-surface characterization of U937-LacZ and U937-MIR2-GFP cells.** This plot compares the relative amount of GFP, HLA-ABC and ICMA-1 (CD54) detected in each of the cell lines. GFP was quantified by its fluorescence, while fluorescently labelled antibodies were used to quantify the other markers. Flow cytometry data presented from 30,000 events collected per trial. This figure was reproduced from the publication being presented in this section.





**Figure 24: CTL Assay.** Shows percent specific lysis of Calcein-labelled target cells (U937-LacZ [white bars] or U937-MIR2-GFP [black bars] cells) in control samples and test samples with varying E:T ratios. (Student's paired *t*-test:  $p < 0.05$  between cell lines for 2:1 E:T ratio; Error bars indicate standard deviation;  $n = 3$ ). This figure was reproduced from the publication being presented in this section.



**Figure 25: NK Assay.** Shows percent specific lysis of Calcein-labelled target cells (U937-LacZ [white bars] or U937-MIR2-GFP [black bars] cells) in control samples and test samples with varying E:T ratios. (Student's paired *t*-test: no significant difference ( $p < 0.05$ ) between cell lines; Error bars indicate standard deviation;  $n = 3$ ). This figure was reproduced from the publication being presented in this section.

**PAPER 8: “RECURRENT HOSPITALIZATIONS IN A RARE CASE OF HEMICORPECTOMY: A CHALLENGING CASE FOR MEDICAL MANAGEMENT” (2018) *BRITISH MEDICAL JOURNAL CASE REPORTS*. DOI 10.1136 PP. 1-5.**

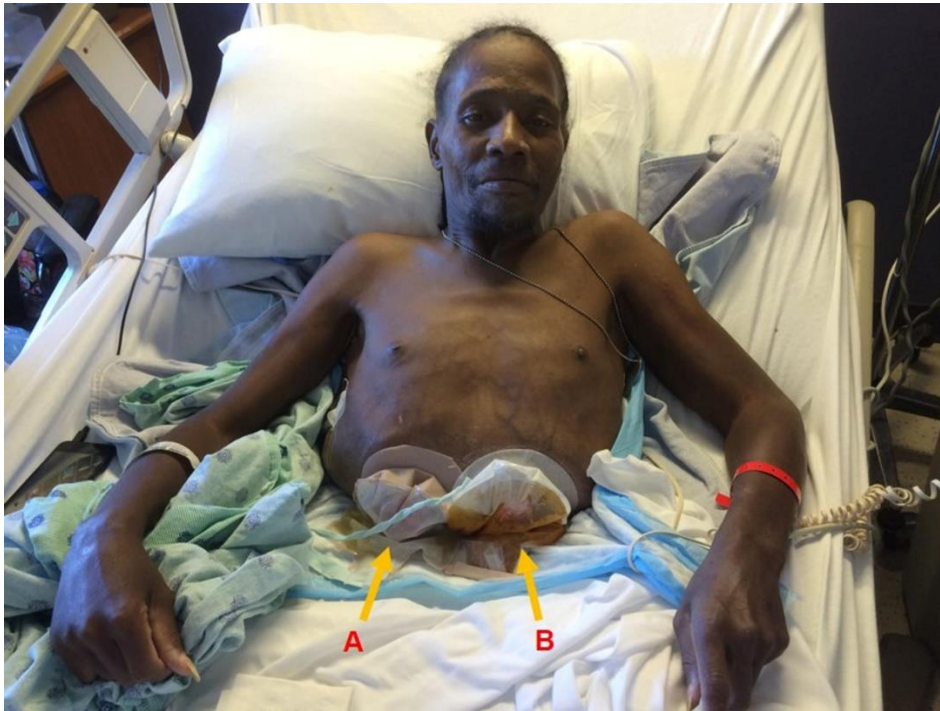
Nanoparticles, microspheres and tissue-engineered constructs can not only be used for cell and drug delivery but can also be engineered to provide a 3D scaffold for wound healing, inflammation suppression, and promotion of tissue regeneration [111,112]. In this paper, we present a patient with recurrent hospitalisations in a rare case of hemicorporectomy due to chronic non-healing pressure ulcers and wound infections (Figure 26).

Hemicorporectomy, or translumbar amputation, is a radical surgery involving the dissection of the body at the lumbar region (commonly between L4-L5) and is usually reserved for complex medical conditions including locally invasive malignancy and terminal pelvic osteomyelitis. Of the 71 reported cases of hemicorporectomy (until Dec 2017), 21 (30%) cases have been reported for terminal pelvic osteomyelitis, 43 (60%) cases for malignancy, 4 cases for benign disease and 3 cases for trauma. Outcomes are generally more favorable for non-malignant vs. malignant indications. For terminal pelvic osteomyelitis, more than 50% of patients survived at least nine years, with an average survival of 11 years post-hemicorporectomy.

We present a 22-year follow up of a 53-year-old African American male who underwent a hemicorporectomy after a series of surgical procedures for terminal pelvic osteomyelitis, chronic advanced pressure ulcers and chronic complicated urinary tract infections, which occurred after he suffered a gunshot wound at T6 causing paraplegia at the age of 31. Unfortunately, these infections persisted post-hemicorporectomy and the patient continued to develop advanced pressure ulcers (grades 1-4) on his back and inferior aspect of his body (Figure 27). Despite repeated courses of broad-spectrum intravenous antibiotics and surgical debridements of his chronic advanced pressure ulcers, this patient suffered recurrent bouts of sepsis. In light of the fact that this patient had been admitted to the hospital on average 10 times/year in recent years, the patient’s family chose to manage his condition conservatively with home hospice, with a focus on palliative care.

This case illustrates the significant challenges in the medical and surgical management of hemicorporectomy patients, which can lead to recurrent hospitalisations with a diminished quality of life and a poor prognosis for patients. However, a significant number of hemicorporectomy patients can prolong their life as well as enjoy a relatively good quality of life with a multi-disciplinary approach to care. After hemicorporectomy, all patients should

undertake a rehabilitation process that involves the integration of different services such as occupational and physical therapy, nutrition, psychological counselling, and specialised wound care with novel biomaterial and tissue-engineering technologies to suppress inflammation and promote healing. Unfortunately, there are currently no guidelines or standards of care for the management of hemicorporectomy patients (inpatient and outpatient). We hope that this case may help healthcare providers anticipate and manage some of the potential complications in similar patients who have undergone hemicorporectomy or other radical surgical procedures.



**Figure 26: Hemisectomy patient.** Image shows A) urostomy with ileal conduit and B) ileostomy. Self-acquired image reproduced from the publication being presented in this section.



**Figure 27: Evolution of pressure ulcers.** A) 09/2011: Stage 4 sacral pressure ulcer 7 x 9.5 x 2.8 cm, B) 01/2013: Stage 3 left thorax pressure ulcer 31.5 x 11 x 0.1 cm, C) 09/2016: Stage 1-4 posterior thorax pressure ulcer 50 x 50 cm. This image reproduced from the publication being presented in this section.

## DISCUSSION

Despite the significant advances in the development of nanoparticles and microspheres for clinical applications, there is a notable paucity of FDA-approved technologies in medicine. This can be attributed to our limitations in understanding how living systems interact with nanoparticles and microspheres, including the significance of the immune system. Here, I will outline some of the major challenges associated with the development of nanoparticles and microspheres for diagnostics and biopharmaceutical delivery in medicine.

### **Challenges associated with QD nanoparticles for diagnostics and drug delivery**

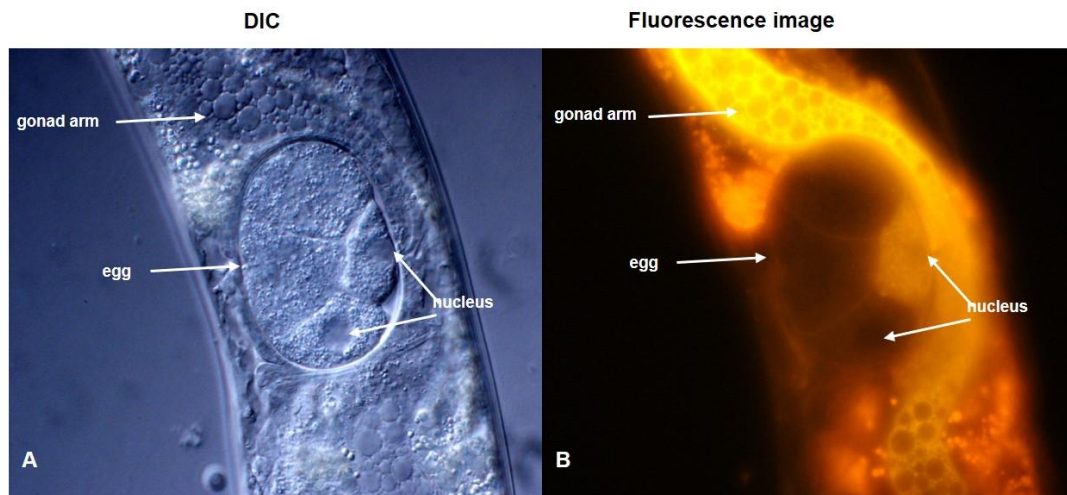
In general, nanoparticles have four major challenges in their development for diagnostics and drug delivery. In this discussion, QD nanoparticles will be used as a case in point to illustrate these challenges. First, most nanoparticles manufacturing processes result in deficiencies in their surface coatings. Although QD have been successfully employed *in vitro*, the application of QD as fluorescent probes in live cells still remains a challenge mainly due to deficiencies in their hydrophilic layer [113]. In 2005, our laboratory used time-lapse imaging experiments in live cells *in vitro* and reported that these coating deficiencies greatly increase QD size (up to 10x) and promote the formation of QD aggregates (Figure 3,4), which trigger the innate immune defenses within cells to recognise and process these foreign objects within lysosomes (Figure 5) [38,40,114,115].

Second, most commercially available nanoparticles are excessively large to function effectively as biological probes. The vast majority of water-soluble QD commercially available have a hydrodynamic diameter of 15-35nm. Given that most intracellular globular proteins are between 1-10nm, it is easy to conceive that a 15nm QD conjugated to the target protein, would greatly influence not only the diffusion of the target protein, but also alter its normal interactions with other intracellular molecules. Previous work has shown that nanoparticles larger than 15nm in diameter have a greatly diminished diffusion capacity within intracellular environments, while nanoparticles larger than 50nm in diameter are effectively immobile in intracellular environments [116,117]. Interestingly, another study showed that nanoparticles smaller than 3nm in diameter can passively diffuse or be actively transported into the nucleus [118]. In 2007, Choi *et al* showed that rodents can renally excrete neutral QD smaller than 5.5nm (hydrodynamic diameter), while QD larger than 15nm are prevented from renal excretion and accumulate in the RES with unknown long-term consequences [46,119,120]. Taken together, these results suggest that with the correct organic QD coating, there may be a small window of nanoparticle size, <15nm, which would be ideal for intracytoplasmic studies while simultaneously avoiding accumulation within the RES, thus making it safer for human use.

Third, most commercially available nanoparticles have a limited ability to cross biological membranes for intracellular delivery. Although previous studies have used techniques such as microinjection and electroporation to successfully deliver QD intracellularly, these techniques are invasive and not easily translatable to all cell types [40]. Non-invasive QD delivery techniques such as pinocytotic loading, receptor-mediated endocytosis, peptide translocation domains and cationic lipids have all been attempted with varying degrees of success, albeit to specific cell lines and QD delivery conditions [40,121]. A more standardised approach to non-invasive intracellular QD delivery, such as our proposed four-component smart 'universal' nanoparticle (Figure 7), is likely required for its successful application in clinical settings.

Fourth, the most concerning aspect of QD application in humans is their potential toxicity. A closer look at their composition reveals that QD are made of inorganic semi-conducting elements. Frequently, the core is composed of elements from group II and VI (e.g. CdS, CdTe, CdSe), groups III and V (eg InP, InAs) or groups IV and VI (eg PbSe), while the shell is frequently composed of ZnS [40,122]. The 2-15nm inorganic core-shell QD is then coated with an organic hydrophilic layer such as thiols, phospholipid micelles and amphiphilic polymers to render them water-soluble. Typically, this organic hydrophilic layer is then functionalised with peptides, antibodies and other ligands of interest. Although many studies have successfully employed QD in various cells types without any adverse effects on cell viability or function, this does not imply that QD do not have any observable effect, as reported in our own live cell studies (Figure 4,5) [5,114,123,124].

Duration of exposure and concentration of QD also seem to influence toxicity. In our own experiments in the *in vivo* setting, QD were microinjected into the oocyte, the gonad arm and the body cavity of a nematode, *C. elegans*, and did not appear to have any observable short-term (up to 48h) toxic effects on the worms (Figure 28). In contrast, other studies have reported significant adverse effects to cell viability and function. For example, Dubertret *et al* showed that high concentrations of QD have an adverse effect on developing *Xenopus* embryos [123]. Moreover, other studies have demonstrated that the rate at which adverse effects (cell viability and function) appeared seemed to be inversely correlated with the degree of QD core-shell protection from the environment [125]. This has been correlated with the leakage of QD core-shell components such as Cd and Se, into the cellular environment and photon-induced free radical formation [116,125,126]. Taken together, these studies suggest that QD toxicity is a function of QD concentration, duration of exposure and efficacy of the organic layer in isolating the core-shell from the cellular environment.



**Figure 28. In vivo QD imaging in live *C. elegans* embryos.** A single cell within a four-cell-stage embryo was microinjected with orange QD in live *C. elegans* and imaged in transmission (A) or epifluorescence (B) microscopy on an inverted Nikon microscope coupled to a CCD camera. The worm and embryo appeared unperturbed for up to 48h. Self-acquired image from unpublished work.

### **Challenges associated with microspheres for biopharmaceutical delivery in medicine**

Multiple clinical studies with microencapsulated cells have revealed partial function and limited survival time of the transplanted cells [98]. The first major challenge is the immune response against the microcapsules themselves, and the cells within. It has been shown that commercially available polymers, including alginate, used to create microcapsules contain pathogen-associated molecular patterns (PAMPs), which are strong initiators of the immune response [127]. In a recent study, Paredes-Juarez *et al* investigated the immune mechanisms of encapsulated cell failure [110]. They suggest that encapsulated cells endure a prolonged phase of ischemia immediately after transplantation and during revascularisation of the region. During this ischemic phase, encapsulated cells are exposed to low-oxygen and low-nutrition levels. The authors showed that encapsulated islet beta-cells in such ischemic conditions release danger-associated molecular patterns (DAMPs) that activate the innate immune response via TLRs *in vitro* [110]. They also found that the selectively-permeable encapsulating membrane only retains relatively large DAMPs, suggesting that the permeability of the microcapsule membrane is a key component in initiating the immune response.

The source of encapsulated cells is another major factor that determines the strength and type of immune response. Xenogeneic cells generate highly immunogenic epitopes such as terminal (1-3) galactosyl residues that provoke a stronger, often hyperacute immune response compared to allogeneic cells [98]. Naturally occurring anti-Gal antibodies can bind galactosyl residues diffusing out of microcapsules and subsequently trigger activation of the classical

complement pathway. This process can trigger the chemotaxis of neutrophils and subsequent neutrophil degranulation near the microcapsules. In addition, an IgM-mediated delayed-type hypersensitivity response against xenogeneic epitopes also occurs [98]. Together, these immune reactions generate chemokines and cytokines that recruit more inflammatory cells and fibroblasts to completely envelop the microcapsules, inducing ischemic changes in the encapsulated cells. This process not only reduces the viability of encapsulated cells, but also changes their proliferation and secretory behaviour.

Finally, inconsistencies in the current methods of encapsulation tends to create variability in the properties of the polymer membrane such as mechanical strength, permeability, surface charge, roughness and protein adsorption characteristics. In addition, current encapsulation methods have been known to create microcapsules with some cells protruding from the surface. These protruding cells can potentially initiate a strong immune response leading to complete fibrosis of the entire transplanted region, which will certainly lower the viability of the cells within. In all the scenarios above, evaluating encapsulated cell viability, proliferation and secretory ability is of critical importance. Our novel flow cytometry assay to assess the viability and proliferation of encapsulated cells provides greater insight into the factors that determine the success and failure of transplanted cells.

## FUTURE WORK

### Prospects for QD nanoparticles in medicine

Current research into Cadmium-free QD for *in vivo* applications is driving the development of the next generation of non-toxic QD that are safe for clinical applications [119,128–131]. Among the most promising alternatives to QD composed of toxic elements Cd and Se, are QD composed of new semiconducting materials called perovskites [132]. Unlike conventional QD, these new semiconductors have a variable ratio of elements, so that their emission spectra can be tailored based on composition and size, providing two degrees of freedom [133]. As an alternative to the use of non-degradable semiconductors, a new generation of ‘organic,’ carbon-based QD are being developed that are highly biocompatible, water-soluble and easily functionalised, yet derive their fluorescence properties due to quantum confinement effects. For example, Yang *et al* have recently developed highly luminescent, water-soluble carbon dots called ‘Cdots’ functionalised with transacting activator of transcription (TAT) peptide (a type of cell penetration peptide) to directly monitor TAT interactions within a living cell membrane using single particle tracking techniques [134]. However, most Cdots currently available have a much lower quantum yield compared to inorganic QD and involved complex fabrication techniques in harsh reaction conditions [134–136]. Alternatively, another type of QD composed of semiconducting polymer called ‘Pdots’ have been particularly advantageous, since they provide a way to circumvent the need to synthesise nanoparticles with a narrow size distribution [137]. Although these organic Pdots can be tunable, up to 30x brighter than traditional inorganic QD of comparable size, and are more likely to be biocompatible, they present new challenges that are yet unresolved. For example, Pdots suffer from a phenomenon known as ‘quenching,’ where tightly packed long chains of polymers diminish the fluorescence quantum yield and thus constrain the size of the nanoparticle [138]. However, other types of organic QD take advantage of this aggregation of polymers within nanoparticles to increase fluorescence quantum yield through aggregation-induced emission (AIE) [139]. These nanoparticles called ‘AIE-dots’ have also been shown to be tunable and up to 40x brighter than traditional QD of comparable size, but have a significant caveat: they have broad emission spectra and their *in vivo* safety and efficacy has not yet been established [140].

Aside from optical characteristics of nanoparticles *in vitro*, imaging *in vivo* presents special optical challenges as ultraviolet and visible light have an extremely limited penetration depth into tissues. However, NIR wavelengths can penetrate up to three centimeters and present an opportunity for deep tissue imaging. Hence, many research groups are currently developing ‘upconversion’ nanoparticles composed of lanthanides to absorb low energy NIR photons and combine them into higher energy photons in the visible and ultraviolet spectra [141]. This



provides a novel photoactive theranostic delivery platform for deep tissue imaging and drug delivery using NIR energy to minimize phototoxicity [142].

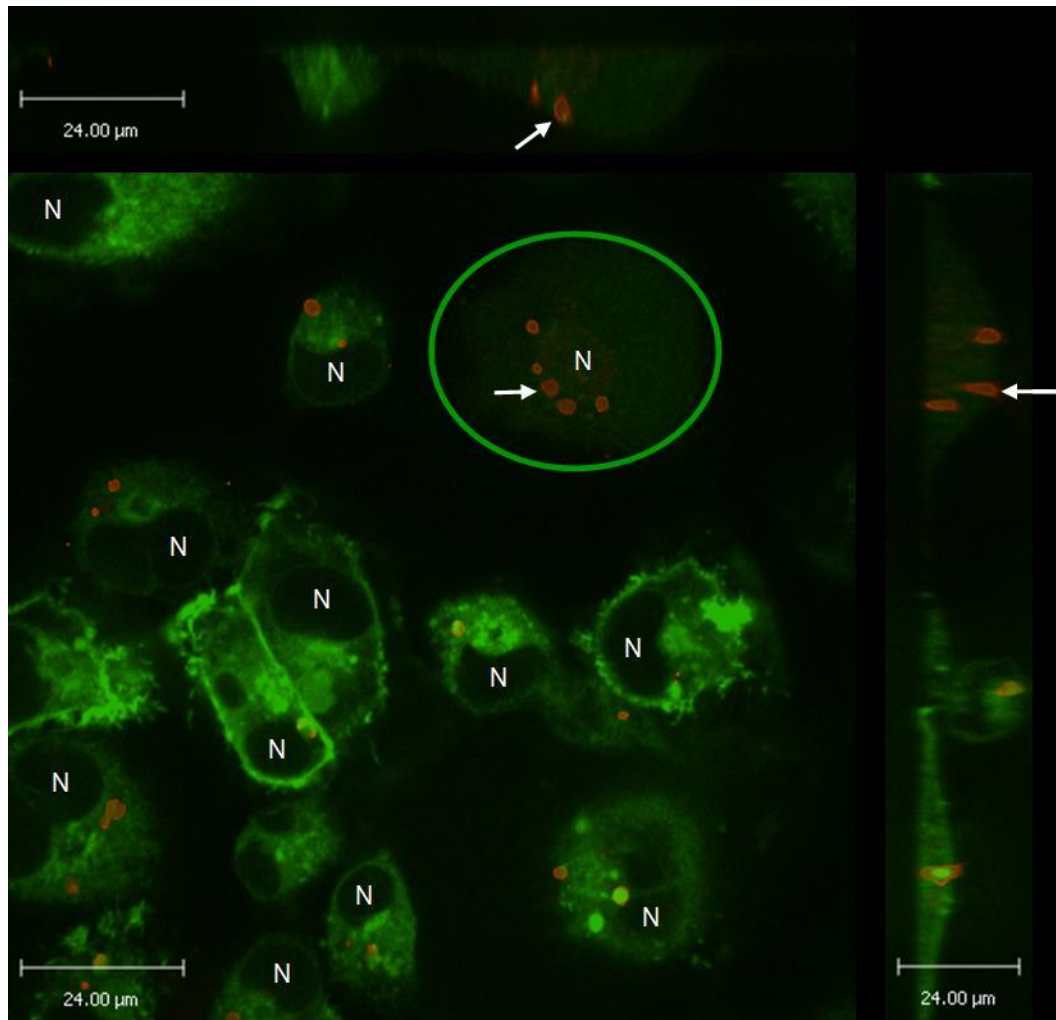
Given that the market for QD technologies has been predicted to grow to over \$5 billion by 2020, it is important to address the potential challenges associated with their use in humans [143,144]. Among the major limitations of QD *in vitro* and *in vivo*, a short blood half-life, undesirable uptake and accumulation in the RES, cellular toxicity, lack of biodegradability, inability to selectively cross target cell membranes and reach the intracellular site of action (cytoplasm or nucleus) significantly hamper the successful application of QD in medicine. Taken together, these observations suggest that the development of QD technologies for clinical applications likely requires a three-pronged approach: 1) standardisation of QD synthesis and functionalisation- surface engineering small QD (<15 nm in diameter) with a thin, neutral PEG organic layer to promote renal excretion, minimise RES uptake and improve intracellular delivery, 2) non-toxic QD- manufacturing heavy metal-free QD, 3) theranostic capabilities- smart multifunctional QD capable of diagnostic and therapeutic capabilities. Overcoming these challenges will allow for the rational design of personalised, multifunctional stimuli-responsive QD to improve their diagnostic and therapeutic value in clinical medicine.

### **Prospects for microspheres in medicine**

Currently microcapsules provide a means of controlled delivery of cells engineered to secrete therapeutic product. However, microcapsule technology is being developed for a multitude of applications in regenerative medicine with parallel delivery of encapsulated drugs, growth factors for improved neovascularisation, extracapsular modification for better integration into the host extracellular matrix and cell-based diagnostics. In addition, encapsulation methods are evolving to improve control over microcapsule size, microcapsule membrane structure and permeability, surface functionalisation with biomolecules, and encapsulated cell placement within microcapsules [98].

Analogous to our proposed smart stimuli-responsive nanoparticles, smart stimuli-responsive microcapsules are also being developed. For example, Luo *et al* recently developed near-infrared light responsive microcapsules to control drug release in a pulsatile manner [145]. The microcapsules can also be engineered to enable precise *in vivo* localisation using traditional imaging modalities such as CT, MRI and US [146–148]. Other research has focused on genetically engineering encapsulated cells with externally inducible suicide genes to inactivate the implanted cells if termination of therapy is desired [149]. Interestingly, genetic engineering of encapsulated cells for fluorescence and bioluminescence imaging provides another novel way to evaluate the viability and proliferation of encapsulated cells *in vivo*. In 2013, Santos *et al* engineered encapsulated myoblasts with a TGL triple-fusion reporter gene with HSV1 thymidine kinase, green fluorescent protein and firefly luciferase, which allows for

the simultaneous imaging with fluorescence and bioluminescence, as well as a biosafety strategy (via a suicide gene) to inactivate the encapsulated cells with ganciclovir [149]. In summary, smart stimuli-responsive microcapsules with encapsulated cells provides a means of multimodal imaging for diagnostics, as well as the long-term delivery of cell-derived and non-cell derived therapeutics that are responsive to internal physiologic feedback from disease-specific stimuli and external signals for clinical applications.



**Figure 29: Prototype of a smart biodegradable polymeric nanoparticle for intracellular nucleotide delivery.** Mammalian cells were pinocytically loaded with the nanoparticle labelled with a fluorescent dye (DiI), fixed in paraformaldehyde, and imaged with a confocal microscope using YFP and Cy3 channel settings (overlaid image presented). The green circle outlines a cell that was analysed in three dimensions. White arrows point to nanoparticle fluorescence localised within this cell (X-Y, X-Z and Y-Z planes) in an endolysosome. Cell nuclei are marked 'N.' Self-acquired image from unpublished work.

## CONCLUSION

It is evident that nanoparticle and microsphere technologies have a vast potential in medicine. Although the technology has been extensively researched and developed for pharmaceutical applications over the last few decades, it is apparent that currently non-viral nanoparticle technologies are more suitable for tissue and subcellular imaging, single particle tracking studies, *in vitro* diagnostics for the detection of biomolecules and *in vivo* applications in animal models. Similarly, viral nanoparticles and microspheres have demonstrated their tremendous potential in the efficient delivery of genes and the sustained delivery of biopharmaceutical products for clinical applications. However, until the major challenges associated with biomaterial interactions with the innate and adaptive immune system have been addressed, these technologies will likely have limited applications in humans *in vivo*. Nevertheless, the next generation of nanoparticles and microspheres are poised to deliver on their promise of multifunctional, targeted and stimuli-responsive modalities for imaging, diagnosis and treatment in clinical medicine.

## BIBLIOGRAPHY

- 1 Thakur A, Fitzpatrick S, Zaman A, *et al.* Strategies for ocular siRNA delivery: Potential and limitations of non-viral nanocarriers. *J Biol Eng* 2012;**6**:7.
- 2 Iga A, Robertson J, Winslet M, *et al.* Clinical potential of quantum dots. *J Biomed Biotechnol* 2007;**2007**:76087.
- 3 Parak WJ, Pellegrino T, Plank C. Labelling of cells with quantum dots. *Nanotechnology* 2005;**16**:R9–25.
- 4 Parak WJ, Gerion D, Pellegrino T, *et al.* Biological applications of colloidal nanocrystals. *Nanotechnology* 2003;**14**:R15–27.
- 5 Jaiswal J, Mattoussi H, Mauro J, *et al.* Long-term multiple color imaging of live cells using quantum dot bioconjugates. *Nat Biotechnol* 2003;**21**:47–51.
- 6 Hohng S, Ha T. Near-complete suppression of quantum dot blinking in ambient conditions. *J Am Chem Soc* 2004;**126**:1324–5.
- 7 Jaiswal JK, Goldman ER, Mattoussi H, *et al.* Use of quantum dots for live cell imaging. *Nat Methods* 2004;**1**:73–8.
- 8 Parak WJ, Boudreau R, Le Gros M, *et al.* Biological uses of semiconducting nanocrystals. *Abstr Pap Am Chem Soc* 2003;**225**:U954–U954.
- 9 Kamila S, McEwan C, Costley D, *et al.* Diagnostic and Therapeutic Applications of Quantum Dots in Nanomedicine. *Top Curr Chem* 2015;**370**:203–24.
- 10 Koo V, Hamilton P, Williamson K. Non invasive in vivo imaging in small animal research. *Cell Oncol* 2006;**28**:127–39.
- 11 Leblond F, Davis S, Valdès P, *et al.* Pre-clinical whole-body fluorescence imaging: Review of instruments, methods and applications. *J Photochem Photobiol B* 2010;**98**:77–94.
- 12 Licha K, Olbrich C. Optical imaging in drug discovery and diagnostic applications. *Adv Drug Deliv Rev* 2005;**57**:1087–108.
- 13 Mérian J, Gravier J, Navarro F, *et al.* Fluorescent nanoprobe dedicated to in vivo imaging: from preclinical validations to clinical translation. *Molecules* 2012;**17**:5564–91.
- 14 Sevick-Muraca E, Sharma R, Rasmussen J, *et al.* Imaging of lymph flow in breast cancer patients after microdose administration of a near-infrared fluorophore.

*Radiology* 2008;**246**:734–41.

- 15 Tagaya N, Yamazaki R, Nakagawa A, *et al.* Intraoperative identification of sentinel lymph nodes by near-infrared fluorescence imaging in patients with breast cancer. *Am J Surg* 2008;**195**:850–3.
- 16 Troyan S, Kianzad V, Gibbs-Strauss S, *et al.* A first-in-human clinical trial in breast cancer sentinel lymph node mapping. *Ann Surg Oncol* 2009;**16**.
- 17 Bruchez M, Moronne M, Gin P, *et al.* Semiconductor nanocrystals as fluorescent biological labels. *Science (80- )* 1998;**281**:2013–6.
- 18 Chan WC, Nie S. Quantum dot bioconjugates for ultrasensitive nonisotopic detection. *Science (80- )* 1998;**281**:2016–8.
- 19 Chan P, Yuen T, Ruf F, *et al.* Method for multiplex cellular detection of mRNAs using quantum dot fluorescent in situ hybridization. *Nucleic Acids Res* 2005;**33**:e161.
- 20 Knoll JH. Human metaphase chromosome FISH using quantum dot conjugates. *Methods Mol Biol* 2007;**374**:55–66.
- 21 Wu X, Liu H, Liu J, *et al.* Immunofluorescent labeling of cancer marker Her2 and other cellular targets with semiconductor quantum dots. *Nat Biotechnol* 2003;**21**:41–6.
- 22 Lidke D, Nagy P, Heintzmann R, *et al.* Quantum dot ligands provide new insights into erbB/HER receptor-mediated signal transduction. *Nat Biotechnol* 2004;**22**:198–203.
- 23 Chen H, Xue J, Zhang Y, *et al.* Comparison of quantum dots immunofluorescence histochemistry and conventional immunohistochemistry for the detection of caveolin-1 and PCNA in the lung cancer tissue microarray. *J Mol Histol* 2009;**40**:261–8.
- 24 Zrazhevskiy P, Sena M, Gao X. Designing multifunctional quantum dots for bioimaging, detection, and drug delivery. *Chem Soc Rev* 2010;**39**:4326–54.
- 25 Heine M, Groc L, Frischknecht R, *et al.* Surface mobility of postsynaptic AMPARs tunes synaptic transmission. *Science (80- )* 2008;**320**:201–5.
- 26 Murcia MJ, Minner DE, Mustata GM, *et al.* Design of quantum dot-conjugated lipids for long-term, high-speed tracking experiments on cell surfaces. *J Am Chem Soc* 2008;**130**:15054–62.
- 27 Dahan M, Levi S, Luccardini C, *et al.* Diffusion dynamics of glycine receptors revealed by single-quantum dot tracking. *Science (80- )* 2003;**302**:442–5.
- 28 Howarth M, Takao K, Hayashi Y, *et al.* Targeting quantum dots to surface proteins in living cells with biotin ligase. *Proc Natl Acad Sci U S A* 2005;**102**:7583–8.

- 29 Varela JA, Dupuis JP, Etchepare L, *et al.* Targeting neurotransmitter receptors with nanoparticles in vivo allows single-molecule tracking in acute brain slices. *Nat Commun* 2016;**7**:10947.
- 30 Hu B, Hu LL, Chen ML, *et al.* A FRET ratiometric fluorescence sensing system for mercury detection and intracellular colorimetric imaging in live HeLa cells. *Biosens Bioelectron* 2013;**49**:499–505.
- 31 Wei W, He X, Ma N. DNA-templated assembly of a heterobivalent quantum dot nanoprobe for extra- and intracellular dual-targeting and imaging of live cancer cells. *Angew Chem Int Ed Engl* 2014;**53**:5573–7.
- 32 Pillai SS, Yukawa H, Onoshima D, *et al.* Fluorescence Quenching of CdSe/ZnS Quantum Dots by Using Black Hole Quencher Molecules Intermediated With Peptide for Biosensing Application. *Cell Med* 2015;**8**:57–62.
- 33 Zhao Y, Liu S, Li Y, *et al.* Synthesis and grafting of folate-PEG-PAMAM conjugates onto quantum dots for selective targeting of folate-receptor-positive tumor cells. *J Colloid Interface Sci* 2010;**350**:44–50.
- 34 Cui B, Wu C, Chen L, *et al.* One at a time, live tracking of NGF axonal transport using quantum dots. *Proc Natl Acad Sci U S A* 2007;**104**:13666–71.
- 35 Zhang Q, Li Y, Tsien RW. The dynamic control of kiss-and-run and vesicular reuse probed with single nanoparticles. *Science (80- )* 2009;**323**:1448–53.
- 36 Cambi A, Lidke DS, Arndt-Jovin DJ, *et al.* Ligand-conjugated quantum dots monitor antigen uptake and processing by dendritic cells. *Nano Lett* 2007;**7**:970–7.
- 37 Roullier V, Clarke S, You C, *et al.* High-affinity labeling and tracking of individual histidine-tagged proteins in live cells using Ni<sup>2+</sup> tris-nitrilotriacetic acid quantum dot conjugates. *Nano Lett* 2009;**9**:1228–34.
- 38 Thakur A, Fradin C. Characterization of quantum dot behaviour in live mammalian cells. *CUPJ* 2005;**3**:7–12.
- 39 Altinoglu EI, Adair JH. Near infrared imaging with nanoparticles. *Wiley Interdiscip Rev Nanomed Nanobiotechnol* 2010;**2**:461–77.
- 40 Michalet X, Pinaud F, Bentolila L, *et al.* Quantum dots for live cells, in vivo imaging, and diagnostics. *Science (80- )* 2005;**307**:538–44.
- 41 Larson DR, Zipfel WR, Williams RM, *et al.* Water-soluble quantum dots for multiphoton fluorescence imaging in vivo. *Science (80- )* 2003;**300**:1434–6.

- 42 Hilderbrand SA, Weissleder R. Near-infrared fluorescence: application to in vivo molecular imaging. *Curr Opin Chem Biol* 2010;**14**:71–9.
- 43 Voura EB, Jaiswal JK, Mattoussi H, *et al.* Tracking metastatic tumor cell extravasation with quantum dot nanocrystals and fluorescence emission-scanning microscopy. *Nat Med* 2004;**10**:993–8.
- 44 Bentolila LA, Ebenstein Y, Weiss S. Quantum dots for in vivo small-animal imaging. *J Nucl Med* 2009;**50**:493–6.
- 45 Kim S, Lim YT, Soltesz EG, *et al.* Near-infrared fluorescent type II quantum dots for sentinel lymph node mapping. *Nat Biotechnol* 2004;**22**:93–7.
- 46 Choi H, Liu W, Misra P, *et al.* Renal clearance of quantum dots. *Nat Biotechnol* 2007;**25**:1165–70.
- 47 Ballou B, Ernst LA, Andreko S, *et al.* Sentinel lymph node imaging using quantum dots in mouse tumor models. *Bioconjug Chem* 2007;**18**:389–96.
- 48 Chen G, Tian F, Li C, *et al.* In vivo real-time visualization of mesenchymal stem cells tropism for cutaneous regeneration using NIR-II fluorescence imaging. *Biomaterials* 2015;**53**:265–73.
- 49 Chen YY, Cheng BR, He ZB, *et al.* Capture and Identification of Heterogeneous Circulating Tumor Cells Using Transparent Nanomaterials and Quantum Dots-Based Multiplexed Imaging. *J Cancer* 2016;**7**:69–79.
- 50 Gupta P, Adkins C, Lockman P, *et al.* Metastasis of Breast Tumor Cells to Brain Is Suppressed by Phenethyl Isothiocyanate in a Novel Metastasis Model. *PLoS One* 2013;**8**:e67278.
- 51 Cai W, Shin DW, Chen K, *et al.* Peptide-labeled near-infrared quantum dots for imaging tumor vasculature in living subjects. *Nano Lett* 2006;**6**:669–76.
- 52 Li Y, Li Z, Wang X, *et al.* In vivo cancer targeting and imaging-guided surgery with near infrared-emitting quantum dot bioconjugates. *Theranostics* 2012;**2**:769–76.
- 53 Kamila S, McEwan C, Costley D, *et al.* Diagnostic and Therapeutic Applications of Quantum Dots in Nanomedicine. *Top Curr Chem* 2016;**370**:203–24.
- 54 Wang C, Gao X, Su X. In vitro and in vivo imaging with quantum dots. *Anal Bioanal Chem* 2010;**397**:1397–415.
- 55 Wu Y-F, Wu H-C, Kuan C-H, *et al.* Multi-functionalized carbon dots as theranostic nanoagent for gene delivery in lung cancer therapy. *Sci Rep* 2016;**6**:21170.

- 56 Park JH, von Maltzahn G, Ruoslahti E, *et al.* Micellar hybrid nanoparticles for simultaneous magnetofluorescent imaging and drug delivery. *Angew Chem Int Ed Engl* 2008;**47**:7284–8.
- 57 Chen C, Sun S, Gong Y, *et al.* Quantum dots-based molecular classification of breast cancer by quantitative spectroanalysis of hormone receptors and HER2. *Biomaterials* 2011;**32**:7592–9.
- 58 Chen C, Peng J, Xia HS, *et al.* Quantum dots-based immunofluorescence technology for the quantitative determination of HER2 expression in breast cancer. *Biomaterials* 2009;**30**:2912–8.
- 59 Chen C, Xia HS, Gong YP, *et al.* The quantitative detection of total HER2 load by quantum dots and the identification of a new subtype of breast cancer with different 5-year prognosis. *Biomaterials* 2010;**31**:8818–25.
- 60 Liu J, Lau SK, Varma VA, *et al.* Molecular mapping of tumor heterogeneity on clinical tissue specimens with multiplexed quantum dots. *ACS Nano* 2010;**4**:2755–65.
- 61 Ghazani AA, Lee JA, Klostranec J, *et al.* High throughput quantification of protein expression of cancer antigens in tissue microarray using quantum dot nanocrystals. *Nano Lett* 2006;**6**:2881–6.
- 62 Tholouli E, Sweeney E, Barrow E, *et al.* Quantum dots light up pathology. *J Pathol* 2008;**216**:275–85.
- 63 Peng CW, Liu XL, Chen C, *et al.* Patterns of cancer invasion revealed by QDs-based quantitative multiplexed imaging of tumor microenvironment. *Biomaterials* 2011;**32**:2907–17.
- 64 Liu X, Peng C, Chen C, *et al.* Quantum dots-based double-color imaging of HER2 positive breast cancer invasion. *Biochem Biophys Res Commun* 2011;**409**:577–82.
- 65 Yezhelyev M, Al-Hajj A, Morris C, *et al.* In situ molecular profiling of breast cancer biomarkers with multicolor quantum dots. *Adv Mater* 2007;**19**:3146–51.
- 66 Kim S, Lim YT, Soltesz EG, *et al.* Near-infrared fluorescent type II quantum dots for sentinel lymph node mapping. *Nat Biotechnol* 2003;**22**:93–7.
- 67 Wang LW, Peng CW, Chen C, *et al.* Quantum dots-based tissue and in vivo imaging in breast cancer researches: current status and future perspectives. *Breast Cancer Res Treat* 2015;**151**:7–17.
- 68 Hama Y, Koyama Y, Urano Y, *et al.* Simultaneous two-color spectral fluorescence lymphangiography with near infrared quantum dots to map two lymphatic flows from



- the breast and the upper extremity. *Breast Cancer Res Treat* 2007;**103**:23–8.
- 69 Kobayashi H, Hama Y, Koyama Y, *et al.* Simultaneous multicolor imaging of five different lymphatic basins using quantum dots. *Nano Lett* 2007;**7**:1711–6.
- 70 Robe A, Pic E, Lassalle HP, *et al.* Quantum dots in axillary lymph node mapping: biodistribution study in healthy mice. *BMC Cancer* 2008;**8**:111.
- 71 de Boer M, van Deurzen CH, van Dijck JA, *et al.* Micrometastases or isolated tumor cells and the outcome of breast cancer. *N Engl J Med* 2009;**361**:653–63.
- 72 Tallet A, Lambaudie E, Cohen M, *et al.* Locoregional treatment of early breast cancer with isolated tumor cells or micrometastases on sentinel lymph node biopsy. *World J Clin Oncol* 2016;**7**:243–52.
- 73 Ojima T, Kinami S, Nakamura K, *et al.* Advantages of the rapid double-staining method for intraoperative detection of micrometastasis in sentinel lymph nodes. *Oncol Rep* 2013;**30**:1067–72.
- 74 Gonda K, Watanabe TM, Ohuchi N, *et al.* In vivo nano-imaging of membrane dynamics in metastatic tumor cells using quantum dots. *J Biol Chem* 2010;**285**:2750–7.
- 75 Takeda M, Tada H, Higuchi H, *et al.* In vivo single molecular imaging and sentinel node navigation by nanotechnology for molecular targeting drug-delivery systems and tailor-made medicine. *Breast Cancer* 2008;**15**:145–52.
- 76 Kosaka N, Bernardo M, Mitsunaga M, *et al.* MR and optical imaging of early micrometastases in lymph nodes: triple labeling with nano-sized agents yielding distinct signals. *Contrast Media Mol Imaging* 2012;**7**:247–53.
- 77 Ma Q, Nakane Y, Mori Y, *et al.* Multilayered, core/shell nanoprobe based on magnetic ferric oxide particles and quantum dots for multimodality imaging of breast cancer tumors. *Biomaterials* 2012;**33**:8486–94.
- 78 Jing L, Ding K, Kershaw S V, *et al.* Magnetically engineered semiconductor quantum dots as multimodal imaging probes. *Adv Mater* 2014;**26**:6367–86.
- 79 Tan W, Jiang S, Zhang Y. Quantum-dot based nanoparticles for targeted silencing of HER2/neu gene via RNA interference. *Biomaterials* 2007;**28**:1565–71.
- 80 Choi Y, Kim S, Choi M, *et al.* Highly Biocompatible Carbon Nanodots for Simultaneous Bioimaging and Targeted Photodynamic Therapy In Vitro and In Vivo. *Adv Funct Mater* 2014;**24**:5781–9.
- 81 Li F, Park S-J, Ling D, *et al.* Hyaluronic acid-conjugated graphene

- oxide/photosensitizer nanohybrids for cancer targeted photodynamic therapy. *J Mater Chem B* 2013;**1**:1678–86.
- 82 Kuo W-S, Chang C-N, Chang Y-T, *et al.* Gold Nanorods in Photodynamic Therapy, as Hyperthermia Agents, and in Near-Infrared Optical Imaging. *Angew Chemie Int Ed* 2010;**49**:2711–5.
- 83 Obaid G, Chambrier I, Cook MJ, *et al.* Targeting the Oncofetal Thomsen–Friedenreich Disaccharide Using Jacalin-PEG Phthalocyanine Gold Nanoparticles for Photodynamic Cancer Therapy. *Angew Chemie Int Ed* 2012;**51**:6158–62.
- 84 Derycke AS, de Witte PA. Liposomes for photodynamic therapy. *Adv Drug Deliv Rev* 2004;**56**:17–30.
- 85 Zhu Z, Tang Z, Phillips JA, *et al.* Regulation of singlet oxygen generation using single-walled carbon nanotubes. *J Am Chem Soc* 2008;**130**:10856–7.
- 86 Tian B, Wang C, Zhang S, *et al.* Photothermally enhanced photodynamic therapy delivered by nano-graphene oxide. *ACS Nano* 2011;**5**:7000–9.
- 87 Tsay JM, Trzoss M, Shi L, *et al.* Singlet oxygen production by Peptide-coated quantum dot-photosensitizer conjugates. *J Am Chem Soc* 2007;**129**:6865–71.
- 88 Papagiannaros A, Upponi J, Hartner W, *et al.* Quantum dot loaded immunomicelles for tumor imaging. *BMC Med Imaging* 2010;**10**:22.
- 89 Sharman WM, van Lier JE, Allen CM. Targeted photodynamic therapy via receptor mediated delivery systems. *Adv Drug Deliv Rev* 2004;**56**:53–76.
- 90 Verma S, Watt GM, Mai Z, *et al.* Strategies for Enhanced Photodynamic Therapy Effects†. *Photochem Photobiol* 2007;**83**:996–1005.
- 91 Schmitt F, Juillerat-Jeanneret L. Drug targeting strategies for photodynamic therapy. *Anticancer Agents Med Chem* 2012;**12**:500–25.
- 92 Ge J, Lan M, Zhou B, *et al.* A graphene quantum dot photodynamic therapy agent with high singlet oxygen generation. *Nat Commun* 2014;**5**:4596.
- 93 Slamon DJ, Godolphin W, Jones LA, *et al.* Studies of the HER-2/neu proto-oncogene in human breast and ovarian cancer. 1989;**244**:707–12.
- 94 HER2+ Breast Cancer. Herceptin. 2018;**2018**.<http://www.herceptin.com/> (accessed 1 Sep 2018).
- 95 Matsumura Y, Maeda H. A new concept for macromolecular therapeutics in cancer chemotherapy: mechanism of tumoritropic accumulation of proteins and the antitumor

- agent smancs. *Cancer Res* 1986;**46**:6387–92.
- 96 Maeda H, Bharate GY, Daruwalla J. Polymeric drugs for efficient tumor-targeted drug delivery based on EPR-effect. *Eur J Pharm Biopharm* 2009;**71**:409–19.
- 97 Maeda H, Wu J, Sawa T, *et al.* Tumor vascular permeability and the EPR effect in macromolecular therapeutics: a review. *J Control Release* 2000;**65**:271–84.
- 98 Orive G, Santos E, Poncelet D, *et al.* Cell encapsulation: technical and clinical advances. *Trends Pharmacol Sci* 2015;**36**:537–46.
- 99 An D, Chiu A, Flanders JA, *et al.* Designing a retrievable and scalable cell encapsulation device for potential treatment of type 1 diabetes. *Proc Natl Acad Sci U S A* 2018;**115**:E263–72.
- 100 Orive G, Hernandez RM, Gascon AR, *et al.* Cell encapsulation: promise and progress. *Nat Med* 2003;**9**:104–7.
- 101 Gray DW. An overview of the immune system with specific reference to membrane encapsulation and islet transplantation. *Ann N Y Acad Sci* 2001;**944**:226–39.
- 102 Game DS, Lechler RI. Pathways of allorecognition: implications for transplantation tolerance. *Transpl Immunol* 2002;**10**:101–8.
- 103 Nienhuis AW, Nathwani AC, Davidoff AM. Gene Therapy for Hemophilia. *Mol Ther* 2017;**25**:1163–7.
- 104 George LA, Sullivan SK, Giermasz A, *et al.* Hemophilia B Gene Therapy with a High-Specific-Activity Factor IX Variant. *N Engl J Med* 2017;**377**:2215–27.
- 105 Robbins PD, Tahara H, Ghivizzani SC. Viral vectors for gene therapy. *Trends Biotechnol* 1998;**16**:35–40.
- 106 Caspi A, Granek R, Elbaum M. Diffusion and directed motion in cellular transport. *Phys Rev E* 2002;**66**.
- 107 Tada H, Higuchi H, Wanatabe T, *et al.* In vivo real-time tracking of single quantum dots conjugated with monoclonal anti-HER2 antibody in tumors of mice. *Cancer Res* 2007;**67**:1138–44.
- 108 Mazumder MAJ, Fitzpatrick SD, Muirhead B, *et al.* Cell-adhesive thermogelling PNIPAAm/hyaluronic acid cell delivery hydrogels for potential application as minimally invasive retinal therapeutics. *J Biomed Mater Res A* 2012;**100**:1877–87.
- 109 Lechler RI, Sykes M, Thomson AW, *et al.* Organ transplantation--how much of the promise has been realized? *Nat Med* 2005;**11**:605–13.

- 110 Paredes-Juarez GA, Sahasrabudhe NM, Tjoelker RS, *et al.* DAMP production by human islets under low oxygen and nutrients in the presence or absence of an immunisolating-capsule and necrostatin-1. *Sci Rep* 2015;**5**:14623.
- 111 Mofazzal Jahromi MA, Sahandi Zangabad P, Moosavi Basri SM, *et al.* Nanomedicine and advanced technologies for burns: Preventing infection and facilitating wound healing. *Adv Drug Deliv Rev* 2018;**123**:33–64.
- 112 Saghezadeh S, Rinoldi C, Schot M, *et al.* Drug delivery systems and materials for wound healing applications. *Adv Drug Deliv Rev* 2018;**127**:138–66.
- 113 Kirchner C, Liedl T, Kudera S, *et al.* Cytotoxicity of colloidal CdSe and CdSe/ZnS nanoparticles. *Nano Lett* 2005;**5**:331–8.
- 114 Parak W, Boudreau R, Le Gros M, *et al.* Cell Motility and Metastatic Potential Studies Based on Quantum Dot Imaging of Phagokinetic Tracks. *Adv Mater* 2002;**14**:882–5.
- 115 Caspi A, Granek R, Elbaum M. Enhanced diffusion in active intracellular transport. *Phys Rev Lett* 2000;**85**:5655–8.
- 116 Smith A, Nie S. Next-generation quantum dots. *Nat Biotechnol* 2009;**27**:732–3.
- 117 Verkman A. Solute and macromolecule diffusion in cellular aqueous compartments. *Trends Biochem Sci* 2002;**27**:27–33.
- 118 Nabiev I, Mitchell S, Davies A, *et al.* Nonfunctionalized nanocrystals can exploit a cell's active transport machinery delivering them to specific nuclear and cytoplasmic compartments. *Nano Lett* 2007;**7**:3452–61.
- 119 Yong K-T, Roy I, Ding H, *et al.* Biocompatible near-infrared quantum dots as ultrasensitive probes for long term in vivo imaging applications. *Small* 2009;**5**:1997–2004.
- 120 Yang R, Chang L, Wu J-P, *et al.* Persistent tissues kinetics and redistribution of nanoparticles, quantum dot 705, in mice: ICP-MS quantitative assessment. *Environ Heal Perspect* 2007;**115**:1339–43.
- 121 Ishii D, Kinbara K, Ishida Y, *et al.* Chaperonin-mediated stabilization and ATP-triggered release of semiconductor nanoparticles. *Nature* 2003;**423**:628–32.
- 122 Samir TM, Mansour MM, Kazmierczak SC, *et al.* Quantum dots: heralding a brighter future for clinical diagnostics. *Nanomedicine (Lond)* 2012;**7**:1755–69.
- 123 Dubertret B, Skourides P, Norris D, *et al.* In vivo imaging of quantum dots encapsulated in phospholipid micelles. *Science (80- )* 2002;**298**:1759–62.

- 124 Hanaki K, Momo A, Oku T, *et al.* Semiconductor quantum dot/albumin complex is a long-life and highly photostable endosome marker. *Biochem Biophys Res Commun* 2003;**302**:496–501.
- 125 Kloepfer J, Mielke R, Wong M, *et al.* Quantum dots as strain- and metabolism-specific microbiological labels. *Appl Env Microbiol* 2003;**69**:4205–13.
- 126 Smith A, Duan H, Mohs A, *et al.* Bioconjugated quantum dots for in vivo molecular and cellular imaging. *Adv Drug Deliv Rev* 2008;**60**:1226–40.
- 127 Paredes-Juarez GA, de Haan BJ, Faas MM, *et al.* The role of pathogen-associated molecular patterns in inflammatory responses against alginate based microcapsules. *J Control Release* 2013;**172**:983–92.
- 128 Li L, Daou T, Texier I., *et al.* Cadmium-free quantum dots for in vivo imaging. *Chem Mater* 2009;**21**:2422–9.
- 129 Gao J, Chen K, Xie R, *et al.* Ultrasmall Near-infrared non-cadmium quantum dots for in vivo tumor imaging. *Small* 2010;**6**:256–61.
- 130 Pons T, Pic E, Lequeux N, *et al.* Cadmium-free CuInS<sub>2</sub>/ZnS quantum dots for sentinel lymph node imaging with reduced toxicity. *ACS Nano* 2010;**4**:2531–8.
- 131 Schipper M, Iyer G, Koh A, *et al.* Particle size, surface coating, and PEGylation influence the biodistribution of quantum dots in living mice. *Small* 2009;**5**:126–34.
- 132 Ning Z, Gong X, Comin R, *et al.* Quantum-dot-in-perovskite solids. *Nature* 2015;**523**:324–8.
- 133 Lim X. The nanolight revolution is coming. *Nature* 2016;**531**:26–8.
- 134 Yang Q, Wei L, Zheng X, *et al.* Single Particle Dynamic Imaging and Fe<sup>3+</sup> Sensing with Bright Carbon Dots Derived from Bovine Serum Albumin Proteins. *Sci Rep* 2015;**5**:17727.
- 135 Xu X, Ray R, Gu Y, *et al.* Electrophoretic analysis and purification of fluorescent single-walled carbon nanotube fragments. *J Am Chem Soc* 2004;**126**:12736–7.
- 136 Sun YP, Zhou B, Lin Y, *et al.* Quantum-sized carbon dots for bright and colorful photoluminescence. *J Am Chem Soc* 2006;**128**:7756–7.
- 137 Massey M, Wu M, Conroy EM, *et al.* Mind your P's and Q's: the coming of age of semiconducting polymer dots and semiconductor quantum dots in biological applications. *Curr Opin Biotechnol* 2015;**34**:30–40.
- 138 Sun K, Chen H, Wang L, *et al.* Size-dependent property and cell labeling of

- semiconducting polymer dots. *ACS Appl Mater Interfaces* 2014;**6**:10802–12.
- 139 Luo J, Xie Z, Lam JW, *et al.* Aggregation-induced emission of 1-methyl-1,2,3,4,5-pentaphenylsilole. *Chem Commun* 2001;:1740–1.
- 140 Li K, Qin W, Ding D, *et al.* Photostable fluorescent organic dots with aggregation-induced emission (AIE dots) for noninvasive long-term cell tracing. *Sci Rep* 2013;**3**:1150.
- 141 Wang F, Deng R, Wang J, *et al.* Tuning upconversion through energy migration in core-shell nanoparticles. *Nat Mater* 2011;**10**:968–73.
- 142 Lin M, Gao Y, Hornicek F, *et al.* Near-infrared light activated delivery platform for cancer therapy. *Adv Colloid Interface Sci* 2015;**226**:123–37.
- 143 New display techs 'worth \$21BN by 2020'. 2015.<http://optics.org/news/6/11/37> (accessed 15 Sep 2018).
- 144 Sanderson K. Quantum dots go large. *Nature* 2009;**459**:760–1.
- 145 Luo R, Cao Y, Shi P, *et al.* Near-infrared light responsive multi-compartmental hydrogel particles synthesized through droplets assembly induced by superhydrophobic surface. *Small* 2014;**10**:4886–94.
- 146 Qie F, Astolfo A, Wickramaratna M, *et al.* Self-assembled gold coating enhances X-ray imaging of alginate microcapsules. *Nanoscale* 2015;**7**:2480–8.
- 147 Yang F, Zhang X, Maiseyeu A, *et al.* The prolonged survival of fibroblasts with forced lipid catabolism in visceral fat following encapsulation in alginate-poly-L-lysine. *Biomaterials* 2012;**33**:5638–49.
- 148 Barnett BP, Arepally A, Stuber M, *et al.* Synthesis of magnetic resonance-, X-ray- and ultrasound-visible alginate microcapsules for immunoisolation and noninvasive imaging of cellular therapeutics. *Nat Protoc* 2011;**6**:1142–51.
- 149 Santos E, Larzabal L, Calvo A, *et al.* Inactivation of encapsulated cells and their therapeutic effects by means of TGL triple-fusion reporter/biosafety gene. *Biomaterials* 2013;**34**:1442–51.

## APPENDIX A: PUBLICATIONS INCLUDED IN THE THESIS

# Characterization of quantum dot behaviour in live mammalian cells

Ajit Thakur<sup>1</sup>, Cécile Fradin<sup>2</sup>

<sup>1</sup>Department of Biology, McMaster University (ajit.thakur@learnlink.mcmaster.ca)

<sup>2</sup>Department of Physics and Astronomy, McMaster University (fradin@physics.mcmaster.ca)

Received 1 February 2005; Accepted 11 February 2005

## Abstract

Quantum dots are semiconductor nanocrystals with exceptional optical properties. To assess their usefulness as fluorescent probes in living systems, we studied the reaction of culture cells to the presence of different types of quantum dots. The quantum dots were characterized in solution using fluorescence correlation spectroscopy and then loaded into mammalian cells and imaged using time-lapse video microscopy. While the cells seemed unperturbed by the presence of single quantum dots, they clearly identified large quantum dot aggregates as foreign bodies. Our results highlight the importance of preventing quantum dot aggregation by using a proper hydrophilic layer.

## Introduction

Fluorescence is the capacity of some molecules called fluorophores to absorb photons of a certain wavelength and then to re-emit photons at a different wavelength. Fluorescence is an important tool for imaging, allowing fluorophore-tagged molecules to be tracked.

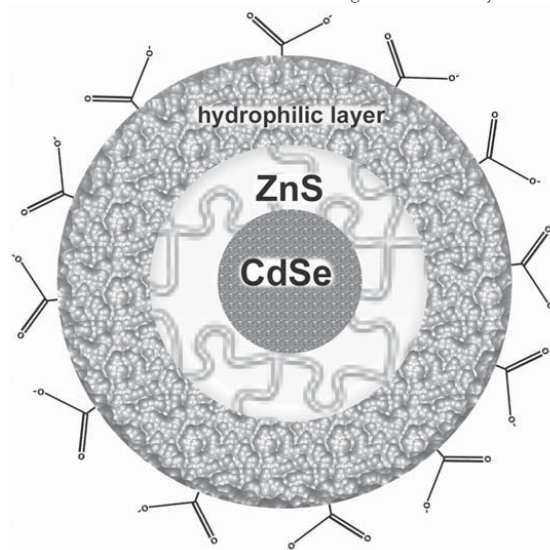
Currently, the dynamics of biological systems are probed primarily using organic fluorophores, which have inherent limitations usually associated with narrow excitation spectra, broad emission spectra, a limited range of colours and a susceptibility to biodegradation. They are also very sensitive to photobleaching, a light-induced inactivation of the fluorophores, which constrains experimental design and data collection procedures. We explored the use of quantum dots (QDs) as a viable alternative to probe live mammalian cells.

The development of QDs as inorganic fluorophores promises to circumvent many of the limitations associated with organic fluorophores<sup>1</sup>. Quantum dots are small (1–10 nm) semiconductor nanocrystals, usually constructed with a CdSe/ZnS core/shell structure<sup>2</sup> (see Figure 1). Quantum dots have very high quantum yields, broad excitation spectra and narrow size-dependent emission spectra that make them perfect for use in single-molecule detection experiments.

Quantum dots are used in experiments where multiple fluorophores need to be detected simultaneously, since a single light source can be used to excite different QDs, whose different emissions are easily separated using standard filter sets. Moreover, QDs display long fluorescence lifetimes and a tendency to blink – two traits that could be useful for the specific identification of single QDs in biological specimens.

In chemical terms, QDs are superior to organic fluorophores due to their customizable size and surface chemistry, allowing multiple molecules to be bound to a single QD. Furthermore, the inorganic composition of QDs makes them resistant to photobleaching and prevents biodegradation in

cells. These properties permit their use as long-term probes in live cells. Overall, QDs have outstanding optical, chemical and physical properties that make them ideal candidates for the investigation of live cell dynamics<sup>1</sup>.



**Figure 1** A diagram of the composition of a single CdSe/ZnS core/shell quantum dot nanocrystal with a hydrophilic layer that provides the COOH groups.



## Ajit Thakur Characterization of quantum dot behaviour in mammalian cells

However, there are several concerns associated with using QDs in biological systems. The semiconductor material is not water-soluble, which means QDs must be coated with a hydrophilic layer prior to use in aqueous environments such as live cells<sup>3</sup>. This layer increases their size and modifies their properties. Secondly, their general optical and chemical properties are not yet fully characterized or understood. For example, although water-soluble QDs have been successfully used in live cells<sup>3-6</sup>, their general compatibility with the cellular environment is not firmly established.

This paper describes observations relating to the reaction of living mammalian cells (rat cells) to the introduction of water-soluble quantum dots with different hydrophilic layers. Our results indicate that a deficient hydrophilic layer promotes aggregation of the QDs in solution. The aggregates not only have compromised optical properties, but also trigger a defensive reaction by the cells, limiting the applicability of QDs as a biological probe.

## Background

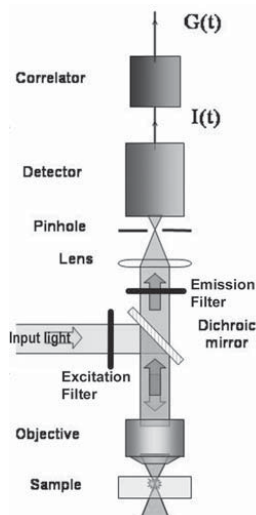
The quantum dots used in this study were acquired from two different companies: Evident Technologies, Inc. (ET) and Quantum Dot Corporation (QDC). The peak emission wavelength of the ET QDs was 600 nm, and that of the QDC QDs was 605 nm. All QDs had a CdSe/ZnS core shell structure, but with different surface chemistries. Two types of QDs were purchased from ET; the first type functionalized with COOH groups (ET600COOH) and the second type with NH<sub>2</sub> groups (ET600NH<sub>2</sub>). Only one type of QDs, functionalized with NH<sub>2</sub> groups, was purchased from QDC (QDC605NH<sub>2</sub>).

The size and tendency to aggregate of these different QDs were characterized by fluorescence correlation spectroscopy (FCS) and time-lapse video microscopy (TLVM). FCS is a technique based on the analysis of fluorescence fluctuations<sup>7,8</sup>. We used FCS to estimate the size of QDs by measuring their diffusion coefficient.

Aggregates are collections of QDs tightly associated with each other mainly through the electrostatic interactions caused by an imperfect hydrophilic layer<sup>2</sup>. Such groupings are expected to behave as large, slow-moving fluorophores with altered fluorescence properties. Hence, they can be easily detected and characterized with FCS studies.

The FCS instrument uses a 543.5 nm helium-neon laser as the excitation light source. The laser beam is tightly focused through a high numerical aperture water immersion objective (60x magnification, 1.33 NA) onto the sample, which is located on a TE2000U Nikon inverted epi-fluorescence microscope (see Figure 2). The sample chambers are made using a glass slide and a coverslip separated by parafilm spacers and sealed with wax. The fluorescence emitted by molecules in the focal volume is collected by the same objective, passed through a dichroic mirror and an emission filter to remove the excitation light, focused through a pinhole to eliminate out-of-focus fluorescence, and detected by a sensitive photomultiplier tube with a time resolution of 60 ns.

In order to characterize the temporal fluctuations of the QDs, the signal is fed into a correlator card that com-



**Figure 2** A schematic of the FCS setup used to measure the radius of different QDs.

putes its autocorrelation function (ACF) using an established algorithm that separates fluctuation events occurring with different characteristic times. Fluorescence fluctuations arise for different reasons, including the diffusion of fluorescent particles across the focal volume. Each kind of fluctuation is reflected in the ACF by a smooth decay rate. In the case of fluctuations due to diffusion, the corresponding decay time observed in the ACF is equal to the average residence time of a fluorescent particle in the focal volume.

Fitting the ACF with an appropriate model allows the extraction of several parameters: the diffusion constant, concentration and molecular brightness of the fluorescent particles. The QD data were fit assuming either that only one species was diffusing in solution (a one-component model) or that two different species were diffusing in solution (a two-component model).

For one fluorescent species diffusing in solution, the autocorrelation function is of the form

$$G(t) = \frac{1/N}{(1+4Dt/w_0^2)\sqrt{1+4Dt/S^2w_0^2}} \left(1 + \frac{Te^{-t/\tau_f}}{1-T}\right), \quad (1)$$

where  $N$  is the average number of fluorescent molecules in the detection volume and  $D$  ( $\mu\text{m}^2/\text{s}$ ) is their diffusion coefficient<sup>8</sup>. The second term uses exponential statistics to account for fast photophysical phenomena, such as blinking due to the existence of a non-fluorescent triplet state of the particles, or for rotation of particles. In the case of blinking,  $T$  is the average fraction of molecules found in the non-fluorescent state and  $\tau_f$  (s) is the characteristic relaxation time associated with the blinking. Both  $S$  and  $w_0$  ( $\mu\text{m}$ ) are constant parameters describing the geometry of the detection volume.

In the case when two different fluorescent species diffuse in solution with respective diffusion coefficients  $D_1$  and  $D_2$  ( $\mu\text{m}^2/\text{s}$ ), the autocorrelation function is

$$G(t) = \left( \frac{1/N_1}{(1+4D_1t/w_0^2)\sqrt{1+4D_1t/S^2w_0^2}} + \frac{1/N_2}{(1+4D_2t/w_0^2)\sqrt{1+4D_2t/S^2w_0^2}} \right) \left(1 + \frac{Te^{-t/\tau_f}}{1-T}\right), \quad (2)$$

where  $N_1$  and  $N_2$  are effective parameters depending on both the concentration and the molecular brightness of the two different fluorophores.

The diffusion coefficients  $D$ ,  $D_1$  and  $D_2$  in Equations (1) and (2) are used to calculate the hydrodynamic radius of the QDs. The hydrodynamic radius is an effective parameter defined as the radius of a sphere with the same diffusion coefficient as the particle in question. The hydrodynamic radius is generally larger than the physical radius of the QD due to the electrostatic attraction of water molecules to the hydrophilic layer of the QDs, which creates a water shell around the QDs. The hydrodynamic radius  $R$  of a molecule is calculated from its diffusion coefficient  $D$  using the Stokes-Einstein relationship,

$$D = \frac{k_B T}{6\pi\eta R}, \quad (3)$$

where  $k_B$  is the Boltzmann constant (J/K),  $T$  is the absolute temperature (K), and  $\eta$  is the viscosity of the solution.

Time-lapse video microscopy (TLVM) uses a fluorescence microscope in conjunction with an image acquisition system to determine the exact location and intensity of light from fluorophores in the field of view at different points in time<sup>4,10,11</sup>. Hence, TLVM can be used to track the motion of fluorophores through the field of view. TLVM was performed on the TE2000U Nikon inverted microscope setup described above, with an infrared-filtered Mercury arc lamp as the light source. Images were collected using a frame transfer camera (Ropers Scientific, MicroMax 512BFT) and accompanying WINView software, and were analyzed using ImageJ and Adobe Photoshop.

The QDs were introduced into the cells using pinocytic loading, a non-invasive method that relies on the natural ability of cells to ingest fluids using its cell membrane. Cells normally ingest fluids by pulling in a portion

## Ajit Thakur Characterization of quantum dot behaviour in mammalian cells

of their cell membrane and pinching the ends to form a fluid-filled compartment called a vesicle. This process allows the cell to intake small soluble molecules along with the fluid.

In order to use this method to introduce the QDs into cells, mammalian Rat1 cells were plated on a coverslip-bottom chambered dish at about 25% confluency approximately 24 hours prior to the experiment. The cells were then incubated for 10 minutes at 37°C in a hypertonic solution containing the QDs.

This hypertonic solution has a high concentration of solutes relative to the cell interior; thus, it dehydrates the cells and accelerates their intake of material (including QDs) from the surrounding hypertonic solution into the membrane-bound vesicles. Next, the cells were placed in a hypotonic solution for 3 minutes. A hypotonic solution has a low concentration of solutes relative to the cell interior so it induces the cells to break these vesicles, releasing the QDs into the cell interior. After that, the cells were allowed to recover in a fresh culture medium – a solution that maintains conditions ideal for cell growth – for at least 7 minutes at 37°C.

We also fluorescently labelled lysosomes – structures used by the cell to degrade organic molecules – to check for the presence of QDs inside them. To label the lysosomes, the cells were further incubated in medium containing 60 nM (nanomoles/liter) of LysoTracker dye for 3 minutes at 37°C and washed with phosphate-buffered saline (PBS), a colourless solution used to maintain a constant pH of 7.4.

Imaging of live cells was performed by TLVM as described above. The cells were placed in PBS, as opposed to a cell growth medium, in order to reduce background fluorescence. The temperature in the sample was maintained at 37°C throughout the experiment by means of a stage and objective heater. A shutter system controlled the excitation light and reduced photodamage. The QDs were excited around 560 nm, and the emission of the QDs was detected around 600 nm using an appropriate filter set and the image acquisition system described above. Similarly, the LysoTracker dye was excited around 480 nm and the emission was detected around 535 nm using a second filter set.

## Results

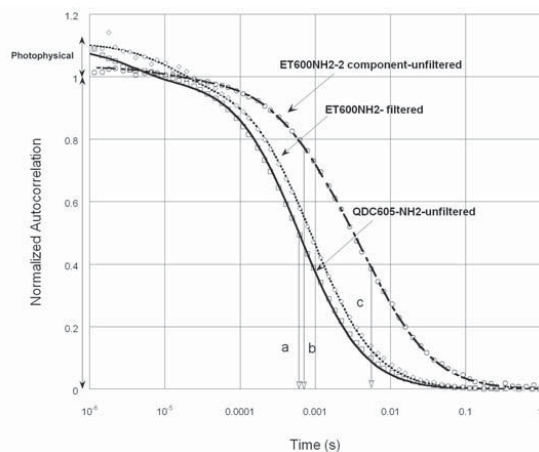
### MEASUREMENT OF THE RADIUS OF THE QUANTUM DOTS

In order to characterize the size of the quantum dots used in this study, FCS data was collected for each of the three types of QDs described above. Some of the recorded autocorrelation functions are shown in Figure 3.

The data obtained for the QDs purchased from the Quantum Dot Corporation were successfully fit using a one-component diffusion model to within an error of approximately 1%. The average particle radius of  $13.9 \pm 0.1$  nm extracted using this model is consistent with the manufacturer's prediction (see Table 1).

Quantum dot type	Radius of the first component (nm)	Radius of the second component (nm)	Brightness per molecule (photons/s)
QDC605NH <sub>2</sub> Unfiltered	$13.9 \pm 0.1$	NA	$62 \pm 1$
ET600NH <sub>2</sub> Filtered	$19.8 \pm 0.1$	NA	$16.0 \pm 0.3$
ET600NH <sub>2</sub> Unfiltered	Fixed at 19.8	$160 \pm 20$	NA
ET600COOH Unfiltered	Fixed at 19.8	$150 \pm 40$	NA

**Table 1** A summary of the FCS data in solution for three types of quantum dots. Unfiltered QDC605NH<sub>2</sub> and filtered ET600NH<sub>2</sub> were fit with a one-component model, while unfiltered ET600NH<sub>2</sub> and unfiltered ET600COOH were fit with a two-component model.



**Figure 3** Autocorrelation functions obtained by FCS for different types of QDs (squares: QDC605NH<sub>2</sub>, circles: ET600NH<sub>2</sub>, diamonds: filtered ET600NH<sub>2</sub>) and fit with Equations (1) or (2). The diffusion of the smaller single QDC605NH<sub>2</sub> quantum dots results in a short diffusion time (a). Two-component modeling of the unfiltered ET600NH<sub>2</sub> QDs gives the diffusion time of the single QDs (b) and that of the aggregates (c). A shift of the ACF decay towards larger time scales, indicating the presence of aggregates, is visible only in the unfiltered ET600NH<sub>2</sub> QDs. A second decay, due to an uncharacterized effect, is indicated by the double headed arrow labeled 'photophysical' at short times for the ACFs of the single QDs only.

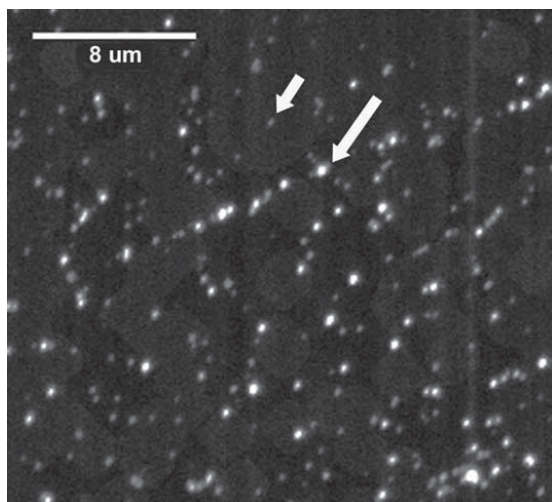
In contrast, the data obtained for the Evident Technologies QDs could not be satisfactorily fit with a one-component model, as shown by a large discrepancy between the experimental autocorrelation function and the fit, which was interpreted as a signature of the presence of aggregates. Using a two-component model yielded better results, determining the aggregate's radius with an error of less than 30%. This two-component model had a fast diffusing component accounting for the presence of single QDs, and a slow diffusing component accounting for the presence of aggregates.

When subjected to an additional 10 minute, 21 000 g centrifugation step (ultra-filtration), the ET QDs exhibited a narrow size distribution with an average radius of  $19.8 \pm 0.1$  nm, in agreement with the manufacturer's specifications (see Table 1). For the fit of the unfiltered ET QD samples, the first species (corresponding to single QDs) was assigned a fixed radius of 19.8 nm by applying the results of the filtered QDs. The diffusion time of the first species was determined within an error of 1% using filtered QDs made of the same material from the same manufacturer. With only one parameter to determine, the radius of the aggregates was estimated at 150 nm (see Table 1). Since it is not expected that aggregates all have exactly the same size, the two-component model was used only as an approximation of the real system.

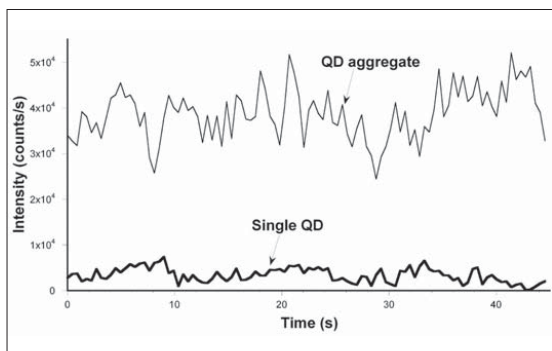
In addition, it was found that the QDC605NH<sub>2</sub> were about 4 times brighter than the ET600NH<sub>2</sub> (see Table 1).

### OBSERVATION OF THE QUANTUM DOTS BLINKING

In order to test the capacity of our fluorescence imaging system to detect single fluorophores, QDs were immobilized in a 5% polyacrylamide gel and imaged using TLVM as described above. A characteristic image is shown in Figure 4a. Some of the bright spots observed in these images had an intensity that greatly fluctuated over time, sometimes reaching an intensity that could not be distinguished from the background intensity (see Figure



**Figure 4a** TLVM image of unfiltered ET600COOH QDs embedded in a 5% polyacrylamide gel. The long arrow points to an aggregate and the short arrow points to a single QD.



**Figure 4b** Fluorescence intensity as a function of time for a particle identified as a single QD (thick black line) and a particle identified as an aggregate (thin grey line). These QDs were embedded in 5% polyacrylamide gel and imaged using TLVM with a time resolution of 100 ms. In each case, the intensity was calculated by adding the intensity value of nine pixels identified as representing the image of the particle. A background value was subtracted from both intensities.

QD type	Directed motion?	Diffusion coefficient ( $\mu\text{m}^2/\text{s}$ )	Velocity ( $\mu\text{m}/\text{s}$ )	Brightness (counts/s)
QDC605NH <sub>2</sub>	No	$0.71 \pm 0.02$	NA	$1800 \pm 40$
Filtered ET600NH <sub>2</sub>	No	$0.19 \pm 0.01$	NA	$1200 \pm 30$
Filtered ET600COOH	Yes	NA	$0.18 - 0.26 \pm 0.02$	$3700 \pm 60$
Unfiltered				

**Table 2** A summary of TLVM data for filtered and unfiltered QDs purchased from QDC and ET, and loaded into Rat1 cells.

4b). This on-and-off fluorescence behaviour, or blinking, is characteristic of single QDs<sup>9,13</sup>.

The intensity of these single QDs did not disappear completely due to the exposure time (100 ms) of the image acquisition system being slightly longer than ideal. However, our ability to distinguish single QDs from aggregate QDs demonstrates the sensitivity of the fluorescence imaging system. Aggregates had a higher absolute intensity, but with lower relative fluctuations in amplitude. Blinking was observed for all three types of QDs studied.

In the FCS curves corresponding to the diffusion of single QDs (QDC605NH<sub>2</sub> and filtered ET600NH<sub>2</sub>), a second decay was observed at microsecond time-scales (see double headed arrow labeled 'photophysical' in Figure 3). This decay was consistently accounted for by the second term in Equations (1) and (2), with an error of less than 7%. This shows that there was a fast photophysical effect, such as blinking due to the non-fluorescent triplet state or rotation, taking place for single QDs that follows exponential statistics as described in the second term of Equations (1) and (2). However, this photophysical effect is different from the blinking effect of single QDs observed by TLVM at longer time-scales, which is known to have power law statistics<sup>12</sup> (see Figure 4b). More work is needed to characterize both of these types of blinking effects.

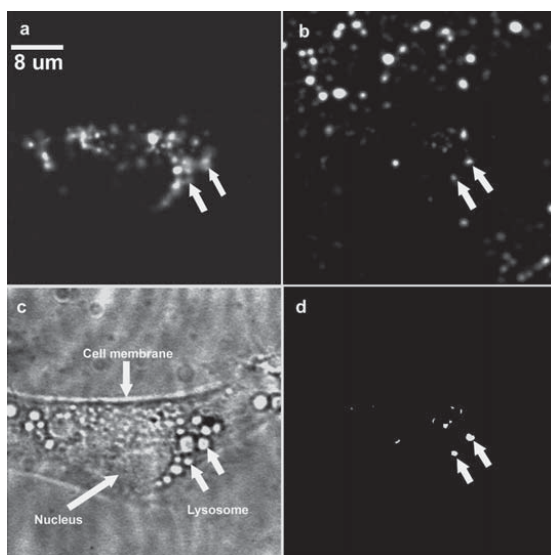
#### CHARACTERIZATION OF THE LOCALIZATION AND MOTION OF QUANTUM DOTS IN LIVE CELLS

In order to study the behaviour of QDs in live cells, each of the three types of dots were introduced into Rat1 cells (mammalian fibroblasts derived from rats) using the pinocytotic loading method described above, and imaged after two hours. Two very different types of behaviour were observed. Aggregated QDs (unfiltered ET600COOH and unfiltered ET600NH<sub>2</sub>) localized into punctuated structures, and did not appear to blink.

We suspected that these structures might be lysosomes – acidic organelles used by cells to degrade organic molecules. In order to test this hypothesis, the cells were imaged after incubation with a LysoTracker dye which stains acidic structures in the cell, particularly lysosomes. Images were taken with different filter sets in order to image either the QDs or the lysosomes for the same cell. The cells recognized both unfiltered ET600COOH and unfiltered ET600NH<sub>2</sub> aggregates, and processed them in similar ways. This indicates that QD aggregates are recognized in cells regardless of their surface composition. Figure 5 illustrates the result of such an experiment, showing that aggregated QDs do indeed colocalize with lysosomes. In contrast, those QDs that behaved as single QDs in solution (QDC605NH<sub>2</sub> and filtered ET600NH<sub>2</sub>) were randomly distributed throughout the cell cytoplasm, did not colocalize with the lysosomes and were blinking (data not shown).

This cellular response to single QDs and aggregates was confirmed by tracking QD motion inside cells. Tracking of QDs was performed by following a QD over time, alternating between the two filter sets described above. Tracking of the unfiltered ET600COOH confirmed that they might be enclosed in lysosomes, as their motion was consistent with the directed motion expected for these organelles. The image sequence in Figure 6 follows the motion of an ET600COOH aggregate. This motion is directed (i.e., it takes place along a linear path) and saltatory (i.e., dwell times are observed where the particles exhibit no visible motion). Given the time elapsed and average displacement between two frames, the average velocity of these QD aggregates was between 0.18 and 0.26  $\mu\text{m}/\text{s}$  (see Table 2). These velocities are consistent with motor protein transport of cargos along microtubules<sup>10,11</sup>.

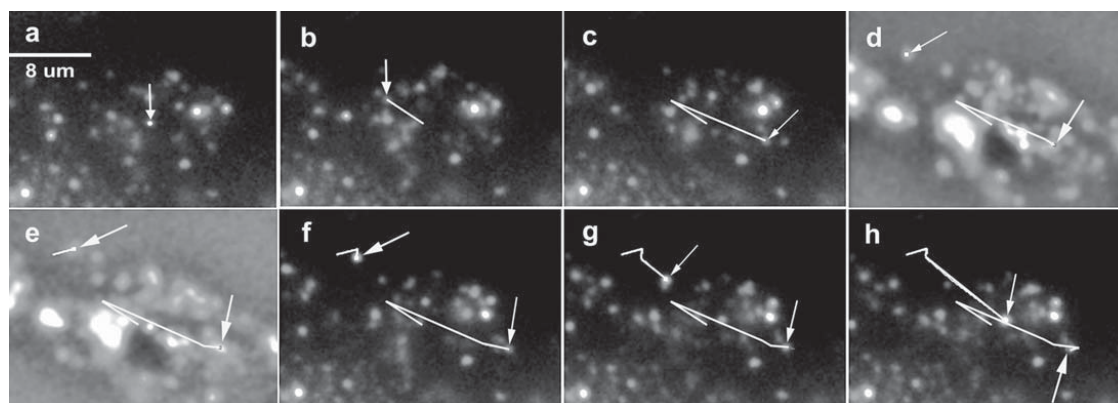
In contrast, tracking of QDC605NH<sub>2</sub> (see Figure 7) and filtered ET600NH<sub>2</sub> (data not included) showed QDs freely diffusing through the cytoplasm, with a trajectory resembling that of Brownian motion. The diffusion coefficients  $D$  of these two types of QDs was determined from their average mean square displacement  $\langle r^2 \rangle$  between two video frames,



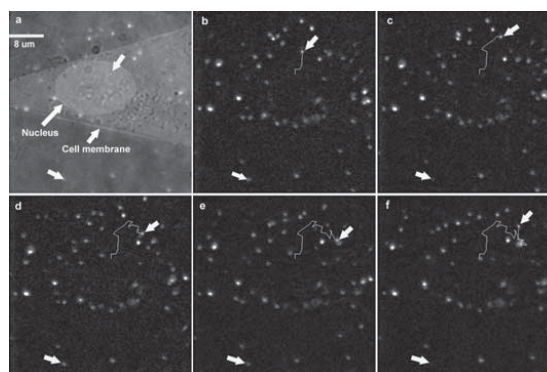
**Figure 5** Different images of the same Rat1 fibroblast cell loaded with unfiltered ET600COOH QDs and stained with a LysoTracker dye. (a) TLVM image showing the position of the lysosomes. (b) TLVM image showing the position of the QDs (note the presence of QDs absorbed on the coverslip outside of the cell). (c) Light microscopy transmission image. (d) TLVM colocalization image showing the overlap of the fluorescence signal coming from the lysosomes and that coming from the QDs. The arrows indicate the position of two lysosomes containing QD aggregates.

$$D = \frac{\langle r^2 \rangle}{4\Delta t} \tag{4}$$

where  $r$  ( $\mu\text{m}$ ) is the displacement and  $\Delta t$  (s) is the time between frames. Image analysis also indicated that QDC605NH<sub>2</sub> was 1.5 times brighter and diffused 3.7 times faster than ET600NH<sub>2</sub> (see Table 2).



**Figure 6** Sequence of TLVM images showing the directed cellular motion (presumably along a microtubule) of two ET600COOH aggregates within lysosomes. The positions of the aggregates are indicated by arrows and their paths by a continuous line. Images (a), (b), (c), (f), (g) and (h) show the fluorescence of the QDs and images (d) and (e) show the fluorescence of the lysosomes. This chronological sequence of images was captured by alternating between two filter sets for imaging QDs and lysosomes.



**Figure 7** Image (a) shows the overlay of a light microscopy transmission image of a Rat1 fibroblast cell with the TLVM image of QDC605NH<sub>2</sub> QDs. Each subsequent image tracks the diffusive motion of a single QD in the cell. The bottom arrow in the image sequence shows the blinking of a single QD attached to the coverslip.

## Discussion

Our comparison of three different types of quantum dots in solution using fluorescence correlation spectroscopy indicates that the surface coating used by Evident Technologies Inc. is more likely to promote aggregation than the coating used by Quantum Dot Corporation, and result in QDs which are significantly dimmer and 30% larger than the Quantum Dot Corporation's QDs.

Consistent with this last observation, we also found that the diffusion coefficient in cells of the QDC QDs was smaller than that of the ET QDs. However, based on the Stokes-Einstein relationship, the diffusion coefficient should be proportional to the radius of the diffusing particle, so that we would expect a 30% difference instead of the observed 73% difference. This discrepancy could be explained either by the binding of QDs to cellular proteins, the aggregation of the ET QDs when placed in the cellular medium, or by the complexity of the cellular environment that invalidate the Stokes-Einstein relationship.



## Ajit Thakur Characterization of quantum dot behaviour in mammalian cells

Our time-lapse video microscopy experiments showed that a tendency to aggregate can have profound consequences for the reaction of cells to QDs irrespective of their surface composition. The Rat1 cells used in this study recognized QD aggregates and packaged them into lysosomes for destruction. However, remarkably, these cells failed to recognize single QDs as foreign objects. These results further demonstrate that single QDs are useful biological probes as long as they have the appropriate surface chemistry to inhibit aggregation and maintain their optical properties.

### Conclusion

Our fluorescence correlation spectroscopy and time-lapse video microscopy experiments show that deficient surface coating promotes aggregation of the QDs in an aqueous environment in vitro. More importantly, colocalization studies and tracking of QDs in living cells indicate that cells recognize aggregates of QDs, but not individual QDs, as foreign bodies. The reaction of cells to QDs is hence immensely dependent upon the surface chemistry of the QDs. An inappropriate surface coating introduces undesirable effects such as aggregation and reduced brightness per molecule and compromises the potential of the QDs to be used as fluorescent probes to study sub-cellular dynamics.

### References

- <sup>1</sup>J.K. Jaiswal and S.M. Simon. "Potentials and pitfalls of fluorescent quantum dots for biological imaging." *Trends in Cell Biology*. (2004) **14**(9), pp. 497–504.
- <sup>2</sup>K. Hanaki, et al. "Semiconductor quantum dot/albumin complex is a long-life and highly photostable endosome marker." *Biochemical and Biophysical Research Communications*. (2003) **302**(3), pp. 496–501.
- <sup>3</sup>W.C. Chan and S. Nie. "Quantum dot bioconjugates for ultrasensitive nonisotopic detection." *Science*. (1998) **281**(5385), pp. 2016–2018.
- <sup>4</sup>M. Dahan, et al. "Diffusion dynamics of glycine receptors revealed by single-quantum dot tracking." *Science*. (2003) **302**(5644), pp. 442–445.
- <sup>5</sup>J.K. Jaiswal, et al. "Long-term multiple color imaging of live cells using quantum dot bioconjugates." *Nature Biotechnology*. (2003) **21**(1), pp. 47–51.
- <sup>6</sup>D.S. Lidke, et al. "Quantum dot ligands provide new insights into erbB/HER receptor-mediated signal transduction." *Nature Biotechnology*. (2004) **22**(2), pp. 198–203.
- <sup>7</sup>D. Magde, E. Elson, and W.W. Webb. "Thermodynamic fluctuations in a reacting system-measurement by fluorescence correlation spectroscopy." *Physical Review Letters* (1972) **29**(11), pp. 705–708.
- <sup>8</sup>M.A. Medina and P. Schwill. "Fluorescence correlation spectroscopy for the detection and study of single molecules in biology." *Bioessays*. (2002) **24**(8), pp. 758–764.
- <sup>9</sup>S. Hohng and T. Ha. "Near-complete suppression of quantum dot blinking in ambient conditions." *Journal of American Chemical Society*. (2004) **126**(5), pp. 1324–1325.
- <sup>10</sup>E. Vignal, et al. "Kinectin is a key effector of RhoG microtubule-dependent cellular activity." *Molecular and Cellular Biology*. (2001) **21**(23), pp. 8022–8034.
- <sup>11</sup>B. Herman and D.F. Albertini. "A time-lapse video image intensification analysis of cytoplasmic organelle movements during endosome translocation." *The Journal of Cell Biology*. (1984) **98**(2), pp. 565–576.
- <sup>12</sup>M. Kuno, et al. "Nonexponential 'blinking' kinetics of single CdSe quantum dots: A universal power law behaviour." *Journal of Chemical Physics*. (2000) **112**(7), pp. 3117–3120.
- <sup>13</sup>M. Kuno, et al. "On/Off fluorescence intermittency of single semiconductor quantum dots." *Journal of Chemical Physics*. (2001) **115**(2), pp. 1028–1040.



**Saint Mary's  
University**  
Halifax, Nova Scotia, Canada

**Department of Astronomy  
and Physics**

### Ph.D. and M.Sc. Programs in Astronomy

- Eleven faculty members in the department, eight of whom have expertise in theoretical astrophysics and observational astronomy
- **Research areas:** stellar evolution, stellar seismology, stellar atmospheres, nuclear astrophysics, MHD astrophysics, extragalactic astronomy, galactic structure, star clusters, interstellar medium, variable stars, star formation, planet formation, and planetary dynamics
- Extensive computational facilities, including those of the Institute for Computational Astrophysics (ICA) and ACEnet
- Full financial support is provided to all full-time students

For more information contact:  
Graduate Coordinator  
Department of Astronomy and Physics  
Saint Mary's University  
Halifax NS B3H 3C3

Phone: (902) 420-5828  
E-mail: [graduate@ap.smu.ca](mailto:graduate@ap.smu.ca)  
URL: [www.ap.smu.ca](http://www.ap.smu.ca)



RESEARCH

Open Access

# Strategies for ocular siRNA delivery: Potential and limitations of non-viral nanocarriers

Ajit Thakur<sup>1\*</sup>, Scott Fitzpatrick<sup>2</sup>, Abeyat Zaman<sup>3</sup>, Kapilan Kugathasan<sup>4</sup>, Ben Muirhead<sup>2</sup>, Gonzalo Hortelano<sup>2,5</sup> and Heather Sheardown<sup>2,6</sup>

## Abstract

Controlling gene expression via small interfering RNA (siRNA) has opened the doors to a plethora of therapeutic possibilities, with many currently in the pipelines of drug development for various ocular diseases. Despite the potential of siRNA technologies, barriers to intracellular delivery significantly limit their clinical efficacy. However, recent progress in the field of drug delivery strongly suggests that targeted manipulation of gene expression via siRNA delivered through nanocarriers can have an enormous impact on improving therapeutic outcomes for ophthalmic applications. Particularly, synthetic nanocarriers have demonstrated their suitability as a customizable multifunctional platform for the targeted intracellular delivery of siRNA and other hydrophilic and hydrophobic drugs in ocular applications. We predict that synthetic nanocarriers will simultaneously increase drug bioavailability, while reducing side effects and the need for repeated intraocular injections. This review will discuss the recent advances in ocular siRNA delivery via non-viral nanocarriers and the potential and limitations of various strategies for the development of a 'universal' siRNA delivery system for clinical applications.

**Keywords:** Biomaterials, siRNA, Drug delivery, Endosomal escape, Nanocarriers, Ocular siRNA delivery, RNAi

## Introduction

### Challenges of posterior segment ophthalmic therapeutics

Pharmaceutical treatment of retinal degenerative diseases affecting the posterior segment of the eye is made challenging by restrictive blood ocular barriers such as the blood aqueous barrier (BAB) and the blood retinal barrier (BRB), which separate the eye from systemic circulation [1]. Additionally, the compartmentalized structure of the eye limits the passage of therapeutics from the anterior chamber to the posterior segment, which houses the light-sensing retina [2]. Finally, once the drug successfully enters the back of the eye, effective clearance mechanisms act to rapidly clear the delivered molecules [2]. In conjunction, these barriers render posterior segment ophthalmic drug delivery particularly challenging. Figure 1 provides a schematic representation of the various physical delivery barriers as well as the clearance mechanisms, which effectively expel drugs that successfully enter the eye.

### Local and systemic routes for drug delivery

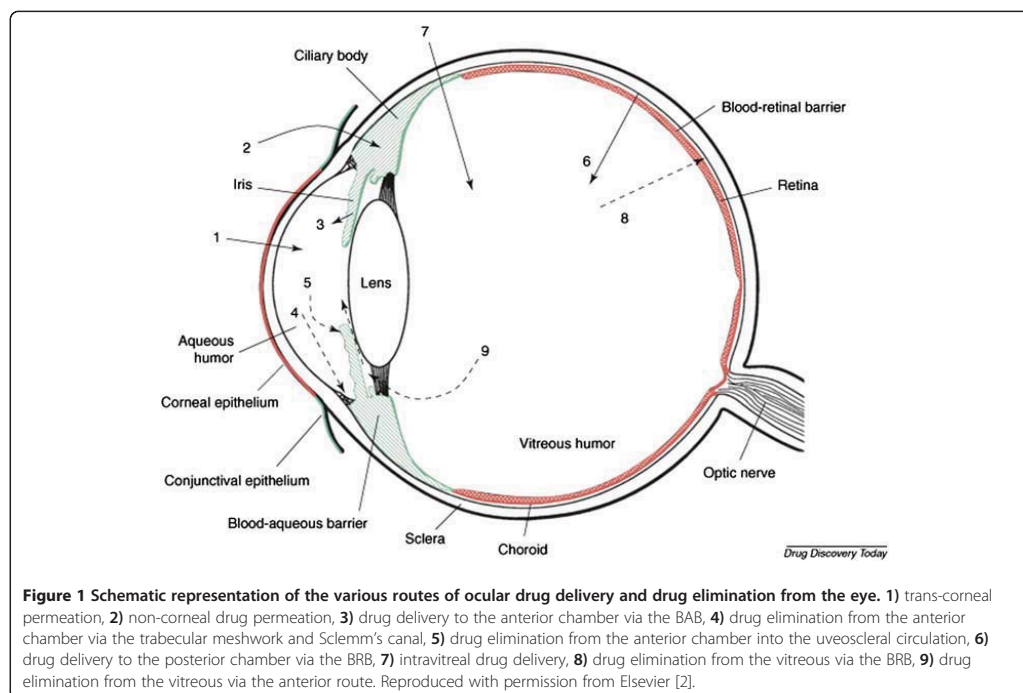
It is estimated that following instillation, only 5% of topically applied drugs enter the anterior chamber of the eye, either through trans-corneal permeation (Figure 1, arrow 1) or non-corneal permeation into the anterior uvea through the conjunctiva and sclera (Figure 1, arrow 2) [2]. Increasing the residence time on the eye through viscous formulation can slightly improve uptake. However, due to the physical barrier created by the corneal and conjunctival epithelium, and the relatively small tear volume (~7  $\mu$ l) available [3], a maximal attainable absorption into the anterior chamber appears to be approximately 10% of the applied dose [4]. Drugs are eliminated from the aqueous humor via aqueous turnover through the Schlemm's canal and trabecular meshwork (Figure 1, arrow 4) and by uptake into systemic circulation through uveoscleral blood flow (Figure 1, arrow 5) [2]. Elimination via the first route occurs through convective flow at a rate of approximately 3  $\mu$ l/min and is independent of drug type. Clearance through uveal blood flow however, is influenced by the ability of the drug to penetrate the endothelial walls of the blood vessels. Thus, lipophilic drugs clear more rapidly than hydrophilic drugs, often

\* Correspondence: thakurajit@gmail.com

<sup>1</sup>Institute of Biomaterials and Biomedical Engineering, University of Toronto, Toronto, ON, Canada

Full list of author information is available at the end of the article





**Figure 1** Schematic representation of the various routes of ocular drug delivery and drug elimination from the eye. 1) trans-corneal permeation, 2) non-corneal drug permeation, 3) drug delivery to the anterior chamber via the BAB, 4) drug elimination from the anterior chamber via the trabecular meshwork and Sclermm's canal, 5) drug elimination from the anterior chamber into the uveoscleral circulation, 6) drug delivery to the posterior chamber via the BRB, 7) intravitreal drug delivery, 8) drug elimination from the vitreous via the BRB, 9) drug elimination from the vitreous via the anterior route. Reproduced with permission from Elsevier [2].

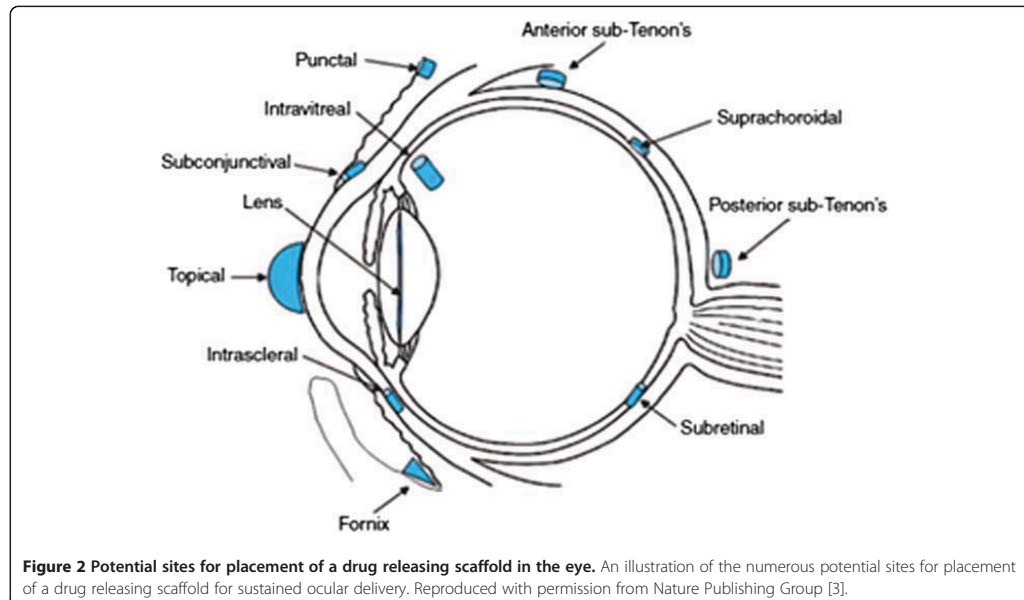
in the range of 20 – 30  $\mu\text{l}/\text{min}$  [2]. Coupled with the physical barrier created by the lens, flow of drugs from the anterior chamber to the posterior segment of the eye is negligible. Therefore, topical drug administration is typically limited to anterior complications. The systemic route is also severely limited in its ability to effectively deliver drugs to the back of the eye. Only an estimated 1 – 2% of compounds delivered via this route successfully cross the BAB (Figure 1, arrow 3) and the BRB (Figure 1, arrow 6) and accumulate within the retinal tissues [1]. With many newly developed pharmaceuticals being protein-based, oral formulations become increasingly difficult to administer, as the drugs need to be protected from degradation within the gastro-intestinal tract. Furthermore, the large concentrations of drug required to achieve therapeutically relevant concentrations within the retinal tissues and the increased potential for off-target interactions makes oral administration an undesirable route of delivery for posterior segment therapies.

There are numerous potential sites surrounding the eye that can house solid drug releasing scaffolds for localized treatment, as illustrated in Figure 2. [3]. Periocular instillation that does not require perforation of the eye wall is desirable as it can minimize invasiveness. However, approaches that utilize this route require drugs to

pass through several layers, including the episclera, sclera, choroid Bruch's membrane and retinal pigment epithelium (RPE), in order to reach the vitreous chamber and the retina [5]. Therefore, due to poor penetration into the posterior segment, this route of delivery lacks clinical significance to date [4]. Subconjunctival injections represent an attractive option for delivery of drugs to the choroid as the sclera is highly permeability to large molecules; however, this approach is less appealing for drug delivery to the retina as the compound must still cross the choroid and the RPE [4].

#### Intravitreal drug delivery

The most efficient means to deliver drugs into the posterior segment is through direct injection into the vitreous cavity (Figure 1, arrow 7) [5]. Using a high-gauge needle, therapeutics may be introduced into the vitreous through simple injection, producing high concentrations of drug locally surrounding the retinal tissues while limiting off-target exposure. However, the concentration of drug is rapidly depleted from the posterior segment via permeation across the BRB (Figure 1, arrow 8) and by diffusion across the vitreous to the anterior chamber (Figure 1, arrow 9), which allows drugs to be cleared through the anterior route [2]. Thus, repeat injections are required, often every 4 – 6 weeks, to maintain



therapeutic concentrations of drug within the posterior segment [6]. Repeat instillations are associated with increasing risk of injection-related complications, such as raised intraocular pressure, vitreous or retinal hemorrhage, retinal detachment, retinal tears, endophthalmitis, cataracts, floaters and transient blurry vision [5]. Rates of endophthalmitis and cataract formation per injection are 0.2% and 0.05% respectively [5]. Repeat injections are also associated with patient discomfort and adherence issues [1]. Therefore, while intravitreal injections have the greatest clinical efficacy, they are also the most risky.

Currently, the most promising solutions to combat the challenges of posterior segment drug delivery are approaches that successfully utilize direct intravitreal delivery and sustain therapeutic concentrations for extended periods of time, thereby decreasing the frequency of intervention. The first commercially successful sustained release intravitreal device for treatment of cytomegalovirus retinitis was Vitrasert (Bausch and Lomb), a non-degrading implant that is surgically implanted at the pars plana [5]. Vitrasert is a US Food and Drug Administration (FDA) approved drug delivery system, which consists of a tablet of ganciclovir coated with polyvinyl alcohol (PVA) and ethylene vinyl acetate (EVA) [5]. The impermeable EVA coating limits the surface area through which ganciclovir can release, forcing drug to diffuse through the small PVA rate-limiting membrane, slowing the release and allowing treatment for a period of 5 to 8 months [1]. However, Vitrasert is a relatively large non-degrading

device and therefore requires an incision for introduction into the vitreous cavity, as well as a secondary surgical intervention for device removal following exhaustion of the drug reservoir. The I-vation (Surmodics) drug delivery system is another example of a non-degrading, sustained intravitreal release device for the treatment of diabetic macular edema. The helical construct was designed to facilitate ease of implantation and removal, maximize surface area available for drug release, and allow sutureless anchorage within the vitreous [7]. The titanium helix is coated with a blend of poly(methyl methacrylate) and EVA, which is loaded with triamcinolone acetonide and provides sustained release for 18–36 months [5,8]. In contrast, the Iluvien (Alimera Sciences) drug delivery system consists of a very small cylindrical polyimide rod loaded with fluocinolone acetonide (FAC) capable of being injected through a 25-gauge needle and releasing low levels of drug for up to 3 years [5,8]. However, as this scaffold is composed of non-degrading materials and is not fixed to the eye wall, it is expected to remain within the patient's orbit following depletion of the drug and is currently under review by the FDA [9]. Ozurdex (Allergan), an FDA approved dexamethasone loaded intravitreal insert for the treatment of macular edema and noninfectious uveitis, is another scaffold capable of introduction into the vitreous via minimally invasive injection using a 22-gauge applicator [7]. However, unlike Iluvien, Ozurdex is composed of degradable poly(lactide-co-glycolide) [10], thereby allowing scaffold degradation and clearance from the eye



and body without the need for secondary surgical intervention [11].

With recent advances in pharmaceuticals, including regulatory approval of multiple pharmacotherapies to treat wet age-related macular degeneration (AMD), and the increasingly elderly demographic at risk of degenerative eye disorders, there has been renewed interest in designing novel drug delivery platforms, particularly nanocarriers, to address the limitations of posterior segment therapeutics [3]. Furthermore, scientific research is continuing to shed new light on the fundamental biochemical pathways implicated in retinal degenerative diseases, which is leading to the discovery of new pharmacological targets and the development of novel therapeutics.

#### **RNA interference and siRNA delivery**

RNA interference (RNAi) is an evolutionarily conserved mechanism that has been observed in most organisms from plants to vertebrates. It is a mechanism that leads to sequence-specific post-transcriptional gene silencing that was first documented in animals by Andrew Fire and Craig Mello in 1998, both of whom subsequently received the Nobel Prize in Physiology or Medicine in 2006 [12,13].

RNA interference can provide a novel therapeutic modality to treat many human diseases by interfering with disease-causing and disease-promoting genes in a sequence-specific manner. Elbashir *et al.* were the first to demonstrate that small interfering RNA (siRNAs) can induce the RNAi pathway in mammalian cells without producing an adverse immune response [14]. This immediately suggested that the RNAi pathway could potentially be manipulated in humans for the treatment of many human diseases. Theoretically, RNAi can be used to selectively alter the expression of any transcribed gene. This new paradigm in therapeutics allows one to address disease states previously considered 'undruggable' [15]. In addition, it creates new opportunities to alter important cellular processes such as cell division and apoptosis, both of which are significantly altered in many cancers [16].

RNA interference is essentially a conserved cellular mechanism that leads to post-transcriptional gene silencing, which can be manipulated for therapeutic applications in humans. Post-transcriptional gene silencing strategies can be broadly divided into four types: 1) single-stranded antisense oligodeoxynucleotides (ODNs)- synthetic molecules that can specifically hybridize with complementary mRNA and sterically inhibit protein translation, 2) ribozymes-catalytically active small RNA molecules that can specifically recognize and cleave single-stranded regions in RNA, 3) microRNA (miRNA)- endogenous, short double-stranded non-coding RNA molecules that play an

important role in health and disease by modulating gene expression, and 4) siRNAs- these 18–25 nucleotide long duplexes are potent activators of the innate immune system that have been shown to initiate sequence-specific post-transcriptional gene silencing. Although all of these strategies can potentially be applied to suppress mRNA translation, it is generally accepted that siRNA technology offers the best combination of specificity, potency and versatility as a therapeutic [15]. In addition, siRNAs are easily synthesized and do not require cellular expression systems or complex protein purification systems, making this technology significantly more cost effective over other small molecule therapeutics [12].

Small-interfering RNA mediates its post-transcriptional gene silencing effects via the RNAi pathway. In brief, when exogenous siRNA duplexes are introduced into mammalian cells, the 5'-end is phosphorylated. This duplex is then assembled into a multiprotein complex called RNA-induced silencing complex (RISC), which includes proteins such as Argonaute 2 (AGO2), Dicer, TRBP (HIV-1 TAR RNA-binding protein) and PACT (dsRNA-binding protein) [17]. The sense strand is then cleaved and unwound, leaving only the antisense strand associated with AGO2. Argonaute 2 is an endonuclease that promotes hybridization of this antisense strand to complementary cellular mRNAs and subsequent cleavage of the mRNA target [17]. This results in 'knocking down' the translation of the target gene [18].

In designing siRNAs, the three most important attributes to be taken into account are: potency (effectiveness of gene silencing at low siRNA concentrations), specificity (minimize homology to other mRNAs) and nuclease stability (resistance against exonuclease and endonuclease activity). Moreover, there are two types of off-target effects that should be minimized: immune stimulation arising from siRNA recognition by the innate immune system, and unintended silencing of genes that share partial homology with the siRNA [15,17].

It is clear that siRNA technology has a great therapeutic potential in medicine. However, one of the major limitations for their application *in vitro* and *in vivo* is the inability of siRNA to cross cell membranes and reach the cytoplasm. The negative charges arising from the phosphate groups in the siRNA backbone electrostatically repel negatively charged cell membranes, therefore limiting siRNA ability to diffuse across cell membranes. In addition, other challenges common to most drug delivery systems, including high molecular weight, short blood half-life, poor specificity and uptake in target tissues, cellular toxicity, and undesirable off-target effects, significantly hamper the successful application of siRNA therapeutics in medicine [12]. Moreover, the intrinsic physical barriers, efficient drug clearance mechanisms and other complexities of ocular tissues such as the

retina and the cornea pose a significant challenge to ocular siRNA delivery. In order to address these problems, several siRNA delivery strategies have been developed for *in vitro* and *in vivo* applications.

Numerous non-viral carriers including natural and synthetic polymers, polyplexes, liposomes, lipoplexes, peptides, dendrimers and free nucleic acid pressurized hydrodynamic injections, as well as virus-based vectors and plasmids encoding for siRNA, have been proposed for siRNA delivery. Although most of these strategies have been attempted with various degrees of success *in vitro* and *in vivo*, strategies for targeted siRNA delivery that are most relevant to ophthalmic applications will be reviewed.

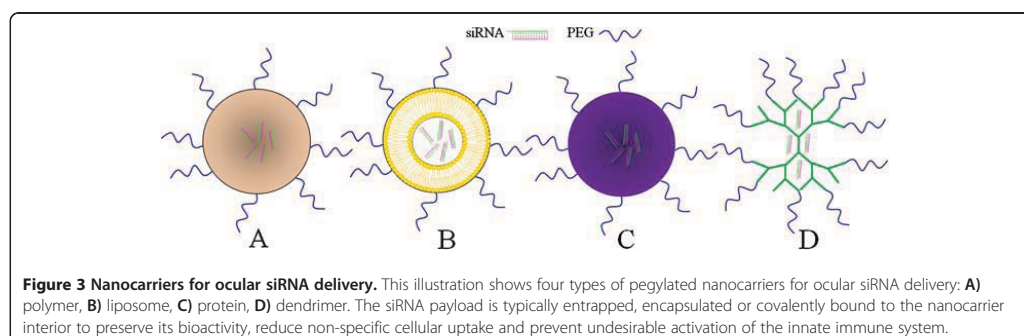
#### Non-viral siRNA delivery systems

In an evolutionary sense, the prevalence of viral infection of cells has likely resulted in highly efficient cellular and systemic defense mechanisms aimed at degrading the naked siRNA molecule *in vivo*. Serum nucleases such as eri-1 [19], renal clearance, and nontargeted bio-distribution make intracellular targets extremely difficult to access. Thus, the most prohibitive barrier faced by siRNA therapeutic strategies is a delivery system [20]. Traditionally, engineered viral particles were tasked with the delivery of nucleic payloads to the eye due to its relative immune-privilege status [21]. Several viral types, particularly adenovirus (Ad), adenoassociated virus (AAV), and lentivirus, are being actively investigated as vectors for RNAi therapy [22]. Exotic modifications of these viral vectors, such as self-complementary AAV (scAAV) or helper-dependent adenovirus (HD-Ad), are the current state-of-the-art in viral delivery, optimizing the properties of earlier generations for ocular gene delivery [23]. However, viral vectors are seen as an acceptable rather than perfect solution to nucleic acid delivery; the potential for mutagenesis, limited loading capacities, appropriate targeting, insertional predictability, high production costs, and adverse immune reactivity severely limit the practicability of viruses [24]. Alternatively, delivering

plasmid vectors expressing siRNA have been attempted with success [25-27], but such DNA-based expression vectors can potentially integrate into the host genome and increase the chances of insertional mutagenesis [26,28]. Engineered, non-viral siRNA delivery systems are being extensively studied because they are relatively safe and can be easily modified with targeting ligands. These artificial vectors are therefore seen as an attractive alternative for viral delivery systems. There are four main types of vectors that are convenient for non-viral siRNA delivery: 1) polymeric, 2) lipid, 3) protein and 4) dendrimeric nanocarrier delivery systems (Figure 3).

#### 1) Polymeric nanocarriers

Although many types of polymers have been used to deliver oligonucleotides, much attention has focused on using cationic polymers for two main reasons: 1) their ability to electrostatically bind siRNA without the need for covalent attachment or encapsulation, and 2) the ability of amine containing cationic polymers to provide endosomal buffering and escape for intracytosolic siRNA delivery. Polyethylenimine (PEI) is perhaps the most investigated synthetic cationic polymer for nucleic acid delivery due to its uniquely high buffering capability at endosomal pH, known as the 'proton sponge' effect, which releases nucleic acid payloads into the cytoplasm after endocytosis [29]. Grayson *et al.* have demonstrated that polyplexes of PEI can effectively deliver siRNA to cells *in vitro* [30]. Kim *et al.* were among the first to employ the use of pegylated (PEG) PEI-siRNA cationic polyplexes targeted against vascular endothelial growth factor-A (VEGFA), vascular endothelial growth factor receptor-1 (VEGFR1) and/or VEGFR2 to significantly reduce herpes simplex virus-induced angiogenesis and stromal keratitis in murine ocular tissues *in vivo* [31]. Notably, these PEG-PEI-siRNA polyplexes were effective in both local and systemic administration of the formulation. Given that PEI-siRNA has been successfully tested *in vivo* for the treatment of



various diseases, it is a promising candidate as a nanocarrier for ocular siRNA delivery [32].

Alternatively, polymeric micelles have been extensively used to deliver nucleic acids. These micelles are colloidal suspensions of amphiphilic copolymers with particle sizes ranging from 5–100 nm [12]. For siRNA delivery, it has been suggested that PEG-polycation diblock copolymers, lactosylated PEG-siRNA and PEG-poly(methacrylic acid) block siRNA encapsulation are well suited [12]. Interestingly, Duan *et al.* have combined the use of a cationic block copolymer (PEI-PEG) with a natural polysaccharide, chitosan, to make 'ternary' nanocarriers to successfully deliver siRNA targeted against the I $\kappa$ B kinase subunit mRNA to human Tenon's capsule fibroblasts *in vitro* [33]. The authors demonstrated that these biodegradable nanocarriers significantly enhanced siRNA delivery and were much less toxic than 25kDa PEI alone. In addition, Ye *et al.* applied these 'ternary' siRNA nanocarriers targeting I $\kappa$ B kinase subunit mRNA *in vivo* in a monkey model of glaucoma filtration surgery and showed that subconjunctival injection of these nanocarriers significantly reduced scar tissue compared to controls [34]. Taken together, these results suggest that pegylated cationic nanocarriers may be suitable candidates for ophthalmic siRNA delivery.

## 2) Lipid nanocarriers

There are many types of lipid-based siRNA delivery systems. However, the most common approaches include: 1) liposomal delivery, where siRNA is encapsulated within vesicles composed of a phospholipid bilayer and 2) lipoplexes, where siRNA complexes with cationic lipids (such as 1,2-dioleoyl-3-trimethylammonium-propane (DOTAP), 1,2-dioleoyl-sn-glycero-3-phosphatidylethanolamine (DOPE), N-[1-(2,3-dioleoyloxy)propyl]-N,N,N-trimethylammonium chloride (DOTMA) and N,N-dioleoyl-N,N-dimethylammonium chloride (DODAC)) and forms nanoscale complexes. Liposomes are probably the most commonly used artificial gene delivery vector since their ability to transport the preproinsulin gene to the liver was demonstrated nearly 30 years ago [35]. Liu *et al.* have successfully demonstrated that 132 nm pegylated liposome-protamine-hyaluronic acid nanocarriers loaded with siRNA targeted against VEGFR1 can not only enhance VEGFR1 knockdown, but also accelerate intracellular delivery to human RPE cells over free siRNA *in vitro* [36]. After intravitreal administration, these nanocarriers were also able to significantly reduce the area of choroidal neovascularization (CNV) in a laser-induced murine CNV model with minimal toxicity, suggesting their suitability for clinical applications [36]. Lipid combinations such as DC-Chol ( $\beta$ -[N-(N',N'-dimethylamino-ethane) carbamoyl]-cholesterol) have also been used to deliver

siRNA successfully and may present opportunities to combine desired features to create novel lipid-based nanocarriers [37].

## 3) Protein nanocarriers

Protein-based siRNA delivery involves the formation of 'proticles,' where proteins are conjugated (electrostatically or covalently) to siRNA for delivery. For example, albumin-protamine-oligonucleotide forms nanocarrier complexes (230–320 nm diameter), which can be safely delivered to cells [38]. Recently, Johnson *et al.* have developed a novel cell-penetrating peptide (CPP) for ocular delivery of small and large molecules, including siRNA, fluorescent probes, plasmid DNA and quantum dots to RPE, photoreceptor and ganglion cells *in vitro* and *in vivo* [39]. Not only do the authors report >50% transgene silencing after peptide-siRNA delivery in human embryonic retinal cells *in vitro*, but they also demonstrate that this peptide-based nanocarrier can transduce approximately 85% of the neural retina within 2 h of intravitreal injection *in vivo* [39]. The lack of toxicity, biodegradability and serum stability of these nanocarriers makes them particularly advantageous as a delivery vehicle [38]. However, protein-based nanocarriers have been known to localize and degrade within endolysosomes after cellular uptake [40]. This problem will likely require additional nanocarrier design considerations such as endosomal escape strategies for its successful application in ocular conditions.

## 4) Dendrimers

Dendrimers represent a group of nanoscale materials that are hyperbranched, monodisperse and have defined molecular weights. Structurally, dendrimers are composed of a central core, repeating units that make up the branches, and surface functional groups [27]. Dendrimers are synthesized in a step-by-step fashion by the sequential addition of repeating units organized in concentric layers, called generations, around the central core. High generation dendrimers have numerous cavities within their hyperbranched structure to allow for the encapsulation of therapeutic agents such as siRNA molecules. The most common dendrimers used for siRNA delivery include poly(amidoamine) (PAMAM) and poly(propylene imine) (PPI) [41]. However, other types of dendrimers composed of amine-containing cationic polymers such as poly-L-lysine have been investigated for ODN (anti-VEGF) delivery to RPE cells *in vitro* [42], and have demonstrated long-term (4–6 months) inhibition (up to 95%) of laser-induced CNV after intravitreal injection in a rat model, without any observable adverse effects [43]. The major advantages of dendrimers include biodegradability, ease of synthesis and customizability, such that they can be synthesized in

**Table 1 Clinical trials involving siRNA therapeutics for ocular diseases**

Company	Drug Name	siRNA target	Carrier	Disease	Delivery method	Clinical status	Reference
Silence Therapeutics/ Quark/Pfizer	PF-655 (formerly REDD14NP and RTP801i)	RTP801/ DNA-damage- inducible transcript 4 gene (DDIT4)	Naked siRNA	AMD	Intravitreal injection	Phase II – completed	(Pfizer 2011a [50]; Quark Pharmaceuticals; 2011a [52]); [55]
Silence Therapeutics/ Quark/Pfizer	PF-655 (formerly REDD14NP and RTP801i)	RTP801/DNA- damage-inducible transcript 4 gene (DDIT4)	Naked siRNA	DME	Intravitreal injection	Phase II – terminated	(Pfizer 2011b [51]; Quark Pharmaceuticals; 2011a [52])
Allergan/Sima	AGN211745 (Sima-027)	VEGFR1	Naked siRNA	AMD	Intravitreal injection	Phase II- terminated	(Allergan 2008 [46]; Allergan 2009) [47]; [48]
Opko Health	Bevasiranib	VEGF	Naked siRNA	Wet AMD	Intravitreal injection	Phase III-terminated	(OpkoHealth 2011 [49])
Syentis	SYL040012	ADRB2	Naked siRNA	Glaucoma, Ocular hypertension	Topical	Phase I-completed	(Syentis 2010 [54])
Quark	QPI-1007	Caspase 2	Naked siRNA	Non-arteritic ischemic optic neuropathy (NAION), Chronic optic nerve atrophy, Glaucoma	Intravitreal injection	Phase I – on going	(Quark Pharmaceuticals 2011b [53])

various sizes and differing number and type of surface functional groups to optimize siRNA delivery. Recently, Agrawal *et al.* have developed dendrimer-conjugated magnetofluorescent nanoworms called 'dendriworms' that significantly enhance intracellular siRNA delivery in a mouse model by optimizing endosomal escape [44]. Alternatively, Han *et al.* have conjugated CPPs, such as HIV transactivator of transcription (Tat), to PAMAM dendrimers for enhanced intracellular siRNA delivery *in vitro* and *in vivo* [45]. Together, these results suggest that dendrimers are ideally suited to serve as nanocarriers, which can be loaded with siRNA and functionalized with PEG and targeting ligands for clinical applications. However, at present, there are no examples of dendrimeric siRNA delivery for ocular applications in the literature.

Despite the multitude of siRNA delivery strategies available, the lack of safe and efficient delivery *in vivo* has limited the clinical translation of siRNA therapeutics. Although a few siRNA therapeutic drugs are currently under clinical trials (Table 1, [46-55]) for ocular applications, none have yet been approved by the FDA. Hence, there is a clear need to develop safe and efficacious methods of ocular siRNA delivery.

#### Chemically modified siRNAs

Various molecular locations on siRNA molecules can be chemically altered to resist hydrolysis and enhance cellular uptake. In order to increase the efficacy of siRNA delivery, much research has focused on increasing the nuclease resistance and therefore serum stability of siRNAs. Nucleases such as eri-1 are involved in the degradation of unmodified siRNA duplexes [19], which have been reported to have a short serum half-life of about 3–5 min. However, it has been shown that siRNA serum half-life can be extended up to 72 h with fully modified duplexes [56].

Among the multitude of possible siRNA modifications, there are two schools of thought regarding the best approach to developing chemically modified siRNA. In one approach, it is believed that extensive chemical modification of siRNA is most likely to lead to the greatest efficacy. For example, Sirna Therapeutics has several patents and products that favour extensive siRNA duplex modifications, where the sense and antisense strands have modified bases (2'-Fluoro-RNA pyrimidines (2'-F-RNA), DNA purines), altered covalent links between the nucleotides (phosphorothioate linkage (PS)) and inverted 5' and 3' abasic end caps [17]. These extensive siRNA modifications translated into increased potency and a much longer serum half-life (48–72 h) in a Hepatitis B virus mouse model [56]. In contrast, the other school of thought is focused on creating stabilized siRNAs with minimal modifications. For example, Alnylam Pharmaceuticals has many siRNA products that are selectively modified (2'-sugar modifications such as 2'-O-methyl or 2'-F-RNA) at

vulnerable sites, such as those susceptible to endonuclease cleavage [15,17,57]. It is important to note that modifications to the RNA backbone can potentially impair siRNA-induced silencing activity, thus many reported modifications have been limited to the sense strand [58,59]. However, the rules for predicting siRNA stability and potency are still unclear since some studies have demonstrated antisense modifications with preserved siRNA functionality [60,61], while other studies have shown sense strand modifications with reduced siRNA efficiency [62,63].

Various chemical modifications to the terminals, backbone, nucleobases and sugars of siRNAs can be implemented to protect the duplex from exonuclease degradation. For example, the phosphodiester (PO<sub>4</sub>) linkages along the RNA backbone can be replaced with PS or boranophosphonate (PB) at the 3' end [64-66]. It has been shown that PS derived oligonucleotides stimulate the physical uptake of siRNA in human cells [67], while siRNAs with PB backbone modifications have less cytotoxicity and a much higher nuclease resistance than native siRNA. Such PB siRNAs are at least 10 times more nuclease resistant than unmodified siRNAs, and have recently been used to treat patients with AMD. The process has reached Phase II clinical trials, and it was found to have no observable side effects [68]. Replacement of sugar moieties at the 2'-hydroxyl group of the ribose backbone with 2'-O-methyl, 2'-fluoro, or 2'-methoxyethyl groups can further improve *in vivo* stability [66,69]. Moreover, various molecules can be conjugated to the 5' or 3' ends of the sense strand, without affecting the activity of the antisense strand needed for silencing [66]. This method can allow for cell specific targeting or visualization of siRNA uptake and distribution by introducing appropriate ligands and fluorophores respectively. However, degradation of these artificially altered siRNA molecules may result in metabolites with unsafe or otherwise unwanted reactivity [66]. Chemical modification of siRNA can increase stability in biological solutions, target specificity and potency [68]. However, the benefits of modification must be measured against the cost and labour of the modification process, as well as its effects on immune stimulation, which are generally difficult to predict and require empirical testing *in vivo*.

#### Immune stimulation and other off-target effects of siRNA delivery

In addition to the gene knockdown effects of the RNAi pathway, there are many other potential consequences that can be initiated by siRNA *in vivo*. Hence, these so called 'off-target effects' need to be considered and evaluated in any siRNA delivery study. For example, it is well known that double stranded RNA (dsRNAs) greater than 30 bp are potent activators of the innate immune response [70]. Although siRNA duplexes are shorter

than 30 bp, many recent studies have begun reporting off-target effects [58,71]. In general, RNAs are recognized by three major types of immunoreceptors: Toll-like Receptors (TLR), protein kinase R (PKR) and helicases. Toll-like receptors are found on cell-surfaces (TLR3) and in endosomes (TLR3,7,8), whereas PKR and helicases (MDA5, RIG-I) are found in the cytoplasm [72,73]. Immune recognition can lead to a host of downstream effects at the cellular level, including cytokine release, interferon response and changes in gene expression. At the whole body level, the use of unmodified siRNAs have been known to induce systemic toxicity, increase serum transaminases, decrease body weight, lymphopenia and piloerection [74]. Thus, proper siRNA design should likely incorporate features to minimize the possibility of undesirable immune activation.

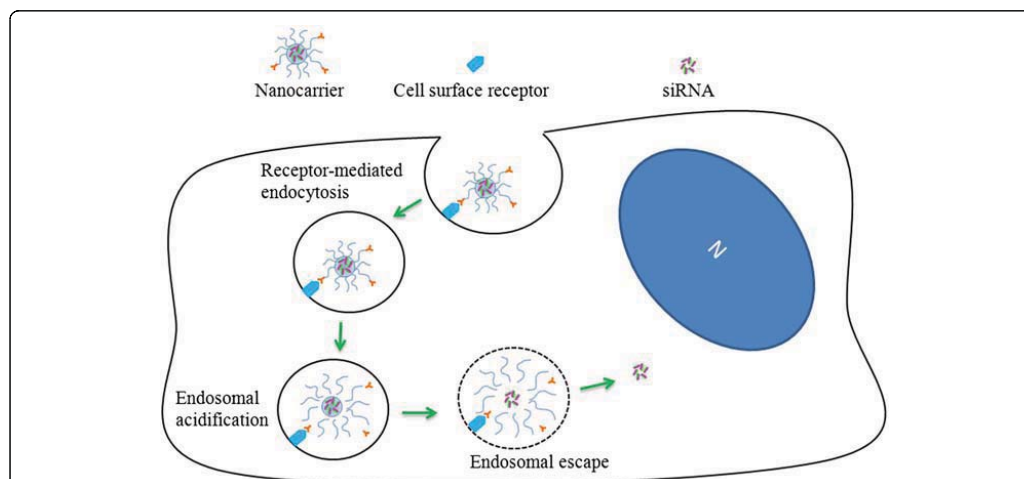
Although immune activation is influenced by many factors such as oligonucleotide length, sequence, chemical modification, mode of delivery and immune cell type involved, it has been previously shown that chemically modified siRNAs can be synthesized so as to reduce their immunostimulatory properties [74]. However, it is interesting to note that immune stimulation may also have desirable consequences, such as anti-angiogenesis via the TLR3 pathway [72]. Although this type of therapeutic immune stimulation may be useful from the standpoint of treating cancer, it can also have potentially severe side-effects [73].

In addition to immune stimulation, other off-target effects can originate from the partial hybridization of the

antisense strand of siRNA with an unintended mRNA. This may lead to the cleavage and subsequent knock-down of the wrong gene [75]. In addition, siRNAs can have their sense strand incorporated into RISC, leading to other off-target effects [75]. To address these problems, siRNA sequences can be carefully selected to minimize complementarity with unwanted mRNAs, and chemically modified siRNAs can be used to increase the selective incorporation of the antisense strand into RISC [62,76]. This highlights the importance of proper siRNA design in mediating target gene knockdown.

#### Cellular uptake of nanocarriers and endosomal escape strategies

Cells can uptake nanocarriers in many ways, including phagocytosis, macropinocytosis, clathrin-mediated endocytosis, non-clathrin-mediated endocytosis and caveolin-mediated uptake [77]. Each of these pathways delivers nanocarriers to specific cellular compartments, which may help or hinder drugs (intracellular, membrane-impermeable type) from reaching their target site. For example, cationic-lipid-DNA complexes and nanocarriers with ligands for glycoreceptors are internalized via clathrin-mediated endocytosis and are destined for the lysosomal compartment (Figure 4) [77]. In contrast, nanocarriers with ligands such as albumin, folic acids and cholesterol are taken up via caveolin-mediated endocytosis, while cell-penetrating peptide (CPP) ligands such as the HIV transactivator of transcription (Tat), facilitate uptake via macropinocytosis [78,79]. In addition to the surface ligand, the size



**Figure 4 Nanocarrier uptake and intracellular siRNA delivery.** This illustration shows that uptake of antibody targeted nanocarriers (10–100 nm) occurs via receptor-mediated endocytosis. The key step in cytoplasmic siRNA delivery involves low pH-triggered nanocarrier disassembly and endosomal escape. A 'smart' nanocarrier can induce endosomal escape by lysing or fusing with endolysosomes upon acidification. The pH change can also be used to trigger the dissociation of the nanocarrier, therefore releasing the siRNA cargo into the cytosol.



and shape of nanocarriers can also influence the mechanism and rate of uptake. Previous nanocarrier uptake studies by Rejman *et al.* have shown that untargeted particles up to 200 nm are exclusively internalized via clathrin-mediated endocytosis, while larger particles enter via a caveolin-dependent pathway [80]. Furthermore, they report an inverse correlation between particle size and rate of uptake. For example, as the particle size was raised from 50 nm to 100 nm, internalization was diminished by 3–4 times. Interestingly, their data also suggests that cells have an upper limit for the size of internalized particles, since 1  $\mu$ m particles were not taken up into mouse melanoma B16 cells *in vitro* [80].

After internalization of nanocarriers into cells, many studies have shown that large fractions of these nanocarriers can remain sequestered in trafficking vesicles and endolysosomes [81]. This implies that some types of nanocarriers may not be suitable for delivering membrane-impermeable therapeutics (such as siRNA) to intracellular targets. Moreover, a lysosomal localization of unmodified naked siRNA will likely result in the degradation of siRNA [79]. Hence, much research has focused on intracellular delivery strategies such as cationic lipid transfection, microinjection and electroporation [82]. However, most of these strategies are limited to *in vitro* conditions due to their invasiveness, variable transfection efficiency, complexity of the procedure and potential for altering/disrupting cellular function. Recent efforts have demonstrated that endosomal escape strategies can be incorporated into nanocarrier design to significantly enhance cytosolic delivery of siRNA [83]. Most commonly, CPPs, pH responsive polymers, fusogenic peptide sequences and hydrophobic molecules have been used for nanocarrier endosomal escape [83]. Nanocarriers functionalized with CPPs such as the T<sub>4</sub>T, VP22, penetratin and polyarginine have been shown to permeate through the plasma membrane for direct cytoplasmic delivery [83–86]. Alternatively, other pH-responsive approaches tend to induce the ‘proton-sponge effect’ for endosomal escape via the clever use of cationic protonable amine-containing polymers such as PEI [87]. In this approach, PEI acts as a buffer against endolysosomal acidification and causes the osmotic swelling and rupture of endolysosomes, releasing the nanocarriers into the cytosol (Figure 4) [88]. In contrast, other approaches attempt to conjugate drugs to fusogenic peptide sequences, such as GALA and KALA, or hydrophobic molecules such that the nanocarrier can traverse membranes [83]. For example, cholesterol-tagging has been shown to improve cytosolic delivery of siRNA with minimal cytotoxicity [89].

Interestingly, lipid-based nanocarriers can also be engineered to fuse with cell membranes, either avoiding endocytosis completely or escaping endolysosomes without

inducing endolysosomal lysis. Although some studies suggest that a net positive surface charge and a high cationic lipid/siRNA molar charge ratio are important factors required to facilitate efficient membrane fusion with lipid-based nanocarriers, it has been reported that these factors also seem to significantly increase toxicity [90]. Recently, Leal *et al.* have reported the development of cationic liposome (CL)-siRNA complexes with novel cubic phase nanostructures, which offer a novel solution to lipid based delivery. Cubic phase lipid delivery systems readily fuse with cell membranes due to their high charge density and positive Gaussian modulus, delivering their cargo through transiently induced pores in the endosomal membrane, which results in highly efficient gene silencing *in vitro* with low toxicity [91,92]. In contrast, some studies have successfully employed non-invasive physical methods to enhance intracellular delivery of siRNA. For example, Du *et al.* recently demonstrated that simultaneous administration of low intensity ultrasound or 15–20% microbubbles can safely enhance the delivery efficiency of siRNA-loaded polymeric nanocarriers to rat RPE-J cells *in vitro* [93]. It is likely that a combination of approaches will need to be tested to determine the optimal strategy for endosomal escape for ocular siRNA delivery.

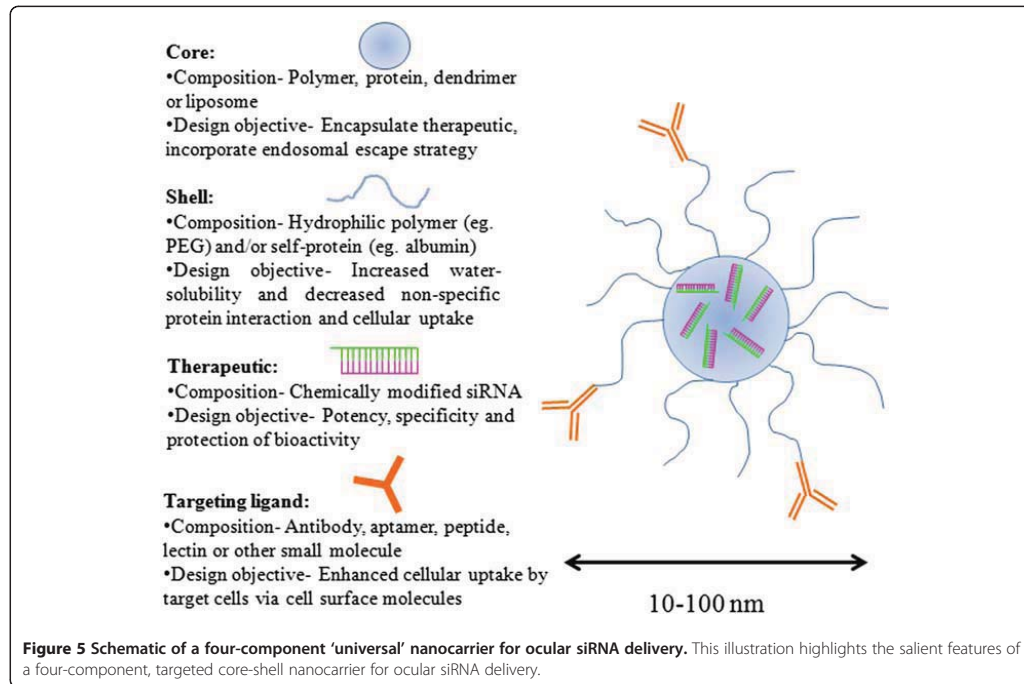
#### **Development of a ‘universal’ nanocarrier for ocular siRNA delivery**

To achieve intracellular ocular siRNA delivery via intravitreal injection, a rational design of a nanocarrier is required that is capable of overcoming the unique biological barriers present in the eye. A review of the literature suggests that several important features including targeting, stealth, siRNA incorporation, size, shape and surface characteristics will have to be taken into consideration for the development of a ‘universal’ nanocarrier for ocular siRNA delivery (Table 2). Turchinovich *et al.* recently demonstrated efficient siRNA delivery into mouse retina *in vivo* using a commercially available transfection reagent [94]. However, this non-targeted method mainly transfected the retinal ganglion cell layer. This suggests that it is likely necessary to use targeting molecules on nanocarriers to control the specific retinal cell type being targeted for transfection. Other studies by Aggarwal *et al.* have shown that nanocarriers exposed to biological fluids in host tissues such as serum are immediately coated with opsonins and other host proteins, creating a ‘molecular signature’ that determines the internalization pathway and fate of nanocarriers taken up by phagocytic cells [95]. Given these observations, many approaches to shield the nanocarriers from such host-induced modification have been developed, among which, a hydrophilic coat of PEG has demonstrated its effectiveness *in vivo*. These PEG coated ‘stealth’ nanocarriers have been shown to significantly reduce non-

**Table 2 Literature review of ocular siRNA nanocarrier delivery**

Target	Carrier	Disease	Model	Delivery method	Results	Implications for ocular diseases	Reference
IKKβ kinase beta (IKKβ)	Cationic nano-copolymers C5-g-(PEI-b-mPEG)	Glaucoma filtration surgery	Rhesus monkey	Subconjunctival injection	Marked reduction in subconjunctival scarring with siRNA treatment in monkeys with trabeculectomy; higher blebs with siRNA compared to PBS treatment; less fibrosis and less destruction of local tissue in siRNA-treated eyes	Improved surgical outcome in glaucoma filtration surgery (less scarring)	[34]
IKKβ kinase beta (IKKβ)	Cationic nano-copolymers C5-g-(PEI-b-mPEG)	Glaucoma filtration surgery	Human	<i>In vitro</i> transfection	Downregulation of IKKβ at the mRNA and protein levels; nuclear factor-κB (NF-κB) inhibited in human Tenon's capsule fibroblasts	Decreased scar formation following glaucoma filtration surgery	[33]
VEGFR1	PEGylated liposome-protamine-hyaluronic acid nanoparticles (PEG-LPH-NP)	Choroidal neo-vascularization	Human RPE cells (ARPE19) and rats	Intravitreal injection	Reduced laser-induced CNV area in rats by PEG-LPH-NP-5 nanoparticles (anti-VEGFR1 siRNA) compared with naked siRNA and PEG-LPH-NP (negative siRNA); downregulated VEGFR1 expression in human RPE cells with siRNA compared to naked siRNA and control group; no significant retinal toxicity	Delivery of siRNA to decrease CNV with low toxicity	[36]
Non-specific commercial siRNA	Transit-TKO transfection reagent	Healthy mice	Mouse	Intravitreal injection	Combination of siRNA with Transit-TKO transfection reagent penetrated through the inner limiting membrane into the retina and accumulated in ganglion cell layer	Uniform delivery to retina through intravitreal injections of siRNA using commercial reagents	[94]





specific cellular uptake and opsonization by phagocytic cells [96].

Moreover, the use of a nanocarrier allows for the control of immune stimulation. Kleinman *et al.* have shown that siRNA can directly mediate CNV suppression *in vivo* via a non-RNAi mediated mechanism involving cell-surface receptor TLR-3 [72]. A therapeutic siRNA shielded from the ocular environment can perhaps avoid such immune stimulation effects of siRNA. However, in some cases, it might be desirable to induce a potentially beneficial immune stimulation effect such as angiogenesis suppression. Given the versatility of nanocarrier systems, it is likely possible to design a carrier that exposes chemically modified, stabilized siRNA to ocular fluids to mediate innate immune stimulation and trigger the TLR-3 pathway for angiogenesis suppression.

A review of successful siRNA delivery nanocarriers *in vivo* strongly suggests that a four component core-shell delivery system is ideal: 1) core- composed of a biodegradable material that entraps, encapsulates or covalently binds siRNA, 2) shell- composed of a hydrophilic polymer such as PEG or a self-protein such as albumin for stability, protection and surface charge modification, 3) drug- chemically modified siRNA for enhanced stability, potency, specificity and efficacy, 4) targeting ligand- antibody,

aptamer, peptide, lectin or other small molecules present on the nanocarrier surface for selective delivery to target cells (Figure 5). In addition, the size, shape and surface characteristics of the nanocarrier are key elements that control their biological interactions. Although the ideal size and shape of nanocarriers for ocular drug delivery have not been systematically tested, the diffusion of nanocarriers through solid tumor models suggest that smaller carriers are preferred over larger ones. Wong *et al.* have recently provided proof-of-principle that gelatin nanocarriers can be designed to change their particle size from 100 nm to 10 nm upon reaching the tumor microenvironment, responding to locally produced matrix metalloproteinase-2 (MMP-2), and can thus penetrate deeper into the tumor tissue [97]. Although most studies involving nanocarrier biodistribution and cellular uptake have been elucidated using spherical nanocarriers, recent studies suggest that the shape of nanocarriers can significantly influence their biological interactions [79,98]. Particularly, a recent study showed that positively charged cylindrical particles with an aspect ratio of 3 (150 nm x 450 nm) were internalized four times more rapidly by HeLa cells than cylindrical particles with an aspect ratio of 1 (200 nm x 200 nm) [98]. This suggests that it is important to consider the size as well as the shape of the nanocarrier in their design. Nanocarrier

biodistribution and uptake in biological systems can also be controlled by manipulating their surface characteristics. The predominant strategy for improving the stability of nanocarriers in biological solutions has involved the grafting of PEG to the surface to render them more hydrophilic and neutral in charge [79]. Some studies suggest that the addition of self-proteins such as albumin via adsorption or covalent modification may reduce non-specific cellular uptake and opsonization [99,100]. Taken together, these data suggest that it is important to optimize the size, shape and surface characteristics for the development of a 'universal' nanocarrier for ocular siRNA delivery.

The proposed four-component nanocarrier system provides a customizable platform for the development of a 'smart' drug delivery system that can be engineered to enhance endosomal escape, control siRNA release intracellularly and manipulate the innate immune response. Particularly, a core-shell nanocarrier structure allows for the incorporation of specific endosomal escape strategies, which can be activated upon endocytosis. For example, the core and shell components can be joined with a cleavable linker that is sensitive to endolysosomal stimuli such as acidic pH and acid-activated proteases. This design effectively allows for the de-shielding of the nanocarrier core, containing siRNA, to induce endosomal destabilization, or to directly traverse the endosomal membrane if the core has a hydrophobic composition. The reducing environment of the cytosol can also be used to further stimulate the dissociation of siRNA from the nanocarrier core via the incorporation of disulphide bonds. The first successful systemic delivery of siRNA via a targeted nanocarrier in humans serves to confirm these important parameters in nanocarrier design [101].

### Conclusions and future directions

Given that we currently lack an ideal siRNA delivery system for ocular disorders, it is instructive to consider the nucleotide delivery strategies found in nature. For example, viruses are essentially targeted biological nanocarriers for the local or systemic delivery of nucleic acids, known to be the causative agents of various human diseases. A virion is indeed a smart nanocarrier, with several key features: environmental stability, monodispersity, bioresponsiveness, biodegradability, immune modulation properties, endosomal escape capabilities, intracellular replicative capacity, and targeted and localized DNA/RNA intracellular delivery to specific cells for controlling gene expression. To this extent, Breitbach *et al.* have recently shown that a modified oncolytic pox virus administered intravenously in human subjects can selectively target cancer cells in solid tumors, without any observable clinical effects on normal cells [102]. This 300 nm enveloped virus delivered ds-DNA to target cells in a dose-dependent manner, similar to that observed in the recent Phase I clinical trial with siRNA-

nanocarrier technology [101]. A nature-inspired nanocarrier design can potentially provide structural insights into developing the optimal solutions to some of the major barriers in ocular and systemic siRNA delivery.

Many groups have employed 'smart' nanocarriers or 'synthetic viruses' that mimic isolated aspects of viral nucleotide delivery with varying degrees of success. For example, Hu *et al.* developed a pH-responsive core-shell nanocarrier designed to release various cargos including proteins, viral particles and siRNA under endosomal acidification [103]. However, most of these single-stimuli responsive nanocarriers are focused on either drug delivery or for diagnostic purposes (imaging and detection), without the ability to combine such useful features. Although multiple stimuli-responsive nucleotide delivery systems are currently under development to address this challenge, a general strategy for intracellular nucleotide delivery has not yet been established [104]. This may be due to the fact that nucleotide delivery systems vary greatly in their composition, such that combining beneficial features of two different nucleotide delivery systems into a hybrid system may not always be possible. In designing a nucleotide delivery system, it is instructive to note that viruses sequentially deploy specific strategies to overcome each barrier at the tissue and cellular level for successful intracellular nucleotide delivery. It follows that any clinically viable nucleotide delivery system will have to take into account the common barriers to siRNA delivery and incorporate specific strategies to overcome each of these barriers, while being flexible enough to combine features that can be adapted to several ocular conditions.

We envision that the ultimate ocular siRNA delivery system would incorporate a combination of nature-inspired desirable features: a biodegradable, multiple stimuli-responsive nanocarrier for controlled and localized siRNA release targeted to specific cell types for manipulating gene expression of specific genes. When combined with a drug delivery device, such a 'smart' nucleotide delivery system would not only address the current challenges of ocular siRNA delivery, with improved biodistribution, bioavailability and reduced toxicity, but also improve therapeutic outcomes for the patient.

### Abbreviations

AAV: Adenoassociated virus; Ad: Adenovirus; AMD: Age-related macular degeneration; AGO2: Argonaute 2; BAB: Blood aqueous barrier; BRB: Blood retinal barrier; CNV: Choroidal neovascularization; CPP: Cell-penetrating peptide; DC-Chol: (3 $\beta$ -[N,N'-dimethylamino-ethane]carbamoyl]-cholesterol; DODAC: N,N-dioleoyl-N,N-dimethylammonium chloride; DOPE: 1,2-dioleoyl-sn-glycero-3-phosphatidylethanolamine; DOTAP: 1,2-dioleoyl-3-trimethylammonium-propane; DOTMA: N-[1-(2,3-dioleoyloxy)propyl]-N,N,N-trimethylammonium chloride; dsRNAs: Double stranded RNAs; EVA: Ethylene vinyl acetate; FAC: Fluocinolone acetonide; FDA: US Food and Drug Administration; 2'-F-RNA: 2'-Fluoro-RNA; HD-Ad: Helper-dependent adenovirus; miRNA: microRNA; MMP-2: Matrix metalloproteinase-2; ODNs: Oligodeoxynucleotides; PACT: dsRNA-binding protein; PAMAM: Poly(amidoamine); PB: Boranophosphonate; PEG: Polyethylene glycol; PEI: Polyethylenimine; PKR: Protein kinase R; PO<sub>4</sub>: Phosphodiester; PPI: Poly

(propylene imine); PS: Phosphorothioate linkage; PVA: Polyvinyl alcohol; RISC: RNA-induced silencing complex; RNAi: RNA interference; RPE: Retinal pigment epithelium; scAAV: Self-complementary AAV; siRNA: Small interfering RNA; Tat: HIV transactivator of transcription; TLR: Toll-like Receptors; TRBP: HIV-1 TAR RNA-binding protein; VEGFA: Vascular endothelial growth factor-A; VEGFR1: Vascular endothelial growth factor receptor-1.

#### Competing interests

No competing interests to declare.

#### Authors' contributions

AT, SF, AZ, KK and BM contributed towards writing and editing the manuscript. GH and HS critically evaluated the manuscript for publication. All authors read and approved the final manuscript.

#### Authors' information

No information to share.

#### Acknowledgements

We would like to thank Prof. Mark Eiteman and the Journal of Biological Engineering for generously waiving the manuscript publication fees.

#### Author details

<sup>1</sup>Institute of Biomaterials and Biomedical Engineering, University of Toronto, Toronto, ON, Canada. <sup>2</sup>School of Biomedical Engineering, McMaster University, Hamilton, ON L8N 3Z5, Canada. <sup>3</sup>Faculty of Medicine, University of Manitoba, Winnipeg, MB, Canada. <sup>4</sup>Faculty of Medicine, University of Toronto, Toronto, ON, Canada. <sup>5</sup>Department of Pathology & Molecular Medicine, McMaster University, Hamilton, ON L8N 3Z5, Canada. <sup>6</sup>Department of Chemical Engineering, McMaster University, Hamilton, ON L8N 3Z5, Canada.

Received: 11 November 2011 Accepted: 26 April 2012  
Published: 11 June 2012

#### References

- Duvvuri S, Majumdar S, Mitra AK: **Drug delivery to the retina: challenges and opportunities.** *Expert Opin Biol Ther* 2003, **3**:45–56.
- Del Amo EM, Urtti A: **Current and future ophthalmic drug delivery systems. A shift to the posterior segment.** *Drug Discov Today* 2008, **13**:135–143.
- Novack GD: **Ophthalmic drug delivery: development and regulatory considerations.** *Clin Pharmacol Ther* 2009, **85**:539–543.
- Urtti A: **Challenges and obstacles of ocular pharmacokinetics and drug delivery.** *Adv Drug Deliv Rev* 2006, **58**:1131–1135.
- Edelhauser HF, Rowe-Rendleman CL, Robinson MR, Dawson DG, Chader GJ, Grossniklaus HE, Rittenhouse KD, Wilson CG, Weber DA, Kuppermann BD, et al: **Ophthalmic drug delivery systems for the treatment of retinal diseases: basic research to clinical applications.** *Invest Ophthalmol Vis Sci* 2010, **51**:5403–5420.
- Kang Derwent JJ, Mieler WF: **Thermoresponsive hydrogels as a new ocular drug delivery platform to the posterior segment of the eye.** *Trans Am Ophthalmol Soc* 2008, **106**:206–213.
- Lee SS, Robinson MR: **Novel drug delivery systems for retinal diseases. A review.** *Ophthalmic Res* 2009, **41**:124–135.
- Kuno N, Fujii S: **Biodegradable intraocular therapies for retinal disorders: progress to date.** *Drugs Aging* 2010, **27**:117–134.
- Campochiaro PA, Brown DM, Pearson A, Ciulla T, Boyer D, Holz FG, Tolentino M, Gupta A, Duarte L, Madreperla S, et al: **Long-term benefit of sustained-delivery fluocinolone acetonide vitreous inserts for diabetic macular edema.** *Ophthalmology* 2011, **118**:626–635. e622.
- London NJ, Chiang A, Haller JA: **The dexamethasone drug delivery system: indications and evidence.** *Adv Ther* 2011, **28**:351–366.
- Eljarrat-Binstock E, Pe'er J, Domb AJ: **New techniques for drug delivery to the posterior eye segment.** *Pharm Res* 2010, **27**:530–543.
- Reischl D, Zimmer A: **Drug delivery of siRNA therapeutics: potentials and limits of nanosystems.** *Nanomedicine: Nanotechnology, Biology and Medicine* 2009, **5**:8–20.
- Fire A, Xu S, Montgomery MK, Kostas SA, Driver SE, Mello CC: **Potent and specific genetic interference by double-stranded RNA in caenorhabditis elegans.** *Nature* 1998, **391**:806–811.
- Elbashir S, Harborth J, Lendeckel W, Yalcin A, Weber K, Tuschl T: **Duplexes of 21-nucleotide RNAs mediate RNA interference in cultured mammalian cells.** *Nature* 2001, **411**:494–498.
- de Fougerolles A, Vornlocher HP, Maraganore J, Lieberman J: **Interfering with disease: a progress report on siRNA-based therapeutics.** *Nature Rev Drug Discov* 2007, **6**:443–453.
- Ahmed SU, Milner J: **Basal Cancer Cell Survival Involves JNK2 Suppression of a Novel JNK1/c-Jun/Bcl-3 Apoptotic Network.** *PLoS One* 2009, **4**:e7305.
- Watts JK, Deleavey GF, Damha MJ: **Chemically modified siRNA: tools and applications.** *Drug Discovery Today* 2008, **13**:842–855.
- Whitehead K, Langer R, Anderson D: **Knocking down barriers: advances in siRNA delivery.** *Nat Rev Drug Discov* 2009, **8**:129–138.
- Kennedy S, Wang D, Ruvkun G: **A conserved siRNA-degrading RNase negatively regulates RNA interference in *C. elegans*.** *Nature* 2004, **427**:645–649.
- Pirollo K, Chang E: **Targeted delivery of small interfering RNA: approaching effective cancer therapies.** *Cancer Res* 2008, **68**:1247–1250.
- Mohan R, Tovey J, Sharma A, Tandon A: **Gene therapy in the Cornea: 2005-present.** *Prog Retin Eye Res* 2012, **31**:43–64.
- Couto L, High K: **Viral vector-mediated RNA interference.** *Curr Opin Pharmacol* 2010, **10**:534–542.
- Wu L, Lam S, Cao H, Guan R, Hu J: **Subretinal gene delivery using helper-dependent adenoviral vectors.** *Cell Biosci* 2011, **1**:15.
- Höbel S, Koburger I, John M, Czubyko F, Hadwiger P, Vornlocher H, Aigner A: **Polyethylenimine/small interfering RNA-mediated knockdown of vascular endothelial growth factor in vivo exerts anti-tumor effects synergistically with Bevacizumab.** *J Gene Med* 2010, **12**:287–300.
- Hirano Y, Sakurai E, Matsubara A, Ogura Y: **Suppression of ICAM-1 in retinal and choroidal endothelial cells by plasmid small-interfering RNAs in vivo.** *Invest Ophthalmol Vis Sci* 2010, **51**:508–515.
- Conley S, Naash M: **Nanoparticles for retinal gene therapy.** *Prog Retin Eye Res* 2010, **29**:376–397.
- Khar R, Jain G, Warsi M, Mallick N, Akhter S, Pathan S, Ahmad F: **Nano-vectors for the Ocular Delivery of Nucleic Acid-based Therapeutics.** *Indian J Pharm Sci* 2010, **72**:675–688.
- Naik R, Mukhopadhyay A, Ganguli M: **Gene delivery to the retina: focus on non-viral approaches.** *Drug Discov Today* 2009, **14**:306–315.
- Boussif O, Lezoualc'h F, Zanta M, Mergny M, Scherman D, Demeneix B, Behr J: **A versatile vector for gene and oligonucleotide transfer into cells in culture and in vivo: polyethylenimine.** *PNAS* 1995, **92**:7297–7301.
- Grayson A, Doody A, Putnam D: **Biophysical and Structural Characterization of Polyethylenimine-Mediated siRNA Delivery in Vitro.** *Pharm Res* 2006, **23**:1868–1876.
- Kim B, Tang Q, Biswas P, Xu J, Schiffellers R, Xie F, Ansari A, Scaria P, Woodlee M, Lu P, Rouse B: **Inhibition of ocular angiogenesis by siRNA targeting vascular endothelial growth factor pathway genes: therapeutic strategy for herpetic stromal keratitis.** *Am J Pathol* 2004, **165**:2177–2185.
- Günther M, Lipka J, Malek A, Gutsch D, Kreyling W, Aigner A: **Polyethylenimines for RNAi-mediated gene targeting in vivo and siRNA delivery to the lung.** *Eur J Pharm Biopharm* 2011, **77**:438–449.
- Duan Y, Guan X, Ge J, Quan D, Zhuo Y, Ye H, Shao T: **Cationic nanocopolymers mediated IKKbeta targeting siRNA inhibit the proliferation of human Tenon's capsule fibroblasts in vitro.** *Mol Vis* 2008, **14**:2616–2628.
- Ye H, Qian Y, Lin M, Duan Y, Sun X, Zhuo Y, Ge J: **Cationic nanocopolymers mediated IKKβ targeting siRNA to modulate wound healing in a monkey model of glaucoma filtration surgery.** *Mol Vis* 2010, **16**:2502–2510.
- Soriano P, Dijkstra J, Legrand A, Spanjer H, Lodos-Gagliardi D, Roerdink F, Scherphof G, Nicolau C: **Targeted and nontargeted liposomes for in vivo transfer to rat liver cells of a plasmid containing the preproinsulin I gene.** *PNAS* 1983, **80**:7128–7131.
- Liu H, Liu Y, Ma Z, Wang J, Zhang Q: **A Lipid Nanoparticle System Improves siRNA Efficacy in RPE Cells and a Laser-Induced Murine CNV Model.** *Invest Ophthalmol Vis Sci* 2011, **52**:4789–4794.
- Zhang Y, Li H, Sun J, Gao J, Liu W, Li B, Guo Y, Chen J: **DC-Chol/DOPE cationic liposomes: a comparative study of the influence factors on plasmid pDNA and siRNA gene delivery.** *Int J Pharm* 2010, **390**:198–207.
- Lochmann D, Weyermann J, Georgens C, Prassl R, Zimmer A: **Albumin-protamine-oligonucleotide nanoparticles as a new antisense delivery**

- system. Part 1: Physicochemical characterization. *Eur J Pharm Biopharm* 2005, **59**:419–429.
39. Johnson L, Cashman S, Kumar-Singh R: Cell-penetrating peptide for enhanced delivery of nucleic acids and drugs to ocular tissues including retina and cornea. *Mol Ther* 2008, **16**:107–114.
  40. Laufer S, Restle T: Peptide-Mediated Cellular Delivery of Oligonucleotide-Based Therapeutics In Vitro: Quantitative Evaluation of Overall Efficacy Employing Easy to Handle Reporter Systems. *Curr Pharm Des* 2008, **14**:3637–3655.
  41. Yuan X, Naguib S, Wu Z: Recent advances of siRNA delivery by nanoparticles. *Expert Opin Drug Deliv* 2011, **8**:521–536.
  42. Marano R, Wimmer N, Kearns P, Thomas B, Toth I, Brankov M, Rakoczy P: Inhibition of in vitro VEGF expression and chorioidal neovascularization by synthetic dendrimer peptide mediated delivery of a sense oligonucleotide. *Exp Eye Res* 2004, **79**:525–535.
  43. Marano R, Toth I, Wimmer N, Brankov M, Rakoczy P: Dendrimer delivery of an anti-VEGF oligonucleotide into the eye: a long-term study into inhibition of laser-induced CNV, distribution, uptake and toxicity. *Gene Ther* 2005, **12**:1544–1550.
  44. Agrawal A, Min D, Singh N, Zhu H, Bhatia S: Functional delivery of siRNA in mice using dendriworms. *ACS Nano* 2009, **3**:2495–2504.
  45. Han L, Zhang A, Wang H, Pu P, Jiang X, Kang C, Chang J: Tat-BMPs-PAMAM conjugates enhance therapeutic effect of small interference RNA on U251 glioma cells in vitro and in vivo. *Hum Gene Ther* 2010, **21**:417–426.
  46. A Dose Escalation Trial of an Intravitreal Injection of Sirna-027 in Patients With Subfoveal Choroidal Neovascularization (CNV) Secondary to Age-Related Macular Degeneration (AMD). [http://clinicaltrials.gov/ct2/show/NCT00363714]
  47. A Study Using Intravitreal Injections of a Small Interfering RNA in Patients With Age-Related Macular Degeneration. [http://clinicaltrials.gov/ct2/show/NCT00395057]
  48. Kaiser P, Symons R, Shah S, Quinlan E, Nguyen Q: RNAi-based treatment for neovascular age-related macular degeneration by Sirna-027. *Am J Ophthalmol* 2010, **150**:33–39.
  49. Safety & Efficacy Study Evaluating the Combination of Bevasiranib & Lucentis Therapy in Wet AMD (COBALT). [http://clinicaltrials.gov/ct2/show/NCT00499590]
  50. Phase II Open Label Multicenter, Prospective, Randomized, Age Related Macular Degeneration, Comparator Controlled Study Evaluating PF-04523655 Versus Ranibizumab In The Treatment Of Subjects With Choroidal Neovascularization (MONET Study). [http://www.clinicaltrials.gov/ct2/show/NCT00713518?term=quark&rank=7]
  51. Prospective, Randomized, Multi-Center, Comparator Study Evaluating Efficacy and Safety of PF-04523655 Versus Laser in Subjects With Diabetic Macular Edema (DEGAS). [http://www.clinicaltrials.gov/ct2/show/NCT00701181?term=degas&rank=1]
  52. Development pipeline: PF-655. [http://www.quarkpharma.com/qbi-en/products/53/]
  53. Safety Study of a Single IVT Injection of QPI-1007 in Chronic Optic Nerve Atrophy and Recent Onset NAION Patients. [http://clinicaltrials.gov/ct2/show/NCT01064505]
  54. Tolerance and Effect on Intraocular Pressure After Administration of SYL040012. [http://clinicaltrials.gov/ct2/show/NCT00990743]
  55. Tiemann K, Rossi J: RNAi-based therapeutics-current status, challenges and prospects. *EMBO Mol Med* 2009, **1**:142–151.
  56. Morrissey D, Blanchard K, Shaw L, Jensen K, Lockridge J, Dickinson B, McSwiggen J, Vargeese C, Bowman K, Shaffer C, et al: Activity of stabilized short interfering RNA in a mouse model of hepatitis B virus replication. *Hepatology* 2005, **41**:1349–1356.
  57. Pipeline: Development Programs. [http://clinicaltrials.gov/ct2/show/NCT00395057. [http://www.alnylam.com/Programs-and-Pipeline/Index.php]
  58. Judge AD, Sood V, Shaw JR, Fang D, McClintock K, MacLachlan I: Sequence-dependent stimulation of the mammalian innate immune response by synthetic siRNA. *Nat Biotechnol* 2005, **23**:457–462.
  59. Prakash T, Allerson C, Dande P, Vickers T, Sioufi N, Jarres R, Baker B, Swayze E, Griffey R, Bhat B: Positional effect of chemical modifications on short interference RNA activity in mammalian cells. *J Med Chem* 2005, **48**:4247–4253.
  60. Czauderna F, Fechtner M, Dames S, Aygün H, Klippel A, Pronk G, Giese K, Kaufmann J: Structural variations and stabilising modifications of synthetic siRNAs in mammalian cells. *Nucleic Acids Res* 2003, **31**:2705–2716.
  61. Morrissey D, Lockridge J, Shaw L, Blanchard K, Jensen K, Breen W, Hartsough K, Machemer L, Radka S, Jadhav V, et al: Potent and persistent in vivo anti-HBV activity of chemically modified siRNAs. *Nature Biotechnol* 2005, **23**:1002–1007.
  62. Samuel-Abraham S, Leonard J: Staying on message: design principles for controlling nonspecific responses to siRNA. *FEBS J* 2010, **277**:4828–4836.
  63. Leuschner P, Ameres S, Kueng S, Martinez J: Cleavage of the siRNA passenger strand during RISC assembly in human cells. *EMBO Rep* 2006, **7**:314–320.
  64. Hall AH, Wan J, Shaughnessy EE, Ramsay Shaw B, Alexander KA: RNA interference using boranophosphate siRNAs: structure-activity relationships. *Nucleic Acids Res* 2004, **32**:5991–6000.
  65. Choung S, Kim Y, Kim S, Park HO, Choi YC: Chemical modification of siRNAs to improve serum stability without loss of efficacy. *Biochem Biophys Res Commun* 2006, **342**:919–927.
  66. Shim M, Kwon Y: Efficient and targeted delivery of siRNA in vivo. *FEBS J* 2010, **277**:4814–4827.
  67. Overhoff M, Sczakiel G: Phosphorothioate-stimulated uptake of short interfering RNA by human cells. *EMBO Rep* 2005, **6**:1176–1181.
  68. Behlke M: Chemical modification of siRNAs for in vivo use. *Oligonucleotides* 2008, **18**:305–319.
  69. Jackson A, Burchard J, Leake D, Reynolds A, Schelter J, Guo J, Linsley P: Position-specific chemical modification of siRNAs reduces "off-target" transcript silencing. *RNA* 2006, **12**:1197–1205.
  70. Minks M, West D, Benven S, Baglioni C: Structural requirements of double-stranded RNA for the activation of 2',5'-oligo(A) polymerase and protein kinase of interferon-treated HeLa cells. *J Biol Chem* 1979, **254**:10180–10183.
  71. Marques JT, Williams BRG: Activation of the mammalian immune system by siRNAs. *Nat Biotechnol* 2005, **23**:1399–1405.
  72. Kleinman ME, Yamada K, Takeda A, Chandrasekaran V, Nozaki M, Baffi JZ, Albuquerque RJC, Yamasaki S, Itaya M, Pan Y, et al: Sequence- and target-independent angiogenesis suppression by siRNA via TLR3. *Nature* 2008, **452**:591–597.
  73. Judge A, MacLachlan I: Overcoming the innate immune response to small interfering RNA. *Human Gene Therapy* 2008, **19**:111–124.
  74. Morrissey DV: Potent and persistent in vivo anti-HBV activity of chemically modified siRNAs. *Nature Biotechnol* 2005, **23**:1002–1007.
  75. Jackson AL, Bartz SR, Schelter J, Kobayashi SV, Burchard J, Mao M, Li B, Cavet G, Linsley PS: Expression profiling reveals off-target gene regulation by RNAi. *Nat Biotechnol* 2003, **21**:635–637.
  76. Walton S, Wu M, Gredell J, Chan C: Designing highly active siRNAs for therapeutic applications. *FEBS J* 2010, **277**:4806–4813.
  77. Zuhorn IS, Kalicharan R, Hoekstra D: Lipoplex-mediated transfection of mammalian cells occurs through the cholesterol-dependent clathrin-mediated pathway of endocytosis. *J Biol Chem* 2002, **277**:18021–18028.
  78. Torchilin V: Cell penetrating peptide-modified pharmaceutical nanocarriers for intracellular drug and gene delivery. *Biopolymers* 2008, **90**:604–610.
  79. Petros R, DeSimone J: Strategies in the design of nanoparticles for therapeutic applications. *Nat Rev Drug Discov* 2010, **9**:615–627.
  80. Rejman J, Oberle V, Zuhorn IS, Hoekstra D: Size-dependent internalization of particles via the pathways of clathrin- and caveolae-mediated endocytosis. *Biochem J* 2004, **377**:159–169.
  81. Fisher D, Ahlemeyer Y, Krieglstein B, Kissel T: In vitro cytotoxicity testing of polyplexes: influence of polymer structure on cell viability and hemolysis. *Biomaterials* 2003, **24**:1121–1131.
  82. Kim BYS, Jiang W, Oreopoulos J, Yip CM, Rutka JT, Chan WCW: Biodegradable Quantum Dot Nanocomposites Enable Live Cell Labeling and Imaging of Cytoplasmic Targets. *Nano Letters* 2008, **8**:3887–3892.
  83. Rajendran L, Knölker H, Simons K: Subcellular targeting strategies for drug design and delivery. *Nat Rev Drug Discov* 2010, **9**:29–42.
  84. Futaki S, Suzuki T, Ohashi W, Yagami T, Tanaka S, Ueda K, Sugiura Y: Arginine-rich peptides. An abundant source of membrane-permeable peptides having potential as carriers for intracellular protein delivery. *J Biol Chem* 2001, **276**:5836–5840.
  85. Ruan G, Agrawal A, Marcus AI, Nie S: Imaging and Tracking of Tat Peptide-Conjugated Quantum Dots in Living Cells: New Insights into Nanoparticle Uptake, Intracellular Transport, and Vesicle Shedding. *J Am Chem Soc* 2007, **129**:14759–14766.
  86. Derossi D, Joliot A, Chassaing G, Prochiantz A: The third helix of the Antennapedia homeodomain translocates through biological membranes. *J Biol Chem* 1994, **269**:10444–10450.

87. Duan H, Nie S: Cell-penetrating quantum dots based on multivalent and endosome-disrupting surface coatings. *J Am Chem Soc* 2007, **129**:3333–3338.
88. Thomas M, Klibanov A: Enhancing polyethylenimine's delivery of plasmid DNA into mammalian cells. *PNAS* 2002, **99**:14640–14645.
89. Gusachenko Simonova O, Kravchuk Y, Konevets D, Silnikov V, Vlassov W, Zenkova MA: Transfection Efficiency of 25-kDa PEICholesterol Conjugates with Different Levels of Modification. *J Biomater Sci Polym Ed* 2009, **20**:1091–1110.
90. Bouxsein N, McAllister C, Ewert K, Samuel C, Safinya C: Structure and gene silencing activities of monovalent and pentavalent cationic lipid vectors complexed with siRNA. *Biochemistry* 2007, **46**:4785–4792.
91. Leal C, Bouxsein N, Ewert K, Safinya C: Highly efficient gene silencing activity of siRNA embedded in a nanostructured gyroid cubic lipid matrix. *J Am Chem Soc* 2010, **132**:16841–16847.
92. Leal C, Ewert K, Shirazi R, Bouxsein N, Safinya C: Nanogyroids incorporating multivalent lipids: enhanced membrane charge density and pore forming ability for gene silencing. *Langmuir* 2011, **27**:7691–7697.
93. Du J, Shi Q, Sun Y, Liu P, Zhu M, Du L, Duan Y: Enhanced delivery of monomethoxypoly(ethylene glycol)-poly(lactic-co-glycolic acid)-poly-L-lysine nanoparticles loading platelet-derived growth factor BB small interfering RNA by ultrasound and/or microbubbles to rat retinal pigment epithelium cells. *J Gene Med* 2011, **13**:312–323.
94. Turchinovich A, Zoidl G, Dermietzel R: Non-viral siRNA delivery into the mouse retina in vivo. *BMC Ophthalmol* 2010, **10**:25.
95. Aggarwal P, Hall J, McLeland C, Dobrovolskaia A, McNeil S: Nanoparticle interaction with plasma proteins as it relates to particle biodistribution, biocompatibility and therapeutic efficacy. *Adv Drug Deliv Rev* 2009, **61**:428–437.
96. Gref R, Minamitake Y, Peracchia M, Trubetskoy V, Torchilin V, Langer R: Biodegradable long-circulating polymeric nanospheres. *Science* 1994, **263**:1600–1603.
97. Wong C, Stylianopoulos T, Cui J, Martin J, Fukumura D: Multistage nanoparticle delivery system for deep penetration into tumor tissue. *PNAS* 2011, **108**:2426–2431.
98. Gratton S, Ropp P, Pohlhaus P, Luft J, Madden V, Napier M, DeSimone J: The effect of particle design on cellular internalization pathways. *PNAS* 2008, **105**:11613–11618.
99. Yokoe J, Sakuragi S, Yamamoto K, Teragaki T, Ogawara K, Higaki K, Katayama N, Kai T, Sato M, Kimura T: Albumin-conjugated PEG liposome enhances tumor distribution of liposomal doxorubicin in rats. *Int J Pharm* 2008, **353**:28–34.
100. Furumoto K, Yokoe J, Ogawara K, Amano S, Takaguchi M, Higaki K, Kai T, Kimura T: Effect of coupling of albumin onto surface of PEG liposome on its in vivo disposition. *Int J Pharm* 2007, **329**:110–116.
101. Davis M, Zuckerman J, Choi C, Seligson D, Ribas A: Evidence of RNAi in humans from systemically administered siRNA via targeted nanoparticles. *Nature* 2010, **464**:1067–1070.
102. Breitbach C, Burke J, Jonker D, Stephenson J, Haas A, Kim D: Intravenous delivery of a multi-mechanistic cancer-targeted oncolytic poxvirus in humans. *Nature* 2011, **477**:99–102.
103. Hu Y, Atukorale P, Lu J, Moon J, Um S, Cho E, Wang Y, Chen J, Irvine D: Cytosolic delivery mediated via electrostatic surface binding of protein, virus, or siRNA cargos to pH-responsive core-shell gel particles. *Biomacromolecules* 2009, **10**:756–765.
104. You J, Almeda D, Ye G, Auguste D: Bioresponsive matrices in drug delivery. *J Biol Eng* 2010, **4**.

doi:10.1186/1754-1611-6-7

Cite this article as: Thakur et al.: Strategies for ocular siRNA delivery: Potential and limitations of non-viral nanocarriers. *Journal of Biological Engineering* 2012 **6**:7.

Submit your next manuscript to BioMed Central and take full advantage of:

- Convenient online submission
- Thorough peer review
- No space constraints or color figure charges
- Immediate publication on acceptance
- Inclusion in PubMed, CAS, Scopus and Google Scholar
- Research which is freely available for redistribution

Submit your manuscript at  
[www.biomedcentral.com/submit](http://www.biomedcentral.com/submit)





## Temperature-sensitive polymers for drug delivery

Scott D Fitzpatrick, Lindsay E Fitzpatrick, Ajit Thakur, Mohammad A Jafar Mazumder & Heather Sheardown

To cite this article: Scott D Fitzpatrick, Lindsay E Fitzpatrick, Ajit Thakur, Mohammad A Jafar Mazumder & Heather Sheardown (2012) Temperature-sensitive polymers for drug delivery, Expert Review of Medical Devices, 9:4, 339-351, DOI: [10.1586/erd.12.24](https://doi.org/10.1586/erd.12.24)

To link to this article: <http://dx.doi.org/10.1586/erd.12.24>



Published online: 09 Jan 2014.



Submit your article to this journal [↗](#)



Article views: 69



View related articles [↗](#)



For reprint orders, please contact [reprints@expert-reviews.com](mailto:reprints@expert-reviews.com)

EXPERT  
REVIEWS

# Temperature-sensitive polymers for drug delivery

*Expert Rev. Med. Devices* 9(4), 339–351 (2012)

Scott D Fitzpatrick<sup>1</sup>,  
Lindsay E Fitzpatrick<sup>2</sup>,  
Ajit Thakur<sup>1</sup>,  
Mohammad A Jafar  
Mazumder<sup>3,4</sup> and  
Heather Sheardown<sup>\*1,3</sup>

<sup>1</sup>School of Biomedical Engineering,  
McMaster University, 1280 Main Street  
West, Hamilton, ON, L8S 4L7, Canada

<sup>2</sup>The Institute of Biomaterials and  
Biomedical Engineering, University  
of Toronto, 164 College Street,  
Toronto, ON, M5S 3G9, Canada

<sup>3</sup>Department of Chemical Engineering,  
McMaster University, 1280 Main Street  
West, Hamilton, ON, L8S 4L7, Canada

<sup>4</sup>Department of Chemistry, King Fahd  
University of Petroleum & Minerals,  
University Blvd, Dhahran-31261,  
Saudi Arabia

\*Author for correspondence:  
Tel.: +1 905 525 9140 ext. 24794  
[sheardown@mcmaster.ca](mailto:sheardown@mcmaster.ca)

The ability to undergo rapid changes in response to subtle environmental cues make stimuli-responsive materials attractive candidates for minimally invasive, targeted and personalized drug delivery applications. This special report aims to highlight and provide a brief description of several of the significant natural and synthetic temperature-responsive materials that have clinical relevance for drug delivery applications. This report examines the advantages and disadvantages of natural versus synthetic materials and outlines various scaffold architectures that can be utilized with temperature-sensitive drug delivery materials. The authors provide a commentary on the current state of the field and provide their insight into future expectations for temperature-sensitive drug delivery, emphasizing the importance of the emergence of dual and multiresponsive systems capable of responding precisely to an expanding set of stimuli, thereby allowing the development of disease-specific drug delivery vehicles.

**KEYWORDS:** drug delivery • intelligent polymers • lower critical solution temperature • *N*-isopropylacrylamide • smart polymers • sustained release • targeted • temperature-sensitive • thermoresponsive

Stimuli-responsive materials have gained considerable attention for their potential to create targeted, tunable and personalized therapeutics that respond directly to the physiologic environment. With recent advances in medical polymer technology, it is becoming increasingly possible to tailor drug-releasing scaffolds to produce on-demand delivery of therapeutic payloads locally in response to physiological requirements [1]. Stimuli-responsive polymers, also termed intelligent, smart, environmentally responsive and sensitive polymers, are a class of materials that undergo significant and rapid physicochemical changes in response to small changes in environmental conditions. There are a number of different classes of responsive polymers, which respond to a distinct set of stimuli, including light, pH, temperature, ultrasound, magnetism, electric field, enzymes, antibodies, or the presence of specific molecules, such as glucose [2]. In addition, the specific response varies depending on the system. Polymers may undergo changes in hydrophobic/hydrophilic balance, solubility, hydration, conformation, shape, degradation or micellization in response to the presence, or absence, of an external stimulus [2]. It is therefore possible to use these materials to generate drug delivery scaffolds that respond with predictable, controllable, predefined response profiles to impart a large degree of control and tunability

over drug dosing. The ability to produce targeted on-demand drug release has implications for a number of different clinical applications, including hormone replacement therapy, chemotherapy, rhythmic heart disorders, diabetes, birth control and posterior segment ocular drug delivery. Of the various stimuli-responsive materials, temperature-sensitive polymers are the most widely studied, and this special report, while not exhaustive, will focus on several of these materials that have particular importance in drug delivery applications. A list of natural and synthetic thermoresponsive homopolymers and copolymers that are relevant to drug delivery is provided in TABLE 1.

## Thermoresponsive polymers & their applicability for controlled release of drugs

Thermoresponsive polymers utilize subtle changes in temperature to trigger macroscopic changes in material properties. Polymers that possess a lower critical solution temperature (LCST) typically undergo a sol–gel phase transition when heated above their LCST, whereas polymers that become soluble upon heating are said to possess an upper critical solution temperature (UCST) [3]. Both systems can be exploited for drug delivery purposes. LCST copolymers can simply be mixed with drug as a liquid suspension at

**Table 1. A list of natural and synthetic thermoresponsive homopolymers and copolymers with their corresponding thermal phase transition temperatures.**

Study (year)	Name	Abbreviation	LCST/ UCST (°C)	Ref.
<i>Synthetic homopolymers</i>				
Laukkanen <i>et al.</i> (2004)	Poly( <i>N</i> -vinylcaprolactam)	PVCL	31	[91]
Schild (1990)	Poly( <i>N</i> -isopropylacrylamide)	PNIPAAm	32	[92]
Cao <i>et al.</i> (2007)	Poly( <i>N</i> -n-propylacrylamide)	PNPAm	25	[93]
	Poly( <i>N,N</i> -ethylmethacrylamide)	PEMA	70	
Liu and Zhu (1999)	Poly( <i>N</i> -ethylacrylamide)	PEA	82	[94]
Geever <i>et al.</i> (2011)	Poly( <i>N,N</i> -diethylacrylamide)	PDEAAm	~28–32	[19]
Uguzdogan <i>et al.</i> (2005)	Poly(ethoxypropylacrylamide)	PEPA	~32	[95]
Yamazaki <i>et al.</i> (1998)	Poly( <i>N,N</i> -bis(2-methoxyethyl) acrylamide)	PBMEA	49	[96]
	Poly( <i>N</i> -(3-methoxypropyl)acrylamide)	PMPAm	>60	
Persson <i>et al.</i> (2000)	Poly(vinyl methyl ether)	PVME	34	[97]
Yuk <i>et al.</i> (1997)	Poly(2-dimethylamino)ethyl methacrylate)	PDMA	50	[98]
Liu and Armes (2001)	Poly(propylene oxide)	PPO	10–20	[99]
Chiu <i>et al.</i> (1986)	Poly(2-ethyl-2-oxazoline)	PEOZ	~62	[100]
Uyama and Kobayashi (1992)	Poly(2-isopropyl-2-oxazoline)	PIPOZ	~36	[101]
Urban (2011)	Polyphosphazenes		~25–99	[81]
<i>Synthetic multi-block copolymers</i>				
Fusco (2006)	Poly(ethylene oxide)-poly(propylene oxide)-poly(ethylene oxide) (Pluronic®)	PEO–PPO–PEO	10–100	[102]
	L42 <sup>†</sup>	PEO <sub>4</sub> –PPO <sub>22</sub> –PEO <sub>4</sub>	37	
	L62 <sup>†</sup>	PEO <sub>6</sub> –PPO <sub>34</sub> –PEO <sub>6</sub>	32	
	L63 <sup>†</sup>	PEO <sub>9</sub> –PPO <sub>32</sub> –PEO <sub>9</sub>	34	
<i>Polyester/PEG block copolymers</i>				
Gao <i>et al.</i> (2010)	Poly(lactic acid-co-glycolic acid)-poly(ethylene glycol)-poly(lactic acid-co-glycolic acid)	PLGA–PEG–PLGA	~37	[103]
Jeong <i>et al.</i> (1997)	Poly(ethylene glycol)-b-poly(D,L-lactic acid-co-glycolic acid)-b-poly(ethylene glycol)	PEG–PLA–PEG	~37	[104]
Lutz <i>et al.</i> (2006)	Poly(oligo(ethylene glycol) methacrylate)	POEGMA	26–90	[105]
Badi and Lutz (2009)	s-poly(ethylene glycol)-b-poly(2-(2-methoxyethoxy) ethyl methacrylate-co-oligo(ethylene glycol) methacrylate)	sPEG-b-P(MEO2MA-co-OEGMA <sub>475</sub> )	35–41	[106]
Lutz <i>et al.</i> (2006)	Poly(2-(2-methoxyethoxy)ethyl methacrylate-co-oligo(ethylene glycol) methacrylate)	P(MEO2MA-co-OEGMA) 5–8% OEGMA units per chain	32–37	[105]
Gong <i>et al.</i> (2009)	Poly(ε-caprolactone)-poly(ethylene glycol)-poly(ε-caprolactone)	PCL–PEG–PCL	~15–50	[107]
		PCL <sub>1000</sub> –PEG <sub>1000</sub> –PCL <sub>1000</sub> (15–35 wt%)	~18–25	[107]
		PCL <sub>1000</sub> –PEG <sub>1500</sub> –PCL <sub>1000</sub> (15–35 wt%)	~39–46	
Dayananda <i>et al.</i> (2008)		PCL <sub>1500</sub> –PEG <sub>1500</sub> –PCL <sub>1500</sub> (15–35 wt%)	~37–45	
		PCL <sub>1950</sub> –PEG <sub>1750</sub> –PCL <sub>1950</sub> (20 wt%)	~42	[108]
		PCL <sub>2110</sub> –PEG <sub>2000</sub> –PCL <sub>2110</sub> (20 wt%)	~44	

<sup>†</sup>Pluronic nomenclature: The first letter in the copolymer name indicates that the physical state of the starting polymer is a liquid (L). The last number indicates the weight content of the PEO block (in terms of weight percent), while the remaining numbers give an indication of the molecular weight of the PPO block (taken from) [102]. Adapted from [111].



**Table 1. A list of natural and synthetic thermoresponsive homopolymers and copolymers with their corresponding thermal phase transition temperatures (cont.).**

Study (year)	Name	Abbreviation	LCST/ UCST (°C)	Ref.
<i>Natural polymers and derivatives</i>				
Chenite <i>et al.</i> (2000) and Molinaro <i>et al.</i> (2002)	Chitosan-glycerophosphate	Chitosan-GP	~37	[50,51]
Persson <i>et al.</i> (2000)	Methylcellulose	MC	50	[97]
Schild (1990)	Hydroxypropylcellulose	HPC	42	[92]
Persson <i>et al.</i> (2000)	Ethyl(hydroxyethyl)cellulose	EHEC	65	[97]
Miyazaki <i>et al.</i> (1998) <sup>†</sup>	Xyloglucan (with 44% removal of galactose)		22–27	[59]
Chilkoti <i>et al.</i> (2006)	Elastin-like polypeptides	ELP	0–100	[109]
Ge <i>et al.</i> (2010)		ELP[V <sub>5</sub> A <sub>2</sub> G <sub>3</sub> -90]	49	[41]
Meyer <i>et al.</i> (2001)		ELP[V <sub>5</sub> A <sub>2</sub> G <sub>3</sub> -150]	40	[48]
		ELP [V <sub>5</sub> A <sub>2</sub> G <sub>3</sub> -160]	55	
Urry <i>et al.</i> (1991)		Poly(VPGVG)	27	[110]

<sup>†</sup>Pluronic nomenclature: The first letter in the copolymer name indicates that the physical state of the starting polymer is a liquid (L). The last number indicates the weight content of the PEO block (in terms of weight percent), while the remaining numbers give an indication of the molecular weight of the PPO block (taken from) [102]. Adapted from [111].

room temperature and delivered via minimally invasive injection techniques directly to hard-to-access target tissues within the body. Heating to physiologic temperature drives a sol–gel phase transition, which entraps the infused drug within a solid depot and can provide sustained release of therapeutic concentrations of drug directly at the site of interest [4]. Drug-releasing polymer systems possessing a UCST may employ temperature-induced swelling or scaffold destabilization to rapidly release drug at a target site [5]. Localized heating (tumor tissues) or the application of an externally applied stimulus (ultrasound, infrared laser and so on) may be utilized to induce the local destabilization of a UCST drug-releasing copolymer scaffold to produce targeted release [6,7].

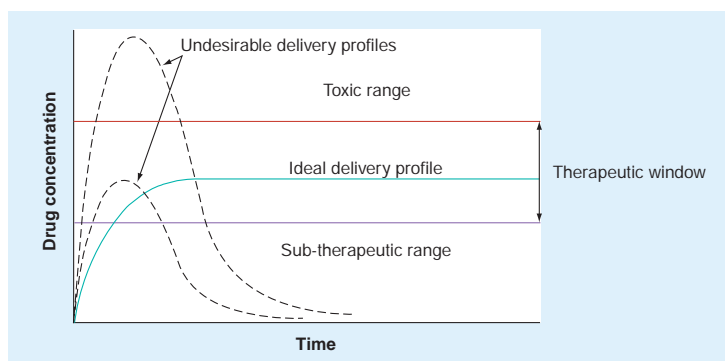
Thermoresponsive drug delivery scaffolds offer numerous advantages, such as eliminating the need for invasive surgical implantation and the ability to bypass physiological barriers, allowing delivery to hard-to-access locations within the body [8]. Furthermore, drug encapsulation within a scaffold may protect the therapeutic agent from enzymatic or environmental degradation. The release rate can be tailored to locally produce persistent levels of therapeutically relevant concentrations of drug, thus overcoming the ineffectiveness of simple injections, which are associated with an initial spike that may lead to toxic levels initially followed by a rapid decrease to levels that possess little to no therapeutic benefit (FIGURE 1) [8].

#### Synthetic thermoresponsive materials

##### Poly(*N*-isopropylacrylamide)

Polymer hydrogels that display reversible volume changes have gained considerable interest since Tanaka observed the tendency of polyacrylamide gels to undergo phase separation in response to temperature or fluid composition [9]. Poly(*N*-isopropylacrylamide) (PNIPAAm) is one of the most widely studied temperature-sensitive

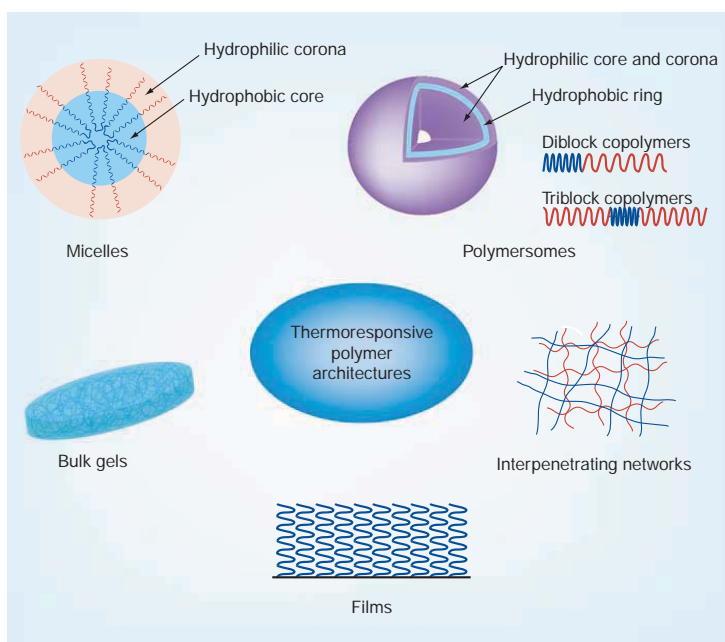
polymers; it exhibits a rapid sol–gel transition when heated above its LCST, approximately 32°C, allowing injection at room temperature and scaffold formation at body temperature [4]. One of the major limitations of PNIPAAm is that it is nondegradable. Degradable drug delivery materials afford elimination of the scaffold following exhaustion of the drug reservoir without the requirement for secondary surgical removal. Therefore, there has been an increased emphasis in recent years on introducing degradability into NIPAAm-based copolymers. Ultimately, it is desirable to preserve the thermal phase transition properties of NIPAAm, while promoting the eventual degradation and clearance from the body following exhaustion of the therapeutic effect. In 1999, Neradovic *et al.* synthesized NIPAAm-based polymers with 2-hydroxyethyl methacrylate–monolactate (HEMA–monolactate) [10]. As the hydrolytically labile lactate ester side groups were cleaved, the hydrophilicity of the copolymer increased, raising the LCST. If the LCST is raised above body temperature, the thermoreversible NIPAAm-based copolymers revert back into a hydrated liquid state, allowing uptake into systemic circulation and clearance from the body, as long as the molecular weight is below the renal filtration limit of 30–50 kDa [11]. Yoshida *et al.* designed NIPAAm-based copolymers that were crosslinked with degradable poly(amino acids), which showed a similar clearance mechanism [12]. Guan *et al.* synthesized a series of protein-reactive NIPAAm-based copolymers, possessing relatively high tensile strength that hydrolyze to produce soluble, nontoxic degradation products through copolymerization with HEMA–polylactide (HEMA–PLA), *N*-acryloxysuccinimide and acrylic acid [13]. Ma *et al.* further improved the mechanical properties through the incorporation of methacrylate–polylactide (MA–PLA) and HEMA [14]. Cui *et al.* developed a series of slow-degrading NIPAAm-based copolymers through copolymerization with dimethyl- $\gamma$ -butyrolactone acrylate (DBA) [15]. These



**Figure 1. Representation of the ideal delivery profile in which drug concentration is maintained within the therapeutic window, below the toxic threshold, but high enough to exert a therapeutic effect.**

copolymers undergo a hydrolysis-dependent opening of the DBA lactone ring structure, capable of increasing LCST above body temperature without producing any degradation products [15,16]. The Sheardown group prepared bioactive NIPAAm/DBA copolymers through copolymerization with *N*-acryloxysuccinimide [17] for posterior segment ophthalmic cell and drug delivery purposes.

oxide) (PEO–PPO–PEO), referred to as Pluronic or Poloxamers, are another family of thermogelling synthetic materials that have been extensively studied for their potential use as drug carriers [23]. Through manipulation of concentration, composition and molecular weight, these copolymers can be tuned to undergo reversible gelation at physiological temperature and pH [23]. The



**Figure 2. Illustration of some of the architectures that can be obtained using thermoresponsive copolymers for drug delivery applications.** The architectures include bulk gels, micelles possessing a hydrophobic core and a hydrophilic corona, polymersomes that have a hydrophobic layer sandwiched between a hydrophilic core and corona, interpenetrating networks and polymer films.

For a list of thermoresponsive homopolymers and copolymers of PNIPAAm, see [18]. There are many other examples of *N*-substituted thermoresponsive polyacrylamides that may be suitable for drug delivery, such as poly(*N,N*-diethylacrylamide [19,20] and poly(*N*-vinyl caprolactam) [21]. For a comprehensive list, see [22]. Similar to PNIPAAm, linear polymers of poly(*N,N*-diethylacrylamide and poly(*N*-vinyl caprolactam) have LCST values of 32°C [19] and 31°C [18], respectively.

Poly(ethylene oxide)-based thermoresponsive copolymers Triblock copolymers possessing an A–B–A configuration of poly(ethylene oxide)–poly(propylene oxide)–poly(ethylene oxide) (PEO–PPO–PEO), referred to as Pluronic or Poloxamers, are another family of thermogelling synthetic materials that have been extensively studied for their potential use as drug carriers [23]. Through manipulation of concentration, composition and molecular weight, these copolymers can be tuned to undergo reversible gelation at physiological temperature and pH [23]. The combination of hydrophilic ethylene oxide and hydrophobic propylene oxide units creates an amphiphilic copolymer that can self-associate into micelles under aqueous conditions when above a critical micelle concentration (CMC) (FIGURE 2). The CMC is highly temperature dependent, as below a critical micelle temperature, both ethylene oxide and propylene oxide blocks are relatively soluble in water [23]. As the temperature of the system increases, the PPO chains become less soluble, resulting in micelle formation. Pluronic micelles typically possess a diameter ranging from 10 to 100 nm and consist of a hydrophobic, PPO-rich core and a hydrated, hydrophilic PEO-rich shell [24]. The PPO core is capable of incorporating up to 30 wt % of water-insoluble drugs, while the PEO corona maintains the micelles in a dispersed state and improves drug stability by shielding the reserves from undesirable interactions with cells and proteins [24]. However, these hydrogels tend to possess poor mechanical strength, limited stability and high permeability, thereby limiting their effectiveness as sustained-release systems [24,25]. Cohn *et al.* have utilized a number of strategies to improve the mechanical integrity of PEO/PPO copolymers. Such strategies include the introduction of *in situ*

crosslinking end-groups, such as carbon-carbon double bonds [26], methacrylate groups [27] and triethoxysilane groups [27] and covalently linking PEO and PPO using carbonyl chloride and diacyl chloride coupling agents [28]. In recent years, there has been an extensive investigation into the synthesis of copolymers of polyethylene glycol (PEG) with degradable polyesters such as PLA, poly(lactide-co-glycolide) (PLGA) and poly(caprolactone) (PCL) to generate thermoresponsive copolymers with improved rigidity that degrade *in vivo*, allowing their ultimate clearance from the body [28–30]. PEG-containing copolymers that have attracted significant interest include PLGA-PEG-PLGA, PEG-PLA-PEG, PCL-PEG-PCL and poly(oligo[ethylene glycol] methacrylate), to name a few [1].

#### Polyphosphazenes

Polyphosphazenes are a thermoresponsive family of hybrid organic-inorganic polymers. These polymers contain an inorganic backbone consisting of alternating nitrogen and phosphorous atoms connected by alternating single and double bonds [31]. Attached to every phosphorous group are two organic groups that impart a high degree of versatility for modification and manipulation of properties and functionality, which can be utilized to impart thermoresponsive properties [4]. Numerous approaches have been explored to develop hydrolytically susceptible copolymers that have highly controllable degradation kinetics, capable of breaking down over periods ranging from hours to years [31–34]. Polyphosphazenes have demonstrated good compatibility with numerous cell lines in culture [35,36] and *in vivo* [37]. Furthermore, the degradation byproducts, namely ammonia, phosphate and alcohol, are well tolerated, and the copolymers can be designed to possess fast *in situ* gelation with tunable release kinetics, making polyphosphazenes attractive candidates for drug delivery [31,38]. For an in-depth review of polyphosphazenes, see [31].

#### Natural thermoresponsive materials

##### Elastin-like polypeptides

Elastin-like polypeptides (ELPs) are synthetic elastin-inspired polymers with a pentapeptide amino acid repeat structure, Val-Pro-Gly-Xaa-Gly, where the Xaa guest residue can be any natural amino acid except proline [39,40]. Below the phase transition temperature ( $T_i$ ), ELPs exist as a clear homogeneous aqueous solution. When heated above their transition temperature, the solution becomes turbid through ELP coacervation into droplets [41]. The ELP droplet size and distribution can be manipulated through concentration and temperature [41], while the transition temperature can be adjusted by varying the concentration, molecular weight, salt content and ELP composition (i.e., through modifying the Xaa guest residue, using variable amino acid sequences or by functionalization with other proteins or polymers) [41]. ELPs are interesting candidates for drug delivery, as they possess tunable characteristics, are well tolerated *in vivo* and degrade into simple amino acid residues [42]. In addition, the molecular weight and composition of ELPs can be precisely controlled through genetic engineering approaches to form narrowly dispersed polymers, which allows an increased level of

control over drug-release performance [43]. Furthermore, ELPs can be expressed in high quantities from *Escherichia coli* and can be easily purified as a result of their thermogelling behavior [44]. The Chilkoti group has extensively studied ELPs for their ability to target tumor tissues [45–48]. In one strategy, the group passively targeted tumor tissues by employing drug-conjugated ELPs with a  $T_i$  that was well above physiologic temperature. The small, soluble, ELPs took advantage of the enhanced permeability of tumor vasculature to accumulate within tumor tissues following systemic delivery [47]. In another approach, ELP-drug conjugates were designed to thermally target tumor tissues. The peptides were engineered to possess a  $T_i$  between 37 and 42°C and externally applied stimuli induced localized hyperthermia, causing the ELP-drug conjugates to aggregate and adhere to the vessel walls [48]. Mild hyperthermia was also used to drive the localized assembly of micelles that possessed a tumor-targeting ligand on the hydrophilic corona, leading to enhanced cellular uptake [46]. In another strategy, ELPs with a subphysiologic  $T_i$  were injected directly into tumorous tissues to produce a sustained-release drug depot directly within the tumor tissues for extended treatment [45].

##### Chitosan

Chitosan is a polysaccharide that is derived from chitin [4]. While on its own, chitosan is not thermoresponsive, it becomes thermoresponsive when it is mixed with glycerophosphate (GP) [4]. At elevated temperatures, GP forms strong hydrogen bonds with chitosan, which leads to gel formation [4]. However, chitosan/GP mixtures tend to possess slow gelation rates. Therefore, for applications requiring more rapid gelation, the derivative chitosan chloride can be used to expedite the gelling process [49]. Chitosan scaffolds also suffer from relatively rapid release of loaded protein and drugs possessing low molecular weight; complete release is often achieved within several hours [4,50]. There are also concerns about the suitability of chitosan/GP hydrogels for *in vivo* application as they have been shown to induce a relatively significant inflammatory response [51].

##### Cellulose derivatives

Several cellulose derivatives, such as methylcellulose (MC) and hydroxypropylmethylcellulose, display LCST behavior that can be exploited for drug delivery and tissue engineering applications [52]. MC and hydroxypropylmethylcellulose display LCST values between 40–50°C and 75–90°C, respectively [53]. However, these values can be substantially lowered using both physical and chemical methods, such as the addition of NaCl or a reduction in the hydroxypropyl content [53,54]. At low temperatures, the macromolecules exist in a fully hydrated state with little polymer-polymer interaction aside from physical entanglement [52]. Upon heating, intermolecular hydrophobic interactions between the methoxy groups result in gradual dehydration and gel formation [53]. Recently, a physical blend of hyaluronan and MC demonstrated rapid thermoreversible *in situ* gelation, degradability, good *in vivo* tolerance and potential for minimally invasive intrathecal drug delivery for spinal cord injuries [55,56]. Formulations

of hyaluronan and MC have also demonstrated favorable results as injectable cell scaffolds for retinal therapeutics [57].

#### Xyloglucan

In its native form, the xyloglucan polysaccharide does not form a gel [58]. However, Miyazaki *et al.* developed a thermally reversible xyloglucan hydrogel through partial degradation of xyloglucan from the seeds of *Tamarindus indica* [59]. When more than 35% of the galactose residues have been removed, xyloglucan exhibits temperature-responsive behavior under dilute aqueous conditions and possesses a relatively high storage modulus [23,25]. Xyloglucan gels have been examined as drug delivery scaffolds for oral [60], ocular [61], rectal [59], percutaneous [62] and intraperitoneal [63] applications.

#### Polymer architecture

A crucial parameter to consider when designing *in situ*-forming drug delivery scaffolds is the type of polymeric architecture that will be most suitable for the intended application. *In situ*-forming hydrogels can form numerous scaffold architectures, such as interpenetrating networks (IPNs), micelles, polymersomes, films and other variations (FIGURE 2). There are two main types of gels: physical gels and crosslinked gels. Physical gels are formed through the physical entanglement of polymer chains or micelle ordering, whereas crosslinked gels are covalently bound [8]. Covalently linked thermoresponsive networks undergo a change in their degree of swelling in response to temperature, while physically linked gels undergo a sol-gel phase transition [8]. Covalently linked networks can either be formed *in situ* or prior to implantation. *In situ* crosslinking minimizes invasiveness of instillation, but requires the use of crosslinking chemistry that is safe *in vivo*.

IPNs consist of two or more polymer networks that are bound through physical entanglement such that the networks can only be separated through bond breakage. IPNs offer a powerful tool for drug delivery as each polymer in the network can introduce specific properties, such as temperature sensitivity, and new properties can arise from the interaction of the various polymers within the network. Furthermore, it is relatively easy to manipulate properties by varying the polymer ratio within the IPN and modifying the polymers within the network. Liu *et al.* have designed transparent silicone/PNIPAAm IPN materials which show temperature transitions that are useful for drug loading and that show particular promise for the delivery of hydrophobic drugs [LIU L, SHEARDOWN H, MANUSCRIPT SUBMITTED]. Semi-interpenetrating copolymer networks (semi-IPNs) contain at least one crosslinked polymer network, either linear or branched [64]. Kim *et al.* prepared thermoresponsive semi-IPNs based on chitosan and poly(acryl amide) in which the hybrid synthetic and natural copolymers displayed high swelling ratios that were dependent on temperature, pH, ion concentration and electric field [64]. Nanoparticle IPNs consisting of poly(acrylic acid) (PAA) and poly(acryl amide) display UCST behavior and rapidly swell in response to heating above a critical temperature [65]. Chen *et al.* prepared semi-IPN nanogels based on hydroxypropylcellulose, which possesses an LCST around 41°C, and PAA, which, as mentioned, possesses UCST behavior [66]. By varying the chemical composition and the degree of crosslinking, the phase

transition properties of these hydroxypropylcellulose-PAA nanogel semi-IPNs could be shifted from UCST to LCST. IPNs and semi-IPNs of thermoresponsive copolymers offer a high degree of flexibility and can be tailored to provide variable release profiles to suit a broad range of applications.

As discussed in the section entitled poly(ethylene oxide)-based thermoresponsive copolymers, amphiphilic block copolymers can spontaneously assemble into micelles with a hydrophilic corona and a hydrophobic core. Therefore, micelles may be particularly useful for cancer therapeutics, as many chemotherapeutics are small hydrophobic compounds with a poor therapeutic index [44]. Micelle drug carriers can increase drug accumulation in tumor tissues, while minimizing off-target effects through the enhanced permeability and retention effect, which allows extravasation of the small drug carriers through the leaky tumor vasculature, as mentioned in the section entitled 'Elastin-like polypeptides' [44]. Quan *et al.* designed an elegant thermoresponsive micelle carrier for tumor-triggered drug release [67]. Upon encountering the subtle physiological changes in tumor physiology (pH 6.8,  $T > 37^\circ\text{C}$ ), PEGylated arginine-glycine-aspartic acid (RGD) peptides were deprotected, allowing internalization by RGD receptor overexpressing tumor cells and destabilization of drug-loaded micelles for localized treatment. Wei *et al.* synthesized a series of NIPAAm-containing thermoresponsive shell crosslinked micelles [68]. They found that the crosslinked shell slowed drug release at temperatures below the LCST (25°C), but the rate accelerated dramatically above the LCST (37°C) as pNIPAAm gelation led to a deformation of the micelle structure.

Polymersomes, also known as polymer vesicles, are similar to micelles in that they are self-assembling amphiphilic block copolymers; however, they arrange to form a hydrophobic ring sandwiched between a hydrophilic core and corona [8]. The polymersome structure allows interior encapsulation of both hydrophilic and hydrophobic drugs, while the hydrophilic shell protects the entrapped drug from undesirable interactions and can help the drug delivery system to evade the immune system. The hydrophilic corona can act as a rate-controlling membrane to modulate the release of drug from the hydrophobic ring, which in turn can serve to impede release from the hydrophilic core [69]. Li *et al.* synthesized thermoresponsive, self-assembling polymersomes consisting of diblock copolymers of poly(*N*-[3-aminopropyl] methacrylamide hydrochloride) and PNIPAAm [70]. In aqueous conditions, the amphiphilic block copolymers existed as unimers at room temperature and transitioned to form vesicles when heated above their LCST, which could be adjusted between 30 and 40°C by varying the composition. The vesicle shells were then crosslinked by polyelectrolyte complexation. Qin *et al.* prepared thermoresponsive, doxorubicin-containing PEG-PNIPAAm-based polymersomes that self-associated upon heating above their LCST and could be destabilized, or ruptured, upon local cooling with either ice or penetrating cryoprobes [71]. These experiments demonstrate how temperature sensitivity can be utilized to create localized drug release following minimally invasive delivery. For an in-depth review of stimuli-responsive polymersomes in targeted drug delivery, see [72].

Thermoresponsive films can also be used as coatings on medical implants to create a stimuli-responsive material capable of modulating the microenvironment surrounding the implant. For example, a rate-controlling thermoresponsive film may increase its release rate in response to slightly elevated increases in temperature due to localized inflammation.

Using thermoresponsive materials, there are numerous design architectures that can be generated, and researchers must decide which type is suitable for their intended application. For an in-depth review on temperature-responsive polymer architecture, see [8] and [69].

### Expert commentary

When designing drug delivery vehicles, an important design question to consider is whether to use natural or synthetic materials. Both choices possess inherent advantages and disadvantages. While natural materials offer great potential for inherent biocompatibility, synthetic materials offer greater flexibility for manipulation and tuning of system performance. With natural materials, we are limited in our ability to modulate the material's properties, unless we resort to the use of synthetic modification techniques. Furthermore, natural materials often possess indefinite composition, poor mechanical strength, variable and uncontrollable degradation kinetics, microbial contamination and compatibility issues [31]. Conversely, synthetic polymers allow a high degree of control over important design constraints, such as mechanical properties, degradation rates, pore size, morphology, scaffold shape and size, drug-release kinetics and biomimetic behavior [31]. It is the opinion of the authors that, moving forward, synthetic polymers inspired by, and potentially augmented by, natural materials will provide valuable tools for the design of novel drug-releasing scaffolds. Patenaude *et al.* synthesized novel hybrids of natural and synthetic materials based on PNIPAAm and various carbohydrate polymers [73]. These studies demonstrated a high degree of control over copolymer properties, such as swelling, degradation, phase transition, and mechanical properties, effectively combining the desired performance features of both natural (degradation and

biological interactions) and synthetic (compositional diversity and thermal sensitivity) materials. TABLE 2 lists some of the advantages and disadvantages of natural and synthetic materials for medical application.

The current state of temperature-sensitive drug delivery copolymers offers minimally invasive implantation of sustained-release scaffolds to hard-to-access regions within the body through simple injection and *in situ* gelation. Furthermore, through utilization of the subtle temperature increase in tumor tissues, it is possible to tailor scaffolds to undergo a sol–gel phase transition upon encountering a tumor, thus targeting the subtle physiological differences and providing localized dosing. Several strategies, such as localized ultrasound application, can induce subtle temperature increases that lead to directed accumulation of drug carriers that possess gelling temperatures slightly above physiologic temperature, and penetrating cryoprobes can induce localized cooling to destabilize drug carriers. Thus, temperature-sensitive drug delivery scaffolds are particularly interesting for cancer therapeutics and applications where minimally invasive procedures are crucial, such as spinal cord [56] and ocular cell and drug delivery purposes [74]. However, temperature-responsive copolymers alone are limited in their ability to respond to the abundance of subtle differences that characterize specific diseased states. Therefore, when used in conjunction with additional stimuli-responsive materials, the degree of control vastly increases, as dual or multiresponsive materials can respond with controllable properties to a number of different physiological states.

There are two classifications of stimuli-responsive materials that can be used to further functionalize temperature-sensitive drug delivery scaffolds: materials that respond to internal stimuli present in the *in vivo* environment, and those that respond to externally applied stimuli. Light, magnetism, electrical impulses and ultrasound are examples of stimuli that can be externally applied to manipulate and regulate the performance of implanted scaffolds [75]. Ionic strength, pH, enzymes, antigen–antibody interactions, or the presence of specific chemicals are examples of internal stimuli that may drive a behavioral change in an

**Table 2. A list of some of the advantages and disadvantages of using naturally derived and synthetic materials in medical applications.**

	Natural materials	Synthetic materials
Advantages	<ul style="list-style-type: none"> <li>Inherent biocompatibility</li> <li>Safe degradation byproducts</li> <li>Defined cellular and biological interactions</li> <li>Natural materials are well suited to 'nature-mimicking' strategies popular in tissue engineering</li> <li>Can provide a close approximation of native extracellular matrix</li> </ul>	<ul style="list-style-type: none"> <li>Synthetic flexibility and compositional diversity</li> <li>High degree of control over performance parameters, such as molecular weight, mechanical properties, elasticity, stimulus-response, release profile, degradation kinetics and so on</li> <li>Easily sterilized</li> </ul>
Disadvantages	<ul style="list-style-type: none"> <li>Limited number of natural polymers, therefore restricted range of attainable properties</li> <li>Batch-to-batch variability with indefinite composition</li> <li>Poor mechanical strength</li> <li>Can illicit an immune response</li> <li>Biological contamination</li> <li>Sterilization can be difficult</li> </ul>	<ul style="list-style-type: none"> <li>Carbon–carbon backbone is not inherently degradable, thus degradation strategies are often required, which can induce inflammation and cytotoxicity</li> <li>Often engineered in attempt to 'mimic' biological tissues, however, unable to recreate 'true' extracellular microenvironment</li> <li>Can illicit a foreign body reaction</li> </ul>



implanted scaffold [76]. Internal stimuli have the ability to act as a negative-feedback loop and generate a direct response to the surrounding physiologic environment. By contrast, externally regulated stimuli-responsive materials require active manipulation from an outside source to generate a change in performance properties. While internal stimuli may provide better on-demand release profiles and tighter regulation of the pathological state, materials requiring external stimuli afford physicians a greater degree of control over the dosing parameters, which is particularly important should complications arise. For an in-depth review of recent advances and future perspectives of various stimuli-responsive materials, see [75–77].

#### **Thermoresponsive & externally regulated stimuli responsive systems**

There are many examples of dual thermo- and externally regulated copolymer systems. Temperature- and light-responsive materials were prepared from photochromic derivatives of ELP, in which one azobenzene moiety was incorporated for every 30 amino acid residues [78]. Irradiation at 350 nm induced a *trans-cis* isomerization, which increased the hydrophilicity of the material and shifted the phase transition temperature from 32–42°C. Irradiation with a longer wavelength was found to reform 50% of the hydrophobic *trans* isomer, thus driving phase separation. Such a system could be used to generate a pulsed-release profile for on-demand release. Zrinyi synthesized thermo- and magneto-responsive polymer beads by incorporating magnetic nanoparticles into crosslinked PNIPAAm and poly(vinyl alcohol) hydrogels [79]. In uniform magnetic fields, the gel beads arranged into linear, chainlike structures. However, in nonuniform fields, the gels formed random aggregates. This study demonstrates the ability to externally manipulate scaffold architecture with externally applied magnetism. This concept could be extended to manipulate gates in a channeled drug-release scaffold, thus creating on–off capabilities and a pulsatile release profile. Kim *et al.* prepared thermo- and electro-responsive IPNs from poly(vinyl alcohol) and PNIPAAm [80]. Electro-responsive materials tend to swell, shrink or bend in response to an applied electric field and are typically comprised of polyelectrolyte hydrogels [81]. As the charged ions are guided towards the cathode or anode side of the gel, deformation of the polyelectrolyte occurs [81]. Ultrasound is a noninvasive stimulus that has been shown to influence drug-release properties within the body by accelerating degradation in degradable polymers and enhancing the permeation of drug in both eroding and non-eroding scaffolds [81]. Ultrasound can be used to disrupt micelle architecture through acoustic destabilization, thus inducing release of the therapeutic payload [81,82]. It can also be used to induce localized heating and aggregation of thermoresponsive drug scaffolds.

#### **Thermoresponsive & internally regulated stimuli-responsive systems**

Thermoresponsive copolymers have also been combined with a number of materials that respond to internal stimuli.

pH-responsive systems have received considerable attention owing to the significant variation of pH within the different locations of the body. In the GI tract, the stomach has an acidic pH between 1 and 3, whereas the pH in the duodenum ranges from 4.8 to 8.2 [3]. Cancer tissue has a slight acidic extracellular pH between 6.5–7.2, whereas normal tissues and blood possess a pH around 7.4 [3]. Furthermore, intracellular variations in pH can be exploited for targeted delivery; the early endosome, late endosome and lysosome have pH values of 6.0–6.5, 5.0–6.0 and 4.5–5.0, respectively [3]. pH-responsive polymers contain weak acids or weak bases, such as carboxylic acids or amines, and thus undergo changes in their ionization state in response to changes in pH [3]. Changes in the ionization state can lead to conformational changes, such as micelle formation or disruption, or changes in the swelling properties of crosslinked gels [2]. Ionizable polymers possessing a dissociation constant (pKa) that closely matches the pH of the target tissues can utilize the conformational pH-induced changes to release drug at a specific location. There are many examples of thermo- and pH-responsive polymer systems. Brazel and Peppas described the synthesis and characterization of temperature- and pH-responsive hydrogels of methacrylic acid and PNIPAAm [83] and Leung *et al.* synthesized microgels with a thermoresponsive core and pH-sensitive shell [84]. These studies demonstrate the potential to target tissues based on their pH and are particularly interesting for cancer therapeutics as tumor tissues possess an elevated temperature and a slightly acidic pH. In addition to pH, antigen-responsive materials are capable of undergoing significant property changes in response to highly specific stimuli recognition. Lu *et al.* reported the synthesis of thermo- and antigen-responsive hydrogels from the combination of a polymerizable antibody Fab' fragment, which was prepared from an antiluorescein monoclonal antibody, with NIPAAm and *N,N'*-methylenebis(acrylamide) [85]. The resulting hydrogels underwent significant reversible volume changes in response to both temperature and the presence of antigens. Glucose-responsive copolymers are of considerable interest for their ability to detect glucose levels and deliver insulin as required [81]. Glucose-responsive polymers typically function either through enzymatic oxidation of glucose via glucose oxidase, through glucose binding with concanavalin A or through reversible bond formation with boronic acids [81]. Thermo- and glucose-responsive copolymers have been synthesized from comb-type graft copolymers of PNIPAAm-co-3-acrylamidophenylboronic acid) [86], and through covalently linking glucose oxidase to copolymers of NIPAAm, methacrylic acid and octadecylacrylate and subsequently immobilizing to the surface of liposomes [87]. Such scaffolds could introduce sustained-release scaffolds that detect blood sugar levels and modify their insulin-release profile accordingly, thus decreasing the frequency of insulin injections and allowing tighter regulation of blood sugar levels.

While temperature-sensitive materials have tremendous potential for targeted drug delivery, combination with dual and multi-responsive polymer systems has the potential to unleash and help realize the true capabilities of these drug release scaffolds to create personalized and on-demand release profiles.

### Five-year view

It is becoming increasingly possible to synthesize drug delivery scaffolds consisting of multiple stimuli-responsive materials that can locally release a multitude of different pharmaceuticals on demand in response to internal physiological feedback and externally applied signals. Such control will allow drastically improved manipulation of the microenvironment of diseased tissues and improve the regulation of systemic conditions. As our understanding of the physiological signature of different diseases increases, so too will our ability to design drug-releasing scaffolds that produce a predictable and controllable response to disease-specific stimuli. As mentioned, temperature-sensitive systems alone are limited in their ability to respond to the surplus of stimuli that characterize a specific disease. Therefore, the true power of thermoresponsive drug-releasing scaffolds will be realized when they are combined with additional stimuli-responsive materials. Such dual and multiresponsive drug delivery scaffolds are beginning to emerge in the literature as temperature-sensitive polymers are combined with materials capable of external regulation through stimuli such as light [88], magnetism [89] and ultrasound [90]. However, a new generation of stimuli-responsive materials is emerging, wherein the identification of differentiating environmental factors characterizing various conditions is allowing the use of intricate internal stimuli to manipulate polymer properties to create a predefined response to disease-specific environmental cues, thus providing on-demand, personalized treatment. A thermoresponsive, glucose-sensitive copolymer that forms an insulin-loaded

scaffold upon injection into the body with release that is dictated by blood sugar levels would mimic the body's natural regulation mechanism and help provide tighter regulation of blood sugar levels for diabetic patients. The generation of such nature-mimicking scaffolds will be driven by the improved understanding of biochemical pathways implicated in various diseases. Better characterization of the chemical signature of various diseases expands the engineer's toolbox for designing novel scaffolds capable of providing personalized treatment. Thus, future generations of drug delivery scaffolds will require a multidisciplinary approach to harness the true potential of stimuli-responsive materials.

### Financial & competing interests disclosure

*The authors would like to acknowledge NSERC and the NSERC 20/20 Ophthalmic Materials Network for funding. H Sheardown is the founder of the 20/20 NSERC Ophthalmic Materials Network, which had/had ties with and receives funding from the following industrial partners: Alimera Sciences, CIBA Vision Corporation, Custom Contact Lenses, GlaxoSmithKline, Fovea Pharmaceuticals, iCo Therapeutics, Siltech Corporation, Take Control Cosmedix, Vista Optics Limited and Walsh Medical Devices Incorporated. The authors have no other relevant affiliations or financial involvement with any organization or entity with a financial interest in or financial conflict with the subject matter or materials discussed in the manuscript apart from those disclosed.*

*No writing assistance was utilized in the production of this manuscript.*

### Key issues

- Temperature-sensitive drug delivery scaffolds allow minimally invasive instillation of sustained-release scaffolds for localized or systemic treatment.
- Encapsulation within a scaffold protects pharmaceuticals from undesirable interactions and enzymatic or environmental degradation. Furthermore, the scaffolds can be designed to generate sustained drug release, maintaining concentrations within the therapeutic window and avoiding complications frequently associated with simple injections.
- There are numerous temperature-responsive polymers and architectures to choose from when designing drug delivery scaffolds. Several design choices include whether to use degradable versus nondegradable scaffolds, natural versus synthetic materials and which architecture (simple hydrogel aggregates, interpenetrating networks, micelles, polymersomes, films and so on) is best suited for the intended application.
- Synthetic materials offer a high degree of flexibility, allowing manipulation of mechanical properties, degradation rates, pore size, morphology, scaffold shape and size, and drug release kinetics, whereas natural materials often possess uncontrollable degradation kinetics, microbial contamination and compatibility issues. Ultimately, combinations of natural and synthetic materials may overcome the limitations while capitalizing on the strengths of both types of materials.
- Temperature-sensitive drug delivery scaffolds are particularly well suited for delivery of chemotherapeutics. Scaffolds designed with a gelling temperature slightly above physiologic value utilize the subtle temperature increase in tumor tissues to drive scaffold formation and accumulation in tumor vasculature and the surrounding tissues.
- *In situ* gelling temperature-sensitive drug delivery scaffolds have tremendous potential for hard-to-access complications requiring minimally invasive techniques, such as ocular and spinal cord therapeutics.
- Combining temperature-sensitive polymers with additional stimuli responsive materials imparts the ability to respond to numerous external and internal stimuli, such as light, magnetism, electrical impulses, ultrasound (external) and ionic strength, pH, enzymes, antigen-antibody interactions or specific chemicals (internal). Such dual and multiresponsive drug delivery scaffolds offer a significant level of control over dosing characteristics and treatment personalization.
- The continued identification of differentiating environmental factors characterizing specific diseases will allow the development of increasingly intricate scaffolds capable of responding to disease-specific cues to provide negative feedback that attempts to mimic the body's natural regulation mechanisms.

## References

- Bikram M, West JL. Thermo-responsive systems for controlled drug delivery. *Expert Opin. Drug Deliv.* 5(10), 1077–1091 (2008).
- Bajpai AK, Bajpai J, Saini R, Gupta R. Responsive polymers in biology and technology. *Polymer Rev.* 51(1), 53–97 (2011).
- Schmaljohann D. Thermo- and pH-responsive polymers in drug delivery. *Adv. Drug Deliv. Rev.* 58(15), 1655–1670 (2006).
- Li Z, Guan J. Thermosensitive hydrogels for drug delivery. *Expert Opin. Drug Deliv.* 8(8), 991–1007 (2011).
- Hoogenboom R, Lambermont-Thijs HML, Jochems MJHC *et al.* A schizophrenic gradient copolymer: switching and reversing poly(2-oxazoline) micelles based on UCST and subtle solvent changes. *Soft Matter* 5(19), 3590–3592 (2009).
- Rapoport N. Physical stimuli-responsive polymeric micelles for anti-cancer drug delivery. *Progr. Polymer Sci.* 32(8–9), 962–990 (2007).
- Hirsch LR, Stafford RJ, Bankson JA *et al.* Nanoshell-mediated near-infrared thermal therapy of tumors under magnetic resonance guidance. *Proc. Natl Acad. Sci. USA* 100(23), 13549–13554 (2003).
- Ward MA, Georgiou TK. Thermoresponsive polymers for biomedical applications. *Polymers* 3(3), 1215–1242 (2011).
- Tanaka T. Collapse of gels and the critical endpoint. *Phys. Rev. Lett.* 40(12), 820–823 (1978).
- Neradovic D, Hinrichs WLJ, Kettenes-Van Den Bosch JJ, Hennink WE. Poly(*N*-isopropylacrylamide) with hydrolyzable lactic acid ester side groups: a new type of thermosensitive polymer. *Macromol. Rapid Commun.* 20(11), 577–581 (1999).
- Ruggiero A, Villa CH, Bander E *et al.* Paradoxical glomerular filtration of carbon nanotubes. *Proc. Natl Acad. Sci. USA* 107(27), 12369–12374 (2010).
- Yoshida T, Aoyagi T, Kokufuta E, Okano T. Newly designed hydrogel with both sensitive thermoresponse and biodegradability. *J. Polym. Sci. A Polym. Chem.* 41(6), 779–787 (2003).
- Guan J, Hong Y, Ma Z, Wagner WR. Protein-reactive, thermoresponsive copolymers with high flexibility and biodegradability. *Biomacromolecules* 9(4), 1283–1292 (2008).
- Ma Z, Nelson DM, Hong Y, Wagner WR. Thermally responsive injectable hydrogel incorporating methacrylate–polylactide for hydrolytic lability. *Biomacromolecules* 11(7), 1873–1881 (2010).
- Cui Z, Lee BH, Vernon BL. New hydrolysis-dependent thermosensitive polymer for an injectable degradable system. *Biomacromolecules* 8(4), 1280–1286 (2007).
- Cui Z, Lee BH, Pauken C, Vernon BL. Manipulating degradation time in a *N*-isopropylacrylamide-based co-polymer with hydrolysis-dependent LCST. *J. Biomater. Sci. Polym. Ed.* 21(6), 913–926 (2010).
- Fitzpatrick SD, Jafar Mazumder MA, Muirhead B, Sheardown H. Development of injectable, resorbable drug-releasing copolymer scaffolds for minimally invasive sustained ophthalmic therapeutics. *Acta Biomater.* 8, 2517–2528 (2012).
- Liu CB, Gong CY, Huang MJ *et al.* Thermoreversible gel–sol behavior of biodegradable PCL–PEG–PCL triblock copolymer in aqueous solutions. *J. Biomed. Mater. Res. Part B Appl. Biomater.* 84(1), 165–175 (2008).
- Geever LM, Lyons JG, Higginbotham CL. Photopolymerisation and characterisation of negative temperature sensitive hydrogels based on *N,N*-diethylacrylamide. *J. Mater. Sci. Lett.* 46(2), 509–517 (2011).
- Patra L, Vidyasagar A, Toomey R. The effect of the Hofmeister series on the deswelling isotherms of poly(*N*-isopropylacrylamide) and poly(*N,N*-diethylacrylamide). *Soft Matter* 7(13), 6061–6067 (2011).
- Beija M, Marty JD, Destarac M. Thermoresponsive poly(*N*-vinyl caprolactam)-coated gold nanoparticles: sharp reversible response and easy tunability. *Chem. Commun.* 47(10), 2826–2828 (2011).
- Advances in Polymer Science.* Aseyev V, Muller AHE, Tenhu H, Borisov O, Winnik FM (Eds). Springer Berlin Heidelberg, Berlin, Germany (2010).
- Klouda L, Mikos AG. Thermoresponsive hydrogels in biomedical applications. *Eur. J. Pharm. Biopharm.* 68(1), 34–45 (2008).
- Batrakova EV, Kabanov AV. Pluronic block copolymers: evolution of drug delivery concept from inert nanocarriers to biological response modifiers. *J. Control. Release* 130(2), 98–106 (2008).
- Wells LA, Lasowski F, Fitzpatrick SD, Sheardown H. Responding to change: thermo- and photo-responsive polymers as unique biomaterials. *Crit. Rev. Biomed. Eng.* 38(6), 487–509 (2010).
- Sosnik A, Cohn D, San Román J, Abraham GA. Crosslinkable PEO–PPO–PEO-based reverse thermo-responsive gels as potentially injectable materials. *J. Biomater. Sci. Polym. Ed.* 14(3), 227–239 (2003).
- Cohn D, Sosnik A, Garty S. Smart hydrogels for *in situ* generated implants. *Biomacromolecules* 6(3), 1168–1175 (2005).
- Sosnik A, Cohn D. Reverse thermo-responsive poly(ethylene oxide) and poly(propylene oxide) multiblock copolymers. *Biomaterials* 26(4), 349–357 (2005).
- Cohn D, Lando G, Sosnik A, Garty S, Levi A. PEO–PPO–PEO-based poly(ether ester urethane)s as degradable reverse thermo-responsive multiblock copolymers. *Biomaterials* 27(9), 1718–1727 (2006).
- Wang Y, Tan Y, Huang X, Xu G. Gelation behavior of thermo-responsive poly(ethylene oxide) and poly(propylene oxide) multiblock polycarbonates. *J. Macromol. Sci. A* 46(4), 397–404 (2009).
- Kumbar SG, Bhattacharyya S, Nukavarapu SP, Khan YM, Nair LS, Laurencin CT. *In vitro* and *in vivo* characterization of biodegradable poly(organophosphazenes) for biomedical applications. *J. Inorg. Organomet. Polymer. Mater.* 16(4), 365–385 (2006).
- Schacht E, Vandorpe J, Dejardin S, Lemmouchi Y, Seymour L. Biomedical applications of degradable polyphosphazenes. *Biotechnol. Bioeng.* 52(1), 102–108 (1996).
- Laurencin CT, Koh HJ, Neenan TX, Allcock HR, Langer R. Controlled release using a new bioerodible polyphosphazene matrix system. *J. Biomed. Mater. Res.* 21(10), 1231–1246 (1987).
- Lee KY, Mooney DJ. Hydrogels for tissue engineering. *Chem. Rev.* 101(7), 1869–1879 (2001).
- Conconi MT, Lora S, Baiguera S *et al.* *In vitro* culture of rat neuromicrovascular endothelial cells on polymeric scaffolds. *J. Biomed. Mater. Res. A* 71(4), 669–674 (2004).
- Bhattacharyya S, Lakshmi S, Bender J *et al.* Preparation of poly bis(carboxylato phenoxy)phosphazene non-woven nanofiber mats by electrospinning. In: *Architecture and Application of Biomaterials*



- and *Biomolecular Materials*. Wong JY, Plant AL, Schmidt CE *et al.* (Eds). Materials Research Society, PA, USA, 157–163 (2004).
- 37 Langone F, Lora S, Veronese FM *et al.* Peripheral nerve repair using a poly(organo)phosphazene tubular prosthesis. *Biomaterials* 16(5), 347–353 (1995).
- 38 Al-Abd AM, Hong KY, Song SC, Kuh HJ. Pharmacokinetics of doxorubicin after intratumoral injection using a thermosensitive hydrogel in tumor-bearing mice. *J. Control. Release* 142(1), 101–107 (2010).
- 39 Chilkoti A, Dreher MR, Meyer DE. Design of thermally responsive, recombinant polypeptide carriers for targeted drug delivery. *Adv. Drug Deliv. Rev.* 54(8), 1093–1111 (2002).
- 40 Ge X, Filipe CD. Simultaneous phase transition of ELP tagged molecules and free ELP: an efficient and reversible capture system. *Biomacromolecules* 7(9), 2475–2478 (2006).
- 41 Ge X, Hoare T, Filipe CD. Protein-based aqueous-multiphase systems. *Langmuir* 26(6), 4087–4094 (2010).
- 42 Bessa PC, Machado R, Nürnberger S *et al.* Thermoresponsive self-assembled elastin-based nanoparticles for delivery of BMPs. *J. Control. Release* 142(3), 312–318 (2010).
- 43 Meyer DE, Chilkoti A. Genetically encoded synthesis of protein-based polymers with precisely specified molecular weight and sequence by recursive directional ligation: examples from the elastin-like polypeptide system. *Biomacromolecules* 3(2), 357–367 (2002).
- 44 McDaniel JR, Callahan DJ, Chilkoti A. Drug delivery to solid tumors by elastin-like polypeptides. *Adv. Drug Deliv. Rev.* 62(15), 1456–1467 (2010).
- 45 Liu W, MacKay JA, Dreher MR *et al.* Injectable intratumoral depot of thermally responsive polypeptide-radionuclide conjugates delays tumor progression in a mouse model. *J. Control. Release* 144(1), 2–9 (2010).
- 46 Dreher MR, Simnick AJ, Fischer K *et al.* Temperature triggered self-assembly of polypeptides into multivalent spherical micelles. *J. Am. Chem. Soc.* 130(2), 687–694 (2008).
- 47 MacKay JA, Chen M, McDaniel JR, Liu W, Simnick AJ, Chilkoti A. Self-assembling chimeric polypeptide-doxorubicin conjugate nanoparticles that abolish tumours after a single injection. *Nat. Mater.* 8(12), 993–999 (2009).
- 48 Meyer DE, Shin BC, Kong GA, Dewhirst MW, Chilkoti A. Drug targeting using thermally responsive polymers and local hyperthermia. *J. Control. Release* 74(1–3), 213–224 (2001).
- 49 Chang Y, Xiao L, Du Y. Preparation and properties of a novel thermosensitive *N*-trimethyl chitosan hydrogel. *Polymer Bull.* 63(4), 531–545 (2009).
- 50 Chenite A, Chaput C, Wang D *et al.* Novel injectable neutral solutions of chitosan form biodegradable gels *in situ*. *Biomaterials* 21(21), 2155–2161 (2000).
- 51 Molinaro G, Leroux JC, Damas J, Adam A. Biocompatibility of thermosensitive chitosan-based hydrogels: an *in vivo* experimental approach to injectable biomaterials. *Biomaterials* 23(13), 2717–2722 (2002).
- 52 Ruel-Gariépy E, Leroux JC. *In situ*-forming hydrogels – review of temperature-sensitive systems. *Eur. J. Pharm. Biopharm.* 58(2), 409–426 (2004).
- 53 Van Vlierberghe S, Dubruel P, Schacht E. Biopolymer-based hydrogels as scaffolds for tissue engineering applications: a review. *Biomacromolecules* 12(5), 1387–1408 (2011).
- 54 Sarkar N. Thermal gelation properties of methyl and hydroxypropyl methylcellulose. *J. Appl. Polymer. Sci.* 24(4), 1073–1087 (1979).
- 55 Gupta D, Tator CH, Shoichet MS. Fast-gelling injectable blend of hyaluronan and methylcellulose for intrathecal, localized delivery to the injured spinal cord. *Biomaterials* 27(11), 2370–2379 (2006).
- 56 Kang CE, Poon PC, Tator CH, Shoichet MS. A new paradigm for local and sustained release of therapeutic molecules to the injured spinal cord for neuroprotection and tissue repair. *Tissue Eng. Part A* 15(3), 595–604 (2009).
- 57 Ballios BG, Cooke MJ, van der Kooy D, Shoichet MS. A hydrogel-based stem cell delivery system to treat retinal degenerative diseases. *Biomaterials* 31(9), 2555–2564 (2010).
- 58 De Freitas RA, Busato AP, Mitchell DA, Silveira JLM. Degalatosylation of xyloglucan: effect on aggregation and conformation, as determined by time dependent static light scattering, HPSEC-MALLS and viscosimetry. *Carbohydr. Polymer.* 83(4), 1636–1642 (2011).
- 59 Miyazaki S, Suisha F, Kawasaki N, Shirakawa M, Yamatoya K, Attwood D. Thermally reversible xyloglucan gels as vehicles for rectal drug delivery. *J. Control. Release* 56(1–3), 75–83 (1998).
- 60 Itoh K, Tsuruya R, Shimoyama T *et al.* *In situ* gelling xyloglucan/alginate liquid formulation for oral sustained drug delivery to dysphagic patients. *Drug Dev. Ind. Pharm.* 36(4), 449–455 (2010).
- 61 Miyazaki S, Suzuki S, Kawasaki N, Endo K, Takahashi A, Attwood D. *In situ* gelling xyloglucan formulations for sustained release ocular delivery of pilocarpine hydrochloride. *Int. J. Pharm.* 229(1–2), 29–36 (2001).
- 62 Takahashi A, Suzuki S, Kawasaki N *et al.* Percutaneous absorption of non-steroidal anti-inflammatory drugs from *in situ* gelling xyloglucan formulations in rats. *Int. J. Pharm.* 246(1–2), 179–186 (2002).
- 63 Suisha F, Kawasaki N, Miyazaki S *et al.* Xyloglucan gels as sustained release vehicles for the intraperitoneal administration of mitomycin C. *Int. J. Pharm.* 172(1–2), 27–32 (1998).
- 64 Kim SJ, Shin SR, Kim NG, Kim SI. Swelling behavior of semi-interpenetrating polymer network hydrogels based on chitosan and poly(acryl amide). *J. Macromol. Sci. Pure Appl. Chem.* A42(8), 1073–1083 (2005).
- 65 Owens DE, Iii, Jian Y, Fang JE, Slaughter BV, Chen Y-H, Peppas NA. Thermally responsive swelling properties of polyacrylamide/poly(acrylic acid) interpenetrating polymer network nanoparticles. *Macromol.* 40(20), 7306–7310 (2007).
- 66 Chen Y, Ding D, Mao Z *et al.* Synthesis of hydroxypropylcellulose-poly(acrylic acid) particles with semi-interpenetrating polymer network structure. *Biomacromolecules* 9(10), 2609–2614 (2008).
- 67 Quan CY, Chen JX, Wang HY *et al.* Core-shell nanosized assemblies mediated by the alpha-beta cyclodextrin dimer with a tumor-triggered targeting property. *ACS Nano* 4(7), 4211–4219 (2010).
- 68 Wei H, Cheng C, Chang C *et al.* Synthesis and applications of shell cross-linked thermoresponsive hybrid micelles based on poly(*N*-isopropylacrylamide-co-3-(trimethoxysilyl)propyl methacrylate)-b-poly(methyl methacrylate). *Langmuir* 24(9), 4564–4570 (2008).
- 69 Stuart MaC, Huck WTS, Genzer J *et al.* Emerging applications of stimuli-

- responsive polymer materials. *Nat. Mater.* 9(2), 101–113 (2010).
- 70 Li Y, Lokitz BS, McCormick CL. Thermally responsive vesicles and their structural 'locking' through polyelectrolyte complex formation. *Angew. Chem. Int. Ed. Engl.* 45(35), 5792–5795 (2006).
- 71 Qin S, Geng Y, Discher DE, Yang S. Temperature-controlled assembly and release from polymer vesicles of poly(ethylene oxide)-block-poly(*N*-isopropylacrylamide). *Adv. Mater.* 18(21), 2905–2909 (2006).
- 72 Meng F, Zhong Z, Feijen J. Stimuli-responsive polymersomes for programmed drug delivery. *Biomacromolecules* 10(2), 197–209 (2009).
- 73 Patenaude M, Hoare T. Injectable, mixed natural-synthetic polymer hydrogels with modular properties. *Biomacromolecules* 13(2), 369–378 (2012).
- 74 Fitzpatrick SD, Jafar Mazumder MA, Lasowski F, Fitzpatrick LE, Sheardown H. PNIPAAm-grafted-collagen as an injectable, *in situ* gelling, bioactive cell delivery scaffold. *Biomacromolecules* 11(9), 2261–2267 (2010).
- 75 Bawa P, Pillay V, Choonara YE, du Toit LC. Stimuli-responsive polymers and their applications in drug delivery. *Biomed. Mater.* 4(2), 022001 (2009).
- 76 Roy D, Cambre JN, Sumerlin BS. Future perspectives and recent advances in stimuli-responsive materials. *Progr. Polymer Sci.* 35, 278–301 (2010).
- 77 McCoy CP, Brady C, Cowley JF *et al.* Triggered drug delivery from biomaterials. *Expert Opin. Drug Deliv.* 7(5), 605–616 (2010).
- 78 Strzegowski LA, Martinez MB, Gowda DC, Urry DW, Tirrell DA. Photomodulation of the inverse temperature transition of a modified elastin poly(pentapeptide). *J. Am. Chem. Soc.* 116(2), 813–814 (1994).
- 79 Zrinyi M. Intelligent polymer gels controlled by magnetic fields. *Colloid. Polymer. Sci.* 278(2), 98–103 (2000).
- 80 Kim SJ, Park SJ, Lee SM, Lee YM, Kim HC, Kim SI. Electroactive characteristics of interpenetrating polymer network hydrogels composed of poly(vinyl alcohol) and poly(*N*-isopropylacrylamide). *J. Appl. Polymer Sci.* 89(4), 890–894 (2003).
- 81 *Handbook of Stimuli-Responsive Materials.* Urban MW (Ed.). Wiley-VCH Verlag GmbH & Co. KGaA, Weinheim, Germany (2011).
- 82 Munshi N, Rapoport N, Pitt WG. Ultrasonic activated drug delivery from Pluronic P-105 micelles. *Cancer Lett.* 118(1), 13–19 (1997).
- 83 Brazel CS, Peppas NA. Synthesis and characterization of thermo- and chemomechanically responsive poly(*N*-isopropylacrylamide-co-methacrylic acid) hydrogels. *Macromolecules* 28(24), 8016–8020 (1995).
- 84 Leung MF, Zhu JM, Harris FW, Li P. Novel synthesis and properties of smart core-shell microgels. *Macromol. Symp.* 226, 177–185 (2005).
- 85 Lu ZR, Kopeckova P, Kopecek J. Antigen responsive hydrogels based on polymerizable antibody Fab' fragment. *Macromol. Biosci.* 3(6), 296–300 (2003).
- 86 Zhang S-B, Chu L-Y, Xu D, Zhang J, Ju X-J, Xie R. Poly(*N*-isopropylacrylamide)-based comb-type grafted hydrogel with rapid response to blood glucose concentration change at physiological temperature. *Polymer Adv. Tech.* 19(8), 937–943 (2008).
- 87 Jo SM, Lee HY, Kim JC. Glucose-sensitivity of liposomes incorporating conjugates of glucose oxidase and poly(*N*-isopropylacrylamide-co-methacrylic acid-co-octadecylacrylate). *Int. J. Biol. Macromolecules* 45(4), 421–426 (2009).
- 88 Ramanan VV, Hribar KC, Katz JS, Burdick JA. Nanofiber-nanorod composites exhibiting light-induced reversible lower critical solution temperature transitions. *Nanotechnology* 22(49), 494009 (2011).
- 89 Fan T, Li M, Wu X, Li M, Wu Y. Preparation of thermoresponsive and pH-sensitivity polymer magnetic hydrogel nanospheres as anticancer drug carriers. *Colloids Surf. B. Biointerfaces* 88(2), 593–600 (2011).
- 90 Nelson JL, Roeder BL, Carmen JC, Roloff F, Pitt WG. Ultrasonically activated chemotherapeutic drug delivery in a rat model. *Cancer Res.* 62(24), 7280–7283 (2002).
- 91 Laukkanen A, Valtola L, Winnik F. Formation of colloidal stable phase separated poly(*N*-vinylcaprolactam) in water: a study by dynamic light scattering, microcalorimetry, and pressure perturbation calorimetry. *Macromolecules* 37(6), 2268–2274 (2004).
- 92 Schild H. Microcalorimetric detection of lower critical solution temperatures in aqueous polymer solutions. *J. Phys. Chem. B* 94, 4352–4356 (1990).
- 93 Cao Y, Zhu X, Luo J. Effects of substitution groups on the RAFT polymerization of *N*-alkylacrylamides in the preparation of thermosensitive block copolymers. *Macromolecules* 40(18), 6481–6488 (2007).
- 94 Liu HY, Zhu XX. Lower critical solution temperatures of *N*-substituted acrylamide copolymers in aqueous solutions. *Polymer* 40(25), 6985–6990 (1999).
- 95 Uguzdogan E, Camh T, Kabasakal O *et al.* A new temperature-sensitive polymer: poly(ethoxypropylacrylamide). *Eur. Polymer J.* 41, 2142–2149 (2005).
- 96 Yamazaki A, Song J, Winnik F, Brash J. Synthesis and solution properties of fluorescently labeled amphiphilic (*N*-alkylacrylamide) oligomers. *Macromol.* 31, 109–115 (1998).
- 97 Persson J, Johansson HO, Galaev I, Mattiasson B, Tjerneld F. Aqueous polymer two-phase systems formed by new thermoseparating polymers. *Bioseparation* 9(2), 105–116 (2000).
- 98 Yuk S, Cho S, Lee S. pH/temperature-responsive polymer composed of poly((*N,N*-dimethylamino)ethyl methacrylate-co-ethylacrylamide). *Macromolecules* 30, 6856–6859 (1997).
- 99 Liu S, Armes SP. The facile one-pot synthesis of shell cross-linked micelles in aqueous solution at high solids. *J. Am. Chem. Soc.* 123(40), 9910–9911 (2001).
- 100 Chiu TT, Thill BP, Fairchok WJ. Poly(2-ethyl-2-oxazoline): a new water- and organic-soluble adhesive. In: *Advances in Chemistry.* American Chemical Society, Washington, DC, USA, 425–433 (1986).
- 101 Uyama H, Kobayashi S. A novel thermosensitive polymer. Poly(2-iso-propyl-2-oxazoline). *Chem. Lett.* 21(9), 1643–1646 (1992).
- 102 Fusco S. Perspectives on: PEO–PPO–PEO triblock copolymers and their biomedical applications. *J. Bioact. Compat. Polym.* 21(2), 149–164 (2006).
- 103 Gao Y, Sun Y, Ren F, Gao S. PLGA–PEG–PLGA hydrogel for ocular drug delivery of dexamethasone acetate. *Drug Dev. Ind. Pharm.* 36(10), 1131–1138 (2010).
- 104 Jeong B, Bae YH, Lee DS, Kim SW. Biodegradable block copolymers as injectable drug-delivery systems. *Nature* 388(6645), 860–862 (1997).
- 105 Lutz JF, Akdemir O, Hoth A. Point by point comparison of two thermosensitive polymers exhibiting a similar LCST: is the age of poly(NIPAM) over? *J. Am. Chem. Soc.* 128(40), 13046–13047 (2006).

- 106 Badi N, Lutz JF. PEG-based thermogels: applicability in physiological media. *J. Control. Release* 140(3), 224–229 (2009).
- 107 Gong C, Shi S, Wu L *et al.* Biodegradable *in situ* gel-forming controlled drug delivery system based on thermosensitive PCL-PEG-PCL hydrogel. Part 2: sol–gel–sol transition and drug delivery behavior. *Acta Biomater.* 5(9), 3358–3370 (2009).
- 108 Dayananda K, He C, Lee DS. *In situ* gelling aqueous solutions of pH- and temperature-sensitive poly(ester amino urethane)s. *Polymer* 49(21), 4620–4625 (2008).
- 109 Chilkoti A, Christensen T, MacKay JA. Stimulus responsive elastin biopolymers: Applications in medicine and biotechnology. *Curr. Opin. Chem. Biol.* 10(6), 652–657 (2006).
- 110 Urry D, Luan C, Parker T. Temperature of polypeptide inverse temperature transition depends on mean residue hydrophobicity. *J. Am. Chem. Soc.* 113(11), 4346–4348 (1991).
- 111 Liu R, Fraylich M, Saunders BR. Thermoresponsive copolymers: from fundamental studies to applications. *Colloid. Polym. Sci.* 287(6), 627–643 (2009).

# Characterization of viability and proliferation of alginate-poly-L-lysine–alginate encapsulated myoblasts using flow cytometry

Ajit Thakur,<sup>1\*</sup> Ruchira Sengupta,<sup>1,2\*</sup> Hideto Matsui,<sup>3</sup> David Lillcrap,<sup>3</sup> Kim Jones,<sup>1,4</sup> Gonzalo Hortelano<sup>1,2,5</sup>

<sup>1</sup>School of Biomedical Engineering, McMaster University, Hamilton L8N 3Z5, Ontario, Canada

<sup>2</sup>Department of Pathology and Molecular Medicine, McMaster University, Hamilton L8N 3Z5, Ontario, Canada

<sup>3</sup>Department of Pathology and Molecular Medicine, Queen's University, Kingston, Ontario, Canada

<sup>4</sup>Department of Chemical Engineering, McMaster University, Hamilton L8N 3Z5, Ontario, Canada

<sup>5</sup>Research and Development, Canadian Blood Services, Ontario, Canada

Received 24 August 2009; revised 15 December 2009; accepted 5 January 2010

Published online 24 May 2010 in Wiley InterScience (www.interscience.wiley.com). DOI: 10.1002/jbm.b.31648

**Abstract:** Genetically modified cells encapsulated in alginate-poly-L-lysine-alginate (APA) are being developed to deliver therapeutic products to treat a variety of diseases. The characterization of the encapsulated cells thus becomes paramount. This study reports a novel method to assess the viability, granularity and proliferation of encapsulated cells based on flow cytometry. The *in vitro* viability of encapsulated G8 murine myoblasts secreting canine FVIII (cFVIII) measured by flow cytometry was comparable to the traditional trypan blue exclusion method and both correlated with cFVIII secretion levels. In contrast, after implantation into mice, only viability measured by flow cytometry correlated with cFVIII secretion. Further, flow cytometry analysis of encapsulated cells maintained *in vitro* and *in vivo* revealed a greater fraction of granular cells compared to free cells, sug-

gesting that encapsulation influences the morphology (cytoplasmic composition) of cells within APA microcapsules. Interestingly, the proliferation study showed that encapsulated cells proliferate faster, on average, and were more heterogeneous *in vivo* compared to *in vitro* culture conditions, suggesting that encapsulated cell proliferation is complex and environment-dependent. In conclusion, we show that flow cytometry analysis allows for a more consistent and comprehensive examination of encapsulated cells to aid in the development of cell therapy protocols. © 2010 Wiley Periodicals, Inc. *J Biomed Mater Res Part B: Appl Biomater* 94B: 296–304, 2010.

**Key Words:** alginate-poly-L-lysine-alginate, myoblasts, gene therapy, viability, proliferation, granularity

## INTRODUCTION

Implantation of microencapsulated cells is a strategy for the continuous delivery of therapeutic protein products, with the potential to treat a wide variety of diseases.<sup>1</sup> Genetically modified cells are immune-isolated within polymeric and biocompatible devices with pore sizes that prevent immune cell-mediated destruction of the enclosed cells after their implantation *in vivo*.<sup>2</sup> In addition, previous studies have shown improved viability of some types of encapsulated cells compared to free cells, attributing this to the increased local concentration of growth factors secreted by encapsulated cells.<sup>2–4</sup> Alginate-poly-L-lysine-alginate (APA) microcapsules have a polyanionic core formed by calcium alginate with a polycationic membrane composed of poly-L-lysine to control permeability and increase strength. The poly-L-lysine is further coated with alginate to improve biocompatibility.<sup>5</sup> Alginate-based microcapsules have been used to encapsulate a wide variety of living cells engineered to deliver a variety of proteins, including coagulation factor VIII, for the treatment of the bleeding disorder, hemophilia A.<sup>5,6</sup>

Viability of the encapsulated cells is a key parameter for interpreting the secretory ability of the encapsulated cells. Therefore, it is critical in cell and gene therapy experiments to use highly reliable and accurate determinations of cell viability. Previous studies employing encapsulated G8 murine myoblasts of fetal origin for FVIII delivery, primarily used the dye-exclusion method to assess cell viability,<sup>7–11</sup> based on selectively staining dead cells with trypan blue. However, the determination of live and dead cells is based on a small sampling of the total number of cells, and can be quite subjective, varying significantly depending on what is perceived by the examiner to be a healthy cell.<sup>12</sup> Moreover, stained smaller cell fragments may distort an accurate determination, and is thus subject to inconsistency.<sup>12</sup> All things considered, this method of measuring cell viability is highly examiner dependent. Similar limitations exist with other dye-exclusion viability tests such as eosin Y, alamar blue, nigrosine, ethidium bromide, alcian blue, among many others. These viability methods also rely on cells having compromised membranes, and face many of the same problems as

**Correspondence to:** G. Hortelano; e-mail: gonhort@mcmaster.ca

Contract grant sponsors: Canadian Blood Services and the Canadian Hemophilia Society; NSERC

trypan blue exclusion, namely reliability, subjectivity and are limited to assessing a small sample of cells.<sup>13,14</sup>

In this study, we compared a flow cytometry-based method of viability analysis with trypan blue exclusion. Current assays for viability, such as trypan blue, can only report the percentage of living cells, but not the health of these living cells. Flow cytometry has four significant advantages over other viability assays: (1) It is able to analyze thousands of particles per second, ensuring a representative sampling of experimental cell populations; (2) It offers a multi-parameter analysis of cell viability and health; (3) It is able to distinguish between implanted cells and host cells in a heterogeneous population of cells; and (4) The measures are objective and easily quantifiable.

Flow cytometry can objectively identify living cells based on fluorescent intensity of the fluorochrome-labeled cell, cell size as determined by the degree of forward scattering (FS), and also the proportion of the living cells that are granular (and morphologically distinct, as determined by the degree of side scattering) (SS) of the cells.<sup>15</sup> The degree of side scatter on a flow cytometry plot is related to the cytoplasmic complexity of the cell (i.e., shape of the nucleus, the amount and type of cytoplasmic granules or the membrane roughness). In essence, side scatter is a measure of the relative granularity of the cell and thus, can be used as an indication of its health.<sup>16–19</sup> An extremely attractive benefit of flow cytometry analysis is the ability to use selected cell surface markers to discriminate host (recipient) cells that may contaminate the encapsulated cells upon their retrieval, thus increasing the accuracy of this technique. Moreover, it allows for an additional level of analysis for cellular morphology (granularity), which other methods of viability cannot assess.

Along with cell viability, cell proliferation is another indicator of normal cell behavior that can be studied using flow cytometry. Proliferation of certain cell lines, such as myoblasts, is limited within the microcapsule.<sup>20,21</sup> Availability of the cell division tracking dye, carboxyfluorescein diacetate succinimidyl ester (CFSE), makes it possible to examine the number of cell divisions during proliferation.<sup>22</sup> CFSE is a simple and sensitive tool for analyzing multiple parameters of cells. This dye, which is retained within cells, allows for one to examine specific populations of proliferating cells and the dye can survive in cells for 7–10 successive cell generations. Once the CFSE molecule diffuses into cells, its acetate groups are cleaved by intracellular esterases, converting it into a fluorescent membrane-impermeable dye. Since CFSE is retained by the cell in the cytoplasm, each round of cell division decreases the relative fluorescence intensity of the dye by half.<sup>22</sup> Encapsulation may affect the proliferation behavior of cells. Studying the changes in proliferation between free cells, encapsulated cells *in vitro* and encapsulated cells *in vivo* may provide additional insights into how to optimize encapsulated cell secretion.

A hurdle for the use flow cytometry to analyze APA encapsulated cells is the complete removal of the capsule material before analyzing cells. Here, we present a modified technique to de-encapsulate cells suitable for flow cytometry. Our data provide new insight into the behavior of encapsulated mouse fetal myoblasts genetically modified to secrete

canine FVIII (cFVIII). This novel analysis may be extended to other cells being used in cell and gene therapy strategies.

## MATERIALS AND METHODS

### Cell culture

G8 is a fetal skeletal myoblast cell line derived Swiss Webster mice (ATCC, Rockville, MD; CRL-1456). G8 cells were transduced with pLenti-EF1- $\alpha$ -BDD-cFVIII as previously described.<sup>23</sup> G8 cells were cultured on 0.01% collagen coated plates in Dulbecco's modified Eagle's medium (DMEM) supplemented with 1.59 g/L sodium bicarbonate (NaHCO<sub>3</sub>), 20% fetal bovine serum (FBS), 1% streptomycin (100  $\mu$ g/mL) and penicillin (100  $\mu$ g/mL) at 37°C in 5% CO<sub>2</sub>. Cells were subcultured at 80% confluency.

### Microencapsulation

Cell encapsulation technique has been described.<sup>6</sup> Briefly, cells were harvested, counted, and resuspended in 1.7% low viscosity (LV) sodium alginate (Improved Kelmar, ISP Alginates, San Diego, CA) to a concentration of  $\sim 5 \times 10^6$  cells/mL. The cell/alginate suspension was extruded at 0.9 mL/min through a 0.35 mm needle in an electrostatic encapsulator (Nisco Engineering, Zurich, Switzerland) at 7 kV. Extrusion of the cell/alginate suspension into a gelling solution of 1.1% CaCl<sub>2</sub> formed beads with a diameter of 360 ( $\pm 26$ )  $\mu$ m. Alginate was then cross-linked with 0.05% poly-L-lysine for 6 min, and further coated with 0.03% alginate for 2 min. The unpolymerized core of alginate was then dissolved with sodium citrate for 6 min. Microcapsules were cultured *in vitro* in DMEM under cell culture conditions described earlier. Microcapsules to be studied *in vivo* were incubated overnight in serum-free media before being implanted into mice to minimize serum-induced antigenic response.

### De-encapsulation of APA capsules

A protocol from de Groot et al. was optimized to completely remove the alginate-poly-L-lysine-alginate layer and release the enclosed cells for viability staining.<sup>24</sup> A sample of 150  $\mu$ L of capsules was added to 10 mL of 0.25% trypsin/EDTA (Gibco, Burlington, Canada) in a sterile centrifuge tube. The capsules were placed in a gently shaking water bath at 37°C for 30 min. After the incubation, the capsules were broken and any remaining cell clumps dislodged by gently pipetting the suspension 2–3 times. Cells were pelleted by centrifugation and re-suspended in 0.5% BSA in PBS (Ca<sup>2+</sup> and Mg<sup>2+</sup> free) for cell staining. Free cells subjected to the same procedure were used as control.

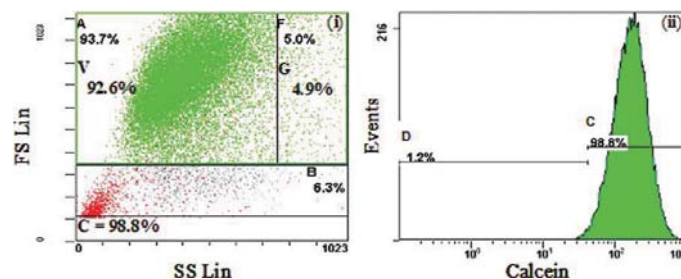
### Trypan blue exclusion

A sample of microcapsules (10  $\mu$ L) were placed on microscope slide and were crushed by a glass cover slip to release the cells, which were subsequently stained with trypan blue (Invitrogen, Burlington, Canada). Live (transparent) and dead (blue) cells were assessed in a given field of view and quantified by light microscopy.

### Flow cytometry

Flow cytometry analysis was carried out using Cytomics Flow Cytometer 500 (Beckman-Coulter) with the CPX





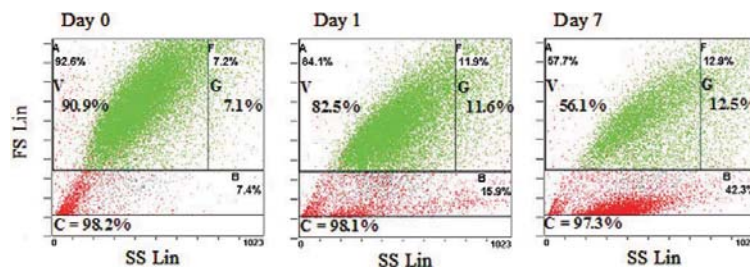
**FIGURE 1.** Flow cytometry-based viability for free G8 cells exposed to the trypsin/EDTA de-encapsulation procedure. (i) The FS/SS plot of Calcein-labeled G8 cells. Box A (>17  $\mu\text{m}$ ) represents live cells (green cells in green box), box B (5–17  $\mu\text{m}$ ) represents dead cells (red) and abnormally small cells and fragments (grey), and box F represents the proportion of cells in box A that were considered granular. The dimensions of all the boxes were held constant when calculating cell viability in all experiments. (ii) The fraction of cells in box A that are brightly labeled with Calcein (live cells in C bracket). The total viability [ $V = (98.8\%/100) \times 93.7\%$ ] and granularity [ $G = (98.8\%/100) \times 5.0\%$ ] of cells was then calculated. The dimly labeled dead cells appear in the D bracket. [Color figure can be viewed in the online issue, which is available at [www.interscience.wiley.com](http://www.interscience.wiley.com).]

software provided. Free or de-encapsulated cells were stained with 1  $\mu\text{L}$  of 50 nM Calcein (Invitrogen, Burlington, Canada), at room temperature in the dark for 20 min, and filtered (40  $\mu\text{m}$  filter), before they were analyzed for viability by flow cytometry. For proliferation studies cells were stained with 2.5 nM carboxyfluorescein succinimidyl ester (CFSE) division tracking dye for 10 min at room temperature, and the reaction stopped with an excess of wash buffer (5% FBS in  $\text{Ca}^{2+}/\text{Mg}^{2+}$  free PBS). The newly labeled cells were re-suspended in media or mixed with alginate for encapsulation. Flow cytometry was used to analyze the CFSE-labeled cells.

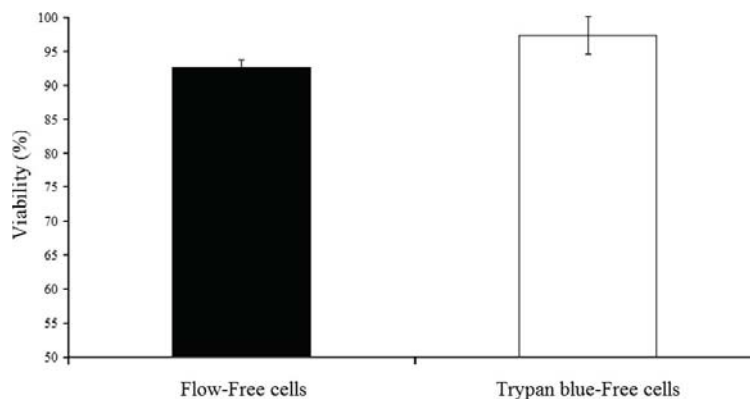
Flow cytometry measures of cell “health” were calibrated against free G8 cells that had been cultured *in vitro* and harvested without being subjected to the mock de-encapsulation procedure. The normal cell size distribution and Calcein-labeling intensity was defined in these healthy cells, and cell viability was calculated using these two parameters. Gated regions on the forward scatter/side scatter (FS/SS) plot were established based on two parameters: cell size (forward scatter) and granularity (side scatter). Box A included cells greater than 17  $\mu\text{m}$ , box B included cells between 5–17  $\mu\text{m}$  and box F included a fraction of the cells

in box A that were considered granular (Figure 1). The cell size cut-offs were determined by the location of the largest population (>90%) of freshly cultured free cells defined in the FS/SS cell density plot, using flow count beads of known size. The granularity (box F) cut-off defined the top 5th percentile of all side-scattered cells that were located in box A. Cell viability was calculated by determining the percentage of all cells in box A that were brightly-labeled (indicative of living cells) with Calcein, as a fraction of total cells (box A and box B) analyzed. The vast majority of freshly cultured free cells were consistently located within one bright population peak. Brightly-labeled cells were defined as the percentage of all cells located within the bright population peak of the Calcein-staining histogram. This distinct bright population peak was selected manually, providing values consistently with a standard deviation of less than 5% for repeat measurements (Figure 1).

The cut-offs for all boxes were uniquely defined for G8 myoblasts and were held constant in all conditions tested (free cells, encapsulated cells and implanted encapsulated cells). It is important to note that without defined cut-offs for cell size and Calcein-labeling intensity, small brightly-labeled cell fragments would be included in the count for



**FIGURE 2.** Representative FS/SS plots of nonimplanted encapsulated G8-cFVIII cells cultured *in vitro*. Samples of G8 cells were de-encapsulated on day 0, 1, and 7, and their viability assessed by flow cytometry. Viability significantly ( $p < 0.05$ ) decreases over the week, as indicated by the increased movement of live cells (green) from box A into box B. Granularity also increases ( $p < 0.05$ ) over the week, as indicated by the movement of cells into box F. (Data presented from ~30,000 events collected). [Color figure can be viewed in the online issue, which is available at [www.interscience.wiley.com](http://www.interscience.wiley.com).]



**FIGURE 3.** Comparison of viability calculated using flow cytometry (black bar) and trypan blue (white bar) for free G8-cFVIII cells cultured *in vitro*. Viability determined using flow cytometry is significantly ( $p < 0.05$ ) different from viability determined by trypan blue. (Error bars indicate standard deviation;  $n = 3$ ).

viability. Approximately 30,000 events were counted per sample of cells. By flow cytometry, brightly labeled (with Calcein) cells larger than  $\sim 17 \mu\text{m}$  were considered alive, while the remaining cells were considered dead (Figure 1).

#### Animal experimentation

C57BL/6 mice were purchased from Charles, River (Montreal, Canada), while FVIII-deficient mice are bred at McMaster University's Central Animal Facilities (CAF). A total of  $20 \times 10^6$  cells each (4 mL) of microcapsules per mouse were injected intra-peritoneally (IP) using a G18 catheter under anaesthesia with isoflurane (Bimeda-MTC, Animal Health, Richmond Hill, Canada) in a small anaesthetic machine (Med-Vet Aesthetic System, Toronto, Canada). Blood samples were taken weekly by retro-orbital bleeding with sodium citrate as anticoagulant (1:9 ratio). Mouse plasma was obtained by centrifugation ( $13,000g$  at  $4^\circ\text{C}$  for 10 min), and stored at  $-70^\circ\text{C}$  until used. All of the animal procedures in animals were performed in accordance with McMaster University's Animal Ethics Guidelines.

#### ELISA assay for cFVIII measurement

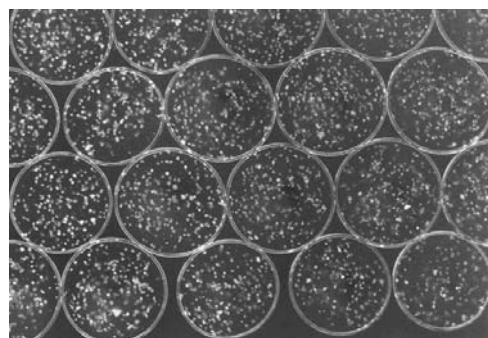
Canine FVIII secretion was quantified using a cFVIII-specific ELISA kit (Affinity Biologicals, Hamilton, Canada), using normal pooled canine plasma (Central Animal Facilities, McMaster University) to generate the standard curves.

#### RESULTS

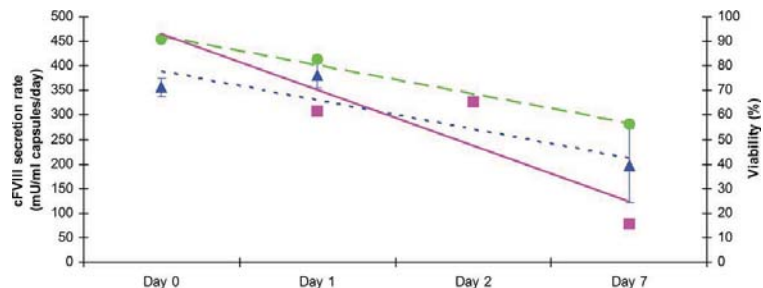
##### Viability of free G8 myoblasts

After establishing the appropriate flow cytometry settings (materials and methods) for running G8 cells and running a sample of 30,000 cells, we calculated that freshly cultured free G8 cells have a viability of 92.6% (Figure 1). The cells located in box F indicated that 4.9% of living free cells in box A were granular, indicating a morphologically distinct subpopulation of live cells. It was imperative that the cells were released from the capsule material before flow analy-

sis could be performed. However, cell de-encapsulation techniques may negatively affect cell viability. Although the de-encapsulation procedure used in this study has been tested before,<sup>24</sup> its effects on myoblasts were investigated. As a control, a sample of free G8 cells were subjected to the same de-encapsulation procedure that was used for encapsulated cells, while a negative control sample was not subjected to trypsin/EDTA. Cell viability was then assessed by flow cytometry. The viability of free cells exposed to the trypsin/EDTA de-encapsulation procedure (92.6%, Figure 1) or free cells exposed to normal cell culture conditions in media without trypsin/EDTA (90.1%, data not shown) was not significantly different ( $p > 0.05$ ) from that of the viability of encapsulated cells on day 0 (90.9%, Figure 2). This indicated that the de-encapsulation procedure did not adversely influence the viability of cells as measured by this method. In addition, we tested and confirmed this result in blood outgrowth endothelial cells (BOECs) (data not shown) as well.



**FIGURE 4.** Murine myoblasts enclosed within APA microcapsules (approximately  $300\text{--}400 \mu\text{m}$  in diameter).



**FIGURE 5.** Relationship between cFVIII secretion rate of non-implanted encapsulated G8-cFVIII cells and viability. Secretion rate (■), trypan blue-based viability (▲) and flow-based viability (●) all significantly ( $p < 0.05$ ) decreased from day 0 to day 7. Trypan blue-based viability and flow cytometry-based viability were not significantly ( $p < 0.05$ ) different. Solid and dashed lines represent the linear regression fit of data presented. (Error bars indicate standard deviation;  $n = 3$ ). [Color figure can be viewed in the online issue, which is available at [www.interscience.wiley.com](http://www.interscience.wiley.com).]

When the viability of free G8 myoblasts as analyzed by flow cytometry and trypan blue exclusion was compared, flow cytometry-based viability produced a more consistent (smaller standard deviations) result ( $92.6\% \pm 1.2\%$ ) than trypan blue exclusion ( $97.3\% \pm 2.7\%$ ). Importantly, the results obtained by the two methods were significantly different ( $p < 0.05$ , Figure 3), with the viability values obtained from trypan blue exclusion being higher.

#### Viability of nonimplanted encapsulated G8-cFVIII cells

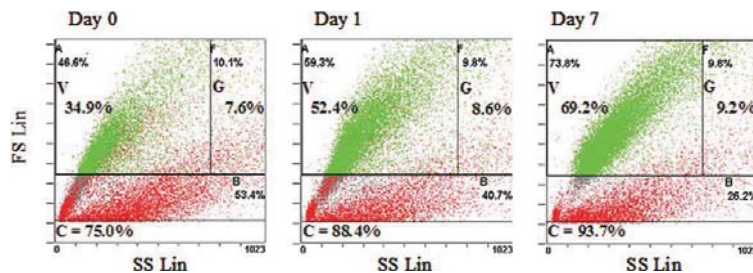
Once the flow cytometry parameters for assessing cell viability were identified, myoblasts were encapsulated and cultured *in vitro* (Figure 4). Samples of G8-cFVIII cells were then de-encapsulated on day 0, 1, and 7, labeled with Calcein and the cell viability calculated by flow cytometry. Cell viability significantly decreased from 90.9% on day 0 to 56.1% on day 7, while at the same time cell granularity (box F) increased from 7.1 to 12.6% from day 0 to day 7 (Figure 2).

Since G8 myoblasts were engineered to secrete FVIII continuously, cFVIII secretion rate (mU/mL of capsules/day) by encapsulated cells was determined and used as another indication of cell viability. Canine FVIII secretion decreased from 306.9 mU/mL capsules/day to 78.3 mU/mL capsules/

day by day 7 ( $p < 0.05$ ), agreeing with both trypan blue exclusion and flow cytometry-based viability techniques (Figure 5). Although the average viability calculated using flow cytometry was consistently higher than viabilities calculated using trypan blue exclusion, the difference was not statistically significant ( $p < 0.05$ ). In addition, we observed similar trends in the data comparing flow cytometry-based and trypan blue-based viabilities using BOECs (data not shown), thereby confirming our results.

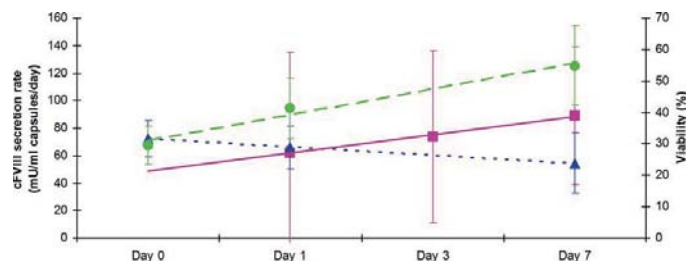
#### Viability of implanted encapsulated G8-cFVIII cells

It is also important to monitor the viability and morphology of encapsulated cells following their implantation *in vivo*. However, such determination can be challenged by potential contamination of the sample with host cells surrounding the microcapsules. Thus, the application of flow cytometry in such conditions was investigated and compared to trypan blue exclusion. A group of C57BL/6 mice were implanted with encapsulated G8-cFVIII myoblasts. After 6 weeks, mice were sacrificed, microcapsules retrieved and cultured *in vitro*. At various time points, samples of cultured microcapsules were de-encapsulated, labeled with Calcein and analyzed by flow cytometry. Initial cell viability on explantation



**FIGURE 6.** Representative FS/SS plots of encapsulated G8-cFVIII cells retrieved 6 weeks postimplantation in mice. The recovered G8-cFVIII cells were subsequently cultured *in vitro*, and samples de-encapsulated on day 0, 1, and 7 to assess their viability using flow cytometry. Viability significantly increases over the week, as indicated by the movement of cells into box B. Granularity slightly increases over the week, as indicated by the movement of cells into box F. (Data presented from  $>25,000$  events collected). [Color figure can be viewed in the online issue, which is available at [www.interscience.wiley.com](http://www.interscience.wiley.com).]





**FIGURE 7.** Relationship between cFVIII secretion rate and viability of encapsulated G8-cFVIII cells cultured *in vitro* after being retrieved from mice. Secretion rate (■) did not significantly increase from day 0 to day 7. Flow-based viability (●) significantly ( $p < 0.05$ ) increased from day 0 to day 7. Trypan blue-based viability (▲) did not significantly decrease from day 0 to day 7. Trypan blue-based viability and flow-based viability were significantly ( $p < 0.05$ ) different. Solid and dashed lines represent the linear regression fit of data presented. (Error bars indicate standard deviation;  $n = 3$ ). [Color figure can be viewed in the online issue, which is available at [www.interscience.wiley.com](http://www.interscience.wiley.com).]

(day 0) was 34.9% and this significantly increased during 7 days of culture to 69.2%, while granularity (box F) of live cells slightly increased from 7.6 to 9.2% from day 0 to day 7 (Figure 6). The increase in viability of encapsulated myoblasts cultured *in vitro* after retrieval was consistent in all data collected ( $n = 3$ ), but the granularity changes were not statistically significant ( $p > 0.05$ ). In contrast, trypan blue-based viability values were significantly different from those yielded by flow ( $p < 0.05$ ).

When the viability measured by trypan blue and flow cytometry were compared to cFVIII secretion, it was interesting to find that the trend displayed in flow cytometry-based viability values positively correlated with the average cFVIII secretion rate (Figure 7), while trypan blue-based viability was negatively correlated with the secretion rate.

Host cells could potentially contaminate the sample of retrieved microcapsules. In particular, professional antigen presenting cells (APCs) such as macrophages or dendritic cells have often been reported to adhere to retrieved microcapsules.<sup>1,6</sup> Thus, in the interest of accuracy, it was important to discriminate between encapsulated and host cells postretrieval. Therefore, four days after retrieval, de-encapsulated cells were stained with anti-CD86 (BD, Franklin Lakes, NJ), a surface marker specific to APCs. No significant staining of CD86 was found, suggesting the absence of antigen presenting cells in the sample (Figure 8).

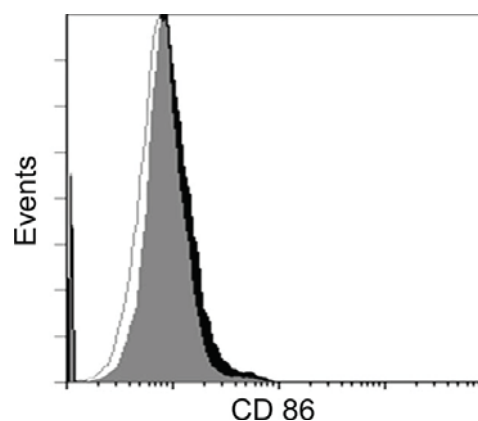
#### Granularity of implanted and nonimplanted encapsulated G8-cFVIII cells

In addition to cell viability, flow cytometry can be used to assess other parameters of cell behavior. In flow cytometry, side scatter is a measure of the relative granularity of the cell and thus, can be used as an indication of its health. In heterogeneous cell samples, granularity can be used as a parameter to morphologically distinguish a subpopulation of cells. Granularity of cells was assessed by setting a threshold (box F) at the extreme end of the forward scatter/side scatter flow cytometry plot (Figure 2) and comparing the relative percentage of cells that appear above this threshold at various time points. The granularity of live free cells (based on cell size and labeling intensity criteria) remained

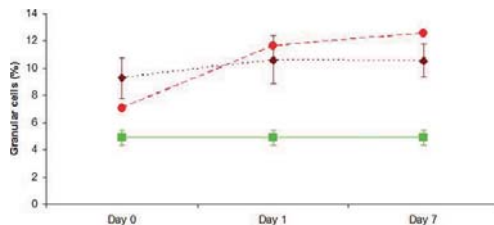
relatively constant for exponentially growing cells *in vitro* (Figure 9). In contrast, both implanted and non-implanted encapsulated cells had a significantly ( $p < 0.05$ ) higher granularity (fraction of live cells in box F) than free cells. There was no significant difference between implanted and non-implanted encapsulated myoblasts at various time points examined. However, we observed that the granularity of G8-cFVIII cells significantly ( $p < 0.05$ ) increased from day 0 (day of encapsulation) to day 7 upon encapsulation and maintenance *in vitro* (Figure 9). A similar increase in the granularity of non-implanted encapsulated cells was also observed in BOECs (data not shown) at equivalent time points.

#### Proliferation of nonimplanted encapsulated G8-cFVIII cells

To study the proliferation behavior of encapsulated cells, G8-cFVIII cells were labeled with CFSE, subsequently encapsulated and cultured *in vitro* for 7 days. A subset of CFSE-labeled free cells was also kept *in vitro* as a control. At



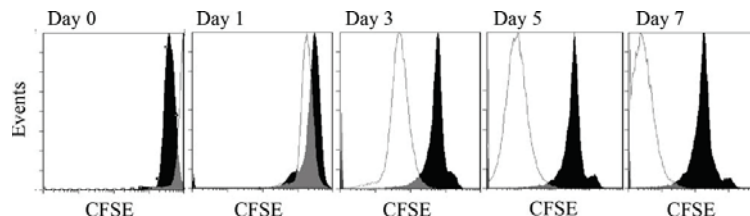
**FIGURE 8.** CD86 staining of de-encapsulated cells postimplantation. The lack of CD86 expression (black) indicates that no CD86 expressing cells were present on the retrieved capsules. White curve represents the isotype control.



**FIGURE 9.** Comparison of the granularity of (■) nonencapsulated (free), (●) nonimplanted encapsulated and (◆) implanted-encapsulated G8 cells. Nonimplanted encapsulated cells were cultured *in vitro*, while implanted-encapsulated cells were retrieved 6 weeks postimplantation (on day 0) and subsequently maintained *in vitro* and deencapsulated on day 0, 1 and 7 to assess their granularity (percentage in box F) using flow cytometry. Free cells had a significantly ( $p < 0.05$ ) lower granularity compared to non-implanted encapsulated and implanted-encapsulated cells. (Error bars indicate standard deviation;  $n = 3$ ). [Color figure can be viewed in the online issue, which is available at [www.interscience.wiley.com](http://www.interscience.wiley.com).]

various time points cells were analyzed by flow cytometry for proliferation. Encapsulated cells cultured *in vitro* proliferated slower (on average) with a doubling time of 1.41 days, while free cells proliferate with a doubling time of 0.59 days (Figure 10). Encapsulated cells also appeared to have multiple sub-populations growing at slightly different rates compared to free cells. In contrast, free cells appeared to divide in synchrony.

The proliferation behavior of encapsulated cells *in vivo* was also examined. A group of C57BL/6 mice were implanted with CFSE-labeled encapsulated G8-cFVIII cells for 7 days. A sample of the prepared microcapsules was kept *in vitro* as a control. On day 7 mice were sacrificed, and microcapsules were retrieved and cultured *in vitro*. The cell proliferation of the implanted microcapsules was compared with the sample kept *in vitro*. Encapsulated cells proliferated slightly faster (on average) *in vivo*, with a doubling time of 1.02 days, while non-implanted encapsulated cells maintained *in vitro* proliferate with a doubling time of 1.20 days (Figure 11). In addition, implanted-encapsulated cells appeared to have a greater range in the rate of cell proliferation, as indicated by the presence of large distinct sub-populations compared to non-implanted encapsulated cells. On day 11, some of the sub-populations in the implanted-encapsulated cells appeared to have become less distinct to the main population of dividing cells.



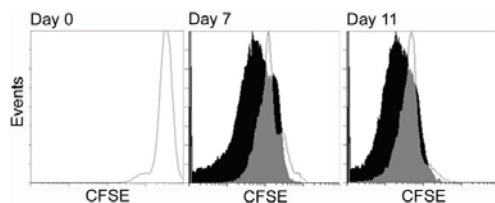
**FIGURE 10.** Proliferation of nonimplanted encapsulated (black) and free (white) G8-cFVIII cells cultured *in vitro*. Encapsulated CFSE-labeled G8-cFVIII cells proliferated slower (on average) than free cells. Representative data presented.

## DISCUSSION

In any microencapsulation-based cell therapy strategy, the accurate assessments of the viability and proliferation of the encapsulated cells are essential for predicting the potential long-term secretion profiles of the therapeutic products. This is the first study to use flow cytometry to evaluate the viability of cells enclosed in alginate-poly-L-lysine-alginate (APA) microcapsules. We developed a flow cytometry-based assay to examine the viability, granularity, and proliferation of cells within the microcapsules, using myoblasts as a model. Our data indicate that flow cytometry yields more consistent viability values than trypan blue, and correlate with cFVIII secretion levels. This could be explained by the fact that trypan blue dye only stains cells with compromised cell membranes.<sup>25</sup> In contrast, Calcein stains live cells based on the enzymatic activity of ubiquitously expressed intracellular esterases. Since dead and unhealthy cells have lower levels of active esterases, they are weakly stained with Calcein. Thus, Calcein fluorescence intensity provides a more accurate estimate of cell viability. A key factor in this technique is the appropriate setting for cell size cut-offs in the flow analysis to exclude small brightly labeled cell fragments from the viability count. It is important to note that in this study the cell size and Calcein-labeling intensity cut-offs were optimized for G8-myoblasts, and although it can be generalized, the parameters are expected to a certain degree be cell line dependant. An additional advantage of this method is that it allows one to determine cell viability without the need for any additional cell surface markers.

When the viability of non-implanted encapsulated cells was measured using flow cytometry and trypan blue exclusion, we found that viability values correlated with each other and with the cFVIII secretion rates, although trypan-based viability was lower than flow cytometry-based viability. This may be due to the more subjective nature of trypan blue staining, where clumps of proliferating cells are generally excluded from the viability estimate due to the difficulty in assessing cell boundaries. Thus, non-aggregated cells are preferentially counted using trypan blue, which perhaps includes a greater proportion of dead cells that reduces the overall viability of encapsulated cells. In addition, our *in vitro* data comparing flow cytometry-based viability and trypan blue exclusion was confirmed using blood outgrowth endothelial cells (BOECs).

We also compared the viability of encapsulated cells implanted into mice, retrieved 6 weeks postimplantation, and found that flow cytometry-based viabilities were significantly



**FIGURE 11.** Proliferation of implanted-encapsulated (black) and non-implanted encapsulated (white) G8-cFVIII cells. Implanted capsules were retrieved after 7 days and cultured *in vitro* until day 11. Implanted-encapsulated CFSE-labeled G8-cFVIII cells proliferate slightly faster (on average) than non-implanted encapsulated cells. Representative data presented from one implantation.

different from trypan blue-based viabilities. However, flow-based viability positively correlated with the cFVIII secretion rate. Given that the average viability of a population of cells is expected to correlate with their average secretion rate, the observed correlation between encapsulated cell viability and cFVIII secretion rate is only supported by flow cytometry data<sup>26,16</sup> (Figure 7). It is also important to note that previous studies have shown that FVIII is able to efficiently diffuse through APA microcapsules in a linear fashion, suggesting that the capsular material is not significantly influencing the average secretion rate. These studies confirm the permeability of the capsules to FVIII, thus validating the correlation between cell viability and secretion.<sup>6</sup>

In addition, the trypsin/EDTA de-encapsulation procedure separated aggregates of proliferating cells into a single cell suspension (data not shown), allowing an accurate analysis by flow cytometry, yet without significantly ( $p > 0.05$ ) affecting cell viability. Furthermore, ~30,000 cells were analyzed by flow compared to the several dozen cells that may be counted by trypan blue. The much larger sample size also resulted in significantly smaller standard deviations ( $p < 0.0001$ ) than those of trypan-based viabilities. The limited sample size feasible and the operator-dependent nature of trypan blue, contribute to more inconsistent viability results. Taken together, this study suggests that the trypsin/EDTA de-encapsulation procedure in conjunction with flow cytometry analysis provides a more objective and consistent estimate of encapsulated cell viability than the traditional trypan blue method.

To address the possibility that host contaminating APCs might potentially be included in our flow cytometry-based viability estimates of encapsulated G8-cFVIII cells, we stained for the presence of the costimulatory molecule CD86 (B7-2), expressed on the cell-membrane of APCs.<sup>27</sup> The absence of cells expressing CD86 among the retrieved myoblasts indicated that there was no APC contamination from the host (Figure 8).

Of note, encapsulated G8 cells were significantly more granular ( $p < 0.05$ ) than free cells. Granularity is a measure of the internal composition of cells based on their light-scattering (quantified by the degree of side-scatter in flow cytometry) properties of their intracellular structures.<sup>17</sup> Free cells have a range of granularity (cytoplasmic heterogeneity) (Figure 5), a reflection of their normal physiology,

which increases upon encapsulation as measured by the percentage of cells in box F (Figures 2 and 6). This indicates that a fraction of live encapsulated cells are morphologically distinct, perhaps representing cells with an altered cFVIII secretion rate. Accumulation of FVIII proteins in the endoplasmic reticulum activates the unfolded protein response (UPR), leading to oxidative stress and apoptosis.<sup>28–30</sup> It is possible that the additional stress of encapsulation itself may have resulted in a greater fraction of cells that are more granular. In agreement with this explanation, Sandhu et al. have shown a correlation between the  $\beta$ -galactosidase secretion of cells and their granularity.<sup>16</sup> This study also demonstrated a positive correlation between the number of viral particles within an infected cell and its granularity.<sup>16</sup> Hence, in our study, FVIII secretion provided a unique opportunity to characterize encapsulated cells.

Our proliferation studies show that encapsulated myoblasts proliferated *in vitro* 2.4-fold slower on average than their free cell counterparts, perhaps attributable to the lack of a proper attachment support of alginate for proliferation.<sup>31–33</sup> The heterogeneous proliferation findings would suggest the presence of subpopulations of myoblasts proliferating at slightly different rates (Figure 10). In contrast, free cells proliferated faster and in synchrony, probably due to the high capacity of the tissue culture-treated surfaces to promote cell adhesion, which allows cells to space themselves uniformly and to adopt an adherent morphology. Interestingly, encapsulated cells that were implanted into mice proliferate 1.2-fold faster on average than non-implanted encapsulated cells (Figure 11), and had multiple subpopulations of cells, proliferating at different rates. These observations suggest that the proliferation behavior of encapsulated cells *in vivo* differs from that of encapsulated cells maintained *in vitro*. It is also possible that the large subpopulations observed in implanted microcapsules represent differentiated myoblasts. *In vivo*, the proinflammatory environment created around the site of implantation may have induced the differentiation of G8 myoblasts into myotube-like non-proliferative cells,<sup>34,35</sup> thus creating the distinct large subpopulation. These data suggest that the proliferation behavior of encapsulated cells is environment-dependent. Given the limited space within microcapsules, it is expected that the proliferation behavior may also have a significant impact on cell viability and consequently their secretion rate.<sup>36</sup> The findings from this study support our previous findings<sup>7,10</sup> and highlight the advantageous characteristic of myoblasts of differentiating into non-proliferative myotubes upon nutrient or cell confluency stress. In contrast to the behavior of proliferative cells such as fibroblasts that can fill the entire capsular space, the proliferation of encapsulated myoblasts is rather limited and will cease when nutrient diffusion is compromised. Therefore, due to the differentiation of myoblasts, capsules are not filled to capacity with cells and can not break as a result of cell proliferation, as we have determined monitoring encapsulated myoblasts retrieved from mice 7 months after their implantation.<sup>7</sup>

As a future challenge, the volume of implanted microcapsules would have to be significantly reduced before

human trials can be considered. A volume of 4 mL of microcapsules used in this study in mice would correspond to several liters when scaled up to human size, a clearly impractical volume.

In conclusion, we propose a novel flow cytometry-based assay to characterize the viability, granularity and proliferation of APA encapsulated cells, which provides a more reliable estimation of viability than trypan blue, and could be of interest in many applications in cell and gene therapy.

#### ACKNOWLEDGMENTS

The authors thank McMaster University's Central Animal Facilities for technical assistance. They also thank Dr. Heather Sheardown for Calcein reagent, and Dr. Frederick A. Oforu and Dr. Murray Potter for reviewing the manuscript.

#### REFERENCES

- Orive G, Tam SK, Pedraz JL, Halle JP. Biocompatibility of alginate-poly-L-lysine microcapsules for cell therapy. *Biomaterials* 2006;27:3691-700.
- Chang T. Therapeutic applications of polymeric artificial cells. *Nat Rev Drug Discov* 2005;4:221-235.
- Kashani SA, Chang T. Effects of hepatic stimulatory factor released from free or microencapsulated hepatocytes on galactosamine induced fulminant hepatic failure animal model. *Biomater Artif Cells Immobilization Biotechnol* 1991;19:565-577.
- Wong H, Chang T. The viability and regeneration of artificial cell microencapsulated rat hepatocyte xenograft transplants in mice. *Biomater Artif Cells Artif Organs* 1988;16:731-739.
- Ponce S, Orive G, Hernandez R, Gascon AR, Pedraz JL, De Haan BJ, Faas MM, Mathieu HJ, De Vos P. Chemistry and the biological response against immunisolating alginate-polycation capsules of different composition. *Biomaterials* 2006;27:4831-4839.
- Garcia-Martin C, Chuah MK, Van Damme A, Robinson KE, Vanzielegem B, Saint-Remy JM, Gallardo D, Oforu FA, Vandendriesche T, Hortelano G. Therapeutic levels of human factor VIII in mice implanted with encapsulated cells: Potential for gene therapy of haemophilia A. *J Gene Med* 2002;4:215-223.
- Hortelano G, Al-Hendy A, Oforu FA, Chang PL. Delivery of human factor IX in mice by encapsulated recombinant myoblasts: A novel approach towards allogeneic gene therapy of hemophilia B. *Blood* 1996;87:5095-5103.
- Hortelano G, Wang L, Xu N, Oforu FA. Sustained and therapeutic delivery of factor IX in nude haemophilia B mice by encapsulated C2C12 myoblasts: Concurrent tumorigenesis. *Haemophilia* 2001;7:207-214.
- Hortelano G, Xu N, Vandenberg A, Solera J, Chang PL, Oforu FA. Persistent delivery of factor IX in mice: Gene therapy for hemophilia using implantable microcapsules. *Hum Gene Ther* 1999;10:1281-1288.
- Wen J, Vargas AG, Oforu FA, Hortelano G. Sustained and therapeutic levels of human factor IX in hemophilia B mice implanted with microcapsules: Key role of encapsulated cells. *J Gene Med* 2006;8:362-369.
- Wen J, Xu N, Li A, Bourgeois J, Oforu FA, Hortelano G. Encapsulated human primary myoblasts deliver functional hFIX in hemophilic mice. *J Gene Med* 2007;9:1002-1010.
- Wehn T, Lorenz T, Behrendt U, Wallerius C, Bontemeyer H, Lehmann J. Determination of animal cell densities and viabilities by the new analyzer CEDX2. *Animal cell technology: Products from cells, cells as products*. In: Proceedings of the 16th ESACT Meeting, Bielefeld. 1999, p 634.
- Jones KH, Senft JA. An improved method to determine cell viability by simultaneous staining with fluorescein diacetate-propidium iodide. *J Histochem Cytochem* 1985;33:77-79.
- Altman SA, Randers L, Rao G. Comparison of trypan blue dye exclusion and fluorometric assays for mammalian cell viability determinations. *Biotechnol Prog* 1993;9:671-674.
- Loken M. *Immunofluorescence Techniques in Flow Cytometry and Sorting*. New York: Wiley; 1990.
- Sandhu KS, Naciri M, Al-Rubeai M. Prediction of recombinant protein production in an insect cell-baculovirus system using a flow cytometric technique. *J Immunol Methods* 2007;325:104-113.
- Bez A, Corsini E, Curti D, Biggiogera M, Colombo A, Nicosia RF, Pagano SF, Parati E. Neurosphere and neurosphere-forming cells: Morphological and ultrastructural characterization. *Brain Res* 2003;993:18-29.
- Murayama A, Matsuzaki Y, Kawaguchi A, Shimazaki T, Okano H. Flow cytometric analysis of neural stem cells in the developing and adult mouse. *Brain* 2002;69:837-847.
- Nordström T, Willamo P, Arvela M, Stenroos K, Lindqvist C. Detection of baculovirus-infected insect cells by flow cytometric side-scatter analyses. *Cytometry* 1999;37:238-242.
- Blau HM, Dhawan J, Pavlath GK. Myoblasts in pattern formation and gene therapy. *Trends Genet* 1993;9:269-274.
- Blau HM, Webster C. Isolation and characterization of human muscle cells. *Proc Natl Acad Sci USA* 1981;78:5623-5627.
- Hawkins ED, Hommel M, Turner ML, Battye FL, Markham JF, Hodgkin PD. Measuring lymphocyte proliferation, survival and differentiation using CFSE time-series data. *Nat Protoc* 2007;2:2057-2067.
- Matsui H, Shibata M, Brown B, Labelle A, Hegadorn C, Andrews C, Hebbel RP, Galipeau J, Hough C, Lillicrap D. Ex vivo gene therapy for hemophilia A that enhances safe delivery and sustained in vivo factor VIII expression from lentivirally engineered endothelial progenitors. *Stem Cells* 2007;25:2660-2669.
- De Groot M, Leuvenink HG, Keizer PP, Fekken S, Schuur TA, Van Schilfgaarde R. Effective removal of alginate-poly-L-lysine microcapsules from pancreatic islets by use of trypsin-EDTA. *J Biomed Mater Res A* 2003;67:679-683.
- Spence DJ, Peyman GA. A new technique for the vital staining of the corneal endothelium. *Invest Ophthalmol* 1976;15:1000-1002.
- Possee RD, Mccarroll L, Thomas CJ, Mann SG, King L. Baculovirus expression vectors: Improving virus-infected cell viability and recombinant protein secretion. In: Al-Rubeai M, editor. *Cell Engineering*. Netherlands: Springer; 1999. pp 108-121.
- De Vos P, Van Hoogmoed CG, De Haan BJ, Busscher H. Tissue responses against immunisolating alginate-PLL capsules in the immediate post-transplant period. *J Biomed Mater Res* 2002;62:430-437.
- Malhotra JD, Miao H, Zhang K, Wolfson A, Pennathur S, Pipe SW, Kaufman R. Antioxidants reduce endoplasmic reticulum stress and improve protein secretion. *Proc Natl Acad Sci USA* 2008;105:18525-18530.
- Srouf MA, Grupp J, Aburubaiha Z, Albert T, Bronckhe H, Oldenburg J, Schwaab R. Modified expression of coagulation factor VIII by addition of a glycosylation site at the N terminus of the protein. *Ann Hematol* 2008;87:107-112.
- Kaufman RJ, Pipe SW, Tagliavacca L, Swaroop M, Moussalli M. Biosynthesis, assembly and secretion of coagulation factor VIII. *Blood Coagul Fibrinolysis* 1997;8:S3-S14.
- De Guzman RC, Ereifej ES, Broadrick KM, Rogers RA, Vandevord P. Alginate-matrigel microencapsulated Schwann cells for inducible secretion of glial cell line derived neurotrophic factor. *J Microencapsulation* 2008;25:487-498.
- Lansdown AB, Payne M. An evaluation of the local reaction and biodegradation of calcium sodium alginate (Kaltostat) following subcutaneous implantation in the rat. *J R Coll Surg Edinb* 1994;39:284-288.
- Augst AD, Kong HJ, Mooney D. Alginate hydrogels as biomaterials. *Macromol Biosci* 2006;6:623-633.
- Nakanishi K, Dohmae N, Morishima N. Endoplasmic reticulum stress increases myofiber formation in vitro. *FASEB J* 2007;21:2994-3003.
- Hawke TJ, Garry D. Myogenic satellite cells: Physiology to molecular biology. *J Appl Physiol* 2001;91:534-551.
- Sitton G, Hansgate A, Srienc F. Transient gene expression in CHO cells monitored with automated flow cytometry. *Cytotechnology* 2006;52:13-24.

## Single-colour flow cytometric assay to determine NK cell-mediated cytotoxicity and viability against non-adherent human tumor cells

Ajit Thakur · Abeyat Zaman · Jeff Hummel · Kim Jones · Gonzalo Hortelano

Received: 22 August 2011 / Accepted: 3 November 2011 / Published online: 21 December 2011  
© Springer Science+Business Media B.V. 2011

**Abstract** A flow cytometry-based cytotoxicity (FCC) assay was developed using a single fluorophore, calcein-acetoxymethyl diacetylester (calcein-AM), to measure NK cell-mediated cytotoxicity. Non-adherent human K562 and U937 target cells were individually labelled with calcein-AM and co-incubated with effector NK cells to measure calcein loss, and

therefore calculate target cell cytotoxicity. This FCC assay also provided a measure of sample viability. Notably, cell viability measured by traditional calcein/7-amino-actinomycin D (7-AAD) double labelling and Trypan Blue methods were comparable to the viability calculated using calcein-loss FCC. This FCC assay may also be used with various effector and target cell types and as a multi-parameter tool to measure viability and immunophenotype cells for tissue engineering purposes.

A. Thakur · K. Jones · G. Hortelano  
School of Biomedical Engineering, McMaster University,  
5380 Glen Erin Dr., Mississauga, ON L5M5C7, Canada  
e-mail: thakurajit@gmail.com

K. Jones  
e-mail: kjones@mcmaster.ca

A. Zaman  
Bachelor of Health Sciences Program,  
McMaster University, 1200 Main Street,  
Hamilton, ON L8N 3Z5, Canada  
e-mail: abeyat.zaman@gmail.com

J. Hummel  
Centre for Gene Therapeutics, McMaster  
University, MDCL Building, Rm. 5070, 1200 Main  
Street, Hamilton, ON L8N 3Z5, Canada  
e-mail: dr.jlh@bell.net

K. Jones  
Department of Chemical Engineering, McMaster  
University, Hamilton, ON L8N 3Z5, Canada

G. Hortelano (✉)  
Department of Pathology & Molecular Medicine,  
McMaster University, Hamilton, ON L8N 3Z5, Canada  
e-mail: gonhort@mcmaster.ca

**Keywords** Calcein · Cell-mediated cytotoxicity · Flow cytometry · Natural killer cells · Viability

### Introduction

Cell-mediated cytotoxicity assays are indispensable in immunology to quantify effector cell [cytotoxic T-lymphocytes (CTLs), natural killer (NK) cells and natural killer T cells (NKT)] function involved in the defence against virally infected cells, allogeneic cells and tumors. Although there are many different assays to measure cytotoxicity, the chromium ( $^{51}\text{Cr}$ )-release assay (CRA) is considered the ‘gold standard’ for measuring the cytolytic activity of effector cells (Ozdemir 2011). Unfortunately, CRA has many disadvantages, primarily related to the use of radioactivity, low sensitivity to apoptotic cell death and speed of analysis (Kim et al. 2007).

The limitations of the CRA has inspired several groups to develop flow cytometry-based cytotoxicity (FCC) assays, which incorporate multi-parameter high-speed analysis at the single-cell level (Papadopoulos et al. 1994; Kasatori et al. 2005; Zimmermann et al. 2005; Klöß et al. 2007; Cao et al. 2010). Flow cytometry allows for the simultaneous measurement of cytotoxic effector cell activation, cell frequency and phenotype, as well as target cell death, in the same sample. In addition, there is a good correlation between the results obtained from FCC assays and the results of the  $^{51}\text{Cr}$ -release and ELISpot assays (Burkett et al. 2005; Zaritskaya et al. 2010). However, most FCC assays require multiple cell labels and/or cell surface markers with extensive cell manipulation. Together, these factors contribute to increased cost and limit the widespread applicability of these assays. In order to address these limitations, we developed an alternative FCC assay that requires only one commonly used fluorophore, calcein-AM, for the determination of NK cell-mediated cytotoxicity of human target cells. Our assay relies on the conversion of a membrane permeable lipophilic compound (calcein-AM) to a brightly fluorescent, membrane impermeable compound (calcein) via the action of ubiquitously expressed intracellular esterases (Bratosin et al. 2005; Gantenbein-Ritter et al. 2008). In a cell-mediated cytotoxicity assay, killed calcein-labelled target cells are either completely or incompletely lysed (mainly perforin and granzyme mediated necrosis), or remain as one entity with a compromised cell membrane (mainly TNF- $\alpha$ , TRAIL and Fas ligand- mediated apoptosis), where calcein is free to diffuse outside the cell (Zaritskaya et al. 2010). Thus, the physical size of dead cells, their internal composition (granularity) and calcein staining intensity distinctly varies from healthy/living cells. These distinguishing characteristics were used to calculate NK-specific target cell cytotoxicity. In the absence of effector cells, we also measured the viability of cells using this method. Our measured viability values were validated against other established assays for viability.

## Materials and methods

### Cell lines and cell culture

U937 is a histiocytic lymphoma-derived monocyte-like human cell line (ATCC, CRL-1593.2). K562 is a human

chronic myelogenous leukemia cell line (ATCC, CCL-243). U937 and K562 cell lines were cultured in RPMI 1640 (Invitrogen, Burlington, Canada) with 10% (v/v) heat-inactivated FBS, 1% penicillin/streptomycin 0.1% gentamycin and 0.1% fungizone in 0.2  $\mu\text{m}$  vented tissue culture flasks at 37°C (humidified, 5%  $\text{CO}_2$ ). All other media additives were purchased from Sigma–Aldrich. Suspension cells were subcultured every 3–4 days. Lymphocytes were cultured in U937 media, with 50  $\mu\text{M}$  2-mercaptoethanol 1 mM sodium pyruvate and 0.1 mM non-essential amino acids. We refer to this media as lymphocyte media (LM). Cells were counted, and viability was measured by Trypan Blue exclusion.

### Enumerating target cell lysis in a cytotoxicity assay using CountBright beads

CountBright beads (Molecular Probes) are small (7  $\mu\text{m}$ ) fluorescent microspheres that were added to a single-cell suspension in order to determine the absolute cell count. In the CTL (cytotoxic T-lymphocyte) assay, we calculated the absolute number of calcein-labelled target cells in control samples (U937 only) and compared them with test samples (co-culture of effector and calcein-labelled target cells) using CountBright beads. Both the control samples and the test samples initially contained the same number (50,000) of calcein-labelled U937 target cells. Briefly, CountBright beads were added to control and test samples at the end of 4 h incubation in the CTL assay to determine the absolute target cell count by flow cytometry. These brightly fluorescent beads were gated unambiguously in the forward scatter/side scatter (FSC/SSC) plot to determine the bead count. Since the concentration of beads and the ratio of the bead solution to cell solution are known, the concentration of cells was calculated according to the manufacturer's instructions (Molecular Probes).

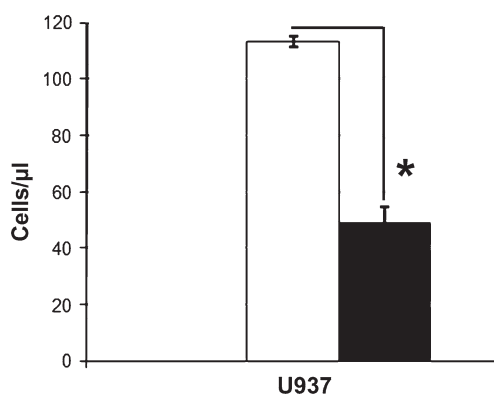
### CTL assay

The CTL assay was conducted as previously described by our laboratory (Thakur et al. 2011). An E:T ratio of 4:1 was used in this assay (Fig. 1).

### Positively selecting NK cells from fresh PBMCs

Peripheral blood mononuclear cells (PBMCs) were isolated from whole blood collected from healthy





**Fig. 1** Enumerating target cell lysis in a cytotoxicity assay using CountBright beads. Comparison between calcein-labelled target (U937) cell concentration in control samples (without effector CTL cells, *open square*) and test samples [with effector CTL cells, *filled square*] measured using CountBright beads. Flow cytometry data presented from ~30,000 events collected per sample. (Error bars indicate standard deviation;  $n = 3$ ; \* indicates significant ( $P < 0.05$ ) difference)

human donors in this McMaster University Research Ethics Board-approved study. The red blood cells (RBC) were lysed using ammonium-chloride (ACK) solution as previously described (Bossuyt et al. 1997). After RBC lysis, the PBMCs were used as a source of NK cells for the NK assay. Briefly, magnetic antibody-coated beads were used to positively select CD56+ cells from PBMCs according to manufacturer's instructions (StemCell Technologies, Vancouver, Canada). After separation, NK cells (CD56+) were resuspended in 4 ml LM.

#### NK assay

Freshly isolated NK cells (CD56+ cells) were first activated with 10 μg/ml Poly I:C (Sigma) and 50 U/ml rh IL-2 (Invitrogen) and incubated at 37°C (humidified, 5% CO<sub>2</sub>) in a 6-well tissue culture plate for 48 h to increase their cytolytic activity. These activated NK cells (lymphokine activated killer cells) were then washed with PBS (Ca<sup>2+</sup> and Mg<sup>2+</sup> free). Target cells were labelled with 100 nM calcein-AM (Invitrogen) for 15–20 min at room temperature. The cells were then washed with PBS (Ca<sup>2+</sup> and Mg<sup>2+</sup> free) three times and finally resuspended in LM as described above. The NK cells were then co-cultured with target cells (NK cells: U937 or K562 cells) at

0.1:1, 0.25:1 and 1:1 in a 96-well round bottom plate in triplicates. Cells were cultured in 200 μl LM. The target cell number was held constant at 50,000 cells, while the effector cell number was varied according to the ratios. Control wells only contained the target cells in LM. After incubating the co-culture for 4 h at 37°C (humidified, 5% CO<sub>2</sub>), 20 μl 7-AAD was added to each well. This was followed by another incubation of 20 min at 22°C (protected from light). The contents of each well were added to 400 μl PBS (Ca<sup>2+</sup> and Mg<sup>2+</sup> free) in separate flow cytometry tubes for analysis.

#### Flow cytometry data acquisition and analysis

A Beckman Coulter FC 500 system (Beckman Coulter Inc., Mississauga, Canada) was used to acquire and analyze the data with the CXP software provided. Calcein was illuminated with an argon (488 nm) laser and fluorescence was collected using a FITC filter set, with the PMT collecting signals centered at 525 nm (BP). 7-AAD was illuminated with an argon (488 nm) laser and fluorescence was collected using an APC filter set, with the PMT collecting signals centered at 675 nm (BP). Flow cytometry data analysis for the NK assay was based on loss of calcein fluorescence from target cells. Briefly, live target cells were gated based on their calcein staining intensity and their relative size (FSC) and granularity (SSC). In addition, the FSC detection threshold voltages were optimized (via CountBright beads) for the cell types used in this study such that apoptotic and necrotic cells were counted, but lysed cell fragments were not counted by the flow cytometer. A live gate was created around the normal FSC/SSC distribution of cells in the control sample (no effector cells) to discriminate between effector and target cells, and to allow intensity analysis on healthy target cells. The population of healthy-bright calcein stained target cells was first determined in the control sample, which contained the same number of cells (50,000) as the test samples, but without any effector cells. After co-incubating effector and target cells (test sample), the population of healthy-bright calcein stained target cells was determined again. The difference between the two values (control and test sample) gives the specific (effector cell-mediated) target cell death [Eq. 1, calculating percent specific death in cell-mediated cytotoxicity assays (Thakur et al. 2011)]. We refer to this calculation as the 'Calcein-loss' method for estimating

specific cell death. A two-tailed Student's *t*-test was performed to determine statistical significance between different E:T ratios and cell lines.

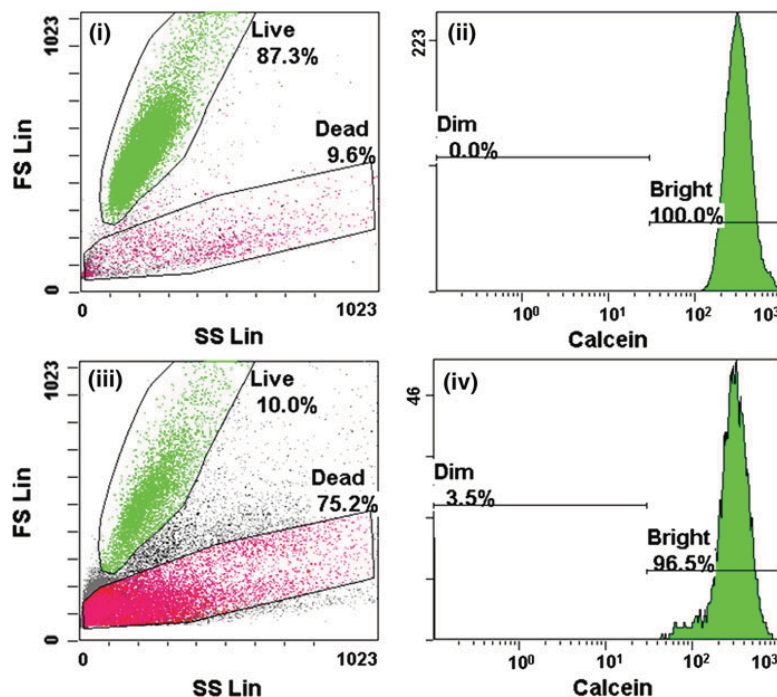
$$\text{Specific death (\%)} = Y_{\text{control}} - \left[ \frac{100 X_{\text{test}}}{Z_{\text{theoretical}}} \right] \quad (1)$$

where  $X_{\text{test}}$  = percentage of calcein-bright cells in co-culture after incubation,  $Y_{\text{control}}$  = percentage of calcein-bright cells in control,  $Z_{\text{theoretical}}$  = percentage of target cells in co-culture before incubation, determined by the effector:target ratio.

#### Viability

Our calcein-loss FCC method of calculating specific cell death relies on the measurement of viability in

controls and co-cultured samples. In order to validate our calcein-loss FCC method, viability of control samples were measured and compared to calcein/7-AAD double labelling and Trypan Blue techniques. The viability of a sample in the calcein-loss method was determined by calculating the number of cells in the live gate that are brightly labelled with calcein as a fraction of the total number of cells (Fig. 2). Calcein/7-AAD viability was determined by calculating the fraction of Calcein labelled cells that were also simultaneously labelled with 7-AAD, indicating late apoptotic/necrotic dead cells with a compromised cell membrane. In contrast, Trypan Blue staining was performed using a hemocytometer, where dead necrotic cells and apoptotic cells with a compromised cell membrane stain blue.



**Fig. 2** NK assay using calcein-loss technique. (i) The FSC/SSC plot of calcein-labelled U937 target cells in the absence of effector NK cells. The live cell bracket (*green* cells) contains the vast majority (>95%) of healthy/live cells, while the dead cell bracket (*red* cells) contains the vast majority (>85%) of unhealthy/dead cells in the sample. (ii) Histogram represents the fraction of cells in the live bracket that are *brightly* ('*Bright*') and *dimly* ('*Dim*') labelled with calcein. The *brightly*

labelled fraction in the live cell bracket ( $Y_{\text{control}} = (100/100) \times 87.3\%$ ) was then calculated. This value also represents the viability of the sample. (iii) FSC/SSC plot of calcein-labelled U937 target cells in the presence of effector NK cells at E:T ratio of 1:1. (iv) The *brightly* labelled fraction in the live cell bracket of this coculture ( $X_{\text{test}} = (96.5/100) \times 10\%$ ) was then calculated. The specific death was calculated to be 68% using Eq. 1



## Results

### Determination of target cell lysis in a cytotoxicity assay

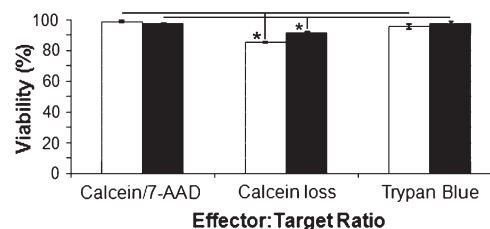
A prime objective of our flow cytometry-based cytotoxicity assays was to determine whether calcein-labelled target cells were being lysed in a necrotic process induced by effector cells as opposed to staying intact with a compromised cell membrane in an apoptotic process. In order to determine the fraction of cells undergoing necrosis/lysis by effector cells, we calculated the absolute number of calcein-labelled target cells in control samples (U937 only) and compared them with test samples (co-culture of effector and target cells) using CountBright beads. The result shown in Fig. 1 suggests that there was a significant ( $P < 0.05$ ) loss of calcein-labelled target cells in the cytotoxicity assay. Only 43% of the target cells (including healthy and apoptotic/necrotic cells) were counted after incubation with CTLs. The remaining necrotic/lysed cells were detected at low FSC and widely distributed over the SSC axis in the FSC/SSC plot.

### Determination of viability and cytotoxicity using the Calcein-loss method

In order to determine specific cell cytotoxicity, the viability of the control sample (containing only target cells) and test sample (effector and target cells) was calculated (Fig. 2i, ii). In the control sample, 87% of cells lie within the live cell gate in the FSC/SSC plot and 100% of the cells within this live gate were brightly stained for calcein, indicating live cells. By contrast, in the test sample only 10% of cells lie within the live gate (Fig. 2iii, iv), with 96.5% of those being brightly labelled with calcein. The specific cell cytotoxicity was determined by comparing the viability of the control and test sample, while accounting for the E:T ratio (Eq. 1).

### Comparison of viability determined using calcein-loss, calcein/7-AAD and Trypan Blue techniques

The calcein-loss method yields a viability that is comparable, albeit significantly ( $P < 0.05$ ) lower than with the calcein/7-AAD and Trypan Blue methods



**Fig. 3** Comparison of viability calculated using calcein/7-AAD, calcein-loss and Trypan Blue techniques in K562 (open square) and U937 (filled square) cell lines. Viability determined using Calcein-loss is significantly ( $P < 0.05$ ) different in U937 (\*) and K562 (\*) cell lines. Viabilities determined using calcein/7-AAD and Trypan Blue are not significantly ( $P > 0.05$ ) different in both cell lines. Error bars indicate standard deviation;  $n = 3$ . Flow cytometry data presented from  $\sim 30,000$  events collected per sample

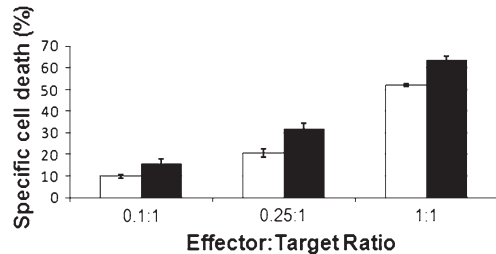
(Fig. 3). However, viability values were consistent, as indicated by the small standard deviations. Viability values determined using calcein/7-AAD and Trypan Blue were not significantly ( $P > 0.05$ ) different. Trypan Blue viability averages were found to have the largest standard deviations of the three techniques. These observations were confirmed in both K562 and U937 cell lines.

### Calcein-loss FCC assay in K562 and U937 cells

The FCC assay using the calcein-loss method shows a significant ( $P < 0.05$ ) increase in the specific cell death of target cells with increasing E:T ratios. This consistent increase in the specific cell death was comparable between K562 and U937 cell lines (Fig. 4).

## Discussion

Our results indicate that the calcein-loss FCC method provides a reliable estimate of NK cell-mediated cytotoxicity that was consistent across both cell lines used in this study. To our knowledge, no other FCC method uses only a single fluorophore to measure specific cell death via necrosis and apoptosis. Our method of analysis defines dead cells as those which have a compromised cell membrane. An apoptotic/necrotic dead cell with a compromised cell membrane is measured by the loss calcein intracellular staining and the change in its size and granularity, while



**Fig. 4** Comparison of NK cytotoxicity (specific cell death) using calcein-loss technique in K562 (*open square*) and U937 (*filled square*) cell lines at three different E:T ratios. Specific cell death values increased with the E:T ratios in both cell lines. Specific cell death values were also significantly ( $P < 0.05$ ) different between all E:T ratios in both cell lines. Error bars indicate standard deviation;  $n = 3$ . Flow cytometry data presented from  $\sim 30,000$  events collected per sample

completely lysed necrotic cells are quantified by the reduction in the expected number of cells counted in the flow cytometer (Bertho et al. 2000; Thakur et al. 2010). This is inherently more sensitive than relying on the ability of a second dye such as 7-AAD or ethidium bromide to label cells with a damaged cell membrane.

Techniques that rely on double labelling of specifically killed target cells, such as Cell Tracker Orange/7-AAD previously used by other groups, may not be suitable for use in cytotoxicity assays since they fail to count early apoptotic and completely lysed necrotic cells (Kim et al. 2007). Data presented here (Fig. 1) indicate that a significant fraction (57%) of specific cell death values (at high E:T ratios) measured in a CTL assay can be attributed to the necrosis/lysis of target cells, which result in necrotic cells and cell fragments that fall below the cell counting limit normally set in flow cytometry. Since CTLs and NK cells rely on similar mechanisms to induce cell-mediated cytotoxicity, it is likely that this result can be extended to NK assays as well. Thus, methods relying exclusively on double labelling of target cells may not be suitable for the assessment of viability and cytotoxicity. However, double labelling of target cells can be easily adapted in our calcein-loss assay to distinguish between apoptosis and necrosis. For example, apoptosis and necrosis can be quantified by the addition of dyes such as 7-AAD and annexin V. Target cells double labelled with Calcein and annexin V (preferentially binds cell membrane phosphatidylserine) will represent early apoptotic cells, while target cells double-labelled with

Calcein and 7-AAD will represent late apoptotic/necrotic cells with a compromised cell membrane. Completely lysed necrotic target cells can be quantified by comparing the absolute number of target cells in controls (target cells only) and test samples (effector and target cells). The reduction in the target cell number in the test sample would provide a direct measure of the completely lysed necrotic target cells.

Calcein-based viability assays are becoming increasingly popular in tissue engineering due to labelling sensitivity, reproducibility, stability of fluorescence in the physiological pH range and their versatility (Gantenbein-Ritter et al. 2008). Viability measurements using the calcein-loss method were found to be consistent across both U937 and K562 cell lines. In comparison to Trypan Blue, the calcein-loss method yielded viabilities with smaller standard deviations. However, our method of analysis likely underestimates the viability since the live gate was restricted by size and granularity in the FSC/SSC plot (Fig. 2). When compared to viability estimates measured by Trypan Blue and calcein/7-AAD, we calculate that our calcein-loss method underestimates the viability by 10% at the most (Fig. 3). We found that expanding the live gate to encompass more cells corrects this viability estimate, but a larger (less stringent) live gate would likely decrease the accuracy of the cytotoxicity measurements. A stringent live gate was applied in this cytotoxicity assay, since cell size (FSC), granularity (SSC) and calcein staining intensity are all parameters that are expected to change when target cells are killed/compromised by effector cells. The specific cell death value was calculated by comparing controls and co-cultured samples, both of which had the same live gate and Calcein staining intensity cut-offs, making it a reliable estimate of cytotoxicity (Fig. 4). Our data show that the specific cell death values are consistent across both cell lines tested at various E:T ratios and are in agreement with previously published NK cytotoxicity values (Papadopoulos et al. 1994; Kasatori et al. 2005).

## Conclusion

We have developed a flow cytometry-based cytotoxicity assay using a single fluorophore, calcein-AM, to measure NK cell-mediated cytotoxicity as well as viability of cell samples. This method can also be

adapted in multi-colour flow cytometry to simultaneously immunophenotype cells in cytotoxicity assays with multiple effector and target cell types. Furthermore, this assay can be conveniently applied in tissue engineering, where cell morphology, spatial distribution and viability are all important parameters that can be assessed using a single fluorophore.

**Acknowledgments** We would like to thank Dr. Heather Sheardown, Dr. Karen Mossman, Dr. Ali Ashkar, Dr. Firoz Mian, Dr. Iran Rashedi, Glenn McClung, Ruchira Sengupta, Faheem Dinath and Dave Morrison for providing us with materials and technical support, and to the Natural Science and Engineering Research Council (NSERC) for their funding to AT and KJ.

## References

- Bertho A, Santiago M, Coutinho S (2000) Flow cytometry in the study of cell death. *Mem Inst Oswaldo Cruz* 95(3):429–433
- Bossuyt X, Marti G, Fleisher TA (1997) Comparative analysis of whole blood lysis methods for flow cytometry. *Cytometry* 30(3):124–133
- Bratosin D, Mitrofan L, Palić C et al (2005) Novel fluorescence assay using calcein-AM for the determination of human erythrocyte viability and aging. *Cytom Part A* 66A:78–84
- Burkett M, Shafer-Weaver K, Strobl S et al (2005) A novel flow cytometric assay for evaluating cell-mediated cytotoxicity. *J Immunother* 28(4):396–402
- Cao L, Krymskaya L, Tran V et al (2010) Development and application of a multiplexable flow cytometry-based assay to quantify cell-mediated cytolysis. *Cytom A* 77(6):534–545
- Gantenbein-Ritter B, Potier E, Zeiter S et al (2008) Accuracy of three techniques to determine cell viability in 3d tissues or scaffolds. *Tissue Eng (Methods)* 14(4):353–358
- Kasatori N, Ishikawa F, Ueyama M et al (2005) A differential assay of NK-cell-mediated cytotoxicity in K562 cells revealing three sequential membrane impairment steps using three-color flow-cytometry. *J Immunol Methods* 307(1–2):41–53
- Kim GG, Donnenberg VS, Donnenberg AD et al (2007) A novel multiparametric flow cytometry-based cytotoxicity assay simultaneously immunophenotypes effector cells: comparisons to a 4 h 51Cr-release assay. *J Immunol Methods* 325(1–2):51–66
- Klöß S, Bochennek K, Huenecke S et al (2007) A novel five-colour flow cytometric assay to determine NK cell cytotoxicity against neuroblastoma and other adherent tumour cells. *J Immunol Methods* 325(1–2):140–147
- Ozdemir O (2011) Flow cytometric mast cell-mediated cytotoxicity assay: a three-color flow cytometric approach using monoclonal antibody staining with annexin V/propidium iodide co-labeling to assess human mast cell-mediated cytotoxicity by fluorosphere-adjusted counts. *J Immunol Methods* 365(1–2):166–173
- Papadopoulos N, Dedoussis G, Spanakos G et al (1994) An improved fluorescence assay for the determination of lymphocyte-mediated cytotoxicity using flow cytometry. *J Immunol Methods* 177(1–2):101–111
- Thakur A, Sengupta R, Matsui H et al (2010) Characterization of viability and proliferation of alginate-poly-L-lysine-alginate encapsulated myoblasts using flow cytometry. *J Biomed Mater Res B Appl Biomater* 94(2):296–304
- Thakur A, Hummel J, Sengupta R et al (2011) Retroviral expression of MIR2 decreases both surface MHC Class I and the alloimmune CTL response. *J Tissue Eng Regen Med* 5(7):520–528
- Zaritskaya L, Shurin M, Sayers T et al (2010) New flow cytometric assays for monitoring cell-mediated cytotoxicity. *Expert Rev Vaccines* 9(6):601–616
- Zimmermann S-Y, Esser R, Rohrbach E et al (2005) A novel four-colour flow cytometric assay to determine natural killer cell or T-cell-mediated cellular cytotoxicity against leukaemic cells in peripheral or bone marrow specimens containing greater than 20% of normal cells. *J Immunol Methods* 296(1–2):63–76

# Retroviral expression of MIR2 decreases both surface MHC class I and the alloimmune CTL response

Ajit Thakur<sup>1</sup>, Jeff Hummel<sup>2</sup>, Ruchira Sengupta<sup>1</sup>, Vasudha Gupta<sup>3</sup>, Karen Mossman<sup>2</sup> and Kim Jones<sup>1,4\*</sup>

<sup>1</sup>School of Biomedical Engineering, Hamilton, Ontario L8N 3Z5, Canada

<sup>2</sup>Centre for Gene Therapeutics, Hamilton, Ontario L8N 3Z5, Canada

<sup>3</sup>Michael G. DeGroote School of Medicine, Hamilton, Ontario L8N 3Z5, Canada

<sup>4</sup>Department of Chemical Engineering, McMaster University, Hamilton, Ontario L8N 3Z5, Canada

## Abstract

The immune response to allogeneic cells in tissue-engineered constructs is a major barrier to their successful application in the treatment of many human diseases. Specifically, the T cell-mediated immune response, initiated through the recognition of cell surface MHCI molecules, is the primary cause of acute cellular allograft rejection. In this study, we altered expression of MHCI through viral immunomodulatory mechanisms to examine whether allogeneic cells could be made to 'mimic' viral evasion of a host CTL response. We demonstrate the successful application of a retroviral vector *in vitro* to overexpress the Kaposi's sarcoma-associated herpesvirus immunomodulatory protein, MIR2, in human monocyte-like myeloid progenitor cells. This approach led to differential downregulation of cell surface MHCI, ICAM-1 and B7-2 molecules. We also demonstrate that downregulation of immunoreactive molecules has the functional effect of significantly reducing T cell-mediated cytotoxicity without altering NK-mediated cytotoxicity *in vitro*. These results provide proof-of-concept that viral immune evasion strategies allow cell-based tissue-engineered constructs to delay or even prevent acute cellular immune rejection *in vivo*. Importantly, this methodology could facilitate the development of universal donor cells for tissue engineering applications. Copyright © 2011 John Wiley & Sons, Ltd.

Received 14 March 2010; Accepted 8 July 2010

**Keywords** tissue engineering; transplantation; immune response; MHC class I; gene therapy; Kaposi's sarcoma-associated herpesvirus; retroviral gene expression

## 1. Introduction

The immune response to allogeneic cells within tissue-engineered constructs has been recognized as a significant barrier to their widespread application in humans (Langer *et al.*, 1993; Jones, 2008). The objective of our work was to engineer human cells that could resist rejection by reducing expression of major histocompatibility complex class I (MHCI) molecules. Experiments by George Snell and colleagues identified the MHC complex as a locus

of polymorphic genes, which code for the targets of allograft recognition (Hurme *et al.*, 1978; Snell, 1979). Since MHCI molecules are expressed on all nucleated cells, they can be recognized by alloreactive T cells and evoke immune responses to virtually all tissue types. Acute cellular rejection is due to activation of alloreactive CD8<sup>+</sup> T cells, which proliferate and differentiate into effector cytotoxic T lymphocytes (CTLs) that specifically kill allogeneic cells (Abbas *et al.*, 2000). Hence, the MHCI recognition capability of T cells responding to the allograft is the most significant event leading to acute cellular rejection (Lechler *et al.*, 2005).

\*Correspondence to: Kim Jones, Department of Chemical Engineering, McMaster University, Hamilton, Ontario L8N 3Z5, Canada. E-mail: kjones@mcmaster.ca

Recognizing this important aspect of immune rejection, several studies have attempted to reduce MHC I expression (Markmann *et al.*, 1992; Osorio *et al.*, 1994a, 1994b). However, a global reduction of MHC I molecules has been shown to increase the susceptibility of cells to natural killer (NK) cells of the innate immune system (Iannello *et al.*, 2006). In humans, many of the MHC I alleles, including human leukocyte antigen B (HLA-B) and HLA-C, are recognized by NK cell inhibitory receptors (Abbas *et al.*, 2000). In the absence of MHC I molecules, NK cells are activated by ubiquitously expressed cell surface receptors such as MICA, MICB and AICL (Welte *et al.*, 2006; Thomas *et al.*, 2008; Nathan *et al.*, 2009). This results in the specific lysis of cells lacking MHC I molecules, which immediately suggests that a general downregulation of MHC I molecules is unlikely to significantly protect allogeneic cells from the immune response. Given that allogeneic stem cells are a promising tissue engineering cell source, many groups have shown that stem cells exhibit immune privilege characteristics, primarily due to their low MHC I expression and their lack of MHC II expression (Li *et al.*, 2004; Wu *et al.*, 2008). However, recent studies by Drukker *et al.* (2002) suggest that stem cell-derived cells do not retain their immune privilege characteristics. For example, human embryonic stem cells (hESCs) upregulate their expression of MHC I upon differentiation by about 10-fold, sufficient to provoke an acute immune response (Drukker, 2008). Overall, these observations suggest that it will be necessary to modulate MHC I molecules expressed on hESC-derived cells to induce active tolerance in the host for these transplanted cells to be successful in tissue-engineering applications.

In preparing a tissue-engineered construct, the cells required are sourced in advance. This provides the opportunity to use genetic engineering to manipulate these cells, such that they evade or suppress the immune response. Viruses have evolved complex genetic mechanisms to evade and suppress detection by the immune responses of the host (Iannello *et al.*, 2006). A tissue-engineered allogeneic construct with cells engineered to utilize these viral mechanisms could elicit a similar response, whereby the construct would not be recognized by the host immune system as foreign. Here, we tested this novel approach by transducing a model human progenitor cell line to express an immunomodulatory protein, modulator of immune recognition (MIR2), from Kaposi's sarcoma-associated herpesvirus (KSHV). This 29 kDa protein is known to downregulate the cell-surface expression of MHC I, ICAM-1, B7-2 and other immunoreactive molecules (Ishido *et al.*, 2000b; Coscoy *et al.*, 2001a, 2001b; Lodoen *et al.*, 2005; Sanchez *et al.*, 2005; Welte *et al.*, 2006; Thomas *et al.*, 2008). In this study, we demonstrate the immunoprotective effect of MIR2-GFP fusion protein (56 kDa) (Sanchez *et al.*, 2002; Cadwell *et al.*, 2005) expression against allogeneic CTLs and NK cells, using flow cytometry-based *in vitro* cytotoxicity assays.

## 2. Materials and methods

### 2.1. Cell line and cell culture

The histiocytic lymphoma-derived monocyte-like myeloid progenitor human cell line U937 (ATCC No. CRL-1593.2) was cultured in RPMI 1640 (Invitrogen Canada Inc., Burlington, ON, Canada) containing 10% v/v heat-inactivated FBS (PAA Labs Inc.), 1% Penn/Strep (Invitrogen), 0.1% Gentamycin (Invitrogen) and 0.1% Fungizone (Invitrogen). Cells transduced with MIR2-GFP (U937-MIR2-GFP) or LacZ (U937-LacZ) cells were cultured in G418 sulphate (1 mg/ml during initial selection or 250 µg/ml for maintenance; Invitrogen)-supplemented media. Human leukocytes (CTLs and NK cells) were maintained in U937 cell culture medium supplemented with 50 µM 2-mercaptoethanol (Invitrogen), 1 mM sodium pyruvate (Invitrogen) and 0.1 mM non-essential amino acids (Invitrogen).

### 2.2. Retroviral vector preparation and transduction

The Viraport™ gene expression system was employed to make the MIR2-GFP retrovirus (Stratagene, La Jolla, CA, USA). The MIR2-GFP cDNA (kind gift of Dr Laurent Coscoy, University of California, Berkeley, CA, USA) was cloned into pFB-Neo using *Bam*HI and *Hind*III restriction sites. Viral particles were generated by co-transfecting pFB-Neo-MIR2-GFP and the retroviral component plasmids pVPack-GP and pVPack-VSV-G into 293T cells, using ExGen500 (Fermentas Canada Inc., Burlington, ON, Canada) according to the manufacturer's protocols. U937 cells were subsequently transduced to generate U937-MIR2-GFP cells, which were selected and maintained in G418 media. This procedure was repeated to generate U937 control cells transduced with LacZ (U937-LacZ).

Transduced U937 cells strongly expressed GFP (fluorescence microscopy data not shown), indicating the expression of the chimeric MIR2-GFP protein. This confirmed that VSV-G pseudotyped MMLV was suitable to deliver genes to U937 cells. Similarly, LacZ transduced cells expressed  $\beta$ -galactosidase (data not shown). Furthermore, the viability of transduced cells (U937-MIR2-GFP, 97.7%; U937-LacZ, 97.4%) was not significantly different from the viability of untransduced U937 cells (98.5%), as measured by 7-AAD staining.

### 2.3. Microscopy

Fluorescent images were collected using a Leica DM IRE2 inverted fluorescence microscope system (Leica Microsystems, Richmond Hill, ON, Canada) with a standard GFP filter set in conjunction with OpenLab imaging software (Improvision Inc., Waltham, MA, USA).

## 2.4. Flow cytometry

A Beckman Coulter FC500 system (Beckman Coulter Canada Inc., Mississauga, ON, Canada) was used to analyse cells with the CXP software provided. Cells were stained with anti-HLA-ABC-PE, anti-CD54-PE, anti-CD56-PE and anti-CD8-PC7 (Beckman Coulter), anti-HLA-E (MEM-08; Abcam Inc., Cambridge, MA, USA), anti-CD86-PE and anti-mouse IgG1-APC secondary antibody (BD, Franklin Lakes, NJ, USA). Prior to antibody staining of cells, cell surface Fc receptors were blocked with heat-inactivated horse serum (Sigma) for 10 min at room temperature. After incubating cells with antibody for 30 min on ice, the cells were washed twice in PBS and passed through a 40 µm cell strainer to remove any cell clumps. Antibodies were used at the manufacturer's recommended concentrations. Cell viability was assessed by 7-AAD staining (Beckman Coulter).

## 2.5. CTL assay

Peripheral blood mononuclear cells (PBMCs) were isolated from whole blood, collected from human donors by ammonium chloride (ACK) lysis of red blood cells. This study was approved by the Research Ethics Board at McMaster University and blood collection was done by a licensed phlebotomist. Human CD8<sup>+</sup> T cells were then negatively isolated using the EasySep Human CD8<sup>+</sup> T Cell Enrichment Kit (Stemcell Technologies, Vancouver, BC, Canada). Isolated ('responder') cells were then stimulated with mitomycin C-treated (25 µg/ml) U937 ('stimulator') cells at a responder:stimulator ratio of 2:1 *in vitro*. This co-culture was incubated in lymphocyte medium supplemented with 10 U/ml recombinant human IL-2 (Invitrogen) at 37 °C (humidified, 5% CO<sub>2</sub>) for 96 h in upright 75 cm<sup>2</sup> tissue-culture flasks to allow the responder population (CD8<sup>+</sup> T cells) to proliferate and differentiate into effector CTLs. In setting up the CTL assay, appropriate effector (CTLs):target (U937-MIR2-GFP or U937-LacZ) ratios were determined (2:1 and 10:1) and the target cell number was held constant at 50 000 cells, while the effector cell number was varied. The appropriate number of target cells were centrifuged at 200 × *g* for 5 min and resuspended in medium and labelled with 100 nM Calcein-AM (Invitrogen) for 15–20 min at room temperature. The cells were washed three times with PBS (Ca<sup>2+</sup>- and Mg<sup>2+</sup>-free) and suspended in lymphocyte medium at the desired concentration. The co-culture was performed in 96-well round-bottomed tissue culture plates. Each effector:target ratio had three repeats for each of the target cell lines. Control wells contained calcein-labelled target cells without effector cells. After incubating the co-culture for 4 h at 37 °C (humidified, 5% CO<sub>2</sub>), the contents of each well (200 µl) were added to 400 µl PBS (Ca<sup>2+</sup>- and Mg<sup>2+</sup>-free) in preparation for flow cytometry.

## 2.6. NK assay

Human PBMCs were used as a source of NK cells. Briefly, NK cells were positively selected from PBMCs using the EasySep Human CD56 Selection Kit (Stemcell Technologies, Vancouver, BC, Canada). Human CD56<sup>+</sup> NK cells were then activated with 10 µg/ml Poly I:C (Sigma-Aldrich Canada Ltd, Oakville, ON, Canada) and 50 U/ml recombinant human IL-2 (Invitrogen) at 37 °C (humidified, 5% CO<sub>2</sub>) in a six-well tissue culture plate for 48 h to enhance their cytolytic ability. After activation of NK cells, appropriate effector (NK cells):target (U937-MIR2-GFP or U937-LacZ cells) ratios were determined (0.1:1, 0.25:1 and 1:1) and the co-culture was set up in a manner similar to the CTL assay.

## 2.7. Data analysis

The percentage of specifically killed target cells was calculated based on loss of calcein fluorescence from target cells after co-incubation with effector cells. Briefly, live target cells were gated based on their calcein staining intensity and their relative size (FSC) and granularity (SSC). A live gate was created around the normal FSC/SSC distribution of cells in the control sample (no effector cells) to discriminate between healthy bright calcein-stained target cells and dead (dim) cells/debris. The population of healthy bright calcein-stained target cells was first determined in the control sample, which contained the same number of cells (50 000) as the test samples but without any effector cells. After co-incubating effector and target cells (test sample), the population of healthy bright calcein-stained target cells was determined again. The difference between the two values (control and test sample) was the percentage specific death (equation 1); any differences observed between the test and control groups were determined using Student's *t*-test; *p* < 0.05 was considered statistically significant:

$$\text{Specific death (\%)} = Y_{\text{control}} - \left[ \frac{100X_{\text{test}}}{Z_{\text{theoretical}}} \right] \quad (1)$$

where  $X_{\text{test}}$  = percentage of calcein-bright cells in co-culture after incubation,  $Y_{\text{control}}$  = percentage of calcein-bright cells in control sample and  $Z_{\text{theoretical}}$  = percentage of target cells in co-culture before incubation, determined by the effector:target ratio.

## 3. Results

### 3.1. Characterization of cell surface molecules in transduced cells

In order to determine the effect of MIR2-GFP expression on cell surface immunoreactive molecules, U937-MIR2-GFP and U937-LacZ cells were stained with antibodies specific to HLA-ABC, CD54, CD86, HLA-E and



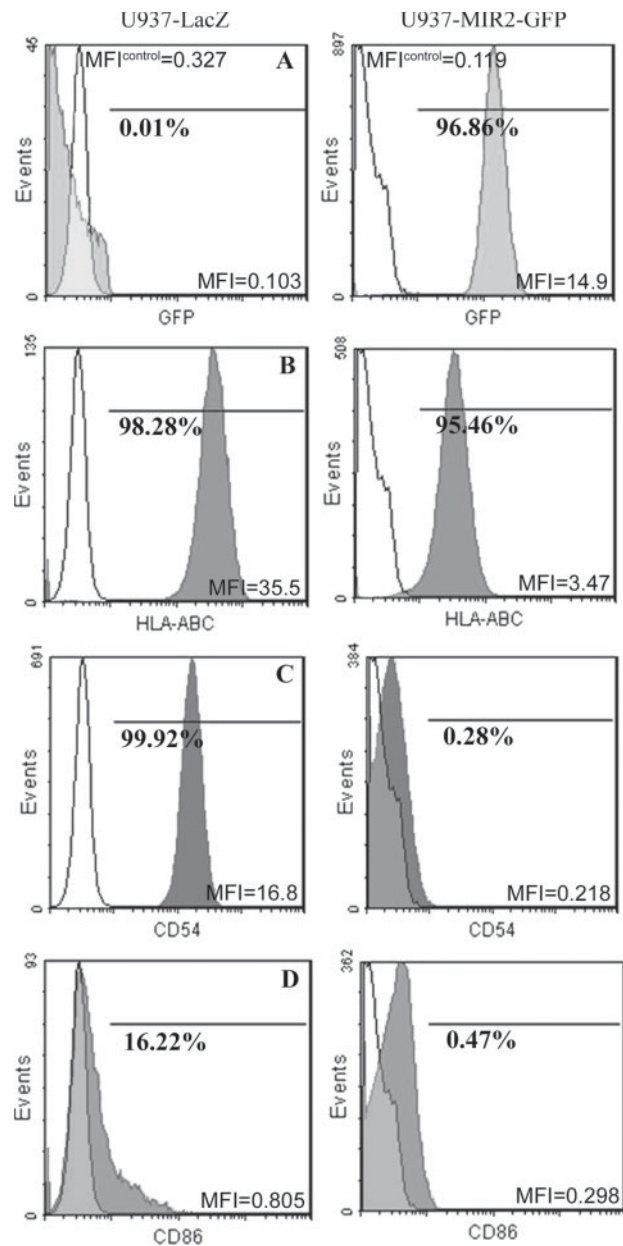


Figure 1. Cell surface characterization of U937-LacZ and U937-MIR2-GFP cells. HLA-ABC, CD54 and CD86 were all downregulated (shaded curves) in U937-MIR2-GFP cells. Expression of MIR2-GFP was quantified by GFP fluorescence, while antibodies were used to quantify all other markers. Mean fluorescence intensity (MFI) values for the shaded curves are indicated at the bottom right corner of each graph, while MFI values of unlabelled cells (white curves) are indicated as MFI<sup>control</sup>. Representative data presented from 100 000 cells analysed per sample; *n* = 2 replicates

HLA-DR. The detection of one strong GFP peak [mean fluorescence intensity (MFI) = 14.9] in U937-MIR2-GFP cells indicated a clonal population. This peak was 145-fold above control cells (MFI = 0.103) (Figure 1A). In

Figure 1B, HLA-ABC expression was shown to be downregulated to 10% (MFI = 3.47) in U937-MIR2-GFP cells compared to the control mean fluorescence intensity value observed for mock transduced cells (MFI = 35.5). We

### MIR2 expression decreases the alloimmune CTL response

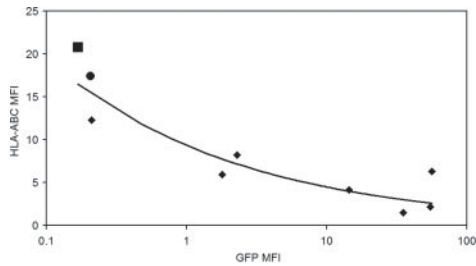


Figure 2. Trend showing MIR2-GFP dose-response effect on HLA-ABC expression. Figure depicts a decreasing trend in the cell surface HLA-ABC level with increasing levels of MIR2-GFP expression (MFI of GFP) as measured by flow cytometry in each of the seven U937-MIR2-GFP clones (◆). Untransduced U937 cells (■) and U937-LacZ cells (●) have high levels of HLA-ABC expression. Line of best fit data presented from 100 000 cells analysed per sample;  $n = 1$  replicate

also noted that CD54 expression was downregulated to 1% (MFI = 0.218), while CD86 was downregulated to 37% (MFI = 0.298) of control MFI values (Figure 1C, D). Cell surface levels of HLA-E and HLA-DR were undetectable in both U937-MIR2-GFP and U937-LacZ cells (data not shown). Transduced U937-LacZ cells did not significantly differ from untransduced U937 cells in their expression of cell surface markers, including HLA-ABC (MFI = 34.3), CD54 (MFI = 12.5) and CD86 (MFI = 0.708).

### 3.2. MIR2-GFP expression decreases surface HLA-ABC in a dose-dependent manner

The relationship between MIR2-GFP expression and the level of HLA-ABC downregulation was determined by collecting GFP fluorescence data from various clones of MIR2-GFP expressing cells. These data were plotted against cell surface HLA-ABC expression data from the same clones. We observed a negative relationship between the expression level (MFI) of MIR2-GFP and the cell surface amount of HLA-ABC (Figure 2). In addition, there was a non-linear relationship between the expression level of MIR2-GFP and HLA-ABC.

### 3.3. Retroviral transduction results in long-term MIR2-GFP expression

In order to assess the long-term stability of MMLV-based retroviral transduction, the MIR2-GFP expression level and the corresponding HLA-ABC level was measured after a clonal population of U937-MIR2-GFP cells was maintained in active culture for 100 days. After 100 days, the GFP signal decreased 2.48-fold to 40.3% (MFI =  $14.1 \pm 2.6$ ) of its original day 0 value (MFI =  $35 \pm 2$ ), while the relative HLA-ABC level increased 2.42-fold from 8.4% (MFI =  $1.46 \pm 4.24$ ) to 20.3% (MFI =  $3.53 \pm 3.52$ )

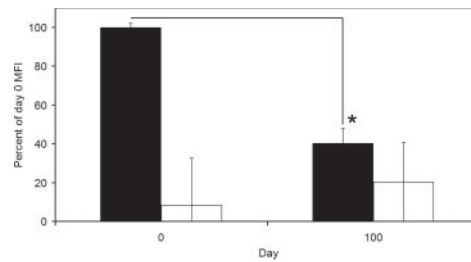


Figure 3. Effect of MIR2-GFP on HLA-ABC expression in transduced cells over 100 days. The black bars show the percentage of day 0 MFI for MIR2-GFP expression in U937-MIR2-GFP cells. The white bars show the percentage of HLA-ABC MFI measured in U937-MIR2-GFP cells relative to its value measured in U937-LacZ cells on day 0. These measurements were acquired from a clonal population of U937-MIR2-GFP cells in active culture for 100 days. Data presented from 100 000 cells analysed per sample;  $n = 3$  replicates; \*, significant difference ( $p < 0.05$ ); error bars indicate SD

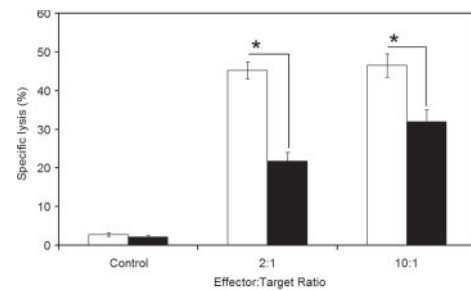


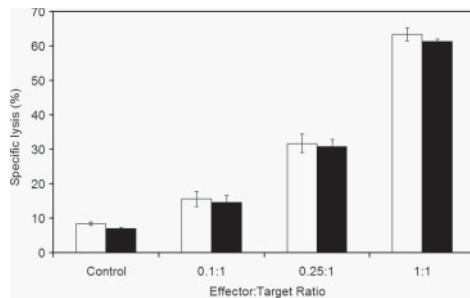
Figure 4. CTL assay. Specific lysis of calcein-labelled target cells [U937-LacZ (white bars) or U937-MIR2-GFP (black bars) cells] in control samples (without CTLs) and test samples (with CTLs) with varying effector:target ratios. \* $p < 0.05$  between cell lines for both effector:target ratios; error bars indicate SD;  $n = 3$  replicates

of its value measured in U937-LacZ cells on day 0 (MFI =  $17.4 \pm 3.5$ ) (Figure 3).

### 3.4. U937-MIR2-GFP cells evade CTL-mediated cytotoxicity

A CTL assay was used to compare the immune evasion of U937-MIR2-GFP cells relative to U937-LacZ cells, as measured by specific cell lysis of target cells. In this assay, flow cytometry measurements confirmed that CD8<sup>+</sup> CTLs comprised approximately 77% of the live effector cell population (data not shown). The CTL assay showed a statistically significant decrease in the specific lysis of target cells transduced with MIR2 at two different ratios (Figure 4). At the 2:1 E:T ratio, there was a 52% reduction in the specific lysis of MIR2 cells, whereas at the 10:1 E:T ratio there was a 31% reduction. This dose-response effect shows that MIR2 expression confers a significant protective effect against CTL-specific cell lysis.





**Figure 5.** NK Assay. Specific lysis of calcein-labelled target cells [U937-LacZ (white bars) or U937-MIR2-GFP (black bars) cells] in control samples (without NK cells) and test samples (with NK cells) with varying effector:target ratios. No significant difference between cell lines ( $p < 0.05$ ); error bars indicate SD;  $n = 3$  replicates

### 3.5. U937-MIR2-GFP cells evade NK-mediated cytotoxicity

The NK assay was used to compare the immune evasion of U937-MIR2-GFP cells relative to U937-LacZ cells, as measured by specific cell lysis of target cells by NK cells. In this assay, flow cytometry measurements confirmed that CD56<sup>+</sup> NK cells comprised 90% of the live effector cell population (data not shown). Although this population of CD56<sup>+</sup> cells included a small fraction of NKT (CD56<sup>+</sup>, CD3<sup>+</sup>) cells, previous studies have demonstrated that this population does not influence the function of CD56<sup>+</sup> cells in this assay (Bonavida *et al.*, 1994; Arrenberg *et al.*, 2009). The NK assay showed no statistically significant difference in the specific cell lysis of target cells transduced with MIR2 when compared to target cells transduced with LacZ at various E:T ratios (Figure 5).

## 4. Discussion

In tissue engineering, the immune response to allogeneic cells is a major barrier impeding the successful transplantation of tissue-engineered constructs. We propose a method to engineer immune acceptance, such that allogeneic cells are selectively modified, using viral strategies that evade the alloimmune response while retaining normal immune function. To our knowledge, this is the first study showing that a multifunctional viral immunomodulatory protein differentially downregulates cell surface molecules in allogeneic cells and results in CTL evasion, without altering NK-specific target cell lysis *in vitro*.

Recently, another research group suggested that viral stealth mechanisms can be exploited for stem cell transplantation. Lee *et al.* (2005) transfected human cytomegalovirus (*hCMV*) *US* genes into human neuronal stem cells (hNSCs) and downregulated surface MHC I molecules by 20–50%. Another study by the same group transfected *hCMV US* genes into a human breast luminal epithelial cell line, which is known to have stem cell

properties, and achieved a 40–60% downregulation of cell surface MHC I molecules (Kim *et al.*, 2005). However, their approach only attempted to globally downregulate MHC I molecules. Given that cell surface MHC I molecules, especially HLA-C and HLA-E, also serve to negatively regulate NK cells, a global downregulation of all types of MHC I molecules is likely to make the cells more susceptible to NK-mediated cytotoxicity (Yokoyama *et al.*, 1993; Lanier, 2005; Iannello *et al.*, 2006). Hence, an increase in NK-mediated cytotoxicity could potentially negate the protective effect of reduced MHC I levels on allogeneic cells from host CTL activity. This presents a potential barrier for the application of global MHC I reduction techniques for the purposes of allogeneic cell transplantation in tissue-engineered constructs. In our study, expression of MIR2 had the effect of protecting allogeneic cells against CTL cytotoxicity without altering the susceptibility of allogeneic cells to NK-mediated cell lysis. This presents a significant advancement in the application of MHC I reduction techniques as a means of evading acute cellular immune rejection for allogeneic cell-based tissue-engineered constructs.

Human U937 cells were used as a model human progenitor cell line, since they are known to express relatively high levels of MHC class Ia (HLA-ABC), ICAM-1 (CD54) and co-stimulatory molecules such as B7-2 (CD86), similar to the expression profile of stem-cell derived cells (Drukker *et al.*, 2002; Marín *et al.*, 2003). Our cell surface characterization of MIR2-GFP-transduced U937 cells showed that MIR2 differentially downregulates immunoactive molecules, such that CD54 levels are decreased to 1%, HLA-ABC levels are decreased to 10% and CD86 levels are decreased to 37% of mock-transduced cells (Figure 1). Although we could not detect cell surface HLA-E in U937 cells, previous groups have detected low levels of HLA-E (Marín *et al.*, 2003). It would be expected that HLA-E levels would remain unaltered in MIR2-GFP-transduced cells (Iannello *et al.*, 2006). In addition, we observed that the expression of MIR2 downregulated surface HLA-ABC in a dose-dependent manner (Figure 2). Overall, these proof-of-concept results suggest that MIR2 can significantly reduce cell surface expression of MHC I, CD86 and ICAM-1 in human progenitor cells. Of particular interest, U937 myeloid progenitor cells have been used in tissue engineering to study monocyte/macrophage responses to decellularized pericardial biomaterials (Ariganello *et al.*, 2009, 2010), poly(ethylene glycol) matrices (Zuckerman *et al.*, 2009) and RGD-grafted gelatin matrices (Gao *et al.*, 2007). Recent work by Roh *et al.* (2010) highlights the importance of mononuclear cell involvement in the development of tissue-engineered vascular grafts. In this study, Roh *et al.* reported that transplanted biodegradable scaffolds seeded with bone marrow mononuclear cells formed into living blood vessels via an inflammatory process of vascular remodelling (Cho *et al.*, 2009; Roh *et al.*, 2010). This immediately presents an opportunity where genetically modified monocytes/macrophages can be employed to direct inflammation, the foreign body

## MIR2 expression decreases the alloimmune CTL response

reaction and wound healing, to ultimately control tissue regeneration (Anderson *et al.*, 2008). Therefore, U937 cells expressing lower levels of immunoactive molecules may provide a relevant model for future studies in tissue engineering involving immune cell activation and tissue remodelling in response to biomaterials.

In genetically engineering cells for allogeneic transplantation, it is important that the introduced viral gene be expressed for a sufficient length of time in order for it to be useful as a general strategy. In this study, retrovirally-transduced U937 cells stably expressed functional MIR2-GFP for at least 100 days, as confirmed by the low cell surface levels of HLA-ABC (Figure 3). Moreover, we found that reduced MIR2-GFP expression over time still resulted in significant downregulation of HLA-ABC (Figures 2, 3). The level of HLA-ABC expression after 100 days suggests that even a reduced amount of MIR2 expression is sufficient to maintain a long-term state of HLA-ABC downregulation. Although this result is promising, safety studies of long-term MIR2 expression using retroviral gene expression systems are likely required to validate its efficacy *in vivo*. Clinical trials have reported adverse events caused by  $\gamma$ -retroviral vector integration, leading to insertional mutagenesis (Howe *et al.*, 2008), clonal expansion of transduced cells (Hacein-Bey-Abina *et al.*, 2003) and two cases of myelodysplasia (Stein *et al.*, 2010). Hence, there has been an impetus towards developing safer integrating vectors for gene therapy. Recently, studies by Montini *et al.* (2006) have demonstrated low genotoxicity of lentiviral vector integration in haematopoietic stem cell gene transfer. Although it is believed that lentiviral vectors may lower the chances of adverse events, a recent case of clonal expansion of lentiviral transduced cells in a  $\beta$ -thalassaemia clinical trial has renewed safety concerns (Kaiser, 2009). Fortunately, newer targeted gene transfer technologies are being developed to lower the risk of adverse events *in vivo*. For example, self-inactivating (SIN) vectors integrate into the transduced cell genome with deleted 3' and 5' long terminal repeats (LTRs) and rely on internal cellular promoters for transgene expression (Nienhuis *et al.*, 2006, 2008; Persons, 2010). Moreover, others groups have showed that 'insulator elements' can be added to the 3' LTR during vector assembly to block enhancer activity, thus reducing the genotoxicity of vector integration (Evans-Galea *et al.*, 2007). Finally, in the event of unexpected allogeneic cell behaviour post-transplantation, Bonini *et al.* (2007) have developed 'suicide' vectors that provide a mechanism by which transduced cells can be selectively killed by administering a drug. Given that viral gene delivery vectors can be modified with such safety features, the results from our study suggest that VSV-G pseudotyped MMLV-based retroviral gene delivery vectors may be suitable for some cell types in tissue engineering.

In addition to concerns about adverse events associated with gene delivery, it is conceivable that long-term MHC1 downregulation may also increase the risk of pathogen propagation in transplanted allogeneic donor cells. However, the MHC1 expression profile in MIR2-expressing

cells suggests that peptide presentation mechanisms are not completely removed, therefore minimizing the risk of pathogen propagation. Perhaps the greatest benefit of expressing MIR2 is its ability to differentially downregulate immunoactive molecules, including MHC1, such that only peptide presentation via HLA-A and HLA-B gene products are significantly reduced, while leaving other HLA peptide presentation mechanisms relatively unaffected. We expect that this will reduce the overall acute allogeneic immune response from CTL and NK cells, while preserving some of the MHC1 peptide presentation routes (via HLA-C) for pathogen detection. Furthermore, this method of donor cell antigen modification does not alter the host or its immune system from mounting a systemic immune response. Taken together, donor cell antigen modification with MIR2 presents a unique opportunity to produce allogeneic cell-based tissue-engineered constructs for transplantation that minimize the potential for adverse events *in vivo*.

Results from the CTL and NK assays in our study suggest that MIR2-GFP expression protects U937 cells against the cytotoxic effects of allogeneic CTLs without altering NK-specific target cell lysis *in vitro*. Specifically, MIR2 expression reduced MHC1 and ICAM-1 levels, which contributed to the decrease in CTL-mediated killing of target cells (Figure 4). Since CD8<sup>+</sup> CTLs recognize MHC1 and adhere to target cells using ICAM-1, it is expected that any decrease in the cell surface expression of MHC1 or ICAM-1 would hinder target recognition and binding capability of CTLs. Immune evasion of MIR2-expressing target cells in our study strongly support this notion.

Unlike the CTL response, NK cell cytolytic activity is inversely proportional to the amount of MHC1 present on the cell surface. As the MHC1 levels decrease on the cell surface, a greater percentage of the target cells are specifically killed by NK cells (Iannello *et al.*, 2006). However, in this study we did not observe any significant increase in NK-mediated cytotoxicity of U937-MIR2-GFP cells and U937-LacZ cells, despite the downregulation of MHC1 (Figure 5). Our results suggest that MIR2 expression maintains constitutive protection against NK-specific cell lysis, while significantly reducing CTL cytotoxicity against allogeneic cells. Hence, MIR2 expression presents a distinct advantage over previously employed techniques for global MHC1 reduction to evade acute cellular immune rejection of allogeneic cells. However, a number of factors could have contributed to the unaltered level of NK-specific target cell lysis. First, cell-surface HLA-C, which is weakly affected by MIR2 expression, might have been sufficient to negatively regulate NK cell specific lysis of target cells (Ishido *et al.*, 2000a, 2000b). Second, the strong downregulation of ICAM-1 (CD54) might have significantly lowered the capacity of NK cells to adhere to MIR2-expressing cells, resulting in decreased NK-specific cell lysis. Third, MIR2-mediated downregulation of other U937 cell surface molecules, such as MHC1-related chains (MICA, MICB) and activation-induced C-type lectin (AICL), might have reduced the activation signal necessary for NK cell activation (Welte

*et al.*, 2006; Thomas *et al.*, 2008; Nathan *et al.*, 2009). It is likely that a combination of the above factors resulted in the observed protective effect of MIR2 expression against NK cell-specific lysis of target cells.

Our method of modifying cell surface molecules has other benefits with respect to the alloimmune response. Differential downregulation of MHC I molecules by MIR2 implies that there is a significant reduction of some classes of MHC I molecules; it does not, however, remove all MHC I molecules from being expressed. The relatively unaltered expression of HLA-C and other non-classical MHC I molecules, such as HLA-E, not only serves to inhibit NK cell-mediated cytotoxicity but might also serve to induce active host tolerance to the allograft. Many studies have previously shown that some expression of the immunantigen is beneficial to maintaining active tolerance. A study by Faustman *et al.* (1991) showed that incomplete masking of MHC I molecules using antibodies can potentially lead to tolerance in murine hosts. This study indicates that donor MHC density was important in inducing tolerance. Hence, our differential downregulation approach to MHC I modulation may effectively create a greater window of opportunity for the induction of systemic tolerance.

In summary, donor antigen modification using viral immunomodulatory strategies to evade the immune response against allogeneic cells represents a new paradigm in the field of tissue engineering. This method of selective immunosuppression may also pave the way to generating universal donor cells. An immediate advantage of universal donor cells in tissue engineering is that they

would enable the development of off-the-shelf technology, which could function immediately in any individual. Furthermore, this technology would provide an alternative to isogenic stem cell technology, which is often laborious and requires time to create, differentiate and expand isogenic stem cells for applications in tissue engineering. We believe that viral strategies of immune evasion can be successfully employed to extend the life of a cell-based tissue-engineered construct in an allogeneic host.

## 5. Conclusion

Expressing a viral immunomodulatory protein, MIR2, in a model human cell line differentially downregulated cell surface levels of MHC I, ICAM-1 and CD86 molecules, which simultaneously resulted in the evasion of acute cellular rejection mediated by allogeneic CTLs without altering NK cell-mediated cytotoxicity. This strategy immediately provides a method for the creation of universal donor cells that could be transplanted into any allogeneic individual.

## Acknowledgements

We would like to thank Drs Heather Sheardown, Carlos Filipe, Ali Ashkar, Laurent Coscoy, Firoz Mian, Neilufar Solaimani, Glenn McClung, Faheem Dinath and Dave Morrison for providing us with materials and technical support, and the Natural Science and Engineering Research Council (NSERC) for their funding.

## References

- Abbas A, Lichtman A, Pober J. 2000; *Cellular and Molecular Immunology*. W. B. Saunders: Philadelphia, PA.
- Anderson J, Rodriguez A, Chang D. 2008; Foreign body reaction to biomaterials. *Semin Immunol* 20(2): 86–100.
- Ariganello M, Labow R, Lee J. 2009; Response of macrophage-like U937 cells to decellularized tissue heart valve materials. *J Heart Valve Dis* 18(2): 187–197.
- Ariganello M, Labow R, Lee J. 2010; *In vitro* response of monocyte-derived macrophages to a decellularized pericardial biomaterial. *J Biomed Mater Res A* 93A(1): 280–288.
- Arrenberg P, Halder R, Kumar V. 2009; Cross-regulation between distinct natural killer T cell subsets influences immune response to self and foreign antigens. *J Cell Physiol* 218(2): 246–250.
- Bonavida B, Braquet M, Lebow L, *et al.* 1994; Qualitative and quantitative analysis of subpopulations of cytotoxic effector cells by flow cytometry. *J Lipid Mediat Cell Signal* 9(1): 19–25.
- Bonini C, Bondanza A, Perna S, *et al.* 2007; The suicide gene therapy challenge: how to improve a successful gene therapy approach. *Mol Ther* 15(7): 1248–1252.
- Cadwell K, Coscoy L. 2005; Ubiquitination on nonlysine residues by a viral E3 ubiquitin ligase. *Science* 309(5731): 127–130.
- Cho S, Kim I-K, Kang J, *et al.* 2009; Evidence for *in vivo* growth potential and vascular remodeling of tissue-engineered artery. *Tissue Eng A* 15(4): 901–912.
- Coscoy L, Ganem D. 2001a; A viral protein that selectively downregulates ICAM-1 and B7-2 and modulates T cell costimulation. *J Clin Invest* 107(12): 1599–1606.
- Coscoy L, Sanchez DJ, Ganem D. 2001b; A novel class of herpesvirus-encoded membrane-bound E3 ubiquitin ligases regulates endocytosis of proteins involved in immune recognition. *J Cell Biol* 155(7): 1265–1274.
- Drukker M. 2008; Recent advancements towards the derivation of immune-compatible patient-specific human embryonic stem cell lines. *Semin Immunol* 20(2): 123–129.
- Drukker M, Katz G, Urbach A, *et al.* 2002; Characterization of the expression of MHC proteins in human embryonic stem cells. *Proc Natl Acad Sci USA* 99(15): 9864–9869.
- Evans-Galea M, Wielgosz M, Hanawa H, *et al.* 2007; Suppression of clonal dominance in cultured human lymphoid cells by addition of the cHS4 insulator to a lentiviral vector. *Mol Ther* 15(4): 801–809.
- Faustman D, Coe C. 1991; Prevention of xenograft rejection by masking donor HLA class I antigens. *Science* 252(5013): 1700–1702.
- Gao Q, Chung A, Kao W. 2007; Monocytic U937 adhesion, tumor necrosis factor- $\alpha$  and interleukin-1 $\beta$  expression in response to gelatin-based networks grafted with arginine-glycine-aspartic acid and proline-histidine-serine-arginine-asparagine oligopeptides. *Tissue Eng A* 13(1): 179–185.
- Hacein-Bey-Abina S, Von Kalle C, Schmidt M, *et al.* 2003; LMO2-associated clonal T cell proliferation in two patients after gene therapy for SCID-X1. *Science* 302(5644): 415–419.
- Howe S, Mansour M, Schwarzwaelder K, *et al.* 2008; Insertional mutagenesis combined with acquired somatic mutations causes leukemogenesis following gene therapy of SCID-X1 patients. *J Clin Invest* 118(9): 3143–3150.

## MIR2 expression decreases the alloimmune CTL response

- Hurme M, Chandler P, Hetherington C, et al. 1978; Cytotoxic T-cell responses to H-Y: correlation with the rejection of syngeneic male skin grafts. *J Exp Med* **147**(3): 768–775.
- Iannello A, Debbeche O, Martin E, et al. 2006; Viral strategies for evading antiviral cellular immune responses of the host. *J Leukoc Biol* **79**(1): 16–35.
- Ishido S, Choi J-K, Lee B-S, et al. 2000a; Inhibition of natural killer cell-mediated cytotoxicity by Kaposi's sarcoma-associated herpesvirus K5 protein. *Immunity* **13**(3): 365–374.
- Ishido S, Wang C, Lee B-S, et al. 2000b; Downregulation of major histocompatibility complex class I molecules by Kaposi's sarcoma-associated herpesvirus K3 and K5 proteins. *J Virol* **74**(11): 5300–5309.
- Jones K. 2008; Effects of biomaterial-induced inflammation on fibrosis and rejection. *Semin Immunol* **20**(2): 130–136.
- Kaiser J. 2009;  $\beta$ -Thalassemia treatment succeeds, with a caveat. *Science* **326**(5959): 1468–1469.
- Kim JY, Kim D, Choi I, et al. 2005; MHC expression in a human adult stem cell line and its downregulation by hCMV US gene transfection. *Int J Biochem Cell Biol* **37**(1): 69–78.
- Langer R, Vacanti J. 1993; Tissue engineering. *Science* **260**(5110): 920–926.
- Lanier L. 2005; NK cell recognition. *Annu Rev Immunol* **23**(1): 225–274.
- Lechler RI, Sykes M, Thomson AW, et al. 2005; Organ transplantation: how much of the promise has been realized? *Nat Med* **11**(6): 605–613.
- Lee EM, Kim JY, Cho BR, et al. 2005; Downregulation of MHC class I expression in human neuronal stem cells using viral stealth mechanism. *Biochem Biophys Res Commun* **326**(4): 825–835.
- Li L, Baroja M, Majumdar A, et al. 2004; Human embryonic stem cells possess immune-privileged properties. *Stem Cells* **22**(4): 448–456.
- Lodoen MB and Lanier LL. 2005; Viral modulation of NK cell immunity. *Nat Rev Microbiol* **3**(1): 59–69.
- Marin R, Ruiz-Cabello F, Pedrinaci S, et al. 2003; Analysis of HLA-E expression in human tumors. *Immunogenetics* **54**(11): 767–775.
- Markmann J, Bassiri H, Desai N, et al. 1992; Indefinite survival of MHC class I-deficient murine pancreatic islet allografts. *Transplantation* **54**(6): 1085–1089.
- Montini E, Cesana D, Schmidt M, et al. 2006; Hematopoietic stem cell gene transfer in a tumor-prone mouse model uncovers low genotoxicity of lentiviral vector integration. *Nat Biotech* **24**(6): 687–696.
- Nathan J, Lehner P. 2009; The trafficking and regulation of membrane receptors by the RING-CH ubiquitin E3 ligases. *Exp Cell Res* **315**(9): 1593–1600.
- Nienhuis A. 2008; Development of gene therapy for blood disorders. *Blood* **111**(9): 4431–4444.
- Nienhuis A, Dunbar C, Sorrentino B. 2006; Genotoxicity of retroviral integration in hematopoietic cells. *Mol Ther* **13**(6): 1031–1049.
- Osorio R, Ascher N, Melzer J, et al. 1994a; Enhancement of islet allograft survival in mice treated with MHC class I specific F(ab')<sub>2</sub> alloantibody. *Transpl Proc* **26**(2): 749.
- Osorio R, Ascher N, Stock P. 1994b; Prolongation of *in vivo* mouse islet allograft survival by modulation of MHC class I antigen. *Transplantation* **57**(6): 783–788.
- Persons D. 2010; Lentiviral Vector Gene Therapy: Effective and Safe? *Mol Ther* **18**(5): 861–862.
- Roh J, Sawh-Martinez R, Brennan M, et al. 2010; Tissue-engineered vascular grafts transform into mature blood vessels via an inflammation-mediated process of vascular remodeling. *Proc Natl Acad Sci USA* **107**(10): 4669–4674.
- Sanchez D, Coscoy L, Ganem D. 2002; Functional organization of MIR2, a novel viral regulator of selective endocytosis. *J Biol Chem* **277**(8): 6124–6130.
- Sanchez DJ, Gumperz JE, Ganem D. 2005; Regulation of CD1d expression and function by a herpesvirus infection. *J Clin Invest* **115**(5): 1369–1378.
- Snell G. 1979; Recent advances in histocompatibility immunogenetics. *Adv Genet* **20**: 291–355.
- Stein S, Ott M, Schultze-Strasser S, et al. 2010; Genomic instability and myelodysplasia with monosomy 7 consequent to EVI1 activation after gene therapy for chronic granulomatous disease. *Nat Med* **16**(2): 198–204.
- Thomas M, Boname J, Field S, et al. 2008; Downregulation of NKG2D and NKp80 ligands by Kaposi's sarcoma-associated herpesvirus K5 protects against NK cell cytotoxicity. *Proc Natl Acad Sci USA* **105**(5): 1656–1661.
- Welte S, Kuttruff S, Waldhauer I, et al. 2006; Mutual activation of natural killer cells and monocytes mediated by NKp80–ALCL interaction. *Nat Immunol* **7**(12): 1334–1342.
- Wu DC, Boyd AS, Wood KJ. 2008; Embryonic stem cells and their differentiated derivatives have a fragile immune privilege but still represent novel targets of immune attack. *Stem Cells* **26**(8): 1939–1950.
- Yokoyama W, Seaman W. 1993; The *Ly-49* and *NKR-P1* gene families encoding lectin-like receptors on natural killer cells: the NK gene complex. *Annu Rev Immunol* **11**(1): 613–635.
- Zuckerman S, Brown J, Kao W. 2009; Identification of regulatory Hck and PAI-2 proteins in the monocyte response to PEG-containing matrices. *Biomaterials* **30**(23–24): 3825–3833.

## Suppression of the MHC Class I-Mediated Alloimmune Response in Human Cells Using a Single-Step Retroviral Transduction Protocol to Express KSHV's Stealth Protein MIR2

Ajit Thakur, Institute of Biomaterials and Biomedical Engineering, University of Toronto  
Abeyat Zaman, The Hospital for Sick Children, University of Toronto  
Scott Fitzpatrick, School of Biomedical Engineering, McMaster University  
Jeff Hummel, Centre for Gene Therapeutics, McMaster University  
Kim Jones, School of Biomedical Engineering, Department of Chemical Engineering, McMaster University

### Abstract

The host immune response is a significant barrier to allogeneic transplantation, and this problem affects almost all types of cell-based, tissue-engineered constructs. In this paper, we test whether a single dose of a retroviral vector is sufficient to transduce a population of human cells to express viral immunomodulatory proteins to suppress the acute cellular alloimmune response *in vitro*. We overexpressed Kaposi's Sarcoma-Associated Herpes Virus (KSHV) modulator of immune recognition (MIR2) protein in human monocyte-like progenitor cells (U937) using the moloney murine leukemia virus (MMLV) to transduce cells in a single transduction step, without any cell selection or amplification. We used fluorescence microscopy and flow cytometry to characterize the heterogeneously transduced MIR2-expressing U937 cells and found that approximately 80% differentially downregulated cell surface levels of Major Histocompatibility Class I (MHCI) and ICAM-1 molecules, which resulted in a significant (30%) reduction in cytotoxic T-lymphocyte (CTL)-mediated killing of target cells, without altering natural killer (NK)-mediated target cell lysis *in vitro*. Our results provide a proof-of-principle that the use of viral immunomodulatory mechanisms in a single-step transduction approach can significantly minimize the acute cellular alloimmune response mediated via CTLs and NK cells. We propose a single-step *ex vivo* gene delivery strategy using retroviral vectors that can potentially be implemented in donor organs, tissues and cell-based tissue engineered constructs to extend the life of allogeneic cells *in vivo*.

### Introduction

Diabetes, chronic renal failure, ischemic heart disease, end-stage liver disease and many others are all incurable diseases with a known solution: organ transplantation. However, transplanted organs or grafts from a human donor (allogeneic transplants) have a limited life-span in the recipient due to the immune response against the foreign cells. Immunosuppressive drugs provide a short-term solution (80-95% 1-year graft survival) in cardiac, renal, lung, liver and pancreatic transplantation.<sup>1</sup> However, immunosuppression is a systemic approach that suppresses the body's immune system, therefore rendering the individual susceptible to opportunistic infections. Moreover, long-term immunosuppressive drug therapy is associated with the risk of severe side effects, such as cytotoxicity, hypertension and cardiovascular disease.<sup>1</sup>

In addition to the potential for graft rejection, significant organ-donor shortages represent a major challenge for the wide spread implementation of organ transplantation as a solution for numerous diseases. The extensive list of requirements for ensuring compatibility between the donor and recipient further reduces the total number of organs available for transplantation. Fortunately, the field of tissue engineering offers many potential solutions to these medical challenges. Tissue engineered constructs can be used as a biological substitute in almost any tissue in the body; hence, their structure and composition can be specifically tailored to the application. However, implantation of cell-based tissue-engineered constructs must overcome the same fundamental challenge surrounding all allogeneic cell, tissue and organ transplantation: immune rejection.

The immune response to allogeneic grafts involves components of both the innate and adaptive immune system. However, the T-cell response of the adaptive immune system is considered to be the most important determinant of acute cellular

Corresponding Author:  
Ajit Thakur, Institute of Biomaterials and Biomedical Engineering  
Email: thakurajit@gmail.com



rejection.<sup>2,3</sup> The T-cell response occurs due to the recognition of 'non-self' alloantigens present on the allograft. Experiments by George Snell and colleagues identified the Major Histocompatibility Complex (MHC) as the locus of polymorphic genes, which code for the targets of allograft recognition.<sup>4,5</sup> Since Major Histocompatibility Complex Class I (MHCI) molecules are expressed on all nucleated cells, they can be recognized by alloreactive T cells and evoke immune responses in virtually all tissue types. This response typically leads to the activation of alloreactive CD8<sup>+</sup> T cells, which proliferate and differentiate into effector cells known as CD8<sup>+</sup> cytotoxic T lymphocytes (CTLs). These CTLs have potent cytolytic activity and specifically target and eliminate allogeneic cells.<sup>2</sup> Hence, the MHCI recognition capability of T cells responding to the allograft is the most significant event leading to acute cellular rejection.

Recognizing this important aspect of immune rejection, many previous studies have attempted numerous techniques to reduce MHCI expression.<sup>6,7</sup> However, a global reduction of MHCI molecules has been shown to increase the susceptibility of cells to natural killer (NK) cells of the innate immune system.<sup>6</sup> Cell surface MHCI acts as a ligand for NK cells and provides an inhibitory signal and decreases their cytolytic activity against allogeneic cells. In humans, many of the Class I alleles, including HLA-B and HLA-C loci, are recognized by NK cell inhibitory receptors.<sup>2</sup> In the absence of MHCI molecules, NK cells are activated by ubiquitously expressed allogeneic cell surface ligands, such as MICA, MICB and AICL.<sup>8,9</sup> This results in the specific lysis of cells lacking MHCI molecules. Therefore, it is clear that a general downregulation of MHCI molecules is unlikely to significantly protect allogeneic cells from the immune response, and that a more elegant method is required.

The immune response is arguably the most significant barrier to allogeneic transplantation and this problem affects almost all types of cell-based, tissue-engineered constructs. Hence, it is imperative that such tissue-engineered constructs address this important challenge. In preparing a tissue-engineered construct, the cells required are sourced in advance. This provides the opportunity to use genetic engineering techniques to manipulate these cells in a fashion that may allow them to evade or suppress the immune response. Viruses have evolved complex genetic mechanisms to evade and suppress detection by the immune responses of the host. A tissue-engineered allogeneic construct with genetically engineered cells that utilizes these viral immune evasion mechanisms might potentially elicit a similar response and not be recognized by the host immune system as 'foreign,' thus preventing rejection. Previous work by our group has shown that clonally selected subpopulations of allogeneic cells employing viral immune evasion mechanisms can indeed suppress the alloimmune response against CTLs and NK cells.<sup>7</sup> However, our approach involved multiple steps post-transduction, including clonal cell expansion, characterization and selection, which required several weeks to implement.<sup>7</sup> Given that organs and tissues harvested from human donors have an extremely limited shelf-life, an alternative, accelerated approach is required to make our immune evasion strategy more applicable to the clinical transplantation of organs, tissues and cell-based, tissue-engineered constructs.

In this paper, we examine the feasibility of applying viral

immune evasion mechanisms to genetically engineer cells in a single-step transduction method, without cell expansion or selection, to suppress the immune rejection of allogeneic model human progenitor cells (U937). In summary, we genetically engineered allogeneic cells using a single dose of a retroviral vector moloney murine leukemia virus (MMLV) to express an immunomodulatory protein called modulator of immune recognition (MIR2) from Kaposi's Sarcoma-Associated Herpes Virus (KSHV). This multifunctional protein is known to differentially downregulate the cell surface expression of MHCI, ICAM-1 and other molecules.<sup>7</sup> In addition, MIR2 also decreases the expression of NK cell activation ligands (MICA, MICB), which are ubiquitously present on most cell types. We tested the effectiveness of using a single dose of retroviral vector to transduce allogeneic cells with MIR2 before challenging them against CTLs and NK cells. The immunoprotective effect of MIR2 expression against allogeneic CTLs and NK cells was tested using an *in vitro* cytotoxicity assay in conjunction with flow cytometry. Our results provide a proof-of-principle that this single-step method of employing viral immune evasion strategies can potentially be applied in the clinical transplantation of organs, tissues and cell-based, tissue-engineered constructs to delay or even prevent acute cellular immune rejection upon implantation into an allogeneic host.

## Materials and Methods

### Cell Line and Cell Culture

The histiocytic lymphoma-derived immortalized monocyte-like myeloid progenitor human cell line (U937) was generously provided by Dr. Karen Mossman at the Centre for Gene Therapeutics, McMaster University, Hamilton, ON. Human U937 cells were cultured using standard culture conditions as described previously.<sup>10</sup>

### Retroviral Vector Construction and Transduction

In order to make the viral vector carrying the MIR2 gene, Stratagene's Viraport<sup>TM</sup> retroviral gene expression system was employed. The MIR2-GFP fusion protein cDNA was a gift from Dr. Laurent Coscoy (University of California, Berkeley). Viral particles were generated according to the manufacturer's instructions (Stratagene's Viraport<sup>TM</sup>). After transducing U937 cells, they were cultured in non-selective media to maintain the composition of the MIR2-GFP-expressing heterologous population (hereby referred to as U937-MIR2-GFP). This procedure was repeated to generate viral particles carrying the LacZ gene, which were subsequently used to generate U937 cells expressing  $\beta$ -galactosidase enzyme. This cell line (hereby referred to as U937-LacZ) served as a control for comparison with U937-MIR2-GFP.

### Fluorescence Microscopy

All transmission light images were collected using an Axiovert 200 (Carl Zeiss MicroImaging, Inc., Germany) inverted fluorescence microscope. Images were acquired using AxioVision 3.1 (Carl Zeiss Vision, USA) software and processed with Adobe Photoshop. Fluorescence images were collected using the aforementioned setup as well as with a Leica DM IRE2 in-

verted fluorescence microscope system (Leica) in conjunction with Openlab imaging software (IMPROVISION).

#### Flow Cytometry

Cells were stained with fluorescently-labelled antibodies specific to cell surface markers of interest. A Beckman Coulter FC500 system (Beckman Coulter Canada Inc., Mississauga, ON, Canada) was used to analyse the cells with the CXP software provided. Data was analyzed as described previously.<sup>7,10</sup> The Student's *t*-test was used to determine statistical significance ( $p < 0.05$ ).

#### CTL Assay

The CTL assay was used to measure the ability of target cells, such as U937-MIR2-GFP, to evade cytotoxicity by effector cells (CTLs) compared to control cells (U937-LacZ). In setting up this assay, effector cells had to be isolated and differentiated from human blood acquired from healthy graduate student volunteers. First, peripheral blood mononuclear cells (PBMCs) were isolated from fresh, whole blood by exposing RBCs to hypotonic ammonium-chloride (ACK) solution. Second, the Human CD8+ T Cell Enrichment Kit (StemCell Technologies) was used to isolate CD8+ T cells from PBMCs. Third, these negatively isolated CD8+ T cells were stimulated with allogeneic 'stimulator' cells (U937-LacZ) *in vitro* to generate CTLs. Fourth, appropriate Effector (CTLs): Target (U937-MIR2-GFP or U937-LacZ) ratios were determined (2:1 and 10:1 respectively) and the number of cells required was calculated. The target cell number was held constant, while the effector cell number was varied according to the predetermined ratios. In setting up the CTL assay, a sufficient number of target cells were labelled with 100 nM Calcein-AM (Invitrogen), which is a live cell fluorescent stain. After incubating the co-culture for 4h at 37 °C (humidified, 5% CO<sub>2</sub>), 7-AAD (Beckman Coulter) was added to each well. Fifth, flow cytometry data analysis was based on the labelling intensity of the target cells with Calcein and 7-AAD. The percentage of specifically killed cells was calculated from the double-labelling of target cells with Calcein and 7-AAD, and comparing this with background target cell death in control wells.<sup>10</sup>

#### NK Assay

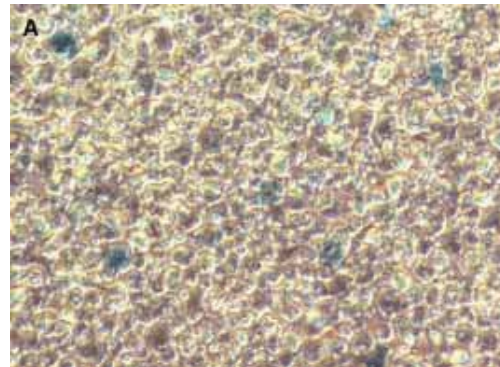
The NK assay was used to measure the ability of target cells (U937-MIR2-GFP) to evade cytotoxicity by effector cells (NK cells) compared to control cells (U937-LacZ). In setting up this assay, effector cells had to be isolated and activated from human blood. First, PBMCs were isolated from fresh, whole blood as described in the CTL assay. Second, the Human CD56 Selection Kit (StemCell Technologies) was used to positively isolate NK cells. Third, NK cells were activated with 10 µg/ml Poly I:C (Sigma) and 50 U/ml rh IL-2 (Invitrogen) to enhance their cytolytic ability. Fourth, appropriate Effector (NK cells): Target (U937-MIR2-GFP or U937-LacZ) ratios were determined (0.1:1 and 0.25:1) and the number of cells required was calculated. The NK assay was setup in a manner similar to the CTL assay.

All studies were performed in accordance with the Research Ethics Board at McMaster University and blood collection was done by a licensed phlebotomist.

## Results

### Retrovirus can Efficiently Transduce Human U937 Cells with LacZ

The MMLV used in this study was pseudotyped, such that it expressed the vesicular stomatitis virus G (VSV-G) coat, which is known to have a broad specificity to almost any mitotic cell. In order to confirm that this VSV-G pseudotyped retrovirus was able to transduce U937 cells, a test transduction was setup. Retrovirus carrying the LacZ gene was generated and used to transduce U937 cells as described in the Materials and Methods section. Figure 1 shows blue staining of β-galactosidase expressing cells, indicating that U937 cells were indeed transducible by VSV-G pseudotyped MMLV. The single dose transduction efficiency varied from 40-70% depending on the conditions. As a result, the transduction produced a heterogeneous population of cells with varying levels of β-galactosidase-expressing cells. This population of cells was subsequently used as a transduction control to compare with U937-MIR2-GFP cells.



**Figure 1. Transduction of U937 cells using MMLV.** Image shows β-galactosidase staining (blue cells) of U937 cells, indicating that these cells are clearly transducible by retrovirus (MMLV).

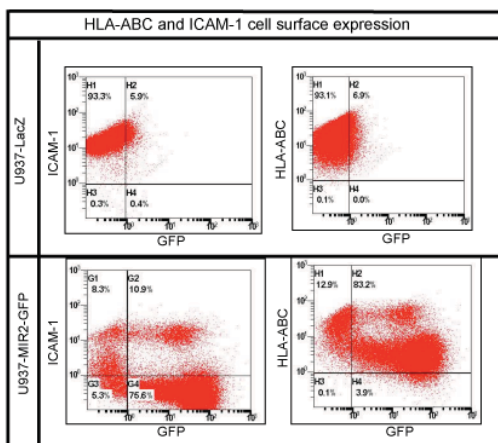
After establishing the transducibility of U937 cells, MMLV carrying the MIR2-GFP gene was generated and used in subsequent transductions. Figure 2 shows a strong GFP signal in transduced U937 cells, indicating the likely expression of the chimeric MIR2-GFP fusion protein. The single dose transduction efficiency varied from 50%-80% depending on the conditions. In addition, the transduction produced a heterogeneous population of cells with varying levels of MIR2-GFP expressing cells, similar to the LacZ transduction.



**Figure 2. MIR2-GFP expression in U937 cells after MMLV transduction.** U937 cells express MIR2-GFP (green) after transduction with retrovirus. Images collected in transmission (A) and fluorescence (B) channels. Image C overlays the two channels.

**MIR2-GFP expression downregulates cell surface HLA-ABC and ICAM-1**

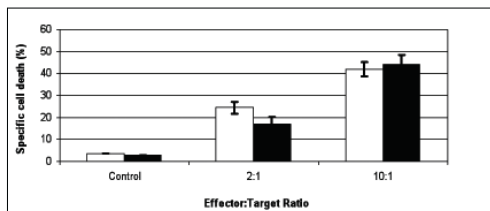
The expression of MIR2-GFP in U937 cells is expected to alter the cell surface expression of important immunoactive molecules such as HLA-ABC and ICAM-1 (CD54). In Figure 3, the top panel depicts the normal distribution in the expression level of HLA-ABC and ICAM-1 in a heterologous population of U937-LacZ cells. In contrast, the bottom panel shows that cell surface ICAM-1 is strongly downregulated, while HLA-ABC is moderately downregulated in U937-MIR2-GFP cells. The detection of GFP in only U937-MIR2-GFP cells confirmed that these cells were likely expressing the MIR2-GFP fusion protein, which produced the observed effects. Upon further analysis (via the CXP software) of the transduced cells expressing GFP, it was also noted that approximately 80% of live cells in the heterologous culture significantly downregulated both cell surface HLA-ABC and ICAM-1. Only a small proportion (~10%) of the heterologous culture of transduced cells expressed GFP without downregulating both cell surface HLA-ABC and ICAM-1. The remaining 5-10% of the heterologous culture did not express GFP and did not downregulate cell surface HLA-ABC or ICAM-1.



**Figure 3. Cell-surface characterization of U937-LacZ and U937-MIR2-GFP cells.** This plot compares the relative amount of GFP, HLA-ABC and ICAM-1 (CD54) detected in each of the cell lines. GFP was quantified by its fluorescence, while fluorescently labelled antibodies were used to quantify the other markers. Flow cytometry data presented from 30,000 events collected per trial (n=3).

**MIR2-GFP expression decreases CTL-induced specific cell death of U937 cells**

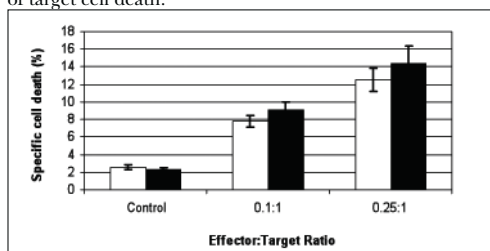
The CTL assay determined the specific cell death of target cells transduced with MIR2 at two different Effector:Target (E:T) ratios (Figure 4). Specifically, at the 2:1 E:T ratio, there was a 30% reduction in the specific lysis of MIR2 cells. However, the protection conferred by MIR2 at the 10:1 E:T ratio was not significant. The control samples did not contain any effector cells and indicate the background levels of target cell



**Figure 4. CTL Assay.** Shows percent specific lysis of Calcein-labelled target cells (U937-LacZ [white bars] or U937-MIR2-GFP [black bars] cells) in control samples and test samples with varying Effector:Target ratios. (Statistics:  $p < 0.05$  between cell lines for 2:1 Effector:Target ratio; error bars indicate standard deviation; n=3).

**MIR2-GFP expression does not alter NK-induced specific cell death of U937 cells**

The NK assay showed no statistically significant difference in the specific cell death of target cells transduced with MIR2-GFP when compared to target cells transduced with LacZ at both E:T ratios (Figure 5). Moreover, it was noted that the increase in the specific cell death of target cells was associated with an increase in the E:T ratio. The control samples did not contain any effector cells and indicate the background levels of target cell death.



**Figure 5. NK Assay.** Shows percent specific lysis of Calcein-labelled target cells (U937-LacZ [white bars] or U937-MIR2-GFP [black bars] cells) in control samples and test samples with varying Effector:Target ratios. (Statistics: no significant difference ( $p > 0.05$ ) between cell lines; error bars indicate standard deviation; n=3).

**Discussion**

In tissue engineering, the immune response to allogeneic cells is a major barrier impeding successful transplantation of tissue-engineered constructs. Previous work by our group has demonstrated that clonally expanded allogeneic cells employing viral immune evasion strategies can significantly suppress the acute cellular alloimmune response mediated by CTLs and NK cells.<sup>7</sup> However, this approach required multiple steps and several weeks of cell expansion, characterization and selection before it could be implemented. In this paper, we test an alternative method to engineer immune acceptance, such that allogeneic cells are modified in a single step to employ viral strategies to suppress the acute cellular



alloimmune response.

In our approach, we used a retroviral vector to deliver the MIR2-GFP chimeric viral gene to allogeneic cells *in vitro*. Our results show that a single dose of VSV-G pseudotyped MMLV is sufficient to transduce model human progenitor cells (U937 cells) and express the LacZ gene or the MIR2-GFP chimeric viral gene at a moderate transduction efficiency (40%-80%) without the need for any cell expansion or selection before transplantation (Figures 1, 2). Furthermore, cell surface characterization of MHCI and ICAM-1 expression confirmed that the levels of transduction efficiency achieved by a single dose of retroviral vector significantly (>90% decrease in mean fluorescence intensity) downregulated both MHCI and ICAM-1 in approximately 80% of the heterologous population of transduced cells (Figure 3). However, approximately 10% of the heterologous population of cells expressed GFP without downregulation of MHCI and ICAM-1. This effect is likely due to the insertional rearrangement of the transduced gene, which has been previously reported.<sup>2,6</sup> In addition, Figure 3 suggests that this single-step transduction approach produced a heterogeneous expression of MIR2-GFP among the transduced cells. This effect is likely due to the varying transgene copy-number in each transduced cell in the heterologous population and simulates the effect that is expected to occur during the transplantation of tissues which have been modified by retroviral vectors. It follows that our approach provides a more realistic measure of the effectiveness of this retroviral vector's ability to transduce cells and tissues for transplantation between donor and recipient. In contrast to the present study, our previous work clonally expanded and selected subpopulations of transduced cells with the desired MIR2 expression level for enhanced suppression of the acute cellular alloimmune response mediated by CTLs and NK cells.<sup>7</sup> Thus, our current study not only confirms the results of our previous work with amplified subpopulations of stably transduced MIR2-expressing cells, it also demonstrates the effectiveness of our retroviral gene-delivery approach over the short term, after a single-step transduction, without involving any cell expansion or selection.

The results of the CTL assay suggest that MIR2-GFP expression in a heterologous population of cells confers a significant (30%) protective effect against allogeneic CTLs at certain E:T ratios (Figure 4). It is also instructive to note that this statistically significant ( $p < 0.05$ ) decrease in CTL-specific cell lysis was measured in a heterologous population of transduced cells, with approximately 20% of cells not downregulating either MHCI or ICAM-1, and with widely varying levels of transgene expression (Figure 3). We have previously observed CTL-specific cell lysis suppression in a heterologous culture of transduced cells ranging from 20-50%, depending on the transduction protocols employed (unpublished data). It follows that the suppression of the acute cellular alloimmune response can be significantly enhanced by optimizing transduction protocols and therefore improving the single-step transduction efficiency. Furthermore, the MIR2-mediated decrease in HLA-ABC (MHCI) and ICAM-1 levels are likely to have synergistically contributed to the decrease in CTL-mediated killing of target cells. Since CD8<sup>+</sup> CTLs rec-

ognize MHCI and adhere to target cells using ICAM-1, it is expected that any decrease in the cell-surface expression of these molecule hinders the target recognition and binding capability of CTLs. This effect likely contributes to the observed immune evasion of MIR2-expressing target cells. It is interesting to note that there was no protective effect at high E:T ratios. This suggests that there likely exists an upper limit for the protective effects of MIR2, which can be abrogated by significantly increasing the E:T ratio. However, E:T ratios above 10:1 are relatively high and may not be encountered by transplanted allogeneic cells *in vivo*.

In the NK assay, no significant difference in specific cell death was observed between U937-MIR2-GFP cells and U937-LacZ cells (Figure 5). Natural killer cell cytolytic activity is inversely proportional to the amount of MHCI present on the cell surface.<sup>6,7</sup> As the MHCI levels decrease on the cell surface, a greater percentage of the target cells should be specifically killed by NK cells. In this experiment, U937 cells expressing MIR2 were shown to downregulate MHCI and ICAM-1 molecules, without increasing NK-mediated specific cell death of target cells in comparison to controls. Therefore, our results suggest that MIR2 expression confers a significant protective effect against NK specific cell death. A number of factors may have contributed to this observed protective effect, including the reduction of ICAM-1, which is involved in NK cell adherence to target cells, and the MIR2-mediated downregulation of other U937 cell surface molecules, such as MICA, MICB and AICL that are involved in NK cell activation.<sup>11,12</sup>

Our method of modifying cell surface molecules may also serve to increase the chances of inducing systemic tolerance against the allograft. Many studies have previously demonstrated that some expression of the immunoantigen is beneficial to maintaining active tolerance.<sup>6,13</sup> For example, a study by Faustman and Coe showed that incomplete masking of MHCI molecules using antibodies can potentially lead to tolerance in murine hosts, indicating that donor MHC density was important in inducing tolerance.<sup>13</sup> Given these observations, the expression of MIR2 in our present study might have the potential to induce a similar tolerance effect against allogeneic cells *in vivo*. MIR2 differentially downregulates MHCI molecules such that it significantly reduces cell surface expression of only some classes of MHCI molecules (HLA-A, HLA-B), without affecting other MHCI molecules (HLA-C, HLA-E).<sup>7</sup> The almost unabated expression of HLA-C and other non-classical MHCI molecules like HLA-E not only serve to inhibit NK cell-mediated cytotoxicity, but may also serve to induce active host tolerance to the allograft. Hence, our differential downregulation approach to MHCI modulation may effectively create a greater window of opportunity for the induction of systemic tolerance.

The results of our present study suggest that this immune evasion strategy can potentially be applied in the clinical transplantation of organs, tissues and cell-based tissue engineering, since it can be effectively implemented in a single step without delay and provides an alternative to using systemic immunosuppressive drugs. Moreover, this method to selectively modify donor antigens may also pave the way to generating 'universal' donor cells. An immediate advantage

of universal donor cells in tissue engineering is that it enables the development of "off-the-shelf" technology, which can function immediately in any individual. Previous work by our group demonstrated that MIR2-expressing cells can maintain their immunoprotective effects against CTLs and NK cells over the long term, making this technique suitable for allogeneic cell-based product development.<sup>7</sup> Given that we employed model human progenitor cells (U937 cells) that mimic the gene expression profile of stem-cell derived cells commonly used in tissue engineering,<sup>14,15</sup> the results of our present study also suggest that our proposed strategy may provide an alternative to isogenic stem cell technology, which is often laborious and requires time to create, differentiate and expand isogenic stem cells for applications in tissue engineering. It follows that this technology will enhance the development of semi-synthetic organs and therefore improve the availability of transplantable organs to better match demand, which would significantly decrease the cost and delays incurred with current medical procedures involving donor organs.

### Conclusion

We characterized the effect of a single-step retroviral MIR2 transduction on the cell surface expression of MHCI and ICAM-1 molecules and assessed their ability to evade CTLs and NK cells, without MIR2-transduced cell expansion or selection. Flow cytometry analysis of the heterogeneously transduced cells showed that MHCI and ICAM-1 molecules were significantly downregulated in approximately 80% of the cells. Our results demonstrate that heterogeneous MIR2 expression in a heterologous culture confers a significant (30%) immunoprotective effect to allogeneic human U937 cells against CTLs, without altering their susceptibility to NK-mediated specific cell death *in vitro*. These results suggest that our single-step method of employing viral immune evasion strategies can potentially be applied in the clinical transplantation of donor organs, tissues and cell-based tissue engineered constructs, which are currently limited by their short shelf-life. It is expected that the observed suppression of the acute cellular alloimmune response mediated by MIR2 expression may significantly delay or even prevent immune rejection upon implantation into an allogeneic host.

### Acknowledgements

We would like to thank Dr. Heather Sheardown, Dr. Karen Mossman, Dr. Ali Ashkar, Dr. Firoz Mian, Dr. Laurent Coscoy, Glenn McClung, Ruchira Sengupta, Vasudha Gupta, Faheem Dinath and Dave Morrison for providing us with materials and technical support, and to the Natural Science and Engineering Research Council (NSERC) for their funding.

### References

1. Lechler R, Sykes M, Thomson A, Turka L. Organ transplantation- how much of the promise has been realized? *Nat Med.* 2005; 11(6):605-13.
2. Abbas A, Lichtman A, Pober J. *Cellular and Molecular Immunology*. Fourth ed. Philadelphia: W.B Saunders Company 2000.
3. Anderson J, Rodriguez A, Chang D. Foreign body reaction to biomaterials. *Semin Immunol.* 2008; 20(2):86-100.
4. Hurme M CP, Hetherington CM, Simpson E. Cytotoxic T-cell responses to H-Y: correlation with the rejection of syngeneic male skin grafts. *J Exp Med.*

- 1978; 147(3):768-75.
5. Snell G. Recent advances in histocompatibility immunogenetics. *Adv Genet.* 1979; 20:291-355.
6. Iannello A, Debbeche O, Martin E, Attalah LH, Samarani S, Ahmad A. Viral strategies for evading antiviral cellular immune responses of the host. *J Leukoc Biol.* 2006; 79(1):16-35.
7. Thakur A, Hummel J, Sengupta R, Gupta V, Mossman K, Jones K. Retroviral expression of MIR2 decreases both surface MHC Class I and the alloimmune CTL response. *Journal of Tissue Engineering and Regenerative Medicine.* 2011; 5(7):520-8.
8. Thomas M, Boname J, Field S, Nejentsev S, Salio M, Cerundolo V, et al. Down-regulation of NKG2D and NKp80 ligands by Kaposi's sarcoma-associated herpesvirus K5 protects against NK cell cytotoxicity. *PNAS.* 2008; 105(5):1656-61.
9. Welte S, Kuttruff S, Waldhauer I, Steinle A. Mutual activation of natural killer cells and monocytes mediated by NKp80-AICL interaction. *Nat Immunol.* 2006; 7(12):1334-42.
10. Thakur A, Kugathasan K, Gupta V, Jones J. A novel method for measuring cell-mediated cytotoxicity and viability using flow cytometry. *IBBME Proceedings.* 2010; 1(1):18-22.
11. Ishido S, Wang C, Lee B-S, Cohen GB, Jung JU. Downregulation of Major Histocompatibility Complex Class I Molecules by Kaposi's Sarcoma-Associated Herpesvirus K3 and K5 Proteins. *J Virol.* 2000; 74(11):5300-9.
12. Ishido S, Choi J-K, Lee B-S, Wang C, DeMaria M, Johnson RP, et al. Inhibition of Natural Killer Cell-Mediated Cytotoxicity by Kaposi's Sarcoma-Associated Herpesvirus K5 Protein. *Immunity.* 2000; 13(3):365-74.
13. Faustman D, Coe C. Prevention of xenograft rejection by masking donor HLA class I antigens. *Science.* 1991; 252(5013):1700-2.
14. Drukker M, Katz G, Urbach A, Schuldiner M, Markel G, Itskovitz-Eldor J, et al. Characterization of the expression of MHC proteins in human embryonic stem cells. *PNAS.* 2002 July 23, 2002; 99(15):9864-9.
15. Marín R, Ruiz-Cabello F, Pedrinaci S, Méndez R, Jiménez P, Geraghty D, et al. Analysis of HLA-E expression in human tumors. *Immunogenetics.* 2003; 54(11):767-75.



With expert hands and creative minds  
it's our mission at PRHC to provide  
exceptional care for our patients.

**PRHC**  
Peterborough Regional  
Health Centre

We value innovative, dedicated and compassionate professionals who can meet the needs of our community. Consider joining PRHC's 350 talented physicians in choosing Peterborough as the place for a dynamic, rewarding and challenging career.

It is an exciting time of progressive change and rapid growth at the Peterborough Regional Health Centre (PRHC). As one of the region's largest employers, our staff is 2,000 strong with more than 600 volunteers, together serving a population of over 300,000 people in four counties.

We recognize what it takes to make a successful career in healthcare. Come and see how much more we can offer you.

PRHC is the place to be for care and career!

Please visit our website or  
contact us at: [careers@prhc.on.ca](mailto:careers@prhc.on.ca)  
[www.prhc.on.ca](http://www.prhc.on.ca)

## CASE REPORT

# Recurrent hospitalisations in a rare case of hemicorporectomy: a challenging case for medical management

Ajit Thakur,<sup>1</sup> Brittney Elliott,<sup>2</sup> Rohan Naik,<sup>1</sup> Nabeel Khan,<sup>1</sup> Shayna McQuaid,<sup>3</sup> Camelia Arsene<sup>1</sup>

<sup>1</sup>Department of Internal Medicine, Sinai-Grace Hospital, Detroit Medical Center/Wayne State University School of Medicine, Detroit, Michigan, USA

<sup>2</sup>Faculty of Medicine, McGill University, Montreal, Quebec, Canada

<sup>3</sup>Eugene Applebaum College of Pharmacy and Health Sciences, Wayne State University, Detroit, Michigan, USA

**Correspondence to**  
Dr Ajit Thakur,  
canindianast@gmail.com

BE and RN contributed equally.

Accepted 9 December 2017

## SUMMARY

Hemicorporectomy, or translumbar amputation, is a radical surgery involving the dissection of the body at the waist and is usually reserved for complex medical conditions including locally invasive malignancy and terminal pelvic osteomyelitis. Only 71 cases have previously been reported. We present a rare case of hemicorporectomy in a 53-year-old patient with terminal pelvic osteomyelitis which occurred after he suffered a gunshot wound at T6 causing paraplegia at the age of 31. Unfortunately, this patient continued to suffer recurrent hospitalisations and sepsis events secondary to chronic, non-healing advanced pressure ulcers and complicated urinary tract infections despite repeated courses of broad-spectrum intravenous antibiotics and surgical debridements. In light of his diminished quality of life and poor prognosis, the patient's family chose to manage his condition conservatively with home hospice. This case illustrates the significant challenges in the medical and surgical management of hemicorporectomy patients.

## BACKGROUND

Hemicorporectomy, or translumbar amputation, is a radical surgery involving dissection of the body at the waist (commonly between L4 and L5). It entails removal of the legs, genitalia, bladder, pelvic bones, anus and rectum, and is commonly performed in two stages, with a colostomy and ileal conduit being created during the first operation and the actual hemicorporectomy being done during the second operation. The first ever hemicorporectomy was performed in 1950, and as of 2017 a total of only 71 cases have been reported.<sup>1,2</sup>

The original indication for hemicorporectomy was locally invasive malignancy of the pelvis for which chemotherapy, radiotherapy or conventional surgeries were not beneficial or possible. In recent years, it has been performed for other indications, including terminal pelvic osteomyelitis, squamous cell carcinoma (SCC) in a pressure ulcer, pelvic chondrosarcoma, severe pelvic trauma, vascular malformations, and in one case gangrene secondary to acute aortic occlusion.<sup>3</sup> Of the 71 reported cases of hemicorporectomy performed, 21 (30%) cases have been reported for terminal pelvic osteomyelitis, 43 (60%) cases for malignancy (13 cases were SCC arising from pressure ulcers), 4 cases for

benign disease and 3 cases for trauma. Outcomes are generally more favourable for non-malignant versus malignant indications.<sup>4</sup> For terminal pelvic osteomyelitis, more than 50% of patients survived at least 9 years, with an average survival of 11 years posthemicorporectomy.<sup>5</sup> The average survival post-procedure decreases to 2.9 years when malignancy is the indication for hemicorporectomy.<sup>5</sup> Overall, one-third of patients survived at least 9 years after hemicorporectomy.<sup>5</sup>

Although published reports suggest prolonged survival (>50% survival for terminal pelvic osteomyelitis at 9 years) posthemicorporectomy, this does not take into account the quality of life and morbidity of patients.<sup>5</sup> In the postoperative period, complications of hemicorporectomy include volume overload, wound dehiscence and delayed healing.<sup>5</sup> Some of the first patients to undergo this procedure died of pulmonary hypertension.<sup>6</sup> For patients with long-term survival, other factors to consider include decreased body mass and circulating blood volume, as well as loss of muscle mass, which is thought to affect fluid, acid-base, electrolyte balance and drug dosing.<sup>7</sup> Moreover, the radical nature of a hemicorporectomy severely distorts the body anatomy and may introduce new problems such as faecal and urine drainage from ostomy sites into dependent areas, with chronic non-healing pressure ulcers causing infections and complicated urinary tract infections (UTIs) resulting in repeated sepsis events requiring multiple hospitalisations. Furthermore, it has also been reported that the loss of body surface area also affects heat dissipation and temperature regulation.<sup>8</sup> Taken together, these factors can potentially diminish the quality of life and increase the morbidity of hemicorporectomy patients, which calls into question the best way to manage the complications of hemicorporectomy patients and provide comprehensive care in the inpatient and outpatient settings.

## CASE PRESENTATION

Here, we present a 53-year-old African-American man who underwent a hemicorporectomy at the level of L2 (at age 49) after a series of surgical procedures for terminal pelvic osteomyelitis, chronic advanced pressure ulcers and chronic complicated UTIs, which occurred after a gunshot wound at T6 causing paraplegia at the age of 31 (box 1, figure 1).



**To cite:** Thakur A, Elliott B, Naik R, et al. *BMJ Case Rep* Published Online First: [please include Day Month Year]. doi:10.1136/bcr-2017-222375

## Rare disease

### Box 1 Timeline of significant medical and surgical events

- ▶ 1994: initially became paraplegic secondary to a gunshot wound at T6.
- ▶ July 2006: elective transverse loop colostomy with subsequent excision and creation of ileostomy.
- ▶ November 2007: right hip disarticulation and amputation due to right femoral head osteomyelitis.
- ▶ December 2007: stage 4 sacral pressure ulcer, left second toe osteomyelitis.
- ▶ January 2008: recurrent urinary tract infections (UTIs) secondary to indwelling Foley catheter.
- ▶ February 2008: suprapubic catheter placed secondary to paraphimosis and erosion of the urethral meatus secondary to the indwelling Foley catheter.
- ▶ April 2008: sepsis secondary to penile shaft necrosis and penile ulcers; suprapubic catheter malfunction, with subsequent sepsis secondary to UTI from urocutaneous fistula.
- ▶ December 2009: ileovesicostomy using ileum as a loop and primary bowel anastomosis.
- ▶ 2011/2012: urosepsis, stage 4 chronic sacral pressure ulcer debridement, septic left hip and sacral bone biopsy consistent with osteomyelitis.
- ▶ April 2012: multiple left lower extremity pressure ulcers with necrotic left toes; subsequent left hip disarticulation and translumbar amputation at L2 leading to his current state: hemicorporectomy.
- ▶ September 2012: enlargement of bilateral back and hip pressure ulcers; excisional debridement.
- ▶ November 2013: revision of colostomy due to prolapse; cystectomy and excision of ileovesicostomy; ileal conduit urinary diversion and bilateral ureteral stent placement.
- ▶ January 2016: prolapsed ileal loop, requiring revised ostomy.
- ▶ September 2016: sepsis due to large chronic back pressure ulcer—50×50 cm, grades 1–4.
- ▶ October 2016: patient dies in hospice care: sepsis secondary to advanced pressure ulcers.



**Figure 1** Hemicorporectomy patient showing (A) urostomy with ileal conduit and (B) ileostomy.

His medical and surgical history was significant for hemicorporectomy with colectomy, splenectomy and creation of ileostomy and urostomy with ileal loop, multiple infected posterior and inferior thoracic pressure ulcers of all stages status post multiple debridements, terminal pelvic osteomyelitis, recurrent multi-drug-resistant complicated UTIs with sepsis, methicillin-resistant *Staphylococcus aureus* (MRSA) and vancomycin-resistant *Enterococcus* (VRE) bacteraemia with sepsis, hypertension, anaemia of chronic disease, chronic kidney disease (CKD), gastritis, oesophagitis, and pulmonary embolism. He presented to the Sinai-Grace Hospital Emergency Department with fever (reported by caregiver to be  $>39^{\circ}\text{C}$  at home) and altered mental status. On admission, he was found to be hypotensive (systolic blood pressure  $\sim 82$  mm Hg), with leukocytosis (white blood count (WBC)  $14.1 \times 10^9/\text{L}$  with neutrophilic predominance and bands of  $1.6 \times 10^9/\text{L}$ ) and acute kidney injury on CKD (creatinine 1.36), and was diagnosed with severe sepsis likely secondary to an infected advanced chronic non-healing posterior thoracic pressure ulcer and a possible complicated UTI. He was intubated and mechanically ventilated in the medical intensive care unit (MICU) for airway protection due to his altered mental status (alert and oriented  $\times 0$ ). He was initiated on empiric antibiotics including intravenous cefepime and clindamycin, along with fluid resuscitation. Infectious disease was consulted for antibiotics management due to the patient's history of multi-drug-resistant organisms (MDROs). However, blood cultures remained negative during this admission. Urinalysis was positive for nitrite and leukocyte esterase, with  $>100$ /high power field (HPF) urine WBCs. Lactic acid was 1.7 on admission. Urine culture grew  $>100\,000$  colony-forming units/mL with multiple organisms present.

The patient's mentation improved (alert and oriented  $\times 3$ ), and he was subsequently extubated on admission day 1. General surgery was consulted for surgical debridement of his extensive, advanced posterior thoracic pressure ulcer spanning  $50\text{ cm} \times 50\text{ cm}$  at various stages (1–4) of healing (figure 2). All necrotic tissue was excised to obtain viable bleeding tissue and haemostasis was achieved. Appropriate postoperative wound care was initiated with daily dressing changes with wet-to-dry dressings, soft care mattress, every 2-hour turns and adequate pain control. His ileostomy bag was replaced to ensure a proper seal to prevent faecal drainage into his posterior thoracic pressure ulcer. In addition, nutrition was consulted to optimise his nutritional intake to support wound healing. Antibiotics were continued for 7 days as per infectious disease recommendations. Our patient was discharged home on admission day 7. He lived with his sister, who was his caregiver and power of attorney. Appropriate postdischarge wound care was initiated with home healthcare services for daily dressing changes, nursing care for ileostomy and urostomy changes, and home physical therapy. In addition, follow-up with the wound care clinic was arranged.

### INVESTIGATIONS

See the Case presentation section.

### TREATMENT

See the Case presentation section.

### OUTCOME AND FOLLOW-UP

Our patient was readmitted 3 weeks later for another episode of sepsis with altered mental status. He was appropriately treated and recovered to his baseline. Psychiatry was consulted, and it was determined that he was not competent to make decisions





**Figure 2** Evolution of pressure ulcers. (A) September 2011: stage 4 sacral pressure ulcer 7×9.5×2.8 cm, (B) January 2013: stage 3 left thorax pressure ulcer 31.5×11×0.1 cm, and (C) September 2016: stages 1–4 posterior thorax pressure ulcer 50×50 cm.

regarding his medical care. In light of the fact that this patient had been admitted to the hospital on average 10 times/year in recent years, with 11 admissions over the last year alone, palliative care was consulted to assess patient and family wishes and determine goals of care. After an extensive discussion with the patient and his family regarding his diminished quality of life and poor prognosis, his sister, the durable power of attorney, decided that it was best for him to enrol in home hospice, with a focus on comfort care. The patient was subsequently admitted to inpatient palliative care 2 weeks later with altered mental status. He subsequently died during this admission in palliative care.

This case highlights the significant medical, surgical, financial and social challenges faced by the families, their caregivers and medical professionals involved in the care of hemipelvectomy patients.

## DISCUSSION

Here we present a case report of a 53-year-old African-American man who suffered a gunshot wound at T6 causing paraplegia at the age of 31 and subsequently underwent a hemipelvectomy at the level of L2 at the age of 49 for terminal pelvic osteomyelitis in a series of body-preserving surgical procedures over a period of 5 years (box 1). This radical surgical procedure prolonged his life, but arguably did not reduce his morbidity and significantly distorted his body anatomy, which presented unique challenges in his medical care. The close proximity of his anterior thoracic urostomy and ileostomy to each other and to his pressure ulcer frequently lead to stool and urine draining into his chronic pressure ulcer located on his posterior and inferior thorax during ileostomy and urostomy bag changes (figure 1). As a result, he required recurrent hospitalisations for sepsis secondary to complicated UTIs and chronic, non-healing advanced pressure ulcers, which gradually progressed and evolved to encompass larger areas of his posterior and inferior thorax, further altering his body morphology (figure 2). Surgeons performing repeated pressure ulcer debridement frequently had difficulty describing the exact location of the ulcer due to his distorted body anatomy. Furthermore, our patient had repeated ostomy prolapses requiring multiple surgical revisions likely due to the high intraperitoneal pressures generated by his body weight on peritoneum without a supporting bony frame (figure 2, box 1).

During each of his numerous hospital admissions, healthcare professionals struggled with his presenting diagnosis and the management of his multidrug-resistant infections, electrolyte abnormalities, monitoring kidney function and blood pressure control. Infectious disease was frequently consulted to manage this patient due to his history of MDROs, and he was invariably placed on multiple broad-spectrum antibiotics. A biopsy of his chronic advanced non-healing pressure ulcer grew *Acinetobacter baumannii* resistant to all major classes of antibiotics (including carbapenems), MRSA and Zosyn-resistant *Pseudomonas aeruginosa*. He also had numerous bouts of VRE and MRSA bacteraemia, which required alternate broad-spectrum antibiotics such as daptomycin for treatment. In addition to

increasing the cost of his medical care, repeated hospitalisations and treatments with broad-spectrum antibiotics also increased the chances of MDRO dissemination to other patients in the hospital.

This patient also required unconventional drug dosing due to his altered body composition and decreased body weight. For example, our patient had a total body weight of 30 kg with a reduced proportion of muscle mass since he was lacking his pelvis, sacrum and bilateral lower extremities. Therefore, his antibiotics, antihypertensive regimen and venous thromboembolism prophylaxis regimen had to be altered to adjust for his body mass and composition. His altered anatomy (urostomy located beside ileostomy) and body composition also presented diagnostic challenges, including persistent pyuria with positive nitrite and leucocyte esterase, which made it difficult to determine if his recurrent sepsis events were attributed to a chronic complicated UTI or his chronic, non-healing advanced pressure ulcers. In addition, he had a baseline systolic blood pressure between 90 and 100 mm Hg, which is not uncommon in patients with hemipelvectomy and paraplegia. In the setting of sepsis, a small reduction in blood pressure when combined with errors in measurement can result in a false diagnosis of septic shock, which in this case frequently prompted placement of a central line and MICU admission as a precautionary measure. These factors undoubtedly increased patient discomfort, length of hospital stay and significantly increased cost burden to the healthcare system.

This case also presented unique challenges for allied health professionals, including nurses and social workers. This patient required long-term specialised urostomy and ileostomy care, as well as wound care and daily dressing changes for his chronic non-healing pressure ulcers. Appropriate outpatient follow-up, education and training for caregivers on aseptic technique and patient hygiene are crucial to decreasing mortality and morbidity and improving the quality of life for hemipelvectomy patients.

The management of chronic non-healing advanced pressure ulcers is generally very costly to the healthcare system and significantly reduces the quality of life of the patient. Alternative treatment options such as maggot debridement therapy and hyperbaric oxygen therapy are currently in development and have shown promising results in institutions that have access to such treatments.<sup>9 10</sup> More research examining the efficacy and cost-effectiveness of various prevention and treatment strategies is needed, ideally with the goal of establishing specific guidelines.

This case also highlights the need to educate the patient and family and establish goals of care in hemipelvectomy patients, with quality of life and patient wishes as the guiding principles. A patient's mental well-being including decision-making capacity, self-image, ability to perform activities of daily living, the potential desire to return to work or school, financial concerns, potential social isolation, pain management and radical changes in ability to perform specific sexual activities must also be addressed. The patient involved in this case had clearly expressed his wish to live and share his life with his son

## Rare disease

and family until late 2016, when his disease burden overtook his ability to make rational decisions, requiring a durable power of attorney for decision-making.

Although the patient in this case provides a unique account of the significant healthcare challenges in managing the potential complications of some hemicorporectomy patients, it is important to highlight that many patients do enjoy a productive life and experience a less complicated posthemicorporectomy course. For example, Peterson and Sardi<sup>11</sup> describe a case of hemicorporectomy for SCC (Marjolin's ulcer), where the patient remained disease-free for at least 7 years (as of November 2003) after hemicorporectomy and was employed as a computer programmer, independent in activities of daily living and retained the ability to drive. Other case reports suggest that some hemicorporectomy patients can live multiple decades despite a grave preoperative diagnosis.<sup>12</sup> A case series of one woman and eight men (all paraplegic) who underwent hemicorporectomy for terminal pelvic osteomyelitis between 1981 and 2005 found that for the four surviving patients at follow-up, none suffered recurrent decubitus ulcers (with a range of survival after surgery of 1.7–22 years).<sup>5</sup> For the patients who died, the cause of death was urosepsis for one patient, a fall for one patient, portal vein thrombosis for one patient and unknown cause for two patients. This makes our patient unique as the majority of posthemicorporectomy patients do not suffer recurrent osteomyelitis and advanced pressure ulcers leading to recurrent sepsis events. However, similar to our patient in this case, these patients had also undergone multiple surgical procedures including wound debridements and local flaps in an attempt to treat chronic pressure ulcers prior to hemicorporectomy. At the time that hemicorporectomy was considered, one patient had an ileostomy, four patients had colostomies and three patients had undergone procedures for urinary diversion.<sup>5</sup>

These notable examples illustrate that a significant number of hemicorporectomy patients can prolong their life as well as enjoy a relatively good quality of life with a multidisciplinary approach to care. After hemicorporectomy, all patients should undertake a rehabilitation process that involves the integration of different services such as occupational and physical therapy for increasing upper body strength and acquiring new mobility skills, nutrition, enterostomal therapy and wound care nursing, and psychological counselling.<sup>5</sup> A previous study showed that patients who survived the procedure for terminal pelvic osteomyelitis and had long-term follow-up were likely to be happy with their decision to have had the procedure as it prolonged their lives and also relieved them from the pain of living with chronic pressure ulcers.<sup>5</sup> Overall the procedure has both benefits and risks, and patients and their families should properly understand both implications and make the best decision while consulting with healthcare providers.<sup>13</sup> Furthermore, Jankowski and Campo-Engelstein<sup>13</sup> suggest that beyond assessing the risks and benefits of hemicorporectomy, the concept of informed consent, justice and resource allocation, and the loss and lived body are important considerations and remain topics of debate.

Unfortunately, there are currently no guidelines or standards of care for the management of hemicorporectomy patients, either on an inpatient or outpatient basis. This is primarily due to the rarity of the procedure and the paucity of subsequent data regarding outcomes, complications and treatments. We hope that this case may help healthcare providers anticipate and manage some of the potential complications in similar patients who have undergone hemicorporectomy or other radical surgical procedures.

## Patient's perspective

The patient died in September 2016 after a recurrent bout of sepsis while he was in home hospice.

## Learning points

- ▶ Hemicorporectomy patients require a multidisciplinary approach to care.
- ▶ Hemicorporectomy secondary to terminal pelvic osteomyelitis has the potential of prolonging life, but may also lead to a significantly diminished quality of life if adequate multidisciplinary care is not provided to the patient.
- ▶ Hemicorporectomy patients present unique challenges for inpatient and outpatient management.
- ▶ Early patient and family education regarding the quality of life and prognosis is required to establish goals of care for decision-making and provide options for comprehensive outpatient care including home healthcare services, physical and occupational therapy, psychiatric care, wound care, and even palliative/hospice care in select patients.

**Acknowledgements** We would like to thank Dr Wasif Hafeez, Dr Hicham Krayem and Dr Susan Seman for their expertise and contribution to the ongoing care of this patient during his multiple admissions to Sinai-Grace Hospital over the years. We would also like to thank the patient's sister (SS) and power of attorney for her cooperation and support in publishing this interesting and rare case of hemicorporectomy.

**Contributors** AT was involved in patient care, the conception, design, critical review and write-up of multiple sections of the case report. BE was involved in the design, write-up of the background and part of the discussion section, and critical review of multiple drafts of the case report. RN was involved in patient care, the conception, design, critical review and write-up of abstract/summary, part of the discussion section and take home messages of the case report. NK was involved in patient care, the background research through 22 years of patient admissions, acquiring patient photographs and critical review of the case report. SM was involved in the design of the paper, analysis of the 22-year case history, write-up of the case presentation section and critical review of the case report. CA was the research supervisor and involved in the conception, design, data analysis and critical review of all sections of the case report. All authors were involved in the final approval and were in agreement regarding the accuracy and integrity of the case report.

**Competing interests** None declared.

**Patient consent** Obtained.

**Provenance and peer review** Not commissioned; externally peer reviewed.

© BMJ Publishing Group Ltd (unless otherwise stated in the text of the article) 2018. All rights reserved. No commercial use is permitted unless otherwise expressly granted.

## REFERENCES

- 1 Crum RW, Lee ES, Patterson FR, *et al.* Back-to-front hemicorporectomy with double-barreled wet colostomy for treatment of squamous cell carcinoma of a pressure ulcer. *Am Surg* 2015;81:E400–2.
- 2 Cavalheiro DP, Marten Teixeira JE, Braga DM, *et al.* Rehabilitation management of hemicorporectomy. *Pm R* 2015;7:777–80.
- 3 Abrams J, Hulbert J, Thompson R, *et al.* Hemicorporectomy for acute aortic occlusion: a case study. *Am Surg* 1992;58:509.
- 4 Ferrara BE. Hemicorporectomy: a collective review. *J Surg Oncol* 1990;45:270–8.
- 5 Janis JE, Ahmad J, Lemmon JA, *et al.* A 25-year experience with hemicorporectomy for terminal pelvic osteomyelitis. *Plast Reconstr Surg* 2009;124:1165–76.
- 6 Yancey AG, Ryan HF, Blasingame JT. An experience with hemicorporectomy. *J Natl Med Assoc* 1964;56:323.
- 7 Lamis PA, Richards AJ, Weidner MG. Hemicorporectomy: hemodynamic and metabolic problems. *Am Surg* 1967;33:443–8.
- 8 Weaver JM, Flynn MB. Hemicorporectomy. *J Surg Oncol* 2000;73:117–24.

- 9 Columbo JA, Ptak JA, Buckey JC, *et al*. Hyperbaric oxygen for patients with above-knee amputations, persistent ischemia, and nonreconstructable vascular disease. *J Vasc Surg* 2016;63:1082–4.
- 10 Felder JM, Hechenbleikner E, Jordan M, *et al*. Increasing the options for management of large and complex chronic wounds with a scalable, closed-system dressing for maggot therapy. *J Burn Care Res* 2012;33:e170–6.
- 11 Peterson R, Sardi A. Hemicorporectomy for chronic pressure ulcer carcinoma: 7 years of follow-up. *Am Surg* 2004;70:507–11.
- 12 Mackenzie AR. Translumbar amputation: the longest survivor—a case update. *Mt Sinai J Med* 1995;62:305–7.
- 13 Jankowski J, Campo-Engelstein L. A better half: the ethics of hemicorporectomy surgery. *J Bioeth Inq* 2014;11:289–94.

Copyright 2017 BMJ Publishing Group. All rights reserved. For permission to reuse any of this content visit <http://group.bmj.com/group/rights-licensing/permissions>.  
BMJ Case Report Fellows may re-use this article for personal use and teaching without any further permission.

Become a Fellow of BMJ Case Reports today and you can:

- ▶ Submit as many cases as you like
- ▶ Enjoy fast sympathetic peer review and rapid publication of accepted articles
- ▶ Access all the published articles
- ▶ Re-use any of the published material for personal use and teaching without further permission

For information on Institutional Fellowships contact [consortiasales@bmjgroup.com](mailto:consortiasales@bmjgroup.com)

Visit [casereports.bmj.com](http://casereports.bmj.com) for more articles like this and to become a Fellow

## APPENDIX B: STATEMENT OF CONTRIBUTION SIGNED BY PRINCIPAL INVESTIGATORS

Much of my research work was conducted over a period of years and I have been unable to reach many of the coauthors listed on my papers via email for signature. Please note that **all** my research was conducted at university academic labs headed by principal investigators who are the only people, apart from me, who fully understand the nature and scale of my contribution to each paper submitted in this thesis. I have been the lead (first) author on seven out of the eight papers submitted in this thesis. The coauthors listed on my papers provided research support in a manner that did not warrant lead (first) authorship. The lead author of paper #3 (published in Expert Review of Medical Devices) has provided his signature attesting to my contribution. The exact nature and scale of my contribution to each of my papers has been described in detail in the 'index of publications submitted and statement of contribution' section, and all the principal investigators have attested (by signature) to my contributions to each of the papers submitted in this thesis. I hope this will satisfy the requirements for thesis submission.



## STATEMENT OF AUTHORSHIP OF PUBLICATION

On behalf of Ajit Thakur

By Prof. Kim Jones

Associate Professor

Associate Chair

Department of Chemical Engineering

McMaster University

1280 Main Street West

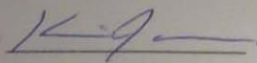
Hamilton, ON, L8S 4L7, Canada

### Publications:

- 1) **A. Thakur**, A. Zaman, J. Hummel, K. Jones, G. Hortelano. (2012). "Single-colour flow cytometric assay to determine NK cell-mediated cytotoxicity and viability against non-adherent human tumor cells." *Biotechnology Letters*. 34(3) pp. 447-53.  
Scale of contribution (%): 90%  
Nature of contribution: Experimental + Writing Paper
- 2) **A. Thakur**, J. Hummel, R. Sengupta, V. Gupta, K. Mossman and K. Jones. (2011). "Retroviral expression of MIR2 decreases both surface MHC Class I and the alloimmune CTL response." *Journal of Tissue Engineering and Regenerative Medicine*. 5(7) pp. 520-528.  
Scale of contribution (%): 90%  
Nature of contribution: Experimental + Writing Paper
- 3) **A. Thakur**, A. Zaman, S. Fitzpatrick, J. Hummel and K. Jones. (2011). "Suppression of the MHC Class I-mediated alloimmune response in human cells using a single-step retroviral transduction protocol to express KSHV's stealth protein MIR2." *University of Toronto Medical Journal*. 89(1) pp. 27-32.  
Scale of contribution (%): 90%  
Nature of contribution: Experimental + Writing Paper
- 4) **A. Thakur**, R. Sengupta, H. Matsui, D. Lillicrap, K. Jones and G. Hortelano. (2010). "Characterization of viability and proliferation of alginate-poly-L-lysine-alginate encapsulated myoblasts using flow cytometry." *Journal of Biomedical Materials Research: Part B*. 94B(2) pp. 296-304.  
Scale of contribution (%): 60%  
Nature of contribution: Experimental + Writing Paper

I confirm the scale and nature of Ajit Thakur's contributions to the above publications.

Signature



Date

FEB 4, 2016

**STATEMENT OF AUTHORSHIP OF PUBLICATION**

**On behalf of Ajit Thakur**

**By Prof. Heather Sheardown**

Professor

Canada Research Chair in Ophthalmic Biomaterials

Department of Chemical Engineering

McMaster University

1280 Main Street West

Hamilton, ON, L8S 4L7, Canada

**Publications:**

- 1) **A. Thakur**, S. Fitzpatrick, A. Zaman, K. Kugathan, B. Muirhead, G. Hortelano, H. Sheardown. (2012). "Strategies for ocular siRNA delivery: potential and limitations of non-viral nanocarriers." *Journal of Biological Engineering*. 6(1) pp. 7.

Scale of contribution (%): 90%.....

Nature of contribution: Writing, editing.....

- 2) S. Fitzpatrick, L. Fitzpatrick, **A. Thakur**, M. Mazumder and H. Sheardown. (2012). "Temperature-sensitive polymers for drug delivery." *Expert Review of Medical Devices*. 9(4) pp. 339-351.

Scale of contribution (%): 15%.....

Nature of contribution: Wrote section.....

I confirm the scale and nature of Ajit Thakur's contributions to the above publications.

Signature 

Date Feb 4/16

## STATEMENT OF AUTHORSHIP OF PUBLICATION

On behalf of Ajit Thakur

By Prof. Cecile Fradin

Associate Professor

Department of Physics and Astronomy

McMaster University

1280 Main Street West

Hamilton, ON, L8S 4M1, Canada

### Publications:

- 1) A. Thakur and C. Fradin. (2005). "Characterization of quantum dot behaviour in live mammalian cells." *Canadian Undergraduate Physics Journal*. 3(3), pp.7-12. **This article was featured on the cover-art of the journal.**

Scale of contribution (%):... 90% .....

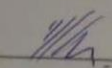
Nature of contribution:... All the experimental work + Most of the writing .....

- 2) R. Peters, J. Goh, J. Dinglasan, A. Thakur, S. Shehata, D. Anderson and C. Fradin. (2010). "Investigation into the photophysics and diffusion properties of water soluble quantum dots using Fluorescence Correlation Spectroscopy." *ECS Transactions: Nanoscale Luminescent Materials*. 28(3) pp. 243-255.

Scale of contribution (%):... 1.5% .....

Nature of contribution:... Experimental support + Editing of manuscript .....

I confirm the scale and nature of Ajit Thakur's contributions to the above publications.

Signature  \_\_\_\_\_

Date Feb 5, 2016 \_\_\_\_\_

**STATEMENT OF AUTHORSHIP OF PUBLICATION**

**On behalf of Ajit Thakur**

**By Dr. Camelia Arsene**

Assistant Professor

Associate Program Director

Department of Internal Medicine

Wayne State University School of Medicine/Detroit Medical Center/Sinai-Grace Hospital

Detroit, Michigan, USA

Publication:

**A.Thakur**, R. Naik, B. Elliott, S. Mcquaid, N. Khan, C. Arsene. (2018). "Recurrent hospitalizations in a rare case of hemicorporectomy: A challenging case for medical management." *British Medical Journal Case Reports*. doi 10.1136 pp. 1-5

Ajit Thakur was the lead author involved in patient care, design, data analysis, critical review, write-up of the paper. He also was the corresponding author for the paper and was the lead editor for paper revisions prior to publication.

I confirm the scale and nature of Ajit Thakur's contributions to the above publication.

Signature



Date

09/17/2018

## STATEMENT OF AUTHORSHIP OF PUBLICATION

On behalf of Ajit Thakur

By Prof. Gonzalo Hortelano

Professor

Department of Biology  
School of Science & Technology  
Nazarbayev University Astana,  
Republic of Kazakhstan

Publications:

- 1) **A. Thakur**, A. Zaman, J. Hummel, K. Jones, G. Hortelano. (2012). "Single-colour flow cytometric assay to determine NK cell-mediated cytotoxicity and viability against nonadherent human tumor cells." *Biotechnology Letters*. 34(3) pp. 447-53.

Ajit Thakur conceived the idea for the study, and took the lead role in experimental work and data analysis. He was the lead author as well as the corresponding author who submitted the manuscript and corresponded with reviewers for paper revisions prior to publication.

- 2) **A. Thakur**, S. Fitzpatrick, A. Zaman, K. Kugathasan, B. Muirhead, G. Hortelano, H. Sheardown. (2012). "Strategies for ocular siRNA delivery: potential and limitations of nonviral nanocarriers." *Journal of Biological Engineering*. 6(1) pp. 7.

Ajit Thakur conceived the idea for this paper and was the lead author involved in the literature review, write-up and critical review. He designed the smart universal nanoparticle for intracellular oligonucleotide delivery. He was also the corresponding author who submitted the manuscript and corresponded with reviewers for paper revisions prior to publication.

- 3) **A. Thakur**, R. Sengupta, H. Matsui, D. Lillicrap, K. Jones and G. Hortelano. (2010). "Characterization of viability and proliferation of alginate-poly-L-lysine-alginate encapsulated myoblasts using flow cytometry." *Journal of Biomedical Materials Research: Part B*. 94B(2) pp. 296-304.

Ajit Thakur conceived the idea for the study and took the lead role in writing the paper, critical data analysis and multiple paper revisions prior to publication. He was assisted by coauthor R Sengupta for experimental work.

I confirm the scale and nature of Ajit Thakur's contributions to the above publications.


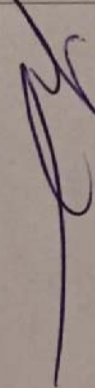
Signature \_\_\_\_\_  \_\_\_\_\_

Date \_\_\_\_\_ 17 September, 2018 \_\_\_\_\_

S. Fitzpatrick, L. Fitzpatrick, A. Thakur, M. Mazumder and H. Sheardown. (2012).  
"Temperature-sensitive polymers for drug delivery." *Expert Review of Medical Devices* 9(4)  
pp. 339-351.

Ajit Thakur co-authored this manuscript with S. Fitzpatrick and was involved in the literature search, write-up, critical review and revisions of the paper.

I confirm the scale and nature of Ajit Thakur's contributions to this publication:

Name	Signature	Date
Scott Fitzpatrick		9/11/2017
Lindsay Fitzpatrick		9/11/2018



APPENDIX C: LIST OF ADDITIONAL PAPERS SUBMITTED AS  
SUPPLEMENTARY MATERIAL

- 1) A. Zaman, **A. Thakur**, I. Rashedi and G. Hortelano. (2012). "Ultrasound-assisted tissue plasminogen activator delivery to ischemic strokes." *Journal of Young Investigators*. 23(5) pp. 16-17.
- 2) R. Peters, J. Goh, J. Dinglasan, **A. Thakur**, S. Shehata, D. Anderson and C. Fradin. (2010). "Investigation into the photophysics and diffusion properties of water soluble quantum dots using Fluorescence Correlation Spectroscopy." *ECS Transactions: Nanoscale Luminescent Materials*. 28(3) pp. 243-255.
- 3) **A. Thakur**, K. Kugathasan, V. Gupta and K. Jones. (2010). "A novel method for measuring cell-mediated cytotoxicity and viability using flow cytometry." *IBBME Proceedings*. 1(1) pp.18-22.
- 4) **A. Thakur**. (2003). "Anthrax and the Three Amigos." *McMaster Meducator*. 1(2) pp.11-13.